Scholar Commons
USF University of South Florida

University of South Florida
Scholar Commons

Graduate Theses and Dissertations | Graduate School

7-15-2005

Processing, Reliability And Integration Issues In Chemical Mechanical Planarization

Parshuram B. Zantye
University of South Florida

Follow this and additional works at: https://scholarcommons.usf.edu/etd

Part of the American Studies Commons

Scholar Commons Citation

Zantye, Parshuram B., "Processing, Reliability And Integration Issues In Chemical Mechanical Planarization" (2005). *Graduate Theses and Dissertations.*
https://scholarcommons.usf.edu/etd/928

This Dissertation is brought to you for free and open access by the Graduate School at Scholar Commons. It has been accepted for inclusion in Graduate Theses and Dissertations by an authorized administrator of Scholar Commons. For more information, please contact scholarcommons@usf.edu.

المنارة للاستشارات

www.manaraa.com

Processing, Reliability And Integration Issues In Chemical Mechanical Planarization

By

Parshuram B. Zantye

A dissertation submitted in partial fulfillment
of the requirements for the degree of
Doctor of Philosophy in Mechanical Engineering
Department of Mechanical Engineering
College of Engineering
University of South Florida

Major Professor: Ashok Kumar, Ph.D.
Rajiv Dubey, Ph.D.
Muhammad Rahman, Ph.D.
Tapas Das, Ph.D.
Julie Harmon, Ph.D.
John Bumgarner, Ph.D.
Yaw Obeng, Ph.D.

Date of Approval:
July 15 2005

Keywords: chemical mechanical polishing (cmp), tribology, polishing pad, slurry, damascene, metrology, end point, delamination, ultrasound, reliability

© Copyright 2005, Parshuram B. Zantye

المنارة للاستشارات

www.manaraa.com

DEDICATION

My entire work in the field of Chemical Mechanical Planarization including this dissertation is dedicated to my Parents, Mrs. Vrinda B. Zantye and Mr. Balkrishna P. Zantye.

للاستشارات المنارة

www.manaraa.com

ACKNOWLEDGMENTS

I would like to generously thank my advisor Prof. Ashok Kumar for giving me an opportunity to pursue research under his able guidance and with his support throughout during my Masters' as well as Doctoral studies at University of South Florida. I would like to thank the Chairman of Department of Mechanical Engineering, Prof. Rajiv Dubey for his constant encouragement and assistance throughout my tenure as a graduate student, and also for serving my dissertation committee. A special thanks goes to Dr. Yaw Obeng (Texas Instruments, Dallas, TX) for his invaluable help in terms of sharing technical know how all along the course of my research during his tenure earlier at psiloQuest Inc, Orlando, FL and later at Texas Instruments, Inc. I wish to thank the Chair of my dissertation committee, Prof. Sunil Saigal for serving on my committee and giving me invaluable suggestions for this past year. I would like to highly acknowledge the help of Dr. Michael Kovac, Director, Nanomaterials and Nanomanufacturing Research Center (NNRC) and all the team of engineers, technicians and support staff working under his able leadership at the NNRC. Special thanks also go to all my committee members: Dr. Mohammed Rahman, Dr. Tapas Das, Dr. Julie Harmon, and Dr. John Bumgarner. Also, I wish to thank Dr. Sergei Ostapenko, who for logistic reasons could not serve on my committee but was actively involved with my research. The financial support for this research came from NSF CAREER Grant #9983535 (Ashok Kumar) and NSF GOALI Grant #DMII 0218141. Part of this research was also supported by USF-Agere High-Tech Corridor Grant #2112-142LO, International Sematech Grant # 2112-139 and psiloQuest, Inc. Florida High Tech Corridor Grant. I would also like to

للاستشارات المنارة

www.manaraa.com

thank Dr. Ashok Das from Applied Materials, Dr. Jeffery Lee from Intel Corporation, Dr. M. Sanganeria from Novellus Systems, and Dr. Jiro Yota from Skyworks Inc., for providing valuable inputs, materials and supplies. Finally, my parents, family, friends, former Post Doctoral fellows (Dr. Arun K. Sikder and Dr. Arun Kumar), and colleagues, especially S. Mudhivarthi, also deserve a very special thank you note at this time for constantly supporting me throughout the thick and thin of my life.

المنارة للاستشارات

www.manaraa.com

TABLE OF CONTENTS

LIST OF TABLES vii

LIST OF FIGURES viii

ABSTRACT xvii

CHAPTER 1: INTRODUCTION 1

1.1 Generalized Semiconductor Fabrication Modules 1

1.2 Increase in Device Density 2

1.3 Scaling and Time Delay 3

1.4 Need for Planarization 9

1.5 Shallow Trench Isolation 10

1.6 Damascene Process 12

1.7 Different Planarization Techniques 13

1.7.1 Doped Glass Reflow 14

1.7.2 Spin Etch Planarization (SEP) 16

1.7.3 Spin on Deposition (SOD) 17

1.7.4 Reactive Ion Etch and Etch Back (RIE+EB) 19

1.7.5 Chemical Mechanical Planarization (CMP) 20

1.8 General Chemical Mechanical Planarization Applications 21

1.9 Overview 26

للاستشارات المنارة

www.manaraa.com

CHAPTER 2: BACKGROUND OF CMP 27

2.1 Evolution of CMP 27

2.1.1 History of CMP 27

2.1.2 Road Map of CMP Process 28

2.2 CMP: A Multi-stage Process 31

2.2.1 Slurry Mixing 33

2.2.2 Slurry Distribution 34

2.2.3 Working of the CMP Process 35

2.2.4 CMP Polisher Consideration 36

2.2.5 First Generation CMP Polisher 37

2.2.6 Second Generation CMP Polisher 38

2.2.6.1 Multi-wafer Per Platen Polisher 38

2.2.6.2 Sequential Rotational Systems 39

2.2.7 Third Generation Polishers 40

2.2.7.1 Sequential Linear Polishers 40

2.2.7.2 Orbital Polishers 41

2.2.7.3 Rotary Inverted 42

2.2.7.4 Pad Feed Polishers 43

2.3 Physics of CMP Process 44

2.4 Parameters Governing CMP Process 46

2.5 Research Objectives 48

المنارة للاستشارات

www.manaraa.com

CHAPTER 3: METROLOGY OF CMP 49

3.1 Need for Effective CMP Metrology 49

3.2 CMP Tester 50

3.3 Coefficient of Friction (COF) and Material Removal Rate (MRR) 52

3.4 Importance of Slurry Flow 55

3.5 CMP End Point Detection (EPD) 58

3.6 In-situ Process Monitoring 63

3.7 Delamination during CMP 72

3.8 Other CMP Defects 76

CHAPTER 4: PROPERTIES OF INTERCONNECT MATERIALS 77

4.1 Need for Evaluation of Material Properties 77

4.2 Effect of Annealing on Copper 78

4.3 Significance of Interfacial Reliability in Damascene Structure 81

4.4 Effect of Annealing on Cu-TaN Interface 82

4.5 Techniques of Interfacial Evaluation of Thin Films 83

4.5.1 Four Point Bend Technique 84

4.5.2 Nanoscratch Testing 86

4.5.2.1 Failure Domain Analysis of Nanoscratch Tests 89

4.5.2.1.1 SEM/Auger Spectroscopy Analysis 89

4.5.2.1.2 FIB Cross section and SEM Analysis 92

4.6 Quantitative Evaluation of Thin Film Adhesion Energy 93

المنارة للاستشارات
www.manaraa.com

4.7 Qualitative Evaluation of Thin Film Adhesion Energy 95

4.8 Low Dielectric Constant Materials (low k materials) 96

4.8.1 CVD Based Low k Materials 98

4.8.2 Spin On Low k Materials 99

4.8.3 Potentially Feasible Low k Materials 100

4.9 Mechanical Characterization of Low k Materials 103

4.10 CMP of Low k Materials 107

4.10.1 Doped and Undoped Ceramic Material Removal 108

4.10.2 Polymeric Material Removal 109

4.10.3 CMP Process Conditions 110

4.10.4 Tribological Properties of Low k Materials 112

4.10.5 Variation of Material Removal Rate for Low k Materials 116

4.10.6 Surface Characterization of Low k Materials 118

4.10.7 Findings of Low k Materials Evaluation 120

CHAPTER 5: INVESTIGATION OF NON UNIFORMITIES IN POLISHING PAD 123

5.1 Significance of Polishing Pad 123

5.2 Method of Mapping and Isolation of Pad Non-Uniformities 124

5.3 Ultrasound Testing System 126

5.4 Evaluation of Mechanical and Tribological Properties of Polishing Pad 128

5.5 SEM Evaluation of Polishing Pad 130

5.6 Isolation of Polishing Pad Coupons 131

5.7 Isolation of 6 Inch Polishing Pad Coupons 133

المنارة للاستشارات

www.manaraa.com

5.8 Pad Dynamic Mechanical Analysis 134

5.9 Frictional Characteristics of Polishing Pad Regions 137

5.10 Summary of Investigations of Polishing Pad Non uniformities 143

CHAPTER 6: INVESTIGATION AND OPTIMIZATION OF APPLICATION SPECIFIC CMP PADS 144

6.1 Application Specific Pad (ASP) for CMP 144

6.2 Scheme for Optimization of ASP Properties 146

6.3 Experimental Techniques for ASP Property Evaluation 147

6.4 Evaluation of ASP Surface Micromechanical Properties 149

6.5 Evaluation of ASP Surface Micromechanical Properties 153

6.6 Evaluation of Static Tribological Properties of ASP 157

6.7 CMP (Dynamic Tribological Property) Evaluation of ASP 158

6.8 Optimization of ASP Total Thickness 163

6.9 Summary of ASP Optimization and Characterization 165

CHAPTER 7: INDENTIFICATION AND MODIFICATION OF CMP SLURRY 167

7.1 Background of CMP Slurry 167

7.2 Effect of CMP Slurry in Global Planarization 167

7.3 Effect of CMP Slurry on Removal Rate 170

7.3.1 Effect of Slurry Chemistry on Removal Rate 171

7.3.2 Effect of Slurry Particle Size Hardness and Concentration 172

7.4 Effect of Temperature on Slurry Performance 174

المنارة للاستشارات

www.manaraa.com

7.5 Novel Nanoparticle Based Slurry 177

7.5.1 Composition of Novel Nanoparticle Based Cu Slurry 178

7.5.2 Mechanism of Polishing of Novel Cu Slurry 179

7.5.3 Polishing Performance of Novel Nanoparticle Cu Slurry 182

7.6 Summary of Investigation and Modification of CMP Slurry 185

CHAPTER 8: SUMMARY 187

8.1 Summary of Research 187

8.2 Major Findings and Contributions 189

8.3 Future Trends in CMP and Potential Areas for Investigation 191

REFERENCES 193

ABOUT THE AUTHOR End Page

المنارة للاستشارات

www.manaraa.com

LIST OF TABLES

Table 1.1	Interconnection Delay (RC) in Silicon VLSI Chip	6
Table 1.2	Advantages of Chemical Mechanical Planarization	23
Table 1.3	Disadvantages of Chemical Mechanical Planarization	24
Table 1.4	Applications of Chemical Mechanical Planarization	25
Table 2.1	Interconnect International Technology Roadmap for Semiconductors	30
Table 3.1	Effect of Slurry Flow rate on COF and AE	56
Table 3.2	STI-CMP Experimental Details	66
Table 4.1	Details of the Samples Undergoing Two Stage Annealing	79
Table 4.2	Details of the Samples Subjected to Interfacial Studies	83
Table 4.3	Relative Concentration of the Elements (at.%) on Scratch Surface	91
Table 4.4	Details of the Different Low k Materials Evaluated	105
Table 4.5	Results of Nanoindentation of the ILD materials	106
Table 4.6	ILD CMP Experimental Details	111
Table 4.7	Surface Roughness (R_{rms}) of the ILD Samples Before and After CMP	120
Table 5.1	Details of the CMP Experiments Performed on the Polishing Pad evaluated by UST	129
Table 6.1	Experimental Details of CMP Process Used for ASP Evaluation	149
Table6.2	Multivariate Correlations between Various Independent Results and PECVD Coating Time	162

المنارة للاستشارات
www.manaraa.com

LIST OF FIGURES

Figure 1.1	Scanning Electron Micrographs of Cross-section of the Structures Fabricated by BEOL Technology: (a) BEOL structure of 0.5 µm CMOS Logic Device and (b) Stacked Contacts and Vias	2
Figure 1.2	Trends Over the Years in Logic and Memory Devices	3
Figure 1.3	Chronology of Key Interconnect Technology Introduction Through the Years. LM Denotes Levels of Metallization	4
Figure 1.4	Variation of RC Time Delay with Minimum Feature Size	7
Figure 1.5	Predicted Future Trends in IC Interconnect Technology, (Courtesy: Jeffery Lee, Intel Corporation)	8
Figure 1.6	Chart Showing Decrease in Intermediate Interconnect Wiring Pitch for Future Generation IC, (Courtesy: Jeffery Lee, Intel Corporation)	8
Figure 1.7	Schematic of a) Non-planarized and b) Planarized MLM structure	10
Figure 1.8	Schematic of a Processes Sequence of Direct STI CMP without Reverse Moat	11
Figure 1.9	Comparison between Subtractive Etch (Conventional Approach) and the Damascene Approach for Metallization	13
Figure 1.10	Schematic Showing Degrees of Surface Global and Local Planarity	14
Figure 1.11	Schematic Showing BPSG Void Formation after Reflow	15

المنارة للاستشارات
www.manaraa.com

Figure 1.12	Schematic of SEP Chamber Showing a Cut-away View of the Process Pot, Four Chambers and Chuck. The Chemical Dispense Arm, Drain Lines and Exhaust Ports also are Indicated	17
Figure 1.13	Schematic showing Spin on Deposition with Partial planarization	18
Figure 1.14	Schematic Showing Smoothening and Partial Planarization using Reactive Ion Etching with Etch Back	20
Figure 1.15	Scanning Electron Micrograph Showing Cross-section of Structure Planarized by SOD RIE EB	21
Fig. 2.1	Flow Chart of the Isolated Industrial CMP Process	31
Fig. 2.2	Schematic of the Slurry Mixing at a Centralized Location	33
Fig. 2.3	Schematic of CMP Slurry Distribution System	34
Fig. 2.4	Schematic of Wafer Planarization by CMP Process	35
Fig. 2.5	Photograph of Speefam (Novellus) Multi Wafer per Platen Polisher	38
Fig. 2.6	Applied Materials Inc., Sequential Rotational CMP Polisher (Courtesy: Ashok Das, Applied Materials, Inc., Santa Clara, CA)	39
Fig. 2.7	Photograph of Sequential Linear Polishing System	41
Fig. 2.8	Schematic of Rotary CMP Polisher	42
Fig. 2.9	a) Set up of Multi Wafer Rotary Inverted CMP Polisher and b) Polishing Action and End Point detection	43
Fig. 2.10	Schematic of a Web-type Polisher	44
Fig. 2.11	Schematic of the Force Field on the Wafer and the Pad during CMP	45
Fig. 2.12	Non-uniformity in Removal Rate with in a Wafer	46

المنارة للاستشارات

www.manaraa.com

Fig. 2.13 Parameters Governing the CMP Dynamics 47

Fig. 2.14 Schematic Showing Objectives of the Current Research 48

Fig. 3.1 Photograph of the CETR CP-4 CMP Tester 51

Fig. 3.2 a) Variation of COF with RPM (platen velocity) for Different Values of Down Pressure (PSI), b) Variation of COF with PSI (Down Pressure) with Different Values of Platen Velocity (RPM) 53

Fig. 3.3 a) Variation of Average Removal Rate with RPM at Different Down Pressure (PSI) for the Evaluated Set of Samples, b) Variation of Average Removal Rate with PSI (Down Pressure) at Different Platen Velocity (RPM) for the Evaluated Set of Samples 54

Fig. 3.4 Average Material Removal Rates Plotted with RPM × PSI. Linear Relation Indicates that Polishing Follows Preston's Equation 55

Fig. 3.5 Schematic of the Positions of Slurry Feeding on the Pad during Polishing for Feeding Position Optimization; Distance 0–1.4 = 15 mm, 0–2.5 = 30 mm, 0–3.6 = 45 mm, 0–7.9 = 45 mm and 0–8 = 25 mm 56

Fig. 3.6 Average Removal Rate with the Slurry Feeding Position on the Lower Platen Position 57

Fig. 3.7 a) Variation of COF at 2 PSI Down Force and Variable RPM in Slurry Cu1; b) Variation of COF at 2 PSI Down Force and Variable RPM in Slurry Cu2; c) Variation of COF at 2 PSI Down Force and Variable RPM in Slurry Ta; and d) Variation of COF at 2 PSI Down Force and Variable RPM in Slurry Cu–Ta 59

المنارة للاستشارات
www.manaraa.com

Fig. 3.8 a) Variation of AE and COF for Different Materials Polished in a Commercial Cu Slurry, b) Variation of COF for 3 Materials Polished in Three Different Slurries 60

Fig.3.9 Cu and TaN Polishing Results (Head 40 RPM, Table 40 RPM, and Pressure 7 PSI) 61

Fig. 3.10 Schematic Illustration of Dishing and Erosion 63

Fig. 3.11 SEM of FIB Cross Section of STI Structure 64

Fig. 3.12 3D AFM Image of the Evaluated STI Structure with Step Height Measurement 65

Fig. 3.13 In-situ Variation of COF during CMP Split in to Different Stages 68

Fig. 3.14 Ex-situ 3D AFM Image of the Evaluated STI Structure with Reduced Step Height before Termination of Stage A 68

Fig. 3.15 Ex-situ 3D AFM image of the Evaluated STI Structure after Process End Point just after Beginning of Stage B 69

Fig. 3.16 In-situ data for Repeatability of 2 Trial Runs Shown to Demonstrate Repeatability 71

Fig. 3.17 a) Picture of Sample Coupons ACL, BCL, and TC after Polishing, b) Variation of AE signal of Three Different Samples 73

Fig. 3.18 SEM Micrographs Showing of Delamination of Different ACL, BCL Samples and No Delamination for TC Sample 74

Fig. 3.19 a) Variation of AE Signal during Polishing in the Time Interval of 230 – 250 s for Three Different Samples. Peaks are Seen for Sample ACL006, b) Sample ACL006 and (c) Sample A006r 75

المنارة للاستشارات

www.manaraa.com

Fig. 4.1 Challenges Surrounding Implementation of Novel Low k Materials Cu in a Damascene Structure (Courtesy: Jeffery Lee, Intel Corporation) 81

Fig. 4.2 Schematic of Four Point Bend Test (University of California, Santa Barabara) Set Up 84

Fig. 4.3 Variation of Load (lbf) Vs Displacement (Microns) during a Four Point Bend Test 85

Fig. 4.4 Schematic of the Nanoscratch Testing Setup 88

Fig. 4.5 Raw Data Showing the Variation of a) Acoustic Emission (AE), b) Frictional Force (F_f) with Time during a Scratch Test. (Sample 1 at Linearly Increasing Downward Force of 2 gm/sec Linear Velocity of 0.2 mm/sec) 88

Fig. 4.6 Surface SEM of the Nanoscratch at Region a) at the Initial Stages of Microscratch, and b) Upon Completion of Delamination 90

Fig. 4.7 FIB Cross-section and SEM Micrograph of the Thin Film Obtained a Region of Onset of Delamination 92

Fig. 4.8 Variation of Interfacial Adhesion Energy for the Different Samples Evaluated by Four Point Bend Technique 93

Fig. 4.9 Elemental Dispersion Spectroscopy Analysis of the Failed Interface after Four Point Bend Analysis 95

Fig. 4.10 Variation of Critical Load for Different Evaluated Samples obtained from the Nanoscratch Test 96

Fig. 4.11 Simplified Classification of Low k Dielectrics 102

المنارة للاستشارات

www.manaraa.com

Fig. 4.12 Typical Curve Showing the Loading and Unloading as a Function of Indenter Penetration Depth 105

Fig. 4.13 Variation of the Normalized Hardness with Dielectric Constant of the Candidate ILD Materials 107

Fig. 4.14 Material Removal Schematic during Ceramic ILD CMP 108

Fig. 4.15 Schematic showing the Action of ILD Slurry on the Polymer Surface during CMP 110

Fig. 4.16 Variation of COF with Down Pressure (PSI) and Linear Velocity (m/s) for a) SiO_2U, b) SiOF, c)Polyimide, and d) BCB 113

Fig. 4.17 Variation of MRR with Pressure (P) and Platen RPM (Linear Velocity V) for a) SiO_2 (U), b) SiOF, c) Polyimide, d) BCB 117

Fig. 4.18 Surface Morphology of the Candidate ILD Samples Before and After CMP for: a) SiO_2 (U), b) SiOF, c) Polyimide and d) BCB 121

Fig. 5.1 Schematic of the Construction of the Ultrasound Testing Equipment 125

Fig. 5.2 Cross-section Scanning Electron Micrograph of the Evaluated Commercial Polyurethane Polishing pad with a Sub-pad 130

Fig. 5.3 Ultrasonic Transmission Maps of the Quarter IC1000/SubaIV pad a) Before and b) After punching of the 1” coupons. Three coupons were punched at the High-Intensity (white) Area and Four Coupons at Low-Intensity (Black) Area. The Effect of Pad Acoustic Homogenization after Punching is Illustrated in Respective Histograms (b, d) 132

Fig. 5.4 a) Pad Mapped Before Punching 6-inch Coupons, b) Area of Pad Remapped after Replacing the Punched HT Coupon, c) Area of Pad

المنارة للاستشارات
www.manaraa.com

	Remapped after Replacing the Punched LT Coupon (All the Values have been Normalized over the Entire Area).	135
Fig. 5.5	a) Variation of Storage Modulus Vs Temperature, b) Variation of loss modulus Vs Temperature c) Variation of tan δ Vs Temperature of Samples Tested from Low and High Intensity region of the Pad	136
Fig. 5.6	Ultrasound Transmission Scan of Pad with Sub-pad	138
Fig. 5.7	Ultrasound Transmission Scan of Pad without Sub-pad	138
Fig. 5.8	Variation of COF for a) Pad 1 and b) Pad 2 during the CMP Process for the Various Values of PSI and RPM	142
Fig. 6.1	Cross-sectional SEM micrograph of a) PsiloQuest's ASP and b) Commercial Polyurethane Polishing pad with a sub pad	150
Fig.6.2	Loading and Unloading Behavior Exhibited by the PsiloQuest's ASP coated for 10 minutes (Pad 1). Note the non-linearity at the Specific Sites of the Loading and Unloading Curve Represent Plastic Deformation under Indentation.	151
Fig.6.3	The Variation of Depth of First Non-linearity of in the Loading Curve (Xa) as a Function of PECVD-TEOS Coating Time for Different Pads Evaluated	152
Fig.6.4	Variation of Elastic Modulus and Hardness with TEOS Coating Time Evaluated by Nanoindentation for Different Evaluated Polishing Pads	153
Fig. 6.5	X Ray Photoelectron Spectroscopy (XPS) Data for Polishing Pads with Different TEOS Surface Coating Time	155

www.manaraa.com

Fig.6.6 Variation in Surface Silanol / Silicates in PECVD-TEOS Coating as a Function of TEOS Deposition Time 156

Fig. 6.7 Variation of Static Wear Rate and Static Coefficient of Friction for Pads with Different PECVD TEOS Surface Coating Time 157

Fig. 6.8 Variation of the Average Value of COF (taken for First 60 Seconds) for the Different Candidate Pads during the Polishing Runs at 2 PSI Down Force and 150 RPM Platen Rotation 158

Fig.6.9 Variation of the Average Value of MRR for the Different Candidate Pads during the Polishing Runs at 2 PSI Down Force and 150 RPM Platen Rotation 159

Fig.6.10 Variation of COF for Different Total ASP Thickness for an Optimized Surface Coating Time of 40 Minutes 164

Fig. 6.11 Variation of MRR for Different Total ASP Thickness for an Optimized Surface Coating Time of 40 Minutes 165

Fig. 7.1 Prime Criteria for Slurry Design 168

Fig. 7.2 Schematic of Microscale and Nanoscale Phenomena during CMP 170

Fig. 7.3 Variation of Rate of Surface Layer Formation in Cu with Different Slurry Chemistry 171

Fig. 7.4 Transient Electrochemical Chronoamperometry Measurements of W 171

Fig. 7.5 Variation of Removal Rate with Particle Size and Concentration 173

Fig. 7.6 Removal Rate of Silica with Different Particle Size and Concentration 174

Fig. 7.7 Variation of COF and MRR with Increase in Slurry Temperature 176

المنارة للاستشارات

www.manaraa.com

Fig. 7.8	Variation of ln of MRR in m/s with Inverse of Temperature (1/T) Showing an Arrhenius Relationship	176
Fig. 7.9	Schematic Showing Mechanism of Polishing Action of Novel Nanoparticle CMP slurry	181
Fig. 7.10	Variation of MRR for Different Trials Using Nanoparticle Slurry without the Surface Catalyst	182
Fig. 7.11	Variation of MRR for Different CMP Trials for Nanoparticle Slurry with Surface Catalyst	183
Fig. 7.12	Variation of COF for Different CMP Trials Using Novel Nanoparticle Based CMP slurry	183
Fig. 7.13	Variation of COF with Time Measured In-situ for Polishing of EP Cu Samples Under 3 PSI Down Pressure and 100 RPM Platen Rotation Using a) Novel Nanoparticle Cu Slurry, and b) Commercial Cu Slurry	184

المنارة للاستشارات
www.manaraa.com

PROCESSING, RELIABILITY AND INTEGRATION ISSUES IN CHEMICAL MECHANICAL PLANARIZATION

Parshuram B. Zantye

ABSTRACT

Global planarization is one of the major demands of the semiconductor industry. Chemical mechanical polishing (CMP) is the planarization method of choice use to achieve the required stringent tolerances essential for successful fabrication of next generation Integrated Circuits (IC). The predominant reason for CMP defects is the shear and normal stresses during polishing to which the material is subjected. Understanding the process of CMP and factor that contribute to overall stress addition during polishing requires an approach that encompasses all the four major categories of variables, namely: a) machine parameters, b) material properties, c) polishing pad characteristics, and d) polishing slurry performance. In this research, we studied the utilized in-situ technique involving acoustic emission (AE) signal monitoring and coefficient of friction (COF) monitoring using a CETR™ Bench Top CMP Tester to evaluate the impact of variation in machine parameters on the CMP process. The mechanical and tribological properties of different candidate materials have been evaluated bring potential challenges in their integration to the fore. The study also involves destructive and non destructive testing of polishing pads performed for characterization and optimization of polishing pad

المنارة للاستشارات
www.manaraa.com

architecture. Finally, the investigation concludes proposing novel nanoparticle CMP slurry which has a predominant chemical component in its polishing mechanism. It was found that the decrease in the mechanical shear and normal loading by: a) operating the process in the low stress regime, b) using potential materials that are mechanically stronger, c) using polishing pads with lesser variation in specific gravity and with a surface that is has its mechanical properties fine tuned to those of the wafer, and d) deploying polishing slurry with a significant chemical component mechanical removal, are some of the approaches that can be employed to meet the future challenges of the CMP process and reduce the defect associated with it.

المنارة للاستشارات
www.manaraa.com

CHAPTER ONE

INTRODUCTION

1.1 Generalized Semiconductor Fabrication Processes

The relentless competitor and customer driven demand for increased circuit density, functionality and versatility has led to evolutionary and revolutionary advances in the "front end" of the chip manufacturing line where the devices are fabricated, and the "back end" where these devices are appropriately wired within the integrated circuit (IC) [1]. Chip interconnections, or "interconnects," serve as local and global wiring, connecting circuit elements and distributing power [2]. To incorporate and accommodate the improvements such as decreased feature size, increased device speed and more intricate designs, research in the 'back end of the line' (BEOL) processes has become equally important as the development of the 'front end of line' (FEOL) processes to reduce gate oxide thickness and channel length. Fig. 1.1 (a and b) shows the multilevel interconnect structure which is fabricated using the BEOL processes. The current viable technologies and future trends in scaling bipolar and Complimentary Metal Oxide Semiconductor (CMOS) devices fabrication and FEOL technologies have been discussed at length by Taur et al. [3].

المنارة للاستشارات
www.manaraa.com

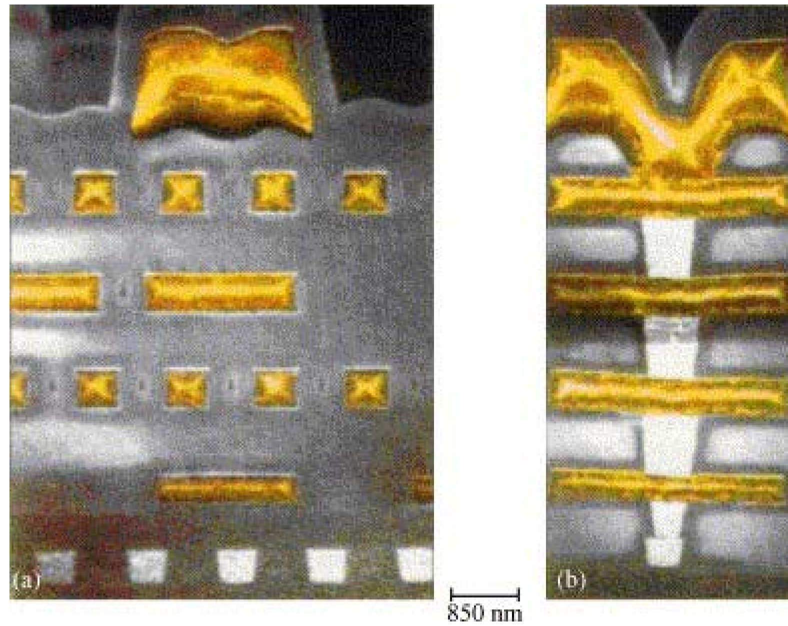

Fig.1.1 Scanning Electron Micrographs of Cross-section of the Structures Fabricated by BEOL Technology: (a) BEOL Structure of 0.5 μm CMOS Logic Device and (b) Stacked Contacts and Vias [1].

1.2 Increase in Device Density

Over the last 20 years, circuit density has increased by a factor of approximately 10^4 (Fig. 1.2), while cost has constantly decreased [e.g., the historical 27% per year decline in price per bit for dynamic random access memories (DRAMs)] [3]. The trend is expected to continue in the future even as 45 nm processes are set for production in 2007 [4]. While recent path breaking innovations in the field of lithography and patterning [5- 9] have brought about progressive device scaling, the development of a planar back-end-of-line approach, which incorporates the use of chemical–mechanical polishing to planarize inter-level dielectrics and metal stud levels, represents a significant advance in BEOL processes. Innovation in BEOL technology is required in each

المنارة للاستشارات
www.manaraa.com

technology generation (Fig. 1.3), since only part of the density increase could be achieved with improvements in lithography (Fig. 1.3). The evolution and progressive improvement in the BEOL technology and processes along with the future trends have been elaborately discussed by Ryan et al [1].

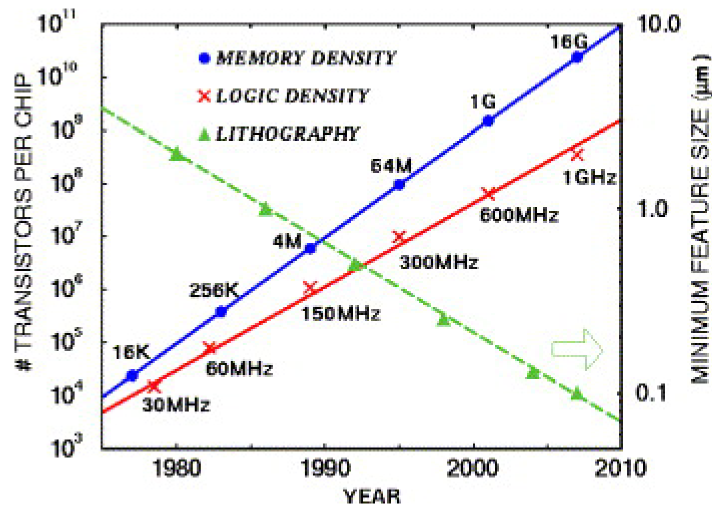

Fig. 1.2 Trends Over the Years in Logic and Memory Devices [6].

1.3 Scaling and Time Delay

At the outset, the CMOS device structure had multiple isolated devices connected by single level of interconnect wiring. Scaling down of the device was very effective in achieving the goals of increased device density, functional complexity and performance. However, scaling down of the devices became less profitable, and speed and complexity were dependant on the characteristics of interconnects that wired the devices [10]. With the single level metallization scheme the total area occupied by the wiring on the chip significantly increased with the increase in the active density of devices on the chip. Keyes [11] cited an example of a bipolar chip with a gate count of

المنارة للاستشارات
www.manaraa.com

1500 gates and a chip area of 0.29 cm^2, fabricated using a single level metal with a pitch of 6.5 µm. The total wiring area occupied by the metal was 0.26 cm^2, which was about 90% of the surface area of the chip!

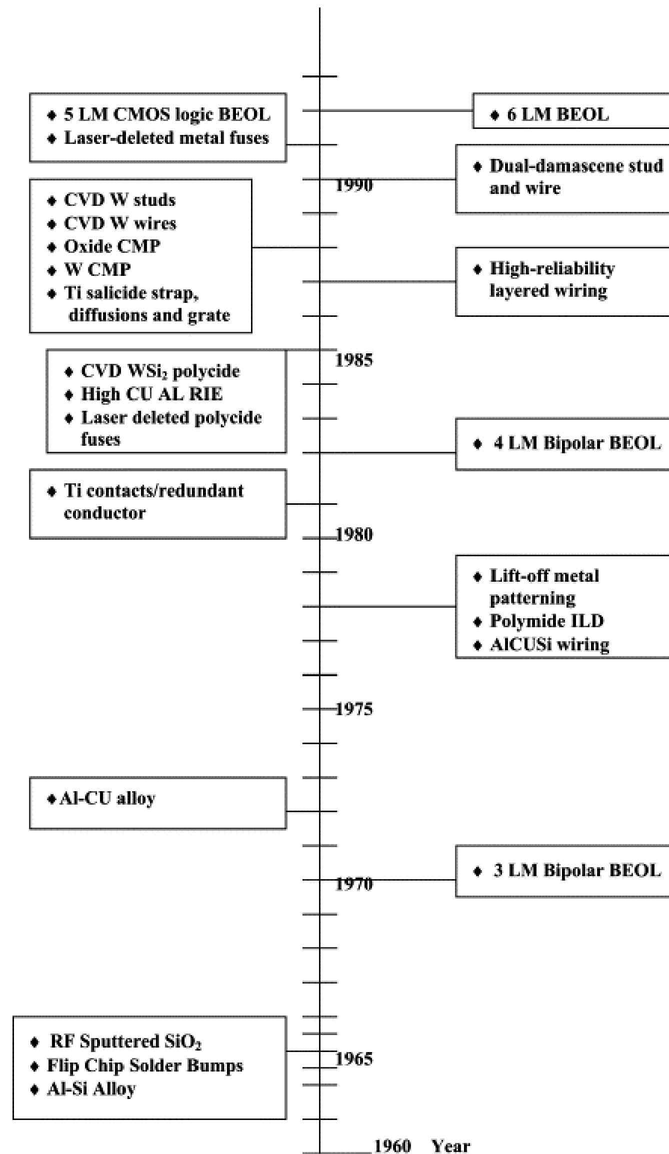

Fig. 1.3 Chronology of Key Interconnect Technology Introduction Through the Years. LM Denotes Levels of Metallization [1].

www.manaraa.com

The total time taken by the voltage at one end of the metal line to reach to 63% of the total value of the step input applied at the other end is known as the interconnect delay and this is due to resistance of the interconnect wiring metal (*R*) and the interlayer dielectric capacitance (*C*) [12]. The RC *(Resistance X Capacitance)* delay can be expressed as shown the following equation:

$$RC = 2\rho\kappa\varepsilon_0 L^2\left[\frac{4}{P^2}+\frac{1}{T^2}\right] \quad (1.1)$$

where ρ is the resistivity of the wiring material, k is the dielectric constant of the ILD, ε_0 is the permittivity of vacuum, L is the length of the interconnect line, P is the interconnect wiring pitch, T is the thickness of the line. It can be seen from (Eq. (1)) that there is an increase in the RC delay with the decrease in interconnect wiring pitch. Hence, in order to decrease the RC delay: 1) Cu has replaced Al as interconnect wiring materials due to its lower resistivity, 2) several novel low k materials are being explored, and 3) multilevel metallization scheme of wiring is being implemented. As Cu cannot be effectively etched due its inability to form non toxic volatile by-products and due to its property of diffusion in neighboring materials, present day MLM structures are fabricated using the damascene process. Table 1 calculates the simple *RC* time constants calculated for a few metals of given R_s (sheet resistance) and 1 mm length on 1 μm thick SiO_2 [12].

The increasing in the levels of the metallization lines means that packing density need not keep pace with the device density and the minimum metal line feature does not have to scale with the same pace as the gate width. The foremost reason behind the implementation of multilevel metallization schemes is the reduction in the length of the metal lines, which in turn reduces the *RC* delay sizably (Eq. (1)).

المنارة للاستشارات
www.manaraa.com

Table 1.1 Interconnection Delay (RC) in Silicon VLSI chip

Metal	Bulk Resistivity ($\mu\Omega$-cm)	Poly crystalline film resistivity ($\mu\Omega$-cm)	Film Thickness (A°)	R_s (Ω/square)	Delay [a] (ps /mm)
Poly-Si	-	~1000	5000	20	690
$CoSi_2$	10	15	2500	0.6	21
$MoSi_2$	~35	~100	2500	4	138
$TaSi_2$	45	55	2500	2.2	76
$TiSi_2$	13	15	2500	0.6	21
W	5.65	8-10	2500	0.32-0.4	11-14
Al	2.65	2.7	2500	0.11	4
Cu	1.67	2.0	2500	0.08	3

[a]Delay = RC = 34.5 R_s (ps/mm) for 1mm length conductor on 1-μm thick SiO_2

المنارة للاستشارات
www.manaraa.com

In places where metal wiring length cannot be reduced, routing can be done at the upper levels without reducing the metal line width, thus reducing the *RC* delay due to the higher surface area. It must be noted that (Eq. (1)) takes in to account only the line to ground capacitance and does not take in to account the capacitance between adjacent metal lines. The line-to-line capacitance is negligible for wide isolated lines but is significantly large in any sub 3 μm interconnect regime. In sub 0.5 μm the line to line capacitance dominates, there by increasing the *RC* time delay significantly with scaling. As seen from Fig. 1.4, there is a dramatic increase in *RC* time delay in sub 0.5 μm feature size interconnect lines. Starting with two levels of metallization, the levels of metallization have increased up to 8 by 2001 [13]. The future trends in the levels of metallization can be seen in Fig. 1.5.

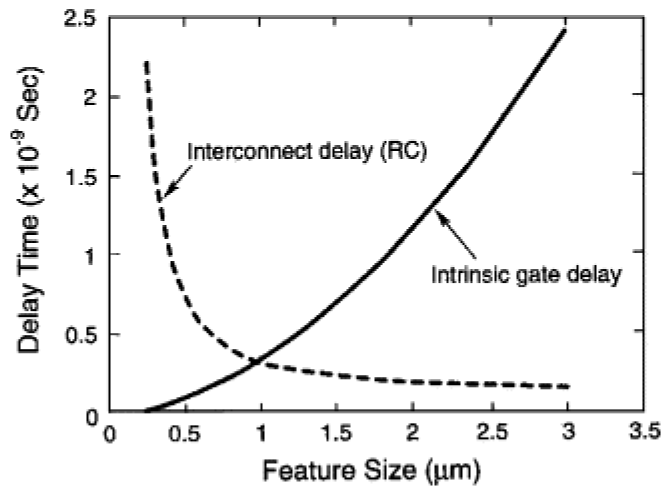

Fig. 1.4 Variation of RC Time Delay with Minimum Feature Size [12].

المنارة للاستشارات
www.manaraa.com

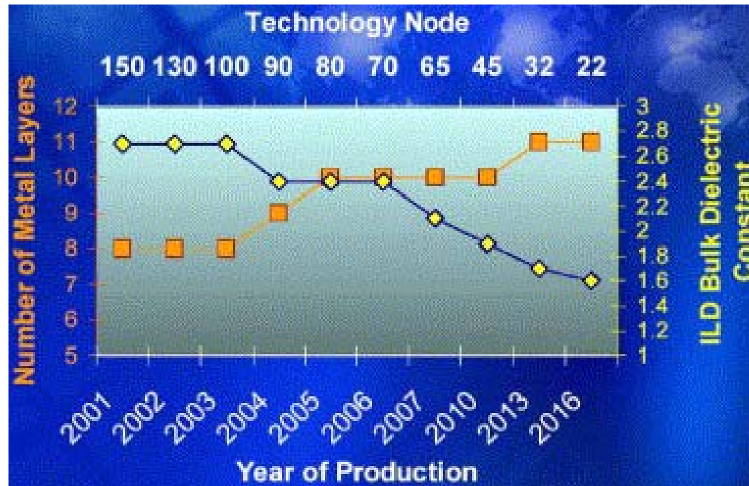

Fig. 1.5 Predicted Future Trends in IC Interconnect Technology, (Courtesy: Jeffery Lee, Intel Corporation) [13-14]

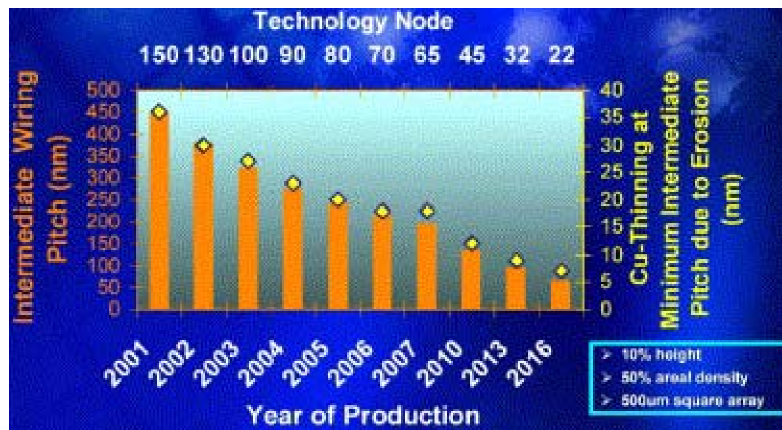

Fig. 1.6 Chart Showing Decrease in Intermediate Interconnect Wiring Pitch for Future Generation IC, (Courtesy: Jeffery Lee, Intel Corporation) [13-14].

The design and layout of interconnect lines is done using the numerous analytical and numerical techniques available. Various techniques have been proposed to investigate the time domain and pulse propagation characteristics of parallel coupled lossless and lossy lines used to model the interconnect lines in the high speed USLI

المنارة للاستشارات
www.manaraa.com

circuits [15, 16]. These techniques include method of characteristics with necessary modifications to incorporate frequency dependant losses [16-18] and congruent modeling techniques where an attempt is made to model the interconnect systems in terms of lumped and distributed circuit elements in computer aided design programs such as SPICE and CADENCE [15, 16]. It is widely accepted that the minimum feature size of the devices on the chip also implies the decrease in the intermediate pitch of the interconnect wring that connects these active devices (Fig. 1.6) [10].

1.4 Need for Planarization

With the decreasing intermediate wiring pitch, non-planarized surface topography results in several processing difficulties. The irregular surface causes a hindrance in conformal coating of the photoresist and efficient pattern transfer with contact lithography. The anomalies in the surface cause the variation of the thickness in fine line widths (sub 0.5 μm) depending upon photo resist thickness. Effectively planarized surface has enormous amount of benefits such as: 1) higher photolithography and dry etch yields, 2) elimination of step coverage concerns, 3) minimization of prior level defects, 4) elimination of contact interruption, undesired contacts and electro-migration effects, 5) reduction of high contact resistance and inhomogeneous metallization layer thickness, and 6) limitation in the stacking height of metallization layers. Fig. 1.7 (a and b) shows a comparison between planarized and non-planarized surface topography.

المنارة للاستشارات
www.manaraa.com

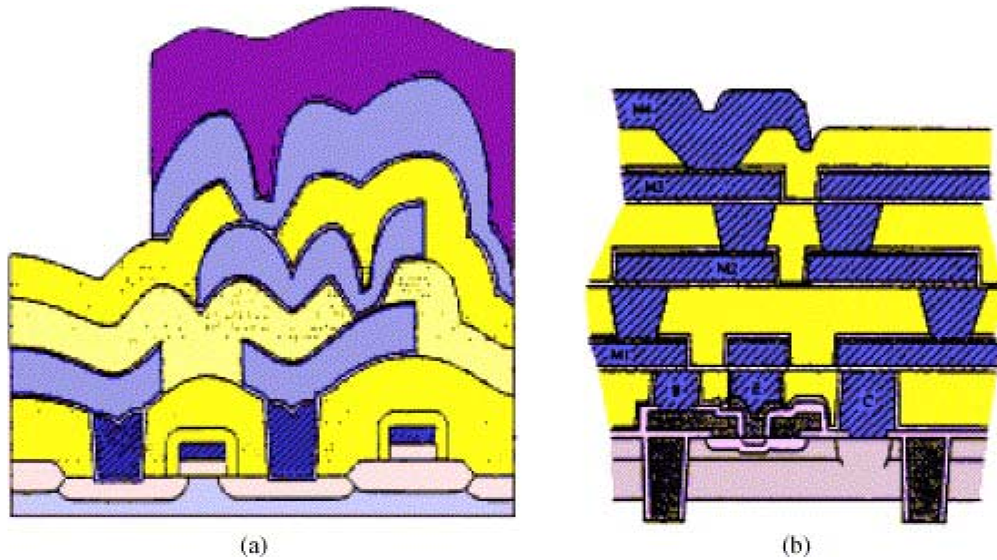

Fig. 1.7 Schematic of a) Non-planarized and b) Planarized MLM structure [19]

1.5 Shallow Trench Isolation

Shallow trench isolation (STI) has become a key technology for device isolation in recent times [20, 21]. The importance and the need for shallow trench isolation have been discussed by Wolf [22]. The method comprises of making a shallow trench on a silicon wafer, depositing SiO_2 thereon, and then planarizing with a chemical mechanical polishing (CMP) process. The method can separate elements within a much narrower area, and shows much better performance than the conventional local oxidation of silicon (LOCOS) method, which causes bird's beak structures [23].

The details of fabrication of STI structures have been elaborately given discussed Jeong et al [24]. Until now, a complicated reverse moat etch process had to be used in the absence of sufficiently selective slurries for SiO to SiN polishing. Using an etch process, the high-density moat regions can be reduced to an acceptable level, and

المنارة للاستشارات
www.manaraa.com

therefore the chip or wafer level polishing uniformity can be greatly enhanced. If direct CMP without the reverse moat etch process was applied with conventional low selectivity slurries, damage might occur to active regions in the case of excessive CMP, whereas, in the case of insufficient CMP, nitride residues might remain in the active regions after the nitride strip process due to oxide residues [20-25]. The schematic representation of the STI structure fabrication reported by Kim and Seo is shown in Fig. 1.8 [26].

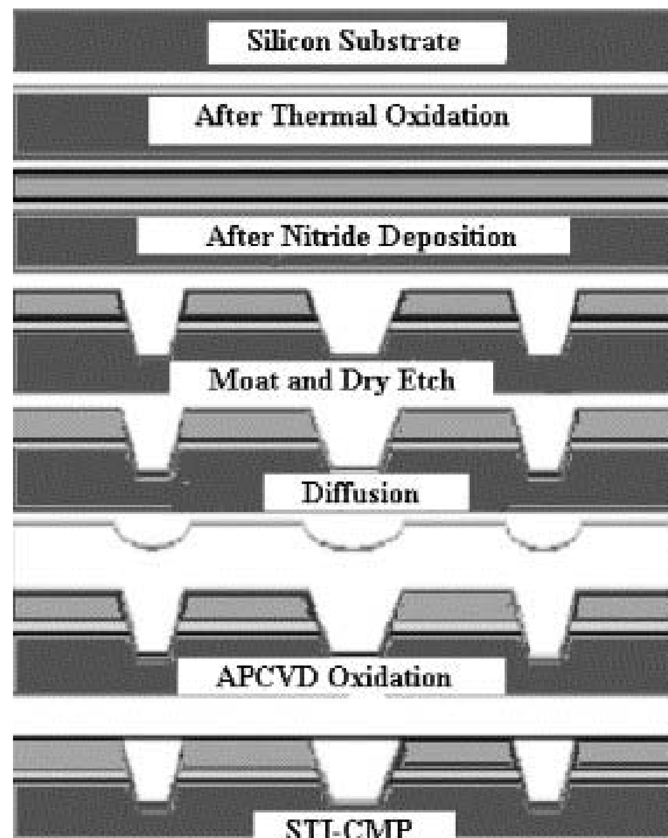

Fig. 1.8 Schematic of a Processes Sequence of Direct STI CMP without Reverse Moat [25]

www.manaraa.com

The process of fabrication of STI structures is still under considerable research [29, 30]. One of the main areas of interest is development of silica and ceria-based high selectivity slurries (HSS) [24] with a high polishing selectivity for silicon oxide and silicon nitride [25, 26]. There is considerable research currently underway in the STI–CMP aspects such as effective and in situ end point detection [20-25], reproducibility [24], defect analysis [27, 28], pattern density effects [26], etc. The STI CMP process has also been extensively modeled [31-33].

1.6 Damascene Process

In the conventional metallization technique as seen in Fig. 1.9, in the conventional metallization technique, the metal deposited on top of the dielectric is positively patterned with photoresist. The metal is then etched out and dielectric material is deposited on top of the metal using processes such spin coating or chemical vapor deposition (CVD) [34]. The dielectric is then planarized and subsequently to make a multilevel metallization structure, more dielectric is deposited on top of the planar dielectric and the process is repeated. In case of the damascene process, the dielectric is negatively patterned, and then etched to form a pattern that is then filled with metal. A seed layer of metal is deposited using physical vapor deposition (PVD). Depending upon the metal, a barrier layer of metal is deposited before the seed layer deposition [35]. The metal is then electroplated on top of the seed layer. The excessive metal is polished off and planarized using the CMP process. For the purpose of making multilevel metallization structures, dielectric is then spin coated or CVD deposited and entire procedure is repeated.

المنارة للاستشارات

www.manaraa.com

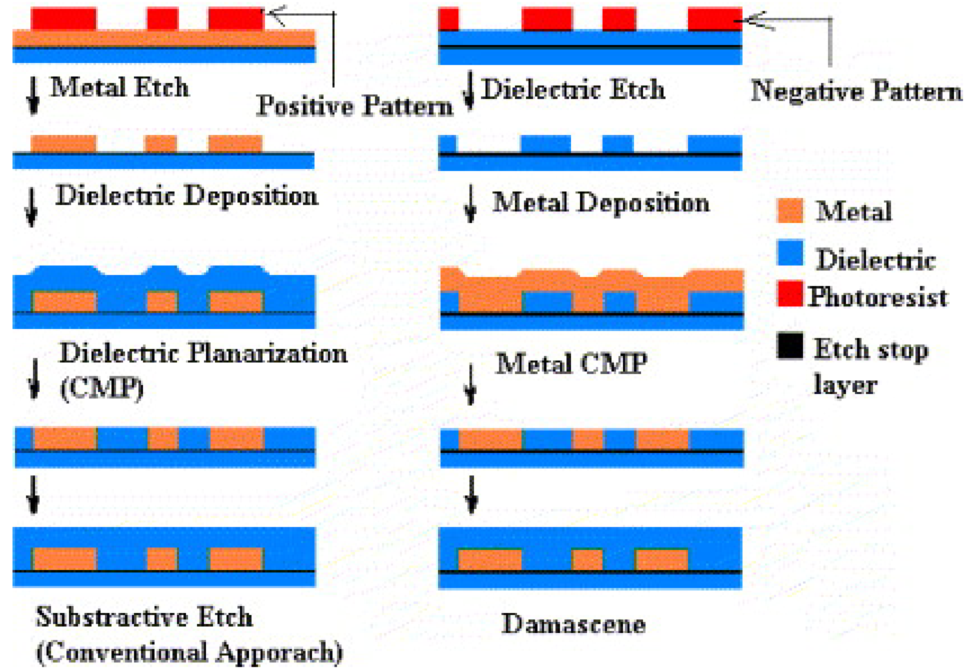

Fig. 1.9 Comparison between Subtractive Etch (Conventional Approach) and the Damascene Approach for Metallization

1.7 Different Planarization techniques

The different degrees of global and local surface planarity [37] can be seen from Fig. 1.10. Techniques such a spin on deposition (SOD), reflow of boron phosphorous silicate glass (BPSG), spin etch planarization (SEP), reactive ion etching and etch back (RIE EB), SOD + EB have been discussed in this section. These are the prominent of several competing technologies presently being used to achieve local and global planarization.

المنارة للاستشارات
www.manaraa.com

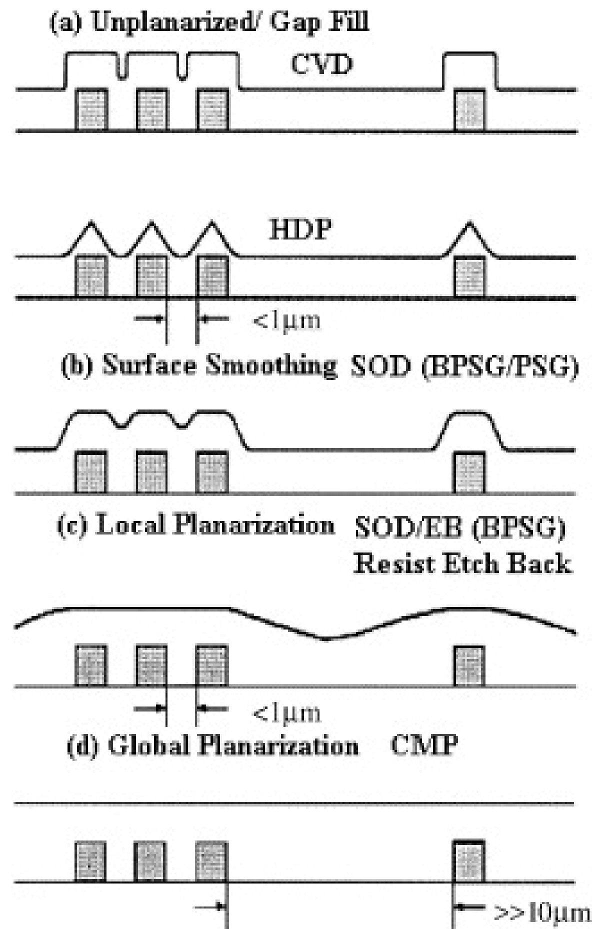

Fig. 1.10 Schematic Showing Degrees of Surface Global and Local Planarity [37]

1.7.1 Doped Glass Reflow

Synthesis of low pressure chemical vapor deposited (LPCVD) boron and phosphorous doped silicon oxide was one of the first planarization techniques in the IC industry used to fabricate the first layer of dielectric (pre metal dielectric) due to its excellent planarization and gettering properties [38-42]. By doping SiO_2 with boron and phosphorous, the film boro-phosphate–silicate glass (BPSG) has better smoothing of step corners and it can be made to reflow at high temperature (850–959 °C).

www.manaraa.com

Kobayashi and co-workers [38-42] have given the details of formation of doped BPSG using n-type lightly doped Si wafers. Dielectric glass layers were deposited on the wafers in a (LP-CVD) reactor equipped with $Si(OC_2H_5)_4$, $B(OCH_3)_3$ and PH_3 gas sources and O_2 and N_2 carrier gases. As the reflow characteristics are mainly controlled by viscosity, which in turn is a function of glass chemical bonding [41, 42] and structure [42], less viscous, non-crystallized glasses are ideally used for reflow and planarization. These glasses are therefore deposited by LPCVD technique, as they are amorphous, more fluid, have low connectivity and have a released structure.

Even though, LPCVD highly boron-containing glasses with low polarizability are favorable for the device planarization in DRAMs and static random access memory (SRAM) cells, these glasses can be used only for the first level of ILD. This is due to the fact that even the low temperature reflow glasses would melt the metal once deposited as the standard temperature of reflow far exceeds melting point of aluminum. Moreover, high temperatures are unsuitable for other metals due to diffusion and electro-migration issues. Also, due to void formation (Fig. 1.11) during reflow, and very high thermal budget, the process of doped glass reflow is not a very widely implemented process of planarization.

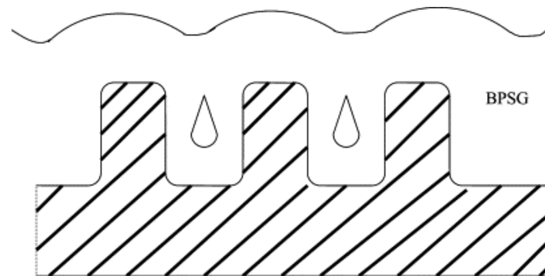

Fig. 1.11 Schematic Showing BPSG Void Formation after Reflow [37]

المنارة للاستشارات
www.manaraa.com

1.7.2 Spin Etch Planarization

The process of CMP gained increasing prominence due to controlled chemical etching of some metals like Cu was not a very feasible task. However, spin etch planarization, a process developed by Levert et al. at SEZ America Inc. [43] is based on the principles of controlled chemical etching of metals. During SEP, the wafer is suspended horizontally on a nitrogen cushion above a rotating chuck (Fig. 1.12). The substrate is held in place laterally with locking pins on the wafer edge. As the chuck and wafer are spun, wet etch chemistries are dispensed onto the wafer. A planar final surface is achieved by using an appropriate etching solution and the spinning of the wafer while removing the excess Cu. Deionized water and nitrogen are then applied onto the wafer to achieve rapid cleaning and dry-in/dry-out-processing. Results show that the etch rates can be as high as 14,000 Å/min. 200 mm electroplated wafers can be planarized with appropriate chemistries and processing parameters [43].

As there is no contact of any external body with the wafer surface, there is no possibility of typical CMP defects like micro scratches, delamination, peel off, etc. There is reduced instance of dielectric dishing and erosion of metal lines and with in wafer non-uniformity is kept as low as 9.2%. Even though this process has some distinct advantages over CMP, this being a totally new process, is yet to be applied in the industry. The process is expected to increase the cost of ownership (CoO), has not been demonstrated on any other materials such as ceramics and insulators. The pattern dependence and etch anisotropy are yet to be further investigated. CMP may be still needed after SEP process to remove pattern dependent bumps on the surface of the wafer. Efficient end point detection mechanisms, in addition to the optical end point detection mentioned by Levert

المنارة للاستشارات
www.manaraa.com

et al. have to be developed for the process. Therefore, for implementation of the SEP further studies, characterization and optimization is necessary.

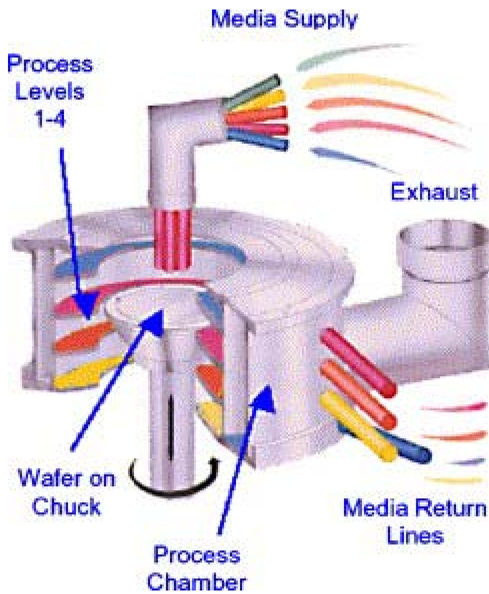

Fig. 1.12 Schematic of SEP Chamber Showing a Cut-away View of the Process Pot, Four Chambers and Chuck. The Chemical Dispense Arm, Drain Lines and Exhaust Ports also are Indicated [43].

1.7.3 Spin on Deposition (SOD)

Porous low-*k* dielectrics, different glasses such as OSG, TEOS used as dielectric materials and polymeric ILD are typically deposited using spin on technique. The precursor solution for the material to be deposited is prepared mostly at room temperature by mixing the base catalyst and suitable organic additives. The wafer surface is pretreated to promote effective sol spreading, followed by dripping the sol on the spinning wafer. Small amount of sol is dripped on wafers that are then rinsed, spun dried, baked and later cured.

المنارة للاستشارات
www.manaraa.com

SOD demonstrates excellent gap filling capabilities but shows very poor global planarization. Spin on deposited hydrogen silsesquioxane (HSQ) (dielectric constant $k = 3.0$), has been reported to be successfully integrated into devices with five levels of Al interconnect [44, 45] and silicon di oxide formed on surface of silicon using silicic acid solution by spin technology [46], has shown relatively good local planarization [47] and is known to have a positive impact on the global planarization of the ILD achieved by CMP.

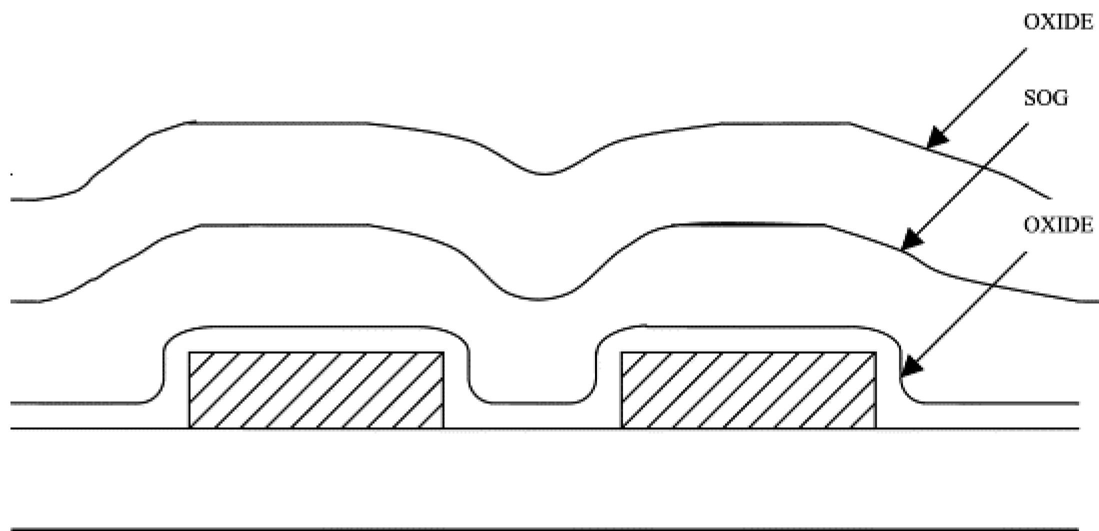

Fig. 1.13 Schematic showing Spin on Deposition with Partial planarization [37]

Numerous defects are known to arise in the spin on deposited materials. There is non-homogeneity in the value of the dielectric constant of these materials with the exposure to plasma in subsequent processing [48]. The spin-on materials also have a tendency to absorb moisture and then release it in the air during the thermal processes. This induces undue stresses in the SOD films there by causing defects such as cracking, shrinking, peel off, degradation, contamination of interconnects and poor thermal

المنارة للاستشارات
www.manaraa.com

stability [49]. For this purpose, techniques such as laser curing need to be implemented to prevent stresses from building into the dielectric film [50]. Thus in spite of the fact that SOD materials show excellent local planarization, blanket SOD materials are not implemented in the industry. SOD materials are implemented only as layers sandwiched between two oxide layers. The schematic of SOD and partial/local planarization can be seen in Fig. 1.13.

1.7.4 Reactive Ion Etch and Etch Back (RIE + EB)

A competing technology for SOD oxide planarization and reflow is the reactive ion etch and etch back (RIE + EB). The technique of reactive ion etching, conventionally used to pattern the thin film on a substrate in this case is used for planarization. The pattern is spin coated with photoresist. The resists fills the trenches and vias of the pattern leaving the hills and mounts on the pattern exposed to the reactive species in the plasma. Typically RIE + EB is used to etch SiO_2 and other dielectrics. Although wet etching is well developed for etching SiO_2, it has inherent limitations due to undercutting of the mask materials, especially for sub micron pattern sizes. A dry etching technique, like RIE + EB, on the other hand, can generate anisotropic etch profiles and for this reason has come into favor. The mechanism of material removal is more due to chemical reaction than due to physical sputtering, although the two mechanisms are synergistic; i.e. the bombardment catalyzes the surface chemical reactions. This leads to anisotropic etching due to the directional nature of the bombardment catalyzed surface chemical reactions [51-54], as well as by physical sputtering. In general, the rate controlling mechanism of etching by the RIE process may

المنارة للاستشارات
www.manaraa.com

be due to physical effects (as in sputtering with inert ions), or chemical phenomena in the sense that the ion bombardment enhances surface chemical reactions with the reactants yielding highly volatile reaction products.

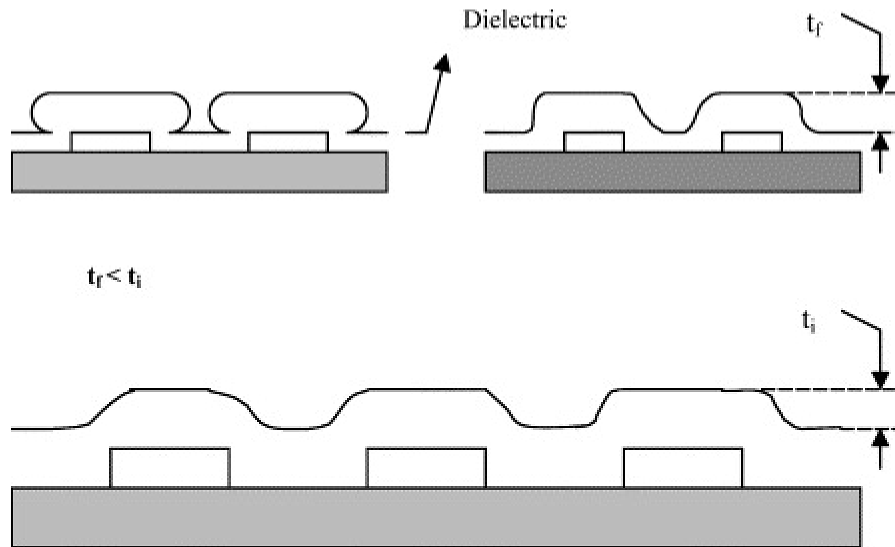

Fig. 1.14 Schematic Showing Smoothening and Partial Planarization using Reactive Ion Etching with Etch Back [37]

Due to the inadequacies of different planarization techniques, the combination of the two techniques has been used in order to compliment each other, with some degree of success. SOD with Etch back has proved particularly useful in this respect. As the spin on deposited glass has the ability to fill voids and gaps permanently, the technique was developed along with the development of the Reactive Ion Etch and Etch Back (RIE + EB) technique. With the emergence of the new spin on polymeric low-*k* dielectrics [51] and other novel spin on materials, techniques like SOD and EB have been pursued with some degree of success in achievement of local planarization on the surface of the wafer.

المنارة للاستشارات
www.manaraa.com

The SOD materials are used to fill the trenches and vias and then RIE process is used to etch back or sacrifice the materials on the higher regions. Subsequently the same material might be deposited using spin on or CVD process to get considerable degree of local planarization. This kind of process is prevalent in gap filling of memory devices (Fig. 1.14).

Even though the usage of both SOD and RIE EB processes together tend to overcome the drawbacks of each of the processes, the extensive optimization is required for the two processes to work in tandem there by giving good surface planarity. Fig. 1.15 shows the cross-section of a device structure planarized using SOD RIE EB process.

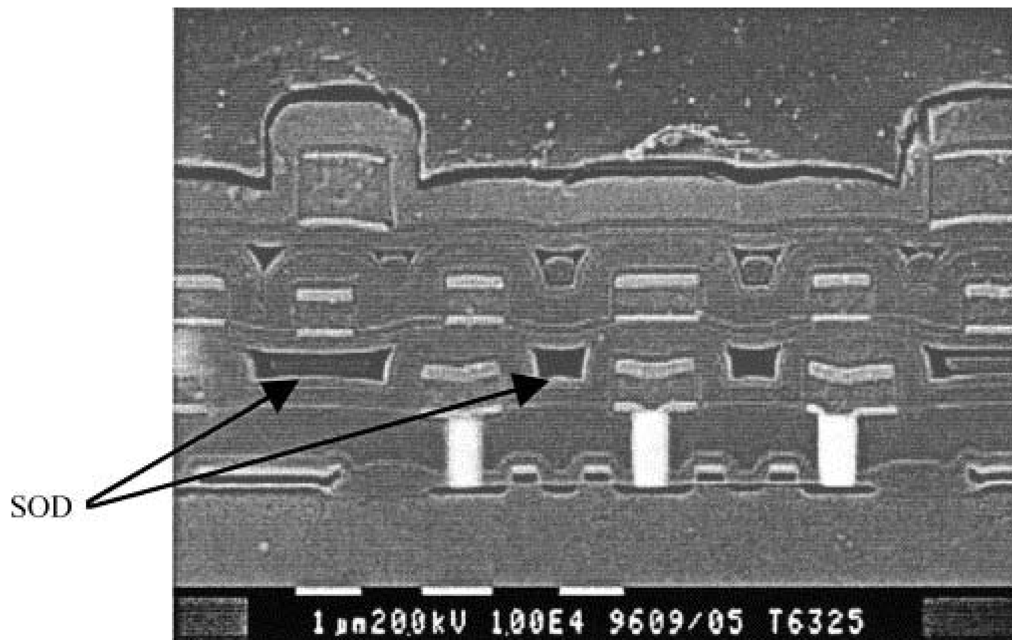

Fig. 1.15 Scanning Electron Micrograph Showing Cross-section of Structure Planarized by SOD RIE EB [37]

المنارة للاستشارات
www.manaraa.com

1.7.5 Chemical Mechanical Planarization

Presently, CMP is the only technique that can offer excellent local and global planarity on the surface of the wafer. CMP has known to yield local planarization of features as far as 30 μm apart as well as excellent global planarization. The plasma enhanced chemical vapor deposited oxides have limited capability of gap filling and are restricted in their gap filling ability below patterns having 0.3-μm feature size. High-density plasma deposited oxides have acceptable gap filling capabilities; however, they produce variation in surface topography or local as well as global level. Even though spin on deposited (SOD) doped and undoped oxides and polymeric materials have acceptable ability for gap filling, CMP is the only technique that produces excellent local and global planarity of these materials. The advantages and disadvantages of the CMP technique have been listed in Table 1.2 and 1.3 respectively. The details and various aspects of CMP are discussed subsequently in different sections of this dissertation.

1.8 General Applications of CMP

The process of CMP was initially developed and implemented for planarization of SiO_2 which is used as interlayer dielectric in multilevel metallization scheme. The initial developmental focus of CMP was oxide planarization [55]. Tungsten is used as an interconnect plug to the source, drain, and gates of transistors in Si microprocessor chips. Initially Ti and TiN barrier layers are deposited, followed by chemical vapor deposition of W to fill the contact vias.

المنارة للاستشارات
www.manaraa.com

Table 1.2 Advantages of Chemical Mechanical Planarization

Benefits	Remarks
Planarization	Achieves Global Planarization
Planarize different materials	Wide range of wafer surfaces can be planarized.
Planarize multi-material surfaces	Useful for planarizing multiple materials during the same polish step.
Reduce severe topography	Reduces severe topography to allow fabrication with tighter design rules an additional interconnection levels
Alternative method of metal patterning	Provides an alternate means of patterning metal, eliminating the need to plasma etch, difficult to etch metals and alloys.
Improved metal step coverage	Improves metal step coverage due to reduction in topography.
Increased IC reliability	Contributes to increasing IC reliability, speed, yield (lower defect density) of sub 0.5µm and circuits.
Reduce defects	CMP is a subtractive process and can remove surface defects.
No hazardous gases	Does a not use hazardous gas common in dry etch process.

المنارة للاستشارات
www.manaraa.com

Table 1.3 Disadvantages of Chemical Mechanical Planarization

Disadvantages	Remarks
New technology	CMP is a new technology for wafer planarization. There is relatively poor control over the process variables with narrow process latitude.
New defects	New types of defects from CMP can affect die yield. These defects become more critical for sub-0.25µm feature sizes.
Need for additional process development	CMP requires additional process development for process control and metrology. An example is the endpoint of CMP is difficult to control for desired thickness.
Cost of ownership is high	CMP is expensive to operate because of costly equipment and consumables. CMP processes materials require high maintenance and frequent replacements of chemicals and parts.

Going ahead from achieving local and global planarization of SiO_2, removal of excessive tungsten from the horizontal surfaces on the wafer pattern proved to be an asset for subsequent Al metallization [56-58]. Hence CMP was developed with a two-fold approach of: 1) planarizing oxide and 2) removing the via fill metal from the horizontal surfaces. The major applications of CMP are given in Table 1.4.

المنارة للاستشارات
www.manaraa.com

Table 1.4 Applications of Chemical Mechanical Polishing [56]

	Materials	Application
Metal	Al	Interconnections
	Cu	Interconnections
	Ta	Diffusion Barrier/Adhesion
	Ti	Diffusion Barrier/Adhesion
	TiN, TiN_xC_y	Diffusion Barrier/Adhesion
	W	Interconnection e-Emitter
Dielectric	Cu-Alloys	Interconnections
	Al- Alloys	Interconnections
	Polysilicon	Gate/Interconnect
	SiO_2	ILD
	BPSG	ILD
	PSG	ILD
	Polymers	ILD
	Si_3N_4 or SiO_xN_y	Passivation Layer, Hard
Other	Aerogels	ILD
	ITO	Flat Panel
	High K Dielectrics	Packaging
	High T_c Superconductors	Interconnections /Packaging
	Optoelectronic Materials	Optoelectronics
	Plastics, Ceramics	Packaging
	Silicon on Insulator (SOI)	Advanced Device /Circuits

Along with its successful implementation for the achievement of the above-mentioned objectives, CMP has now extended to 1) polishing of different metals like Al, Cu, Pt, Au, Ti, Ta, etc., 2) polishing of different insulators like SiO_2, Si_3N_4, various low-*k* dielectrics, doped and undoped oxides of silicon, 3) polysilicon, 4) ceramics like SiC,

المنارة للاستشارات
www.manaraa.com

TiN, TaN, etc., 5) multichip modules, 6) packaging, 7) optoelectronic components, 8) flat panel displays, 8) microelectromechanical systems (MEMS), and 9) magnetic recording heads and CD read write drives [56].

1.9 Overview

This dissertation begins with the need for device scaling and implementation of novel materials in the present day semiconductor industry. The importance of planarization and the various available planarization techniques with emphasis on CMP have been discussed in Chapter 1. Chapter 2 gives an overview of the CMP process in general and gives the background of the process and equipment used to carry out the process. The different types of equipment used for CMP process and innovations there in have been discussed in this section. The CMP findings of the studies involving in-situ metrology of CMP and detection of process end point, slurry selectivity, as well CMP defects using the CETR™ CMP tester have been discussed in Chapter 3. Chapter 4 elaborates the various issues surrounding integration of Cu and novel low dielectric constant materials in the next generation damascene structures. The investigation of specific gravity non uniformities and the use of application specific pads with novel pad architecture have been discussed in Chapter 5 and 6 respectively. The investigation of CMP slurry and synthesis of novel nanoparticle based Cu CMP slurry has been dealt with Chapter 7. Finally, Chapter 8 summarizes the research, highlights significant contributions and gives an idea of the future directions in which CMP is heading.

المنارة للاستشارات
www.manaraa.com

CHAPTER TWO

BACKGROUND OF CMP

3.1 Evolution of chemical mechanical polishing

By definition, chemical mechanical polishing is a process whereby a chemical reaction increases the mechanical removal rate of a material. CMP is mostly used for material removal by polishing the "hills" on the wafer and "flattening" the thin film. The chemical reaction between the slurry and wafer is tailored to enhance material removal and bring about quicker planarization of the thin film.

2.1.1 History of CMP

The modern day application of CMP process in the semiconductor industry was for polishing the surface raw silicon wafers to achieve a global flatness over raw silicon wafers. After sawing, the single crystal silicon rod and removing the mechanically damaged surfaces, the wafer needs to be flattened globally and a uniform scratch free surface needs to be made available for fabrication of semiconductor devices. The idea of using colloidal silica, then made by Monsanto, instead of standard abrasives, was developed by Bob Walsh in 1961 [59] and thus, the first wafers polished using CMP were commercially available in the early 1960s [59, 60]. Before its implementation in polishing raw single crystal silicon wafers, the process of CMP was traditionally used in

المنارة للاستشارات

www.manaraa.com

glass polishing. One of the most wide spread application of CMP outside the semiconductor industry is optical lens polishing. In fact, the first machinery used by Monsanto was very similar to the commercial machine used in the optical industry. The first semiconductor CMP machine was an innovation of the optical lens polishing machine. The proper polishing abrasives in presence of the slurry chemicals were used to achieve a superior degree of precision and flatness to meet the demands of the semiconductor industry. By supplementing mechanical polishing with high hardness abrasives such as silica in an alkaline medium, there are significant gains in material removal and reduction the process time.

A further improvement to the CMP process was made at IBM in the late seventies and early 80 s. The new process was faster than the previous silica-based polishing method and resulted in ultra flat, ultra smooth surface to meet the stringent requirements of the IC industry [61]. The slurry was later tailored to reduce defects and surface non-planarity introduced by the etching and deposition processes.

The IBM process was then applied for trench isolation by the late 1980s in Japan for various logic and DRAM devices. There was wide spread industrial implementation of the different variants of the CMP by companies such as NEC, National Semiconductor, Hitachi, etc. This led to the introduction of the first commercial polisher designed specifically for CMP by Cybeg in Japan in 1988. Later, International SEMATECH identified CMP as a technology critical for the future of IC manufacturing and launched a project to develop competitive, advanced CMP tools in the US [62].

المنارة للاستشارات
www.manaraa.com

2.1.2 Road Map of CMP Process

The semiconductor industry has effectively adapted its CMP technology for the 300 mm wafer [63]. Beyond the adoption of copper interconnects, several technologies are necessary to continue the shrinkage of device dimension and the increase of packing density in ULSI manufacturing. The use of ultra low-*k* materials as interlayer dielectrics has been at the forefront for decreasing the "*C*" of the "*RC* delay". However, polishing of ultra low-*k* dielectrics which are soft mechanically and weak is a daunting task in itself. The single and dual damascene structures comprising of ultra low-*k* porous or polymeric materials are more prone to buckling and crushing failures. It can be seen from Table 2.1, that these materials have significantly lower hardness and Young's modulus as compared to silicon di oxide which has a dielectric constant of about 3.2–4.0 available in the market today. According to the ITRS roadmap [14] materials with dielectric constant 2.2 will be integrated in the IC by year 2007 (Table 2.1). The difference between the polishing rates of copper and the low-*k* materials available will significantly affect post-CMP surface planarity. New processes must be developed to address the problems associated with this non-uniform polishing phenomenon as well as the complexity of the materials structures. Also, there needs to be a marked improvement in slurry selectivity for accurate end point detection when the constituent layers of the damascene structure namely, metal, hard mask, cap layer, barrier layer and dielectric are polished [64]. Furthermore, it is necessary to explore the niche of the CMP process in shallow trench isolation and other applications such as backside polishing and the fabrication of micro-electro-mechanical systems (MEMS). The CMP process there must be integrated horizontally and vertically to achieve high thorough put and performance.

المنارة للاستشارات
www.manaraa.com

Table 2.1 Interconnect International Technology Roadmap for Semiconductors [14]

YEAR OF PRODUCTION	*2001*	*2002*	*2003*	*2004*	*2005*	*2006*	*2007*
DRAM ½ PITCH (nm)	*130*	*115*	*100*	*90*	*80*	*70*	*65*
MPU/ASIC ½ PITCH (nm)	*150*	*130*	*107*	*90*	*80*	*70*	*65*
MPU PRINTED GATE LENGTH (nm)	*90*	*75*	*65*	*53*	*45*	*40*	*35*
MPU PHYSICAL GATE LENGTH (nm)	*65*	*53*	*45*	*37*	*32*	*28*	*25*
Number of metal levels	8	8	8	9	10	10	10
Number of optional levels—ground planes/capacitors	2	2	4	4	4	4	4
Total interconnect length (m/cm^2)—active wiring only, excluding global levels [1]	4086	4843	5788	6879	9068	10022	11169
FITs/m length/cm^2 × 10^{-3} excluding global levels [2]	1.22	1.03	0.86	0.73	0.55	0.50	0.45
Jmax (A/cm^2)—wire (at 105°C)	9.6E5	1.1E6	1.3E6	1.5E6	1.7E6	1.9E6	2.1E6
Imax (mA)—via (at 105°C)	0.32	0.29	0.27	0.24	0.22	0.20	0.18
Local wiring pitch (nm)	350	295	245	210	185	170	150
Local wiring A/R (for Cu)	1.6	1.6	1.6	1.7	1.7	1.7	1.7
Cu thinning at minimum pitch due to erosion (nm), 10% × height, 50% areal density, 500 µm square array	28	24	20	18	16	14	13
Intermediate wiring pitch (nm)	450	380	320	265	240	215	195
Intermediate wiring dual Damascene A/R (Cu wire/via)	1.6/1.4	1.6/1.4	1.7/1.5	1.7/1.5	1.7/1.5	1.7/1.6	1.8/1.6
Cu thinning at minimum intermediate pitch due to erosion (nm), 10% × height, 50% areal density, 500 µm square array	36	30	27	23	20	18	18
Minimum global wiring pitch (nm)	670	565	475	460	360	320	290
Global wiring dual Damascene A/R (Cu wire/via)	2.0/1.8	2.0/1.8	2.1/1.9	2.1/1.9	2.2/2.0	2.2/2.0	2.2/2.0
Cu thinning global wiring due to dishing and erosion (nm), 10% × height, 80% areal density, 15 µm wide wire	67	57	50	48	40	35	32
Cu thinning global wiring due to dishing (nm), 100 µm wide feature	40	34	30	29	24	21	19
Conductor effective resistivity (µΩ-cm) Cu intermediate wiring	2.2	2.2	2.2	2.2	2.2	2.2	2.2
Barrier/cladding thickness (for Cu intermediate wiring) (nm) [3]	16	14	12	10	9	8	7
Interlevel metal insulator —effective dielectric constant (κ)	3.0-3.6	3.0–3.6	3.0–3.6	2.6–3.1	2.6–3.1	2.6–3.1	2.3–2.7
Interlevel metal insulator (minimum expected) —bulk dielectric constant (κ)	<2.7	<2.7	<2.7	<2.4	<2.4	<2.4	<2.1

White–Manufacturable Solutions Exist, and Are Being Optimized
Yellow–Manufacturable Solutions are Known
Red–Manufacturable Solutions are NOT Known

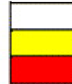

In MEMS applications horizontal integration ensures reliability and good performance of a specific CMP process run. The development of new polishing pads and pad architecture, novel slurries, new metrology techniques, etc. comes with in the scope of horizontal CMP integration. Vertical integration ensures success of every successive CMP operation. This includes the integration of the upstream processes such as Cu/barrier deposition and etching and downstream processes such as ILD deposition and

www.manaraa.com

lithography. This opens a wide scope for research for further optimization and development of Cu CMP process.

3.2 CMP: A Multi-stage Process

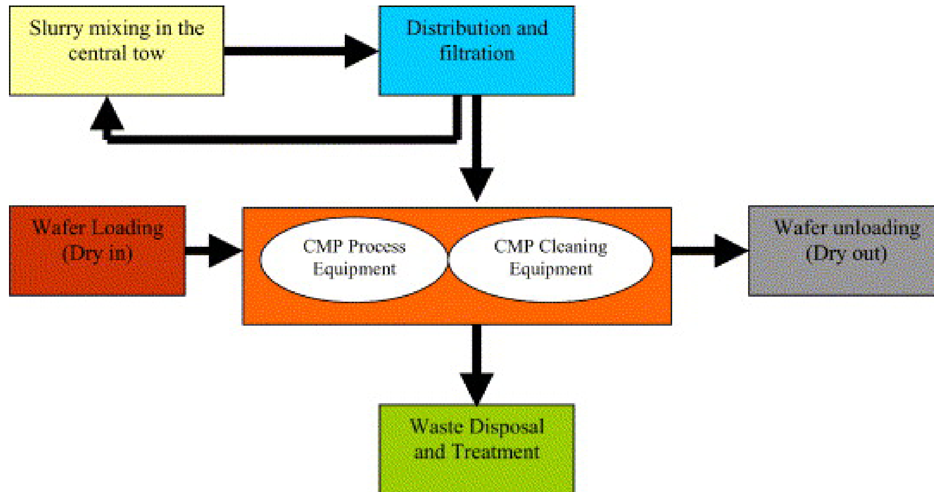

Fig. 2.1 Flow Chart of the Isolated Industrial CMP Process

The recent developments in the semiconductor industry described previously imply that CMP is fast becoming the established technology for planarizing metal and interlayer dielectrics of multilevel sub-0.5 μm devices. Along with the rapid growth of CMP and its application for polishing various materials, have come a variety of slurries, different pads, complex process recipes, more complex slurry mixing and distribution systems and an increase in the volume of wastewater. Polishing of different materials and customized needs of the various semiconductor industries have given birth of more complex CMP equipment with different process dynamics such as linear, orbital and fixed head machines. Reliable filtration and waste distribution are also required to avoid

المنارة للاستشارات
www.manaraa.com

hazardous environmental implications, as the increase in the number of CMP process steps have given rise to a large amount of disposable slurry waste. The schematic of the industrial CMP process (isolated from the other process in the fabrication line) is as shown in Fig. 2.1.

As seen from Fig. 2.1, the slurry is mixed in a tow at a central location from where it is distributed to the various CMP machines in the fabrication. The slurry that not used for feeding any machines is then returned back to the tow for recirculation. The slurry that is used for CMP process is later disposed off. The wafer which is dry from the previous process is loaded in the CMP process equipment where it undergoes polishing and then cleaning. It is then dried in the CMP cleaning station (which may be integrated with the polisher). Most machines follow this dry in dry out methodology.

2.2.1 Slurry Mixing

CMP slurry feeder equipment is composed of a stock solution unit, a mixing and circulation unit, and the CMP equipment. The thick slurry supplied from the stock solution unit is diluted to a fixed density in the mixing and circulation unit using ultra pure water. The mixed and diluted solution is then supplied to the CMP equipment. All of the equipments are manufactured in a clean room with high degree of cleanness, under strict quality checking. Consistent construction method is used from the manufacturing of the slurry feeder unit to local piping, wiring, cleaning and the trial run adjustment of the system. The system thus needs to be of high quality and stability. A tolerance of about 1% is maintained in meeting the recommended slurry parameters. The schematic of the slurry mixing is shown in Fig. 2.2. In this section, the various physical aspects of the

المنارة للاستشارات
www.manaraa.com

CMP process are discussed in detail in order to give a better understanding of the general working of the industrial CMP process and the various parameters associated with it [65].

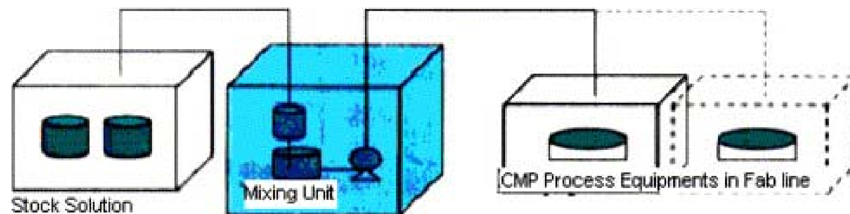

Fig. 2.2 Schematic of CMP Slurry Distribution System

2.2.2 Slurry Distribution

Fig. 2.3 gives a simplified physical representation of a semiconductor fabrication line in which, the slurry distribution to the various CMP tools is shown. As seen from the diagram, the slurry is mixed and blended at a centralized location from which it is distributed to the various machines through the distribution lines. The distribution loop shown in the schematic ensures that the "good" slurry, which is unused for the process, is delivered back the mixing chamber or the tow, in order to prevent slurry wastage. Although CMP slurries are composed of very fine particles up to 200 nm (0.2 μm), "large" particles of 1–3 μm and greater are often present in slurries at the point of dispense. Such particles can be formed as a result of agglomeration or the presence of foreign material. Metal CMP slurries, in particular, are prone to formation of aggregates. The agglomerated slurry particles often cause numerous defects in the wafer during CMP. Microscratching is the most prominent defect which occurs mainly due the agglomerated particles present in the slurry delivered to the machine as well as such particles embedded in the pads [67]. This makes the continuous mixing of the slurry in

المنارة للاستشارات
www.manaraa.com

the tow absolutely imperative. In order to prevent the particle agglomeration [67] during the distribution stage, dispense filters are installed on each of the machine which filter out the agglomerated particles before slurry delivery. Care must be taken that the filtration of the agglomerated particles does not change the particles distribution and concentration of the slurry. Most often, a series of filters are used in order to minimize the drop in the slurry pressure and flow. The slurry after being used for the actual CMP process in the tool is then disposed off using appropriate methods and environmental damage is restricted [68].

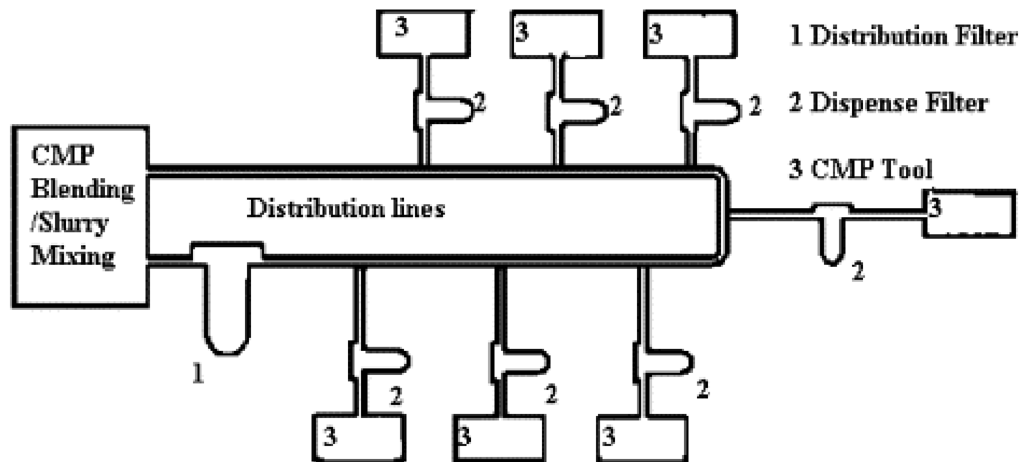

Fig. 2.3 Schematic of CMP Slurry Distribution System [68]

2.2.3 Working of the CMP Process

Current semiconductor fabrication technology for logic and memory devices requires CMP to achieve the required multilevel interconnections densities. Indeed, each silicon wafer can be exposed to 15 or more CMP steps before final device assembly. A schematic diagram of the CMP process is shown in Fig. 2.4. During CMP, the wafer is

المنارة للاستشارات
www.manaraa.com

pressed face down against a rotating polishing pad, while a chemically and physically (abrasive) active slurry planarizes the wafer. As wafer size grows, devices sizes shrink and process requirements grow more stringent, within die/wafer uniformity and removal rate increase becomes a greater concern. Different CMP processes attempt to achieve a balance between removal rate and global/local planarization through a combination of solution chemistry, speed, applied pressure and pad properties [56, 65]. Often a change in slurry or operating conditions lead to conflicting performance.

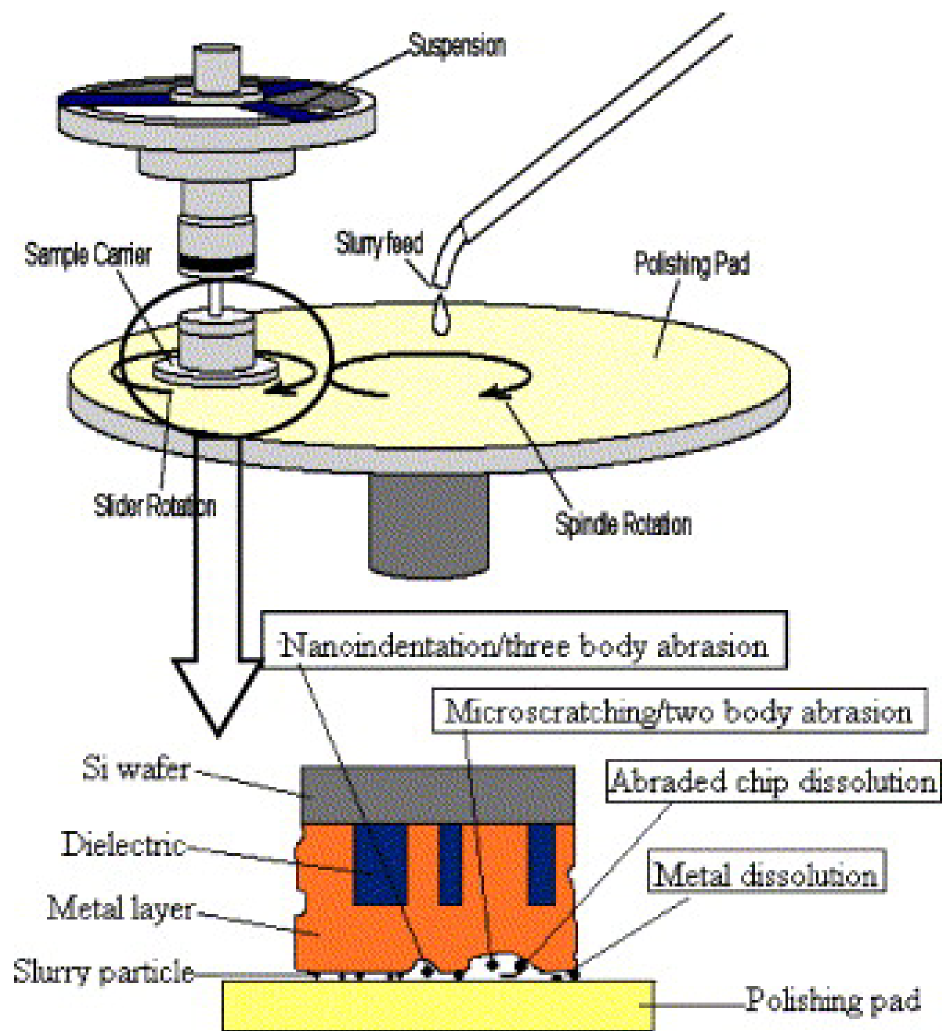

Fig. 2.4 Schematic of Wafer Planarization by CMP Process

المنارة للاستشارات
www.manaraa.com

2.2.4 CMP Polisher considerations

The key issues affecting industry use of CMP during the semiconductor chip manufacturing are the high cost of ownership (CoO), the lack of industry wide CMP technology and less than thorough understanding of the knowledge of the underlying science behind the CMP process [65]. Improvement in CoO has been brought about in the fast few years due to: 1) higher raw throughput, 2) in situ film thickness metrology, 3) dry in dry out configuration ensuring low defectivity [68], and 4) process equipment, implementation and integration support from CMP vendors [68].

The first generation CMP tools based on rotational platen had low throughput values of about 10–18 wafers/h [65]. The second generation tools emphasized on evolutionary improvements while the third generation equipment designs were modified to stay in production for long period of time by giving them adaptability to future technology modifications. The throughput of the machine can be enhanced by increasing the removal rate and improving the wafer handling. However, for effective CMP of materials, the increase in removal rate by increasing the down force should not be brought about by compromising on the defectivity (like increase in wafer to wafer and within wafer non-uniformity, delamination, dishing, erosion, etc.) [70, 71] of the wafer. For this reason sometimes, the throughput is compromised to polish the wafers at lower down force there by increasing the polishing time [72].

2.2.5 First Generation CMP Polisher

The first generation CMP polishers use a single robot system to move the wafer and hold it on the carrier. The polisher is comprised of two rotating platens; one

المنارة للاستشارات
www.manaraa.com

covered with a hard pad for bulk material removal and other with relatively soft pad for buffing. The wafer is pressed face down on the pad by the carrier and the slurry is deposited close to the center of the pad, from where the centrifugal force spreads it all over. The mechanical properties, surface morphology, structure, absorbency, etc. strongly affect the slurry distribution and polishing [73]. The polishing platen on these tools is around 22 in. in diameter which is more than 7.5 times the size of a 200 nm wafer [65]. The actual slurry utilization of these processors is poor and the pH of the slurry changes during use as there is an absence of any slurry reprocessing unit [74]. The amount of slurry that is actually used for processing at the interface is function of pad properties [75], pad conditioner [76], pad topography [77] and slurry viscosity [78]. Thus, the pads must be conditioned to: 1) bring the pad back to flat, 2) remove materials from pores, and 3) rebuild the nap. Simple manipulation of the machine parameters is sufficient to increase the material removal rate in these polishers. However, issues such as platen wobble need to be taken care off in order to deliver CMP wafers in the acceptable range. The schematic of the first generation polishers is similar to that shown in Fig. 2.5.

2.2.6 Second Generation CMP Polishers

The second generation polishers like, are basically made of rotating carrier and platen designs but have numerous changes to improve the raw throughput. The second generation polishers can be classified broadly in two distinct types: 1) single large (22 in.) platen polishing numerous wafer concurrently on the same pad, and 2) single wafer per platen, multi-platen systems [65].

المنارة للاستشارات
www.manaraa.com

2.2.6.1 Multi-wafer Per Platen Polishers

There is a natural increase in the throughput due to the increase in the number of polishing heads per platen. However, this approach presents several challenges. The most severe issue is the quantity of the wafer put at risk at one time. If one wafer breaks, the pieces can damage several wafers at one time. The more subtle issue is that of load balancing. As long as all the carriers on the platen are loaded with wafers, polishing can be consistent. However in certain cases, like application specific integrated circuit (ASIC) fabrication where in just one or two wafers need to be polished at one time, this issue is of considerable importance. The schematic of multi wafer per platen polisher is shown in Fig. 2.6.

Fig. 2.5 Photograph of Speefam (Novellus) Multi Wafer per Platen Polisher [78]

2.2.6.2 Sequential Rotational Systems

Another approach usually adopted to avoid the risk of damaging more number of wafers due to pad anomalies is sequential polishing of wafers on different platens. This

المنارة للاستشارات
www.manaraa.com

approach involves multi-step polishing wherein the first platen is used for bulk material removal without particular regard to superficial surface defects; the second platen is used for global planarization while the third platen is used to for a fine buff to get a defect free mirror like surface. However, synchronization of all these processes is an issue that the process engineer needs to tackle with this approach. This implies the process speed is limited by the slowest process. This is especially a problem when polishing metals such as copper as the corrosion might results due to the wafer staying wet in the slurry for a longer duration of time [79, 80]. Also, small damage to the pad can result in damage to all wafers in the sequential polishing run and it is sometimes hard to determine the damage on the pad and hence, all pads need to be changed. In case of tool failure, all the processes need to be stopped until repairs and tool utilization is limited due to tool inflexibility. Fig. 2.7 shows an illustration of sequential rotational CMP polisher**.**

Fig. 2.6 Applied Materials Inc., Sequential Rotational CMP Polisher (Courtesy: Ashok Das, Applied Materials, Inc., Santa Clara, CA) [69]

المنارة للاستشارات
www.manaraa.com

2.2.7 Third Generation CMP Polishers

The third generation polishers have a series of evolutionary and revolutionary systems built in them or integrated in them as modules. Dry in dry out feature is one of the most prominent enhancements in this kind of polishers. This considerably reduces the wafer defects especially in metal CMP as corrosion of the metal is drastically reduced as a result of cleaning after the polishing step. The addition of in situ metrology modules such as motor current detection [81], sensor array for integrated steering [82], thin film reflectivity [83] in situ optical end point detection method [84] have markedly improved CMP process performance and reduced defectivity. There are several new end point detection and other metrology modules such are integration of acoustic emission sensor [85], force sensor [86] and Cu radioactivity detection [87] that are candidates for implementation in the third generation polishers.

2.2.7.1 Sequential Linear Polishers

The sequential linear third generation polishers are generally used in CMP for STI and rarely in ILD structures. The polishers have a moving belt on which the wafer is pressed device side down and rotated slowly about the carrier axis. The belt which is held in tension between rollers moves rapidly [88]. This type of polisher can achieve high removal rate owing to high belt speed and can achieve faster planarization as for STI application where large amount of material needs to be removed from a relatively lower pattern density structure. The low down force and high relative velocity polishing regime limits the damage to the film [13]. The linear polishers require new set and architecture of polishing pads which comprise of single polyurethane belt without foam or felt (sub-pad).

المنارة للاستشارات
www.manaraa.com

The concurrent polishing pad conditioning is obtained by means of a novel polishing pad design where polishing pads have to be mounted in a cylindrical configuration and not on a the conventional flat surface configuration [89]. A special polishing pad conditioner is provided to refurbish the polishing pad [90]. With more and more publication of data showing improved CMP performance at low down force and high linear velocity, this type of polisher is finding increasing acceptance in the semiconductor processing industry. Fig. 2.8 shows a photograph of a sequential linear polisher.

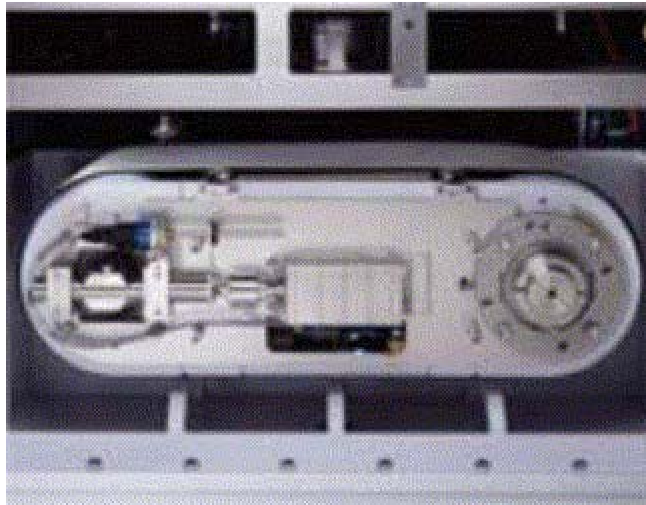

Fig. 2.7 Photograph of Sequential Linear Polishing System [97]

2.2.7.2 Orbital Polishers

Several CMP tool concepts have been developed based on orbital motion. Some orbit the carrier with rotating the carrier [91-93] while others orbit the platen while rotating the carrier [94]. Some of the polishers also involve arbitrary non rotational motion on a fixed polishing pad. In these types of polishers the fundamental principle of relative motion between the wafer and pad to remove the material is used, however,

المنارة للاستشارات
www.manaraa.com

unlike the first generation polishers, slurry is delivered directly at the pad area used for polishing thus improving slurry utilization efficiency. The schematic of the orbital polisher is shown in Fig. 2.9. The preferred mode of operation of orbital polishers is low down force with high relative velocity. With the recent popularity of the contact retaining ring method for polishing, the pad remains compressed at the edges of the wafer and reduces the area of the die lost due to edge exclusion [95]. The planarization capabilities of these tools are known to be better than the first and second generation polishers. These of machines are also known for their small down times due to the rapid change individual polishing heads.

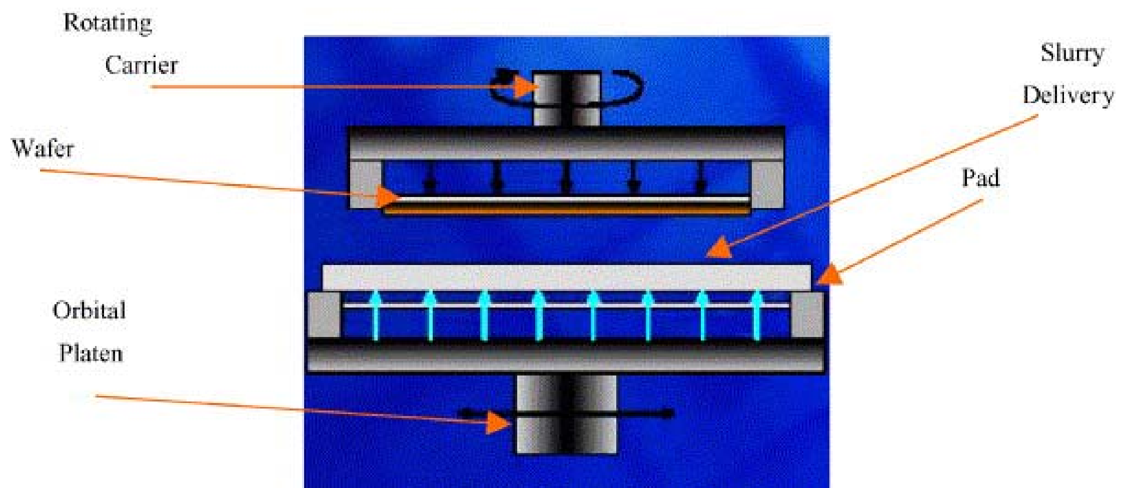

Fig. 2.8 Schematic of Rotary CMP Polisher [13]

2.2.7.3 Rotary Inverted

Recently, Nikon Inc. has developed high-precision CMP systems applying proprietary technology based on its long experience in lens polishing and optical measurement [96]. The system's special face-up polishing uses small pads applied at very

المنارة للاستشارات
www.manaraa.com

low pressure and high-speed rotation. The compact polishing pad as seen in (Fig. 2.10 a) enables high-speed rotation. Its light-weight, less pad deformation feature allows superior planarity. These features are especially advantageous ultra low-*k* polishing process. Through the compact polishing pad the slurry is supplied onto polishing area of the wafer efficiently. This enables less slurry consumption compared to the conventional polishing equipment (Fig. 2.10 b). Face-up polishing at the polishing station enables continuous optical end-point measurement. It helps improve S/N ratio while minimizing slurry effect for end-point detection. Mounting of wafer and pad are also convenient with this system. In spite of some initial excitement about this system, it is yet to have a proven track record in the semiconductor fabrication environment.

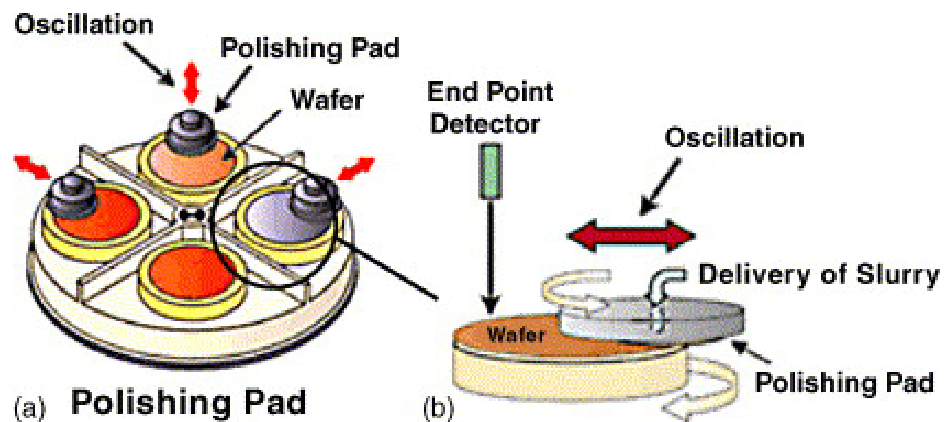

Fig. 2.9 a) Set up of Multi Wafer Rotary Inverted CMP Polisher and b) Polishing Action and End Point detection [96]

2.2.7.4 Pad feed Polishers

The pad feed polishers are based on a recently developed pad type that is held in rolls. These polishing pads are fed to the wafer polishing tables, the wafer is polished,

المنارة للاستشارات
www.manaraa.com

pad is conditioned and then the pad moves further (Fig. 2.11). This methodology is especially useful for pads that have very repeatable first polish performance and their characteristics either degrade or change with subsequent polishing runs. This polisher unlike others does not have to be turned off for changing the pad there by maximizing the equipment utilization time [97, 98]. This technology is still in its nascent stage and various industrial giants continue to develop it even further in order to make a positive impact on the CMP polisher market.

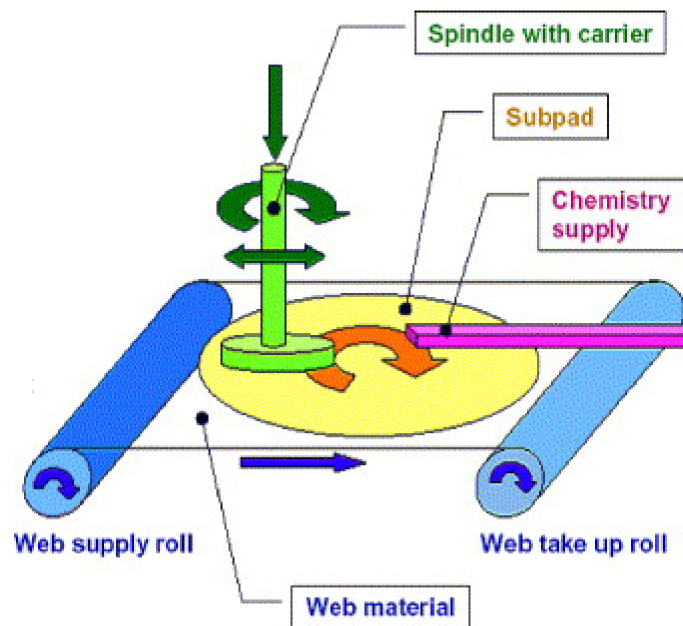

Fig. 2.10 Schematic of a Web-type Polisher [98, 99]

3.3 Physics of CMP Process

In 1927, the Preston equation was developed (Eq. (2.1)) [99], for modeling the mechanical effects of pressure and velocity in the CMP process:

$$R = KPV \quad (2.1)$$

المنارة للاستشارات
www.manaraa.com

where R denotes the polish rate, P is the applied downward pressure, V is the linear velocity of the wafer relative to the polishing pad, and K is a proportionality constant, called the Preston coefficient. As seen in Fig. 2.12 r_{cc} is the linear distance between the centers of the wafer carrier and the platen, which is mostly assumed to be constant, r_H (H stands for head) is the positional vector at any point Q on the wafer from the center of the carrier and this varies with the position of the point Q, r_{th} is the positional vector of any point Q on the wafer from the center of the platen (this distance varies with the location of Q). V_Q is the velocity of any point Q on the wafer. V_T and V_H are the linear velocities of the table (platen) and wafer head. ω_T, ω_H are the rotational velocities of the platen and wafer carrier. Assuming that $\omega_T \neq \omega_H$ velocity V_Q will vary from point to point over the wafer. The variation in velocity will call cause changes in the removal rate across the wafer in accordance with the Preston's equation.

$$r_{th}=r_{cc}+r_H \quad (2.2)$$

$$V_Q=V_T+V_H=-(\omega_T \times r_T)+(\omega_H+r_H), \text{ where } V_Q=(\omega_T \times r_{cc})=[r_H(\omega_T-\omega_H)] \quad (2.3)$$

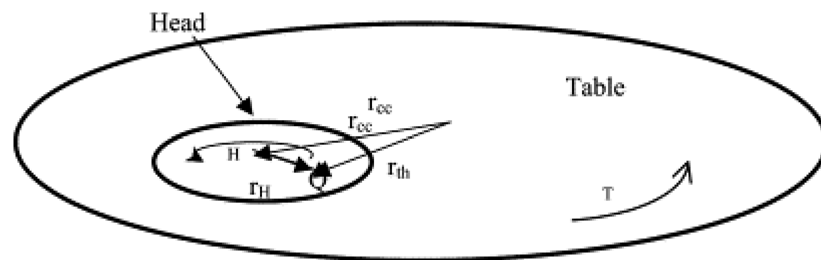

Fig. 2.11 Schematic of the Force Field on the Wafer and the Pad during CMP [37, 70]

However, if ω_T is set equal to ω then linear velocity will be independent of the location of the wafer for $V_Q = -[\omega_T \times r_{cc}]$. This with the V_Q maintained as shown before, the velocity of all points on the wafer will be the same and then there will be no change

www.manaraa.com

in the removal rate of the material. This force field analysis is taken in to account to fundamentally design any CMP process [37, 70]. In any event, many times, the process engineers are still confronted with the problem of wafer to wafer and within wafer non-uniformity (WIWNU and WTWNU) (Fig. 2.13) [33].

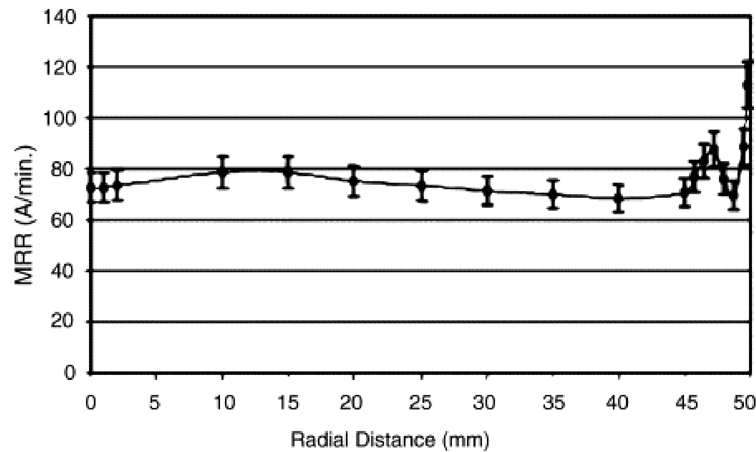

Fig. 2.12 Non-uniformity in Removal Rate with in a Wafer [33]

3.4 Parameters Governing CMP process

The physical forces acting upon the wafer govern only a part of the entire tribo-chemical phenomenon of CMP. The process of CMP is governed by various input variables that act on a micro as well as nanoscale to produce desirable or undesirable output parameters. The interplay and interaction of different micro and nanoscale parameters takes place sequentially or simultaneously, predominantly at the pad wafer interface, during the entire CMP polishing run. Though machine parameters when input in the Preston's equation may appear to be the dominant in any CMP output, the entire governing dynamics of industrial scale CMP is much more complex. Fig. 2.14 is an attempt to correlate the various parameters in the CMP governing dynamics.

المنارة للاستشارات
www.manaraa.com

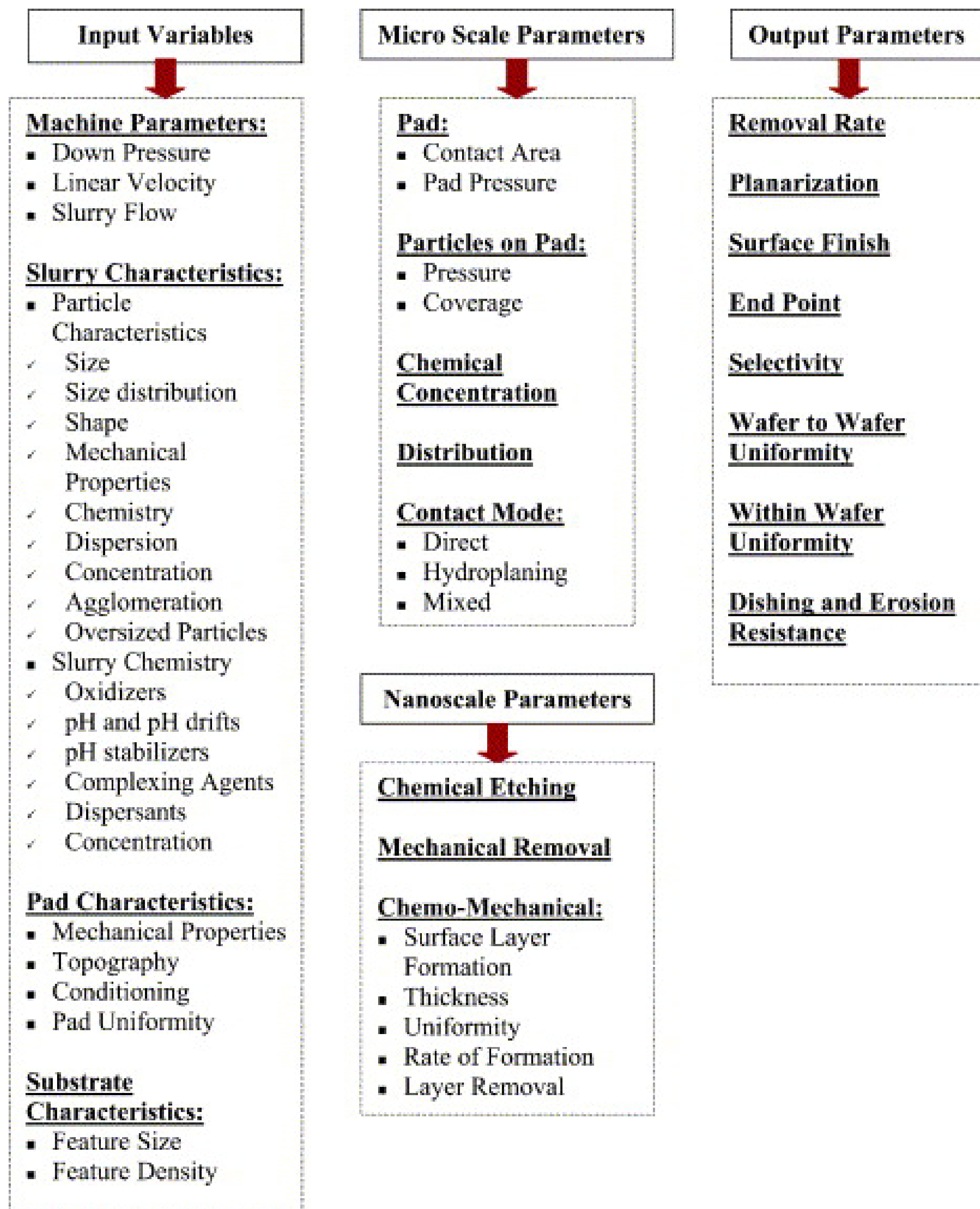

Fig. 2.13 Parameters Governing the CMP Dynamics [101]

المنارة للاستشارات
www.manaraa.com

3.5 Research Objectives

The broader objective of this research is to understand the process of CMP which has been more of an art that science. The specific objectives, milestones and subjects of investigation along with the expected outcome are shown in Fig. 2.15.

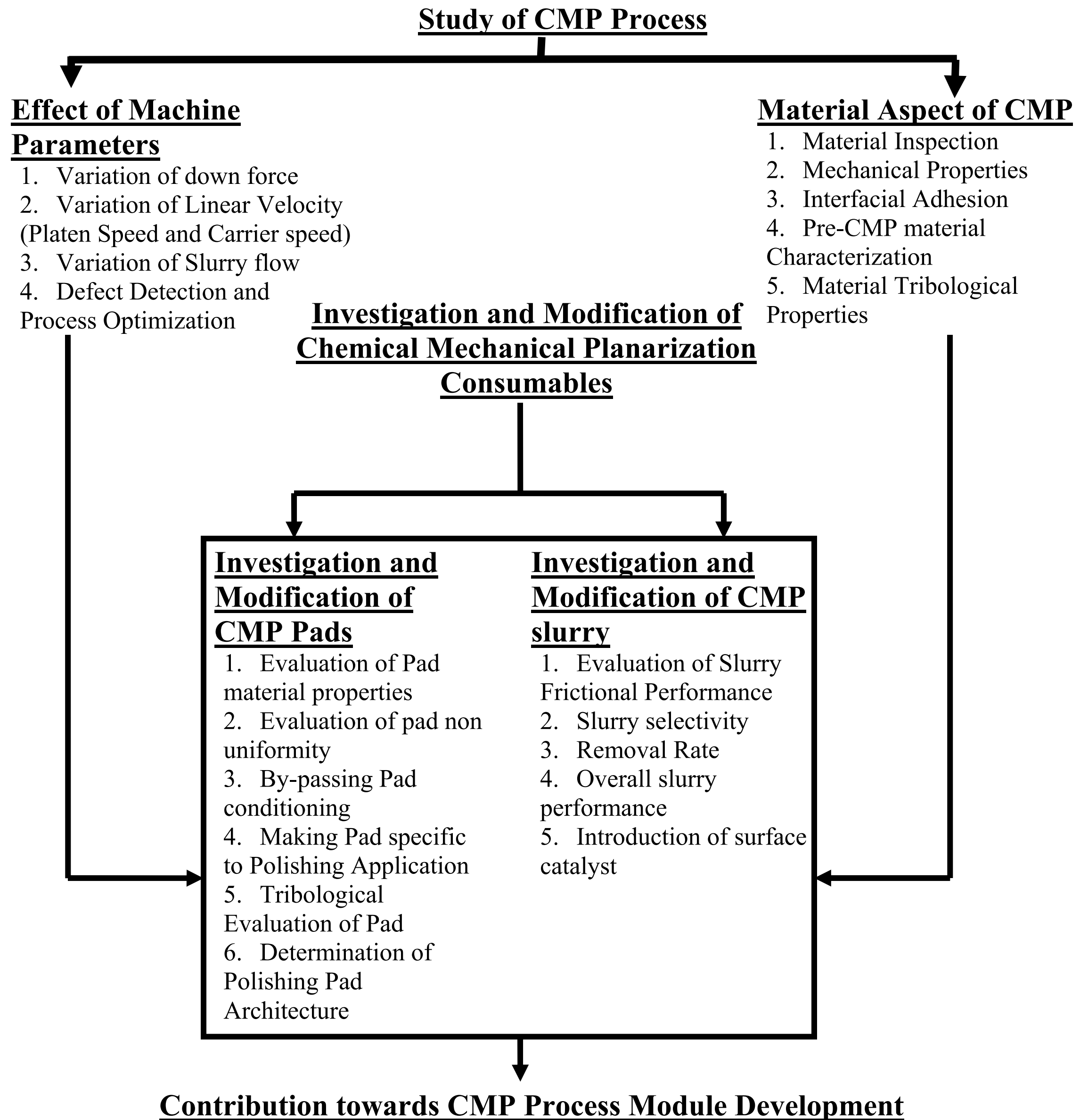

Fig. 2.14 Schematic Showing Objectives of the Current Research

المنارة للاستشارات
www.manaraa.com

CHAPTER THREE

METROLOGY OF CMP

3.1 Need for Effective CMP Metrology

The CMP process combines mechanical and chemical removal mechanisms in a synergistic effect. This synergy has been the subject of many studies, but focus in the past has been primarily on mechanical effects due to the difficulty of identifying the reaction mechanisms of the chemical effect. However, mechanical effects alone cannot provide the type of polishing necessary for IC manufacturing. Chemical effects contribute to the increased global planarity and reduced micro roughness required for successful IC fabrication. As discussed in the earlier section, the fundamental basis for designing any CMP process module, the force field analysis of the wafer–pad–slurry abrasion system is made. The variations in the machine parameters to obtain optimal results are the first adjustments made to refine the CMP process. Until recently, slurry flow and slurry flow rate was not given much importance variation of machine parameters [65], however, with the ever-growing demands for enhanced yield and low defects, and also with the knowledge of the heat transfer behavior of the slurry [100], the slurry flow is also brought in the CMP process control equation. This section discusses the broader impact of these machine parameters on the CMP process. A better understanding on the effect of machine parameters on the CMP process can be obtained by performing repetitive CMP

www.manaraa.com

experiments on a prototype CMP tester in which process data is monitored in situ. We have used the CETR bench top. for studying the CMP process in detail. The details of the CMP tester are described below and also can be obtained in literature [102].

3.2 CMP Tester

Most of the CMP processes during this research were performed on a CMP tester (CETR, Inc, CA) with variety of process parameters. A photograph of the tester is shown in Fig. 3.1. The lower platen can hold a pad up to 6" in diameter. The upper carriage can hold two inch wafers or sample coupons up to 1.5" X 1.5". The upper carriage can rotate about its own axis and oscillate radially with the pad during planarization process. A strain gauge force sensor (0-200 N) can record both vertical and friction forces and hence co-efficient of friction (COF) is monitored during the process. The system is also equipped with a high frequency acoustic emission sensor. AE-Analysis is an extremely powerful technology that can be deployed within a wide range of usable applications of non-destructive testing: metal pressure vessels, piping systems, reactors, and similar. All solid materials have certain elasticity. They become strained or compressed under external forces and spring back when released. The higher the force and, thus, the elastic deformation, the higher is the elastic energy. If the elastic limit is exceeded a fracture occurs immediately if it is a brittle material, or after a certain plastic deformation. If the elastically strained material contains a defect, e.g. a welded joint defect, a non- metallic inclusion, incompletely welded gas bubble or similar, cracks may occur at heavily stressed spots, rapidly relaxing the material by a fast dislocation. This rapid release of elastic energy is what we call an AE event. It produces an elastic wave

المنارة للاستشارات
www.manaraa.com

that propagates and can be detected by appropriate sensors and analyzed. The impact at its origin is a wideband movement (up to some MHz). The frequency of AE testing of metallic objects is in the range of ultrasound, usually between 100 and 300 kHz. The acoustic emission sensor employed in this tester has a frequency range between 0.5 to 5 KHz. The AE sensor, in conjunction with COF, has been used to detect the delamination, endpoint, and debris during polishing (described later) during the course of this research.

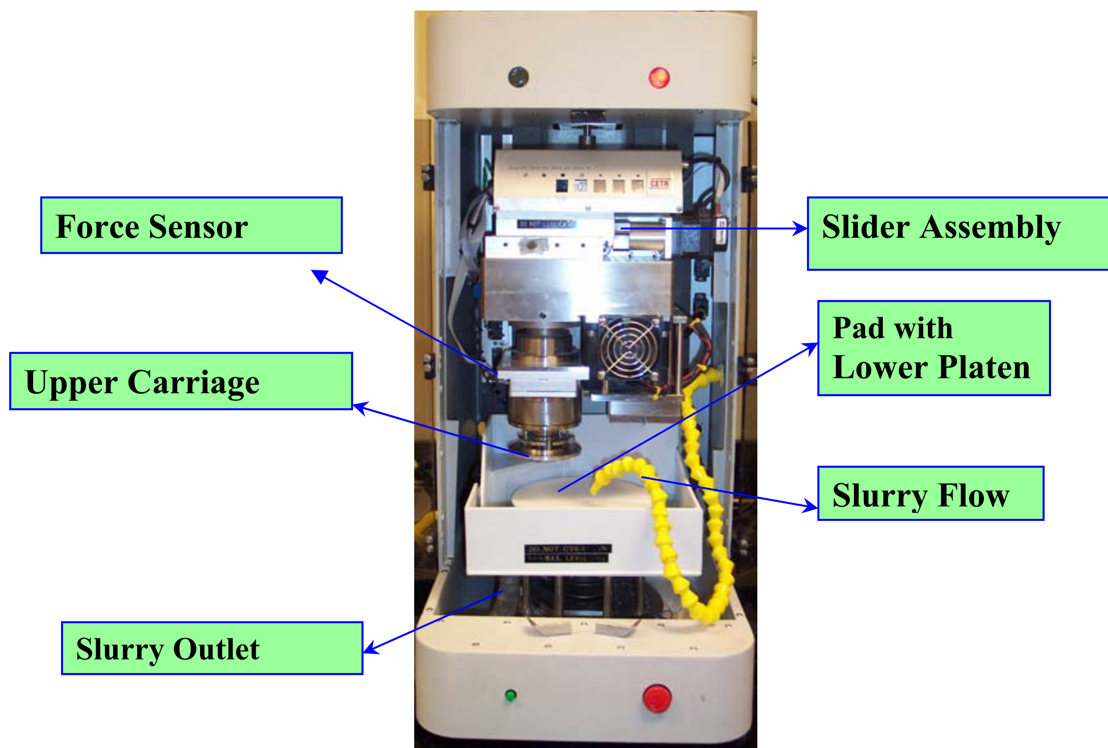

Fig. 3.1 Photograph of the CETR CP-4 CMP Tester

The state-of-the-art CMP tester is a testing tool and thus the following assumption are made when different pads, slurries and materials were evaluated: 1)Due to the lack of uniformity on the surface of the coupon, an average of the material removal rate measured at different points from the center to the edge was assumed to be the MRR

www.manaraa.com

of the polishing run, 2)During the in-situ detection of MRR using COF and AE, the non uniformity of the sample surface brought about gradual tapering of the signals even for blanket samples. The end point was assumed to have occurred when more than 70 % of the material was removed from the surface and further material removal brought insignificant change in the AE and COF signals.

3.3 Coefficient of Friction (COF) and Material Removal Rate (MRR)

To understand the variation of COF and MRR, which are the primary output variables of any given CMP process, the polishing tests on the CETR tribometer. The samples used in this case were 1 in. × 1 in. PECVD SiO_2 using Klebesol 1501 (Rodel Inc., DE) colloidal silica slurry (pH 10–11) on an IC 1000/IV pad with linear velocity 5 mm/s and a radial distance of 50 ± 2.5 mm. The down force used was 4 PSI and the platen rotation was 150 RPM. Influence of machine parameters such as down force, relative velocity, slurry flow on the acoustic emission (AE), coefficient of friction (COF) and material removal rate (MRR) was observed. For removal rate calculations, thickness of oxide was measured at nine points using the ellipsometer. The wear rate was calculated by re-measuring the sample after polishing at nine points.

COF is an important tribological property of films and pad as it gives an estimate of the surface shear which directly affects the MRR. The COF was recorded during all the tests. Fig. 3.2 (a, b) shows the COF versus RPM and PSI, respectively, during polishing. With higher RPM, COF decreases, whereas, decrease of COF is very small with the increase of PSI.

المنارة للاستشارات
www.manaraa.com

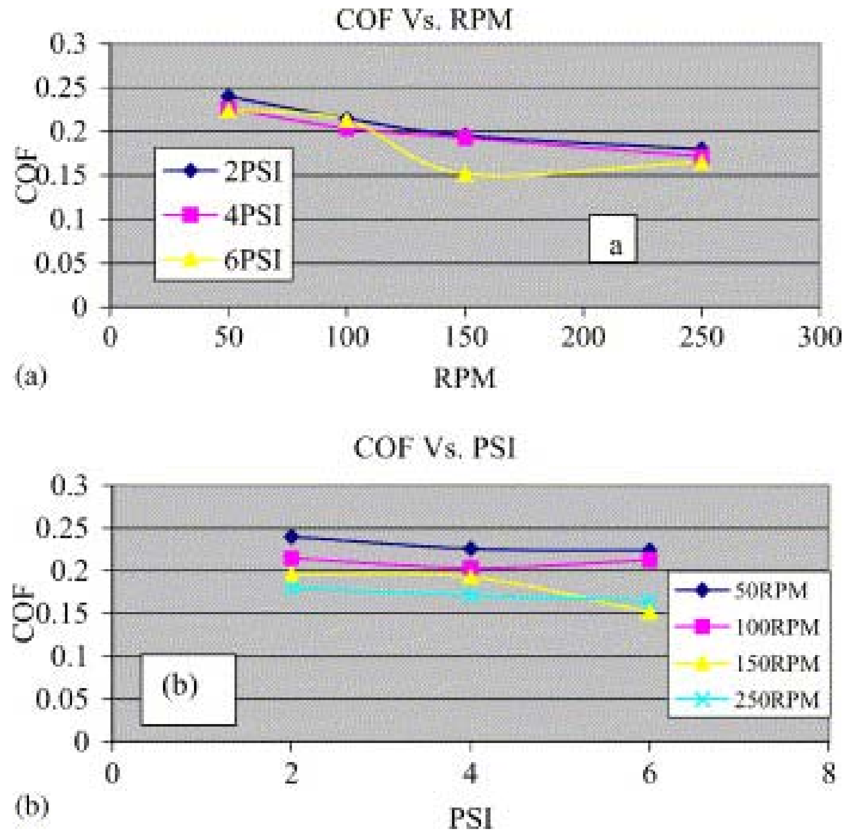

Fig. 3.2 a)Variation of COF with RPM (platen velocity) for Different Values of Down Pressure (PSI), b) Variation of COF with PSI (Down Pressure) with Different Values of Platen Velocity (RPM)

Fig. 3.3 a, b shows the variation of MRR as a function of RPM and PSI, respectively. Experiments on two sets of samples show the same trend. Removal rate increases with both RPM and PSI. Removal rate decreases slightly at platen rotation 250 RPM. This may be due to inadequate slurry flow under the sample at higher platen rotation. As COF decreases with increasing RPM and PSI, a lower COF may be related to the higher removal rate in CMP process. Fig. 3.4 shows the removal rate versus RPM × PSI and the linear relation indicates that polishing of oxide follows Preston's equation [99].

المنارة للاستشارات
www.manaraa.com

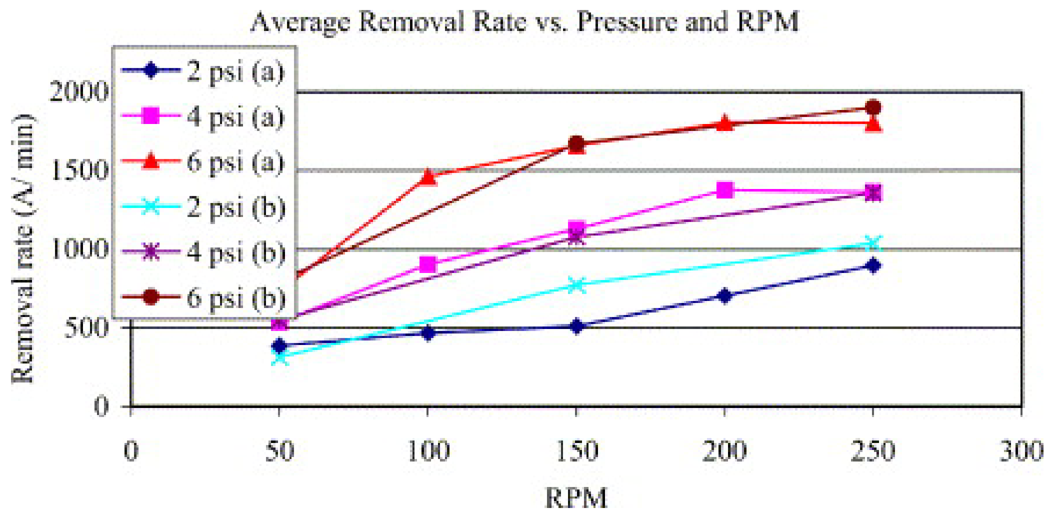

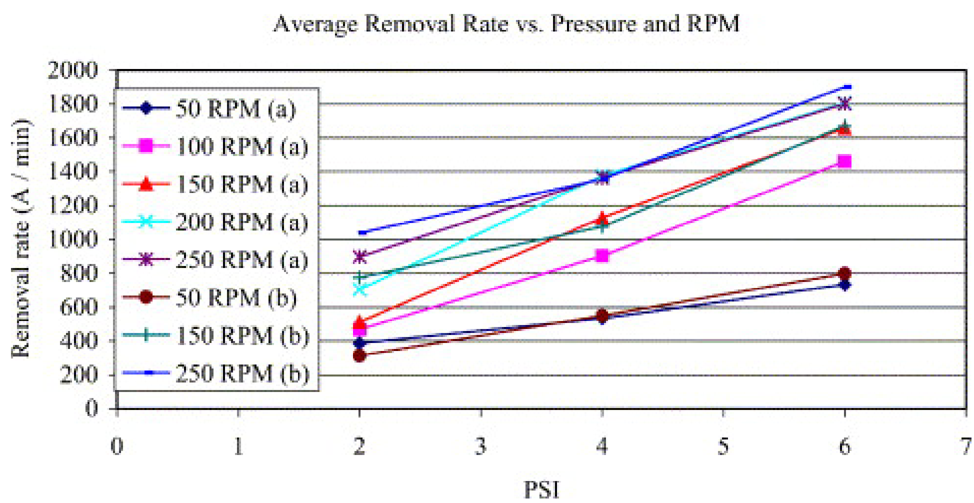

Fig. 3.3 a) Variation of Average Removal Rate with RPM at Different Down Pressure (PSI) for the Evaluated Set of Samples, b) Variation of Average Removal Rate with PSI (Down Pressure) at Different Platen Velocity (RPM) for the Evaluated Set of Samples

المنارة للاستشارات
www.manaraa.com

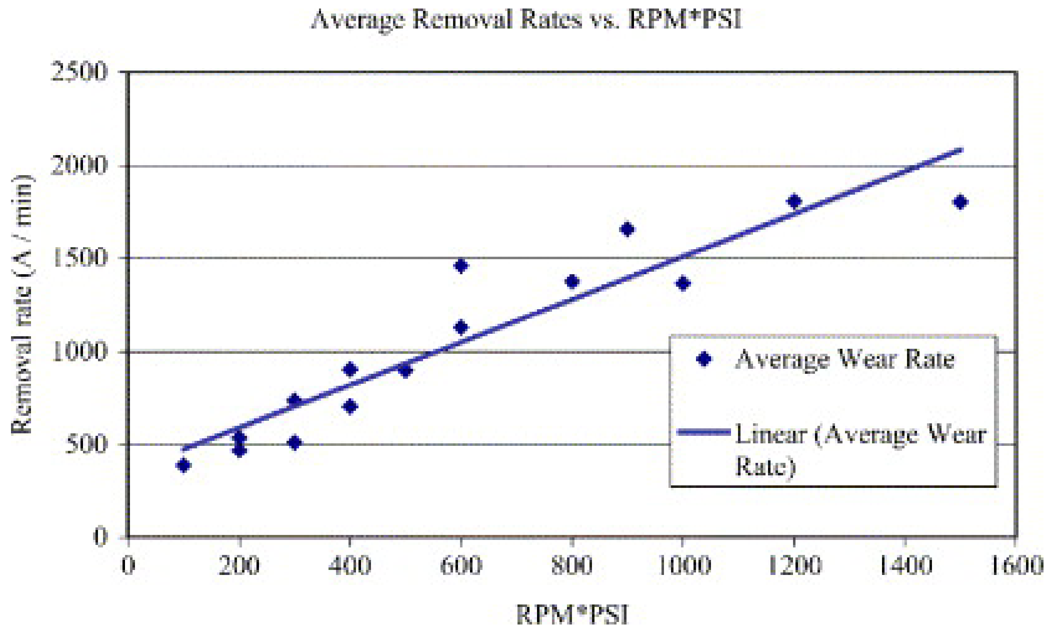

Fig. 3.4 Average Material Removal Rates Plotted with RPM × PSI. Linear Relation Indicates that Polishing Follows Preston's Equation

3.4 Importance of Slurry Flow

It is important to optimize the effect of slurry flow rate on the COF and AE signal. Results of the optimization experiments are summarized in Table 3.1. It can be seen from Table 3.1 that COF decreases slightly while no significant change can be noticed in AE signal. Decrease of COF may be attributed to the higher slurry flow rate during polishing. Therefore, the data suggests that flow rate may not affect the AE signal. The flow pattern of the slurry on the pad affects the polishing rate as well as the WIWNU. Due to the rotation of the lower platen the flow pattern will be different as we feed the slurry at different positions of the pad. Fig. 3.5 shows the different positions of slurry feeding on the platen. If the slurry cannot reach uniformly at the pad-film contact points material will not be removed uniformly. It can be seen from Fig. 3.6 that center

www.manaraa.com

position and position “8” (very near to the center) are two better positions to feed slurry while platen is moving clockwise.

Table 3.1 Effect of Slurry Flow rate on COF and AE

Run #	Slurry flow (ml/min)	COF	AE signal (arbitrary unit)
1	35	0.3977	0.4013
2	75	0.3949	0.4533
3	100	0.3932	0.4184
4	155	0.3911	0.4133
5	195	0.3888	0.4189

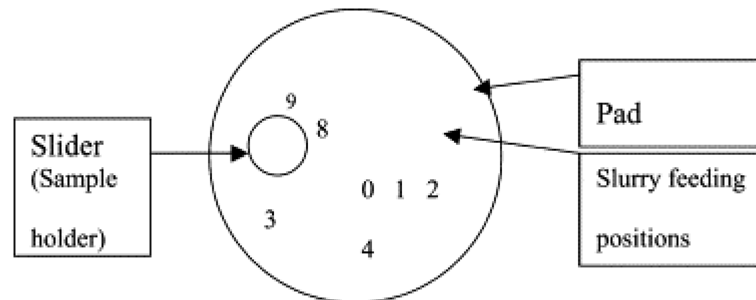

Fig. 3.5 Schematic of the Positions of Slurry Feeding on the Pad during Polishing for Feeding Position Optimization; Distance 0–1.4 = 15 mm, 0–2.5 = 30 mm, 0–3.6 = 45 mm, 0–7.9 = 45 mm and 0–8 = 25 mm

The friction generated during CMP brings about over all increase in the temperature at the wafer pad interface. Certain CMP processes such are silicon polishing are exothermic. Hence, there is a natural increase in the temperature at the interface. The increase in temperature changes the reaction kinetics of the slurry with the wafer, mostly

المنارة للاستشارات
www.manaraa.com

increasing the removal rate. However, the increase in removal rate due to the increased chemical action of the slurry at elevated temperature does not always translate in to greater removal rate during the CMP process [65]. The increase in temperature makes the viscoelastic polyurethane pad softer, there by reducing the removal rate due to the reduction in hardness [103]. Hence, an optimum slurry flow must be maintained during the process and should be changed if necessary in order to strike a balance with optimum temperature for enhanced slurry action and non-degradation of the pad [65]. Novel CMP process developers have adopted a new recipe to change the slurry flow during the CMP process for optimization of slurry utility and maintaining the temperature during the CMP process [104,105].

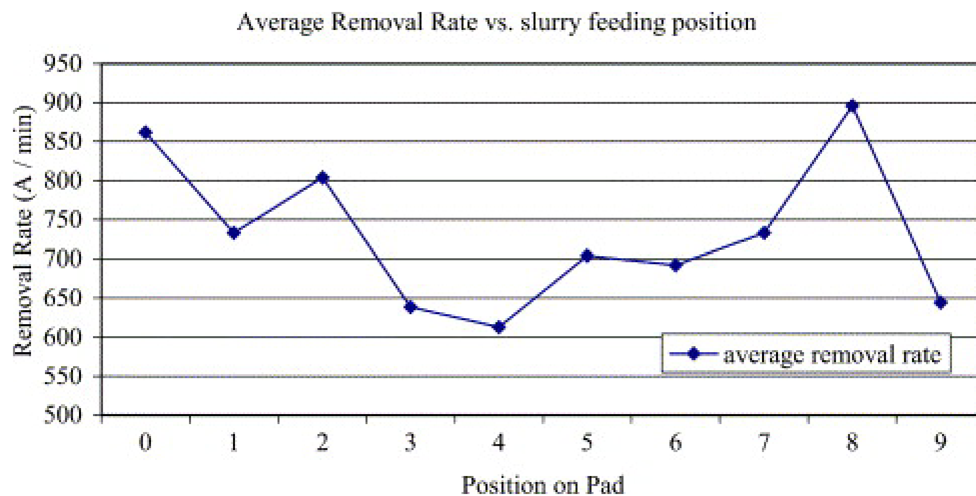

Fig. 3.6 Average Removal Rate with the Slurry Feeding Position on the Lower Platen Position

المنارة للاستشارات
www.manaraa.com

3.5 CMP End Point Detection (EPD)

The difference in removal rate of one material as compared to another in a given slurry yields the measure of the selectivity of that slurry for those two materials. Higher the slurry selectivity, the more effective is the end point detection for a particular CMP process step as there is a marked change in the tribological properties of the material being polished and the under layer. Selectivity is a very important criterion in designing any slurry. For STI, slurry used needs to act on the oxide that is being planarized and not act on the underlying nitride. For polishing Cu, the slurry needs to act selectively on Cu and spare the barrier layer Ta and underlying layers of silica or low-*k* dielectric material. Typically slurry selectivity of 10–25 has been reported for Cu polishing [101]. The selectivity could be considerably improved up to 1000 by introducing particle free slurry [106, 107]. The reduction in mechanical component due to lack of abrasive implies that majority of material removal takes place due to solution chemistry which can be made highly selective. Slurries with high selectivity facilitate easy end point detection as the tribological properties of the material say Cu being polished in a highly selectivity slurry are markedly different from the properties of the barrier layer Ta or underlying silica layer when polished in the same slurry. The difference in tribological properties can be monitored in situ using techniques such as motor current or force and acoustic emission sensor.

The variation in coefficient of friction and acoustic emission for polishing of blanket Cu, Ta and ultra low-*k* dielectric ($k = 2.2$) has been studied. The candidate materials have been polished in the form of 1 in. × 1 in. coupons on the bench top CMP tester (mentioned in Section 3.2) [102] to evaluate the selectivity of the slurry. The

www.manaraa.com

slurries evaluated were: 1) Cu selective alumina particle slurry (Cu1), 2) Cu selective particle less slurry (Cu2), 3) Ta selective slurry with colloidal abrasives (slurry Ta), and 4) non-selective slurry (slurry Cu–Ta). Fig. 3.7 a–d shows the variation of COF and AE at 2 PSI and different platen speeds. It can be seen from the figure that the value of COF for a particular material for one polishing condition is unique and hence monitoring the value of COF can give an estimate of the end point of the process.

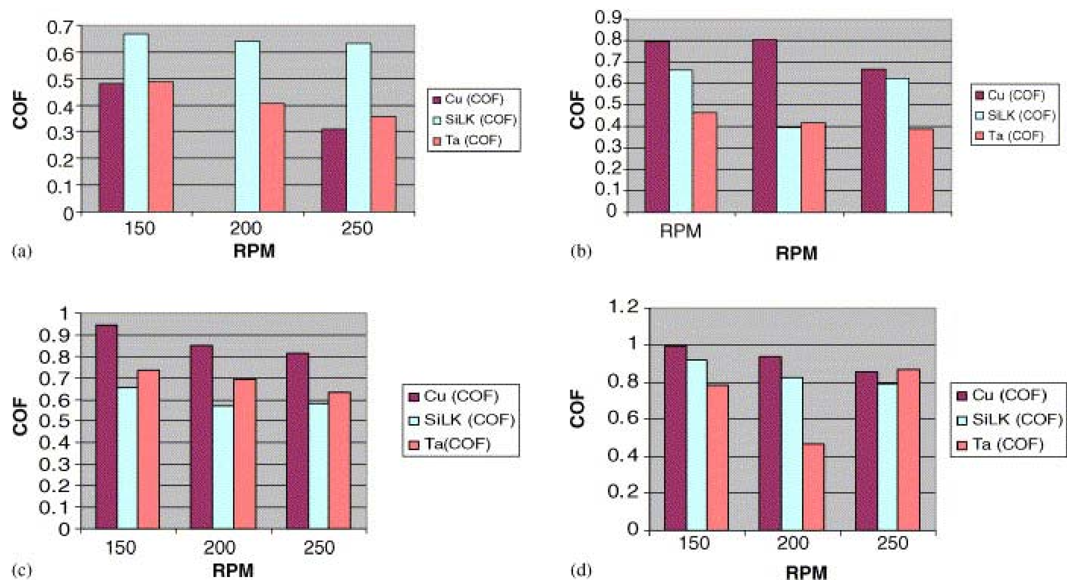

Fig. 3.7 a) Variation of COF at 2 PSI Down Force and Variable RPM in Slurry Cu1, b) Variation of COF at 2 PSI Down Force and Variable RPM in Slurry Cu2, c) Variation of COF at 2 PSI Down Force and Variable RPM in Slurry Ta, and d) Variation of COF at 2 PSI Down Force and Variable RPM in Slurry Cu–Ta [85, 86]

Just as the COF is a strong function of the down pressure, platen and carrier velocity, and the choice of the slurry and pad, the acoustic emission during CMP is already affected by the choice of the aforementioned CMP variables. The variation of

المنارة للاستشارات
www.manaraa.com

AE and COF for different materials polished in a commercial Cu slurry is shown in Fig. 3.8 a. It must also be noted here that the same materials displays different COF with polished using different slurries. This can be seen from Fig. 3.8 b where different materials, namely Cu, SiLK^{TM} (ILD material) and Ta are polished in commercial slurries named here are "Cu2", "Ta" and "Cu-Ta". The slurry Cu2 is selective to Cu while Ta is selective to Tantalum. The slurry Cu-Ta is a non selective slurry.

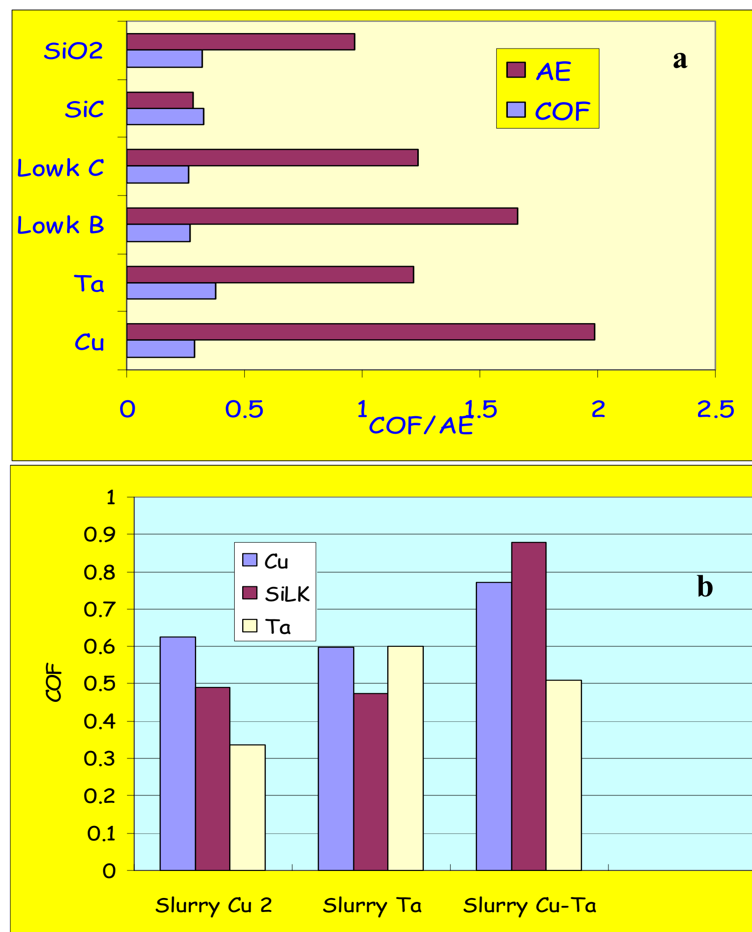

Fig. 3.8 a) Variation of AE and COF for Different Materials Polished in a Commercial Cu Slurry, b) Variation of COF for 3 Materials Polished in Three Different Slurries

المنارة للاستشارات
www.manaraa.com

Addition of specialized chemicals that can act as catalysts in the chemical interaction between slurry and the polished material there by increasing the rate of the chemical reaction with the material being removed considerably is a common approach for improving the selectivity of the slurry. Tetra-methyl ammonium hydrate (TMAH) can be added to Cu slurries to considerably decrease silica polishing rate [108, 109]. Phosphoric acid added to alumina and colloidal silica TaN slurry has also shown accelerated chemical reaction with TaN. Fig. 3.9 shows the increase in the polishing rate of TaN with addition of phosphoric acid in alumina and colloidal silica slurry [110]. The effect of surface catalyst in the slurry has been investigated and details have been reported in later in this dissertation.

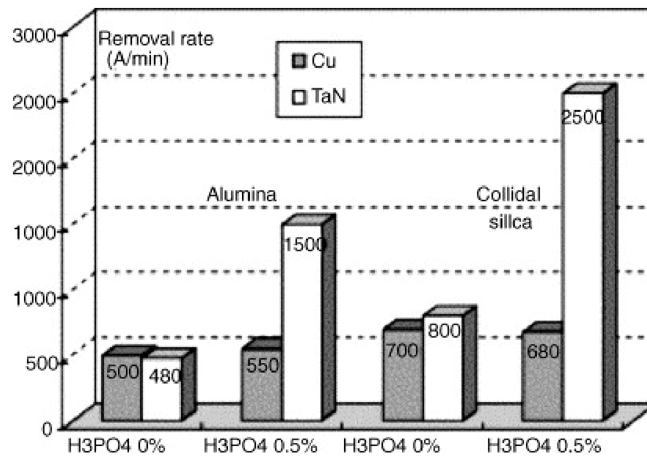

Fig. 3.9 Cu and TaN Polishing Results (Head 40 RPM, Table 40 RPM, and Pressure 7 PSI) [110]

www.manaraa.com

Among the several different models proposed for friction and interfacial heat dissipation, pad-wafer interactions during CMP tend fall in the molecular friction model at a nanoscale. The molecular friction model essentially postulates that when two different surfaces come in contact, the imbalanced Van der Vaal forces of the surface molecules results in adhesion or “stiction” between the two interfaces. It must be mentioned here that if one of the surface is significantly rougher than the other (as is the case with CMP when pad is significantly rougher than the polished wafer), macro-scale parameters such as “asperity lock-in” also govern the friction phenomena. In the event of an abrasive containing fluid present at the pad wafer interface, the overall energy required to overcome the combined effect of the Van der Vaal’s interaction of pad, slurry and abrasive materials with the polished wafer. Hence, the choice of the polished material, polishing pad, and CMP slurry will directly influence the friction force and hence the COF at the pad wafer interface during polishing. This interaction of the different aforementioned materials will also impact the strain to which the material subjected to during polishing at the given polishing conditions. The strain and the strain relaxation which is the root cause of the elastic wave sensed by the AE sensor will thus change for different process recipes and parameters. Upon complete removal of polished material, the exposure of the material underneath will change one of the variables (the polished material) in the interactions taking place at the interface of pad and wafer. This will in turn affect the COF and AE values measured in-situ. This principle could be used for effective CMP end point detection. The time taken for complete material removal can give an reasonable estimate of the material removal rate during CMP. If the polishing is

المنارة للاستشارات
www.manaraa.com

continued for sustained period of time, then the time taken for the complete material removal of the buried layers can give an idea of the selectivity of the slurry.

3.6 In-situ Process Monitoring and Slurry Selectivity

The previous section described in-situ monitoring of CMP process of predominantly blanket samples. However, in reality, wafers that undergo CMP have an intricate pattern based upon the design layout. This gives many new paradigms to the CMP process monitoring. However, the knowledge gained from in-situ process monitoring of blanket samples can be used for studying the CMP of STI structures. The variation in pattern density in the topography of the wafer can accentuate a special type of defect known as 'dishing' [111, 112]. A schematic illustration of dishing and erosion defects is shown in Fig. 3.10. This dishing effect is characterized by high polishing rates in localized regions where the pattern is significantly different from its surrounding. The formation of the trough shaped dish has been attributed to excessive over polishing in these areas. Efficient end point detection (EPD) helps prevent these and numerous other CMP defects.

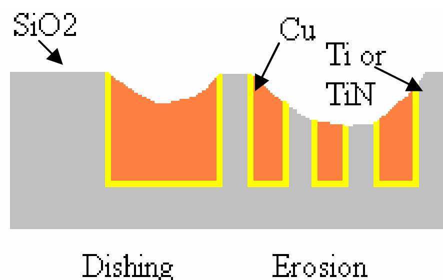

Fig. 3.10 Schematic Illustration of Dishing and Erosion

www.manaraa.com

The overview of the STI process has already been given in Chapter 1. However, before the process monitoring of STI CMP is discussed, it is important to understand the background and layout of the evaluated structures that would undergo CMP. In STI structures, the field oxide is embedded in the Si wafer in order to clearly separate the device active areas. This allows smaller device pitches and higher packing density. Fig. 3.11 shows an SEM micrograph of the Focused Ion Beam (FIB) cross section of an STI structure.

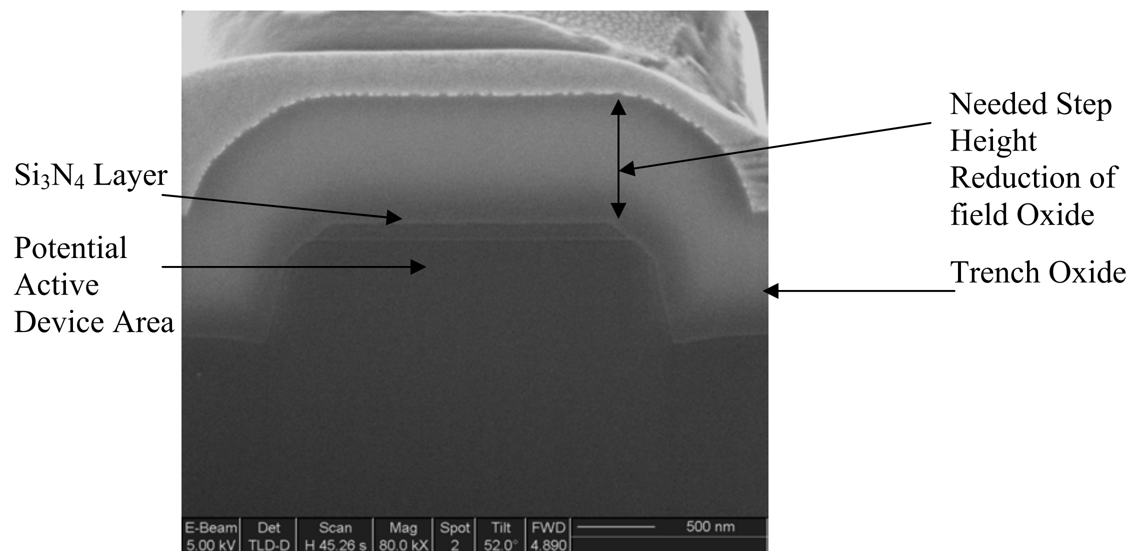

Fig. 3.11 SEM Cross-section of STI Structure

The process of the fabrication of STI structures (besides minor possible process variations) is relatively well characterized and is already discussed in literature [113]. Some of the teething challenges in STI process are: 1) effective trench oxide filling, 2) thermal stability and wet etch resilience of the oxide, 3) with in die non uniformity after CMP of field oxide, 4) incomplete polishing of the oxide, 5) oxide dishing and nitride erosion, etc. Most of these STI process challenges can be resolved

المنارة للاستشارات
www.manaraa.com

using effective process EPD. It can be argued that during the polishing of STI structures, the COF will change when the nitride layer is exposed after removal of field oxide.

In this study, we used the variation of COF during the CMP process for in-situ EPD. CMP polishing run was carried out for an extended period of time to determine the oxide and nitride MRR and oxide to nitride selectivity of the slurry. The surface of the wafer was characterized ex-situ using Atomic Force Microscopy (AFM) before, in the middle, and after process end point.

The evaluation of sample surface morphology was done using AFM in the tapping mode. The surface morphology before polishing showed 3.5 µm X 3 µm pedestals with 2 µm device area (Fig. 3.12). The AFM characterization was also performed after partial removal of oxide during CMP as well as the complete removal of field oxide. The process parameters specifically studied were: 1) variation of COF with time, and 2) variation of material removal rate (MRR) for each material under different polishing conditions. The details of the experiments are shown in Table 3.2.

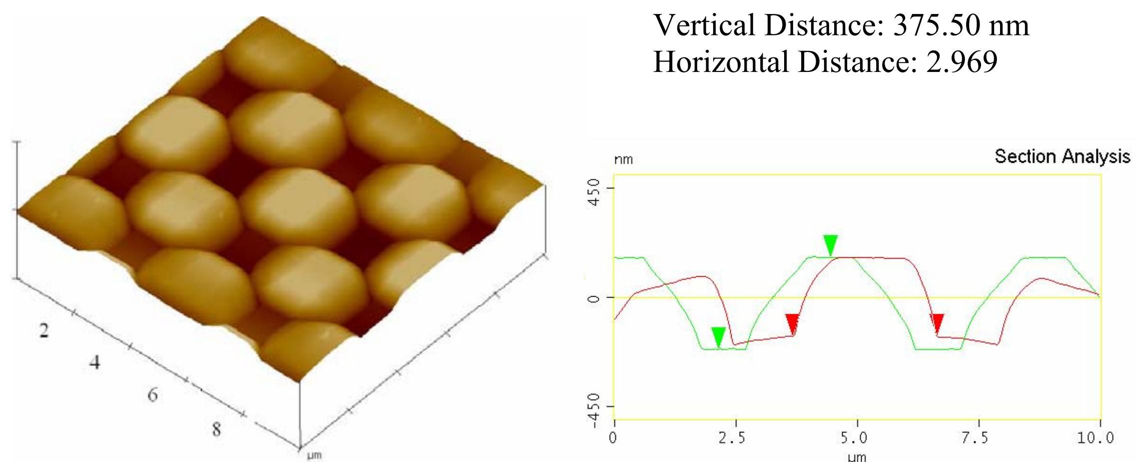

Fig. 3.12 3D AFM Image of the Evaluated STI Structure with Step Height Measurement

المنارة للاستشارات
www.manaraa.com

The COF, which is the ratio of the shear force (F_s) to the normal force (F_N) ($COF = \frac{F_s}{F_N}$), is measured in situ during the process. When a patterned wafer (in this case STI) is pressed face down on the surface of the polishing pad under a particular value of down pressure, the pressure is distributed uniformly over the entire topography. The density of the pattern thus strongly affects the local pressure on the surface of the wafer. The step height reduction takes place at a brisk rate during the initial stages of the CMP process due to the higher local pressure. As the material removal from the surface of the wafer takes place primarily due to shear, higher shear force generated due to the aforementioned mechanism is the cause of higher values of COF after carrier touch down. The shear force also depends upon the chemically modified surface layer that results due to the interaction of the surface and the slurry.

Table 3.2 CMP Experimental Details

#	Parameter	Conditions
1	Down Pressure	4 PSI for EPD experiments, 8 PSI for Slurry Selectivity
2	Platen Rotation	200 RPM Platen Rotation, 195 Carrier Rotation
3	Slider	35mm ± 5mm (position) @ velocity of 5 mm/ sec
4	Slurry	ILD 1300 (pH~10.5) with colloidal silica abrasives
5	Pad	Rodel, Inc. IC1000 Suba IV A4 perforated
6	Time of polishing	Until Process End Point
7	Polishing Specimen	1” X 1” coupon

المنارة للاستشارات
www.manaraa.com

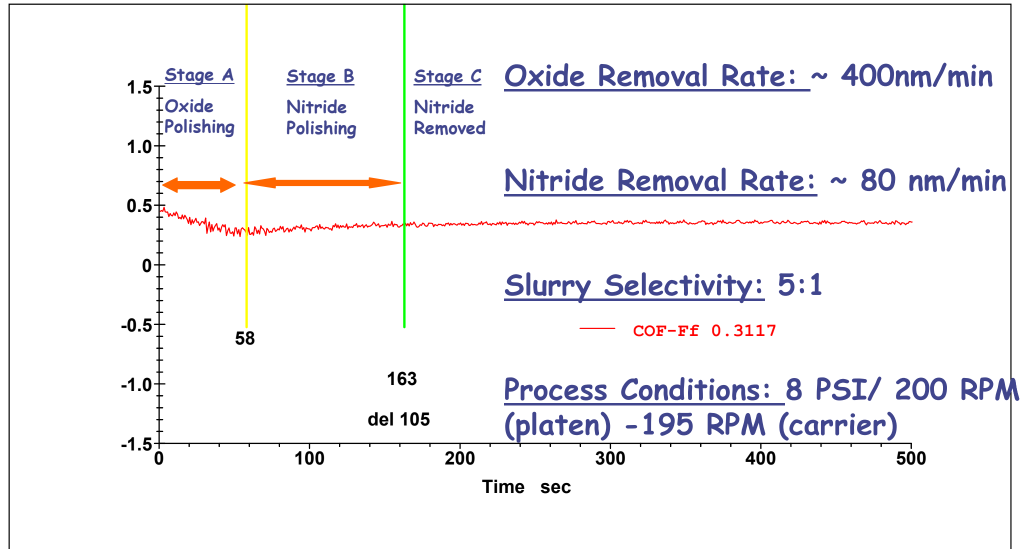

Fig.3.13 In situ Variation of COF during CMP Split in to Different Stages

In case of STI patterns being polished by ILD slurry designed to planarize SiO_2, the planarization chemical mechanism involves: 1) penetration of water in the material surface in presence of an alkaline medium, 2) surface layer dissolution, 3) removal of hydrolyzed material by particle impact, 4) Partial redeposition of dissolved products, 5) reaction of surfactant on the abrasive on material removal [114]. Any change in the material removal mechanism will cause the change in the nature of interactions at the pad wafer interface. There is a drastic change in the slurry-surface interaction when the Si_3N_4 layer is exposed after the removal of field oxide. In comparison with SiO_2, the hydroxylation of the Si_3N_4 surface is markedly reduced. Also, silicon nitride being significantly harder than SiO_2, the silica particles tend to roll over the surface due to the slurry flow and show lesser tendency for indentation. This causes lesser shear for a given down force, which in turn implies that COF values when Si_3N_4 is polished by silica ILD slurry are lesser as compared to SiO_2. However the COF measured during Si_3N_4 polishing

المنارة للاستشارات
www.manaraa.com

is the combined COF of the Si_3N_4 pads and surrounding trench SiO_2. Hence, though there is a difference in COF value when Si_3N_4 is being polished, the magnitude of the COF is not markedly different (Fig. 3.13). The COF value again changes when the Si_3N_4 is completely removed and field oxide is polished. The CMP experiments were first performed on 1"X 1" STI coupons at a down force of 8 PSI and 200 RPM platen/ 195 RPM carrier rotation for 500 seconds.

During the stage A, the COF continuously goes down after the initial high at touch down. Another CMP process run was performed and stopped before completion of Stage A. Based upon the previous discussion, it can be thus hypothesized that progressive decrease of COF during the first stage corresponds to SiO_2 material removal. As COF is a characteristic of particular material for the given set of polishing conditions and consumables, after complete removal of SiO_2, and exposure on the nitride regions, there is a change in the COF. This transition can be seen to reach after 58 seconds for the polishing run reported in Fig. 3. 13.

For exposure of Si_3N_4, the step height of the oxide has to be removed, along the surrounding excess field oxide. The height reduction was approximated to 400 nm and it implied that SiO_2 material removal rate (MRR) during the process run was approximately to 400 nm and that implied that SiO2 material removal rate (MRR) during the process run was 400 nm/ min. Further polishing of sample coupon showed that CMP of Si_3N_4 produced 80 nm/min MRR. Thus the oxide to nitride selectivity of the slurry at the given process condition was found to be around 5:1. This selectivity ratio is in agreement with the industry standards [115].

المنارة للاستشارات
www.manaraa.com

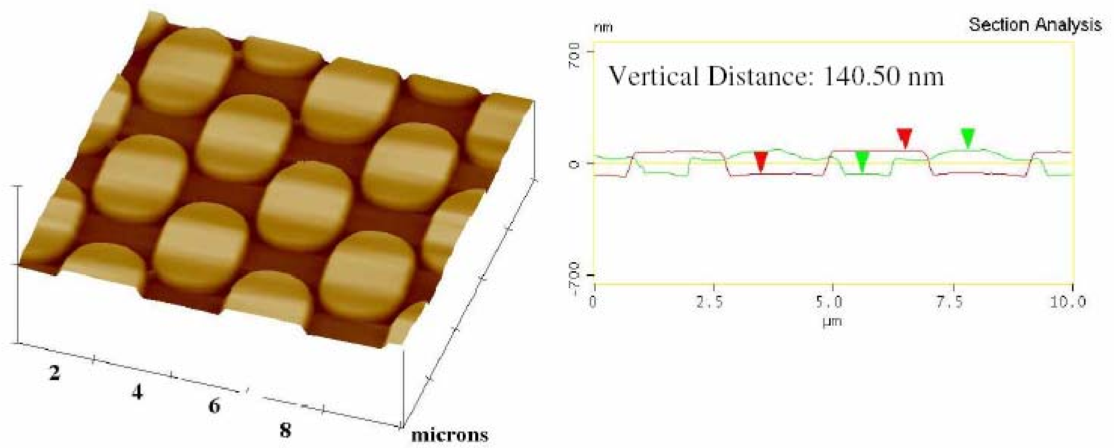

Fig. 3.14 Ex-situ 3D AFM Image of the Evaluated STI Structure with Reduced Step Height before Termination of Stage A (ref. Fig. 3.13)

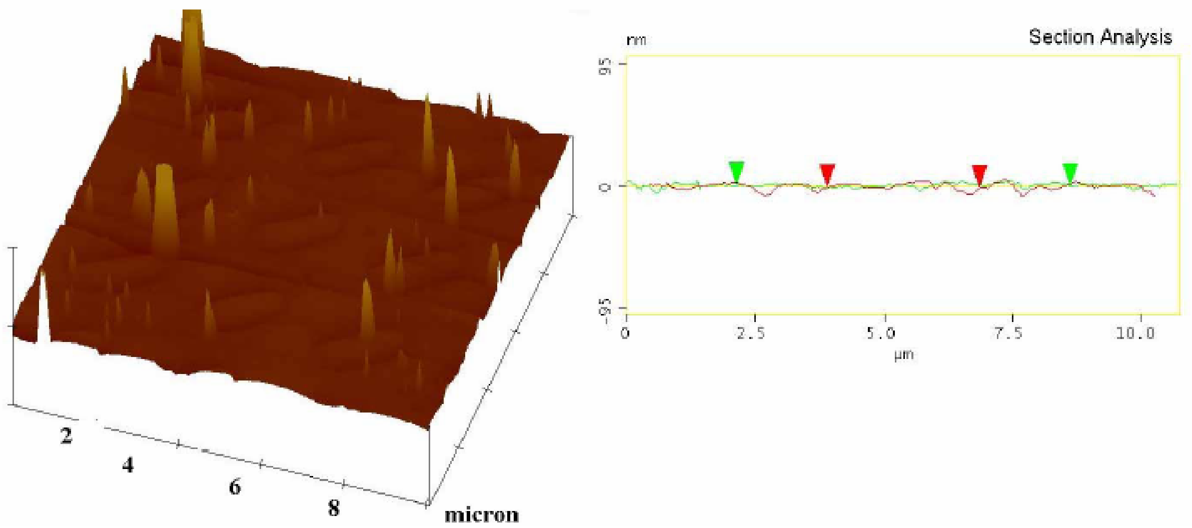

Fig. 3.15 Ex-situ 3D AFM Image of the Evaluated STI Structure after Process End Point just after Beginning of Stage B (ref. Fig. 3.15)

المنارة للاستشارات
www.manaraa.com

Another polishing run was performed till the process end point was reached (ref Fig. 3.13) and COF transition was observed. The sample coupon polished just until the beginning of Stage B was characterized ex-situ using AFM as shown in Fig. 3.14. It can be seen from Fig. 3.15 that, the nitride regions on the surface of the samples are exposed. This shows that the CMP process has reached its end point due to the complete removal of the field oxide. The "spikes" on the surface of the AFM 3D image are due to the particle adhesion. The particles adhered to the surface due to non availability of an efficient post CMP set up. The AFM section analysis shows a planar surface with and surface variations can be primarily attributed to the surface roughness. The evaluated COF during the entire stage B is a combination of the COF of nitride and oxide. With progressive decrease of nitride layer during CMP, the value of COF tends to increase till nitride is completely removed and oxide is exposed. To evaluate the repeatability of the hypothesis, CMP runs were performed at different values of down pressure and platen rotation. The data of the two of such trials performed at a down pressure of 4 PSI, 200 RPM platen rotation and 195 RPM carrier rotation is shown in Fig. 3.16. It can be seen from the figure that the CMP process end point occurs at 200 sec. for both process trials. Also the variation of COF follows a similar trend for both the trials. Thus it can be inferred that for the given process conditions and parameters, the process end point is reached at almost a similar time with in margin of acceptable error. The spikes in the COF data could be attributed to the noise during data collection. In order to filter the noise, obtained sharp transitions of end point, and study the "events" such as microscratching, dishing, erosion etc., during the process, the COF data needs to be further filtered using specialized signal processing filters. As the COF is data is non

المنارة للاستشارات
www.manaraa.com

stationary and even random to some extent (depending upon process defects or "events"), the COF signal has to be filtered in time as well as frequency domain. Wavelet based techniques have been found appropriate for sharp end point detection from using COF [116].

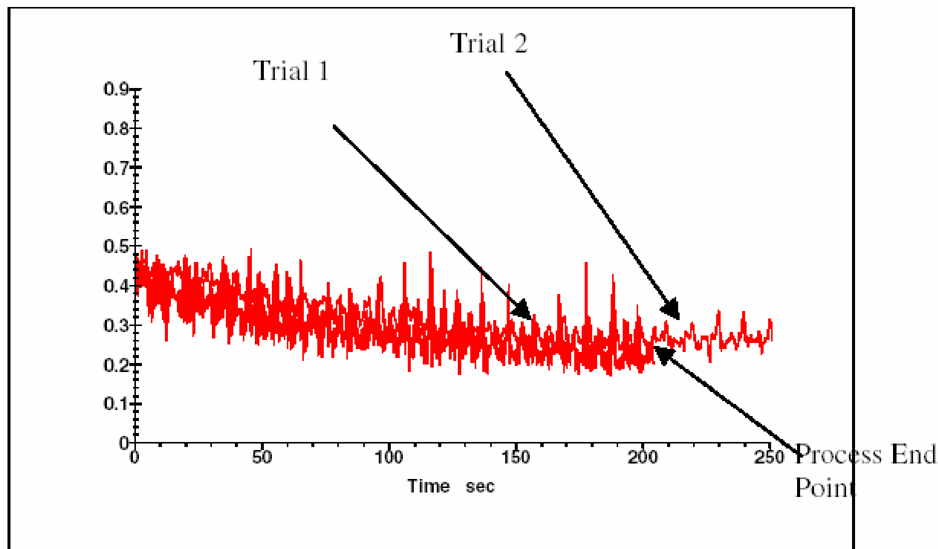

Fig. 3.16 In-situ data for 2 Trial Runs Shown to Demonstrate repeatability

Thus, it can be concluded from this study that real time monitoring of the CMP process can give valuable information which otherwise would need ex-situ metrology for evaluation. The values of COF being the "signature" of a particular pattern, material, pad, slurry and polishing conditions can be used as a fingerprint of a particular STI CMP process run. The work could be further extended in evaluating different pattern densities and different High Selectivity Slurries for STI CMP.

المنارة للاستشارات
www.manaraa.com

3.7 Delamination during CMP

The next generation low-κ materials are generally porous in nature and poor adhesion of dielectrics in a stack may result in delamination during the CMP process. Loading forces and rotation rates may also affect the reliability of the structure. Delamination can occur due to either: 1) adhesive failure at the low-κ and barrier layer interface, 2) failure within the low-κ material, or3) failure of the cap layer and low-κ interface. The process conditions must be adjusted in such a way that the overall hardness of the pad surface does not cause the aforementioned defects. It has been found that the density and size of abrasives along with the CMP process conditions have a strong effect on delamination during material planarization [117].

To understand and demonstrate the phenomenon of delamination, three different types of materials namely: 1) Patterned Cu samples with low-k A (A) (k~<2), 2) Patterned Cu samples with low-k B (B) (k~2.0), 3) Patterned Cu samples with SiO2 (TEOS) (k~4.0). Henceforth, these samples will be referred to as ACL, BCL, and TC respectively. Small coupons (2cm X 2cm) of samples were used to polish on either 6” or 9.5” pad coupon at different rotation of platen (0.2 to 1.5 m/s) and down force (1-10 PSI). Upper specimen was allowed to oscillate back and forth by 5 mm (47.5-52.5 mm) with a speed of 1 mm/s. Polishing slurry was fed into the interface continuously with the rate of 55 ml/min. On some occasions, tests were stopped before 300 sec due to high vibration and sample holder rotation. Slider movement for these experiments were 50±2.5 with a velocity 1 mm/s. Slurry flow was fixed at 55 ml/min. Polishing pad was a perforated IC1000/SubaIV while alumina based Cu selective slurry was fed continuously at the center of the pad.

المنارة للاستشارات
www.manaraa.com

Fig. 3.18(a) shows the AE signal variation while polishing with active upper rotation and Fig. 3.18 (b) shows the optical picture of the coupons after polishing. As it is seen for the samples polished with non upper rotational machine, highest AE signal is recorded for sample ACL and lowest signal for sample TEOS while a little smaller value is recorded for sample B than sample A. As sample ACL consists of Cu-ultra low-k samples with lowest k values, delamination may be more for this sample. It can be seen from Fig. 3.18 (b) samples get polished more uniformly with an upper rotation whereas samples gets more polished at the leading edge only for no upper rotation. From the samples it could also be seen that all the ACL and BCL samples are delaminating whereas TEOS has no sign of delamination.

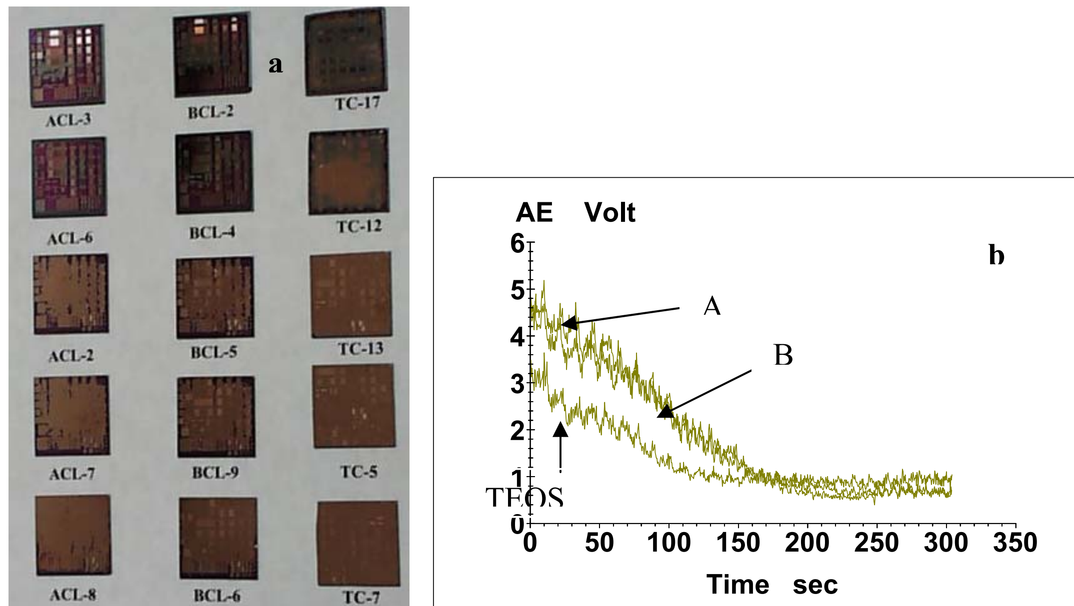

Fig. 3.17 a) Picture of Sample Coupons ACL, BCL, and TC after Polishing, b) Variation of AE signal of Three Different Samples

Further analysis of the samples with SEM, shown in Fig. 3.18, reveals that

www.manaraa.com

during the process Cu either gets peeled off or delaminated. Even delamination of underlying interlayer dielectric films could be seen. In all conditions, and experimental setups AE signal was higher for sample A and B than TEOS. Also, sample ACL produced more AE signal than sample BCL. It is prudent to mention that the only difference among the three samples is the underlying ultra low-k ILD film. High AE for ACL and BCL sample may be an indication of delamination of Cu from barrier and ILD interface. As Low-k B has slightly higher k values, which implies better mechanical strength, sample B shows better resistance to the CMP process. Lower magnitude of AE for sample BCL than sample ACL is the reason for this conclusion.

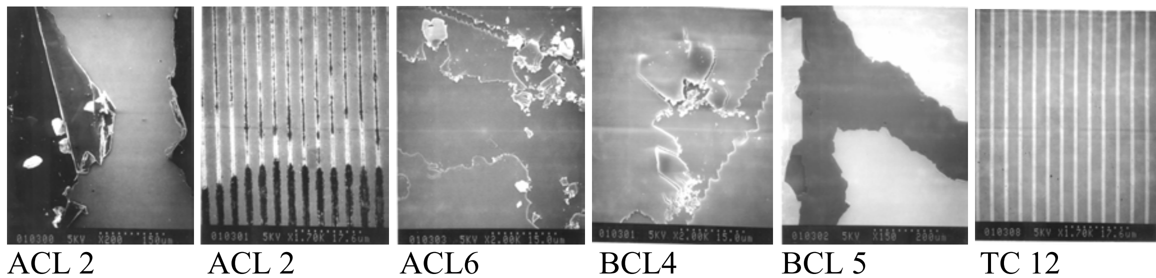

Fig. 3.18 SEM Micrographs Showing of Delamination of Different ACL, BCL Samples and No Delamination for TC Sample

Severe delamination or scratching on the surface could be monitored with the AE sensor, which produces spikes during the unusual polishing. Two ACL samples were run in the same conditions along with a TEOS sample. The expanded AE signals for all three samples are shown in Fig 3.19(a). Optical and SEM picture of the sample coupons are also shown in Fig. 3.19 (b) and (c). It can be seen from Fig. 3.19 (a) that several

www.manaraa.com

spikes occur for the sample with visible scratch on it. AE signal for TEOS shows very smooth and reduced noise level.

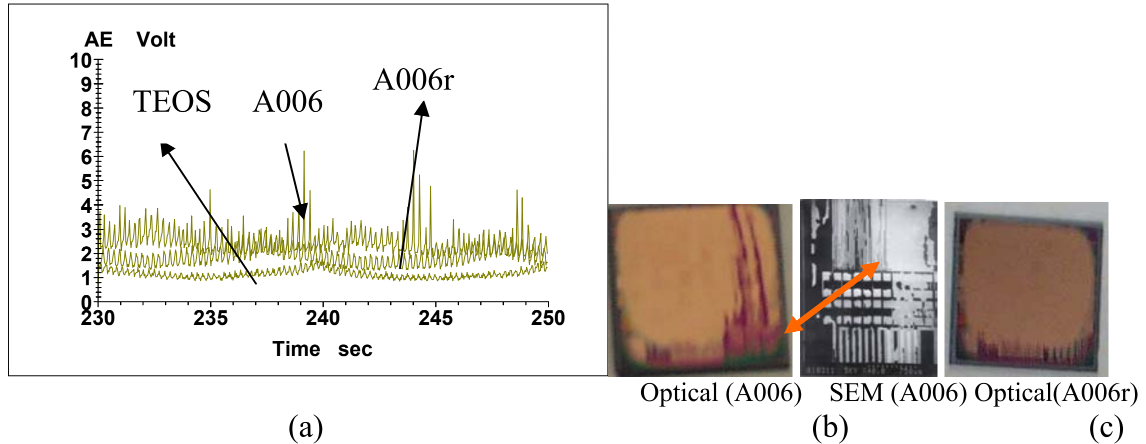

Fig. 3.19 (a) Variation of AE Signal during Polishing in the Time Interval of 230 – 250 s for Three Different Samples. Peaks are Seen for Sample ACL006, (b) Picture of Sample ACL006 and (c) Picture of Sample A006r

As mentioned earlier, the AE signal monitors the elastic acoustic wave in the ultrasound range during the CMP process. The shear generated by the down pressure and platen rotation brings about a strain in the thin film that is being polished and thus is also responsible for material removal. If the shear force is sufficient enough to overcome the interfacial adhesion of the thin film and the buried layer, the interfacial adhesion energy is dissipated in the form of acoustic vibration, besides other modes. This excessive emission of acoustic energy during polishing due to interfacial delamination is also sensed by the AE sensor. This results in the higher magnitude of AE signal in the event of delamination during the CMP process. In-situ monitoring of the AE signal during

المنارة للاستشارات
www.manaraa.com

CMP can thus give a qualitative estimation of delamination. Filtering of AE sensor data using frequency and time domain filtering (Wavelet based approach) can provide further meaningful information of the CMP process. In-situ isolation and quantification of the phenomenon of delamination may also be helpful in setting up a feed back mechanism which based upon statistical process control principles. Work related to Wavelet based AE signal filtering and analysis has been published in literature [118].

3.8 Other CMP Defects

Besides, delamination and faulty end point detection, several defects plague the process of CMP. The defect of microscratching results in the event of indentation or impingement of abrasive being deeper than the modified surface. Excessive surface passivation during polishing results in the predominantly mechanical removal of material and reduces the MRR during CMP. The loss in global planarity and poor surface finish that my sometimes result after CMP can have severe implications on the subsequent lithography step. Due to these reasons, it is important to understand the behavior of candidate materials from a CMP perspective and understand the challenges surrounding the successful integration of these materials. These and allied issues will be discussed in the subsequent chapter.

المنارة للاستشارات
www.manaraa.com

CHAPTER FOUR

PROPERTIES OF INTERCONNECT MATERIALS

4.1 Need for Evaluation of Material Properties

As elaborately discussed in Chapter1, there is a general agreement on the choice of Cu as the interconnect material for subsequent generations of microprocessors for the time being. However, integration of Cu alone (without taking the low-k dielectric into consideration) in the damascene process also comes with its share of challenges. Copper is typically much softer (microhardness: ~ 80 Kg/mm^2; Mohs scale: 2.5) than the conventional materials presently being used (tungsten and silica) in the interconnect CMP technology. This is in sharp contrast with the slurry abrasives made up of silica (hardness: 1200 kg/mm^2; Mohs scale: 6-7) or alumina (hardness: 2000 kg/mm^2; Mohs scale: 9). Hence, use of these abrasives results in formation of pits, craters, micro and macro scratches on the surface after CMP [6]. Before developing a CMP process for Cu, one has to evaluate the tribological properties of Cu under different process conditions. Also, certain peculiar traits Cu such as self annealing and varying impact of post electroplating annealing also need to be considered before implementation of Cu. Besides Cu, the polishing performance other materials such barrier layer Ta or TaN and different novel low- k materials is also important to determine the process CMP process recipe. Several low-κ materials do not meet thermal, mechanical and electrical requirements for

المنارة للاستشارات
www.manaraa.com

their integration with metal in the damascene structure. For CMP applications, low-κ materials have to be strong enough to prevent delamination and mechanical breakdown. Due to all these reasons, it is important to devote some part of studies performed on materials from a CMP to their reliability issues which may surface during or after processing. In this chapter will study the properties of different materials that potentially may undergo CMP in the future. For this, we will elaborately discuss the impact of multistage annealing on the properties that may have implications for Cu processing. Also we will understand the effect of decreasing dielectric constant and its implication on the mechanical and tribological properties of low k materials.

4.2 Effect of Annealing on Copper

Electroplated Cu films undergo a structural transition even at room temperature, which involves grain growth and texture changes [119, 120]. This so-called self-annealing process takes place over a period of hours or days after the deposition. Its kinetics depends on various deposition and post-deposition parameters such as electrolyte composition, current density, film thickness, seed layer composition, substrate morphology, annealing temperature, etc. [121-129]. This phenomenon, which leads to a dramatic drop of the resistivity over time, is associated with evolution of the microstructure at room temperature. The self-annealing for EP Cu films has become a constraint for reliability and reproducibility of Cu interconnect process, because changes of grain size and hardness have influence on electromigration and CMP process [130, 131].

المنارة للاستشارات
www.manaraa.com

Table 4. Details of the Samples Undergoing Two Stage Annealing

Sample #	Oxide (nm)	Barrier (nm)	PVD Cu (nm)	EP Cu (nm)	Aging	1st Anneal	2nd Anneal
1	500	30	150	No	No	No	No
2	500	30	150	500	7days in air	150˚C, 60min	250˚C, 60min
3	500	30	150	500	7days in air	200˚C, 60min	250˚C, 60min
4	500	30	150	500	7days in air	250˚C, 60min	No
5	500	30	150	500	No	150˚C, 60min	250˚C, 60min
6	500	30	150	500	No	200˚C, 60min	250˚C, 60min
7	500	30	150	500	No	250˚C, 60min	No

For most reliability tests, knowledge of the thin film constitutive mechanical behavior is required. Mechanical properties of thin films often differ from those of the bulk materials. Hence there is a need for evaluation of mechanical properties at nanoscale using state-of-the-art evaluation techniques like Nanoindentation [132, 133]. To

www.manaraa.com

understand the impact of multi-stage annealing on the material properties of Cu, investigations have been focused on the Si/SiO_2/TaN/SeedCu/EPCu thin film stack annealed at different stages with different temperatures and duration. The details of the evaluated samples can be seen Table 4.1.

Grazing incident x-ray diffraction pattern showed stronger x-ray reflections form Cu (111) and (220) planes but weaker reflections from (200), (311) and (222) planes in all the electroplated Cu samples. This implies that all the Cu films have preferential crystallization along the Cu (111) and (220) planes as compared to (200), (311) and (222) planes. The Cu samples that did not undergo multi-step annealing, had lower hardness and modulus values. Nanoindentation was performed on all the samples using the continuous stiffness measurement (CSM) technique. The elastic modulus varied from 121 to 132 GPa while the hardness varied from 1 to 1.3 GPa depending on the annealing conditions. The surface morphology and roughness of Cu films were characterized using atomic force microscopy. The tribological properties of the copper films were measured using the Bench Top CMP (chemical mechanical polishing) tester. Nanoindentation was performed on the samples after CMP and an increase in hardness and modulus was observed. This may be attributed to the work hardening of the Cu films during CMP.

In addition, the hardness and modulus values increase with the increase in temperature of the first-step annealing. Samples annealed in one stage (sample 4 and 7) show better mechanical properties, which may be due to higher (111) oriented crystallites. The Cu seed layer is very smooth and has lower COF and AE values during CMP. No distinctive trend is found for the COF and AE values for annealed Cu samples.

المنارة للاستشارات
www.manaraa.com

Improved mechanical properties on post-CMP samples may indicate the work hardening of the Cu surface due to the high shear force applied on the sample surface during CMP. The surface roughness of annealed Cu samples increased with the increase in temperature of the first-step annealing. Annealing at higher temperature may reveal further insight of the microstructural evolution of electroplated Cu films, which is the key in successful implementation of Cu as an interconnect material. These results have been reported in literature and though these properties do have a bearing on the CMP performance of Cu, this chapter will focus on the interfacial adhesion of Cu and TaN barrier layer which directly dictates the maximum amount of down force and platen rotation during CMP process.

4.3 Significance of Interfacial Reliability in Damascene Structures

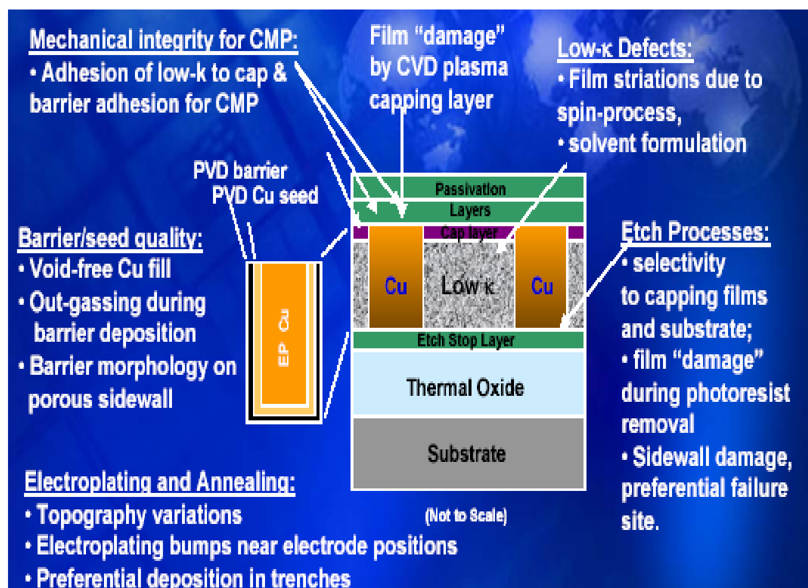

Fig. 4.1 Challenges Surrounding Implementation of Novel Low k Materials Cu in a Damascene Structure (Courtesy: Jeffery Lee, Intel Corporation)

المنارة للاستشارات
www.manaraa.com

Normally in copper damascene process, low-*k* materials are protected from exposure to CMP environment. In dual-damascene Cu-interconnect system CMP is a two step process. In first step Cu is being polished with a copper selective slurry and barrier layer, which acts as a protecting layer of low-*k* system. In second step barrier layer is being removed with barrier selective slurry and a hard inorganic mask/dielectric capping layer is typically used to provide mechanical support and prevent interaction between the slurry and the low-*k* materials. Fig. 4.1 outlines some of the significant challenges on the roadmap before successful implementation of damascene and dual damascene structures containing next generation ultra low k materials. The challenge pertaining to the mechanical integrity of the interface of the constituent thin films and the effect of annealing on the same has been elaborately discussed in this chapter.

4.4 Effect of Annealing on Cu-TaN interface

To implement novel materials in the MLM schemes for next generation interconnect systems, the interfacial reliability of material thin films needs to be extensively studied. In this direction, we have evaluated the effect of annealing on the metal-barrier interface. To demonstrate the impact of multi-stage annealing on Cu-TaN interface, the aforementioned stack (Si/SiO_2/TaN/SeedCu/EPCu thin film) with different In this research, interfacial reliability of blanket samples of Cu (interconnect wiring material) /TaN (barrier / adhesion layer) / Tetraethylorthosilicate (TEOS) (dielectric) has been evaluated. Also, Cu has been annealed at different temperature and duration to study the effect of annealing on the interface. Even though studies have revealed that, the problem of delamination is more teething at the low k- cap layer interface [134]; this

المنارة للاستشارات
www.manaraa.com

study aims at demonstrating a proof of concept for improvement of interfacial reliability of Cu-barrier interface by treatments such as annealing after self annealing of Cu is mostly complete [119]. The details of the samples evaluated during this investigation are shown in Table 4.2.

Table 4.2 Details of the Samples Subjected to Interfacial Studies

Sample Designation	Thickness Cu (seed + EP)	Aging	1st Anneal (N_2 atmosphere)	2nd Anneal (N_2 atmosphere)
1	6500 Å	7days in air	150°C , 60min	250° C, 60min
2	6500 Å	7days in air	200°C , 60min	250° C, 60min
3	6500 Å	7days in air	250°C , 60min	No
4	11500 Å	7days in air	150°C , 60min	250° C, 60min
5	11500 Å	7days in air	200°C , 60min	250° C, 60min
6	11500 Å	7days in air	250°C , 60min	No

4.5 Techniques for Interfacial Evaluation of Thin Films

Before proceeding to study the impact of annealing on thin film interface, it is important to understand the techniques used to evaluate the interfacial adhesion and fracture toughness. During this study, the interfacial adhesion was qualitative evaluated using the four point bend technique. The results of this technique were compared to qualitative evaluation of interfacial adhesion using a novel nanoscratch technique developed by us.

المنارة للاستشارات
www.manaraa.com

4.5.1 Four Point Bend Technique

The four point bending technique is commonly used to evaluate the thin film stacks in microelectronics applications. The technique involves extensive sample preparation and post failure analysis [135-138]. The sample preparation procedure includes dicing, curing and notching, which may induce permanent damage into soft and weak materials. Due to the extensive human element involved in the entire testing setup, there is a high possibility of erroneous results. In order to correlate the thin film interface performance with the CMP results, large statistical set of samples need to be evaluated for accurate estimation of the interfacial adhesion energy of the thin films in a stack.

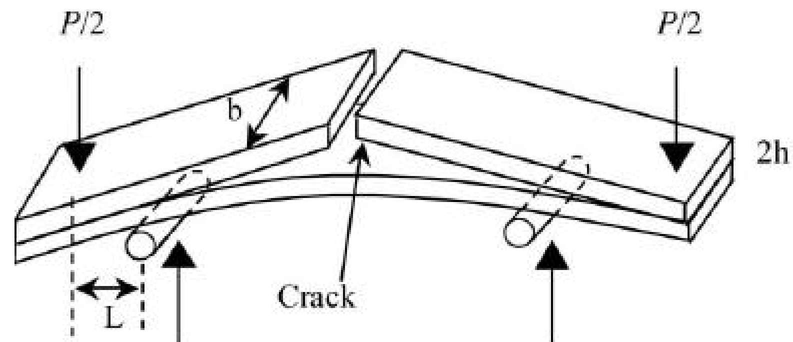

Fig. 4.2 Schematic of Four Point Bend Test (University of California, Santa Barabara) Set Up [137, 138]

In the test, two 60 mm X 10 mm specimens of with the aforementioned thin films on them were bonded to each other using an epoxy resin. The samples were cut using a diamond coated dicing saw and epoxy was coated manually. The samples with the sandwiched epoxy were then cured for 2 hours and later notched used a dicing up to a

www.manaraa.com

depth approximately equal to one third of the thickness of the substrate .The samples were then gradually loaded in the conventional four point bend set up, the details of which are already published [135-138].The upper substrate is notched up to roughly one third of its thickness. The sandwich specimen was gradually loaded in the set up which is schematically shown in Fig. 4.2.

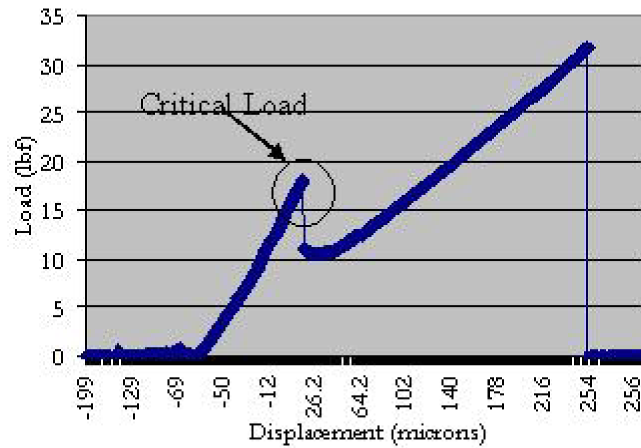

Fig. 4.3 Variation of Load (lbf) Vs Displacement (microns) during a Four Point Bend Test

When the critical load is reached, the crack propagates through the substrates and kinks through the interface having the lowest interfacial adhesion energy. This can be clearly seen from the load Vs displacement curve obtained from the test as seen in Fig. 4.3. The interfacial adhesion energy (G) of the weakest interface is calculated using the critical load (P) of interfacial fracture from the equation 4.1 [137].

$$G = \frac{2l(1-v^2)P^2L^2}{16Eb^2h^3} \quad (4.1)$$

المنارة للاستشارات
www.manaraa.com

In equation 4.1, E is the Young's modulus of Cu, ν is the Poisson's ration, l is the length of the entire specimen and L, b, h are shown in the Fig 4.2. The interfacial failure domain analysis was performed using the Elemental Dispersion Spectroscopy (EDS). The EDS was performed on a 10 lt EDAX Dewar standard EDS detector couples with a Hitachi Scanning Electron Microscopy (SEM). EDS is used to detect the elemental composition of the surface exposed after failure of the specimen due to crack propagation. The results from EDS analysis are thus helpful in determining the weakest interface in the given specimen.

4.5.2 Nanoscratch Tests

The nanoscratch technique has been developed by fabricating a modified suspension and set up on the CETR Bench Top CMP tester. This technique mostly involves a sharp diamond tip (in this case Berkovich indenter tip), which directly processes the surface of material. The diamond tip may have different shapes such as cylindrical, conical, three or four sided pyramidal, rounded etc. The variation of the frictional forces induced is monitored in-situ or ex-situ to analyze the failure of the thin film being evaluated [139]. A standard three-sided Berkovich tip has been utilized on a modified setup incorporated in the CMP tester described before. An edge of the pyramid will cut through the material surface to finish a scratch test. The schematic of the proposed scratch testing setup is shown in Fig. 4.4. The tip has been will be mounted on a stainless steel holder with a custom designed housing. The holder has been then fit into a CETR tester with a specialized suspension. A light-duty sensor setup has been used during testing as the magnitude of down force applied during nanoscratch testing is significantly

المنارة للاستشارات
www.manaraa.com

lower than that applied during CMP. The light duty suspension gives better resolution for monitoring and controlling the down force and frictional force. The variation of AE and COF signals upon film delamination will produce an in-situ qualitative metrology of interfacial adhesion. The load at which the onset of delamination is recorded has been termed as the "critical load". The parametric optimization of nanoscratch testing will include the study of the effect of: 1) down loading, 2) scratch tip velocity, 3) thin film thickness, 4) thin film mechanical properties (Hardness and Young's Modulus) on the magnitude of critical load obtained from the scratch test.

The scratch tests were started by downward loading (F_z) of 5 gm on the tip and progressively increasing the load at the rate of 2 gm /sec. The ultimate load used for each test was 105 gm. The linear velocity of the scratch tip was kept constant at 2 mm/ sec. The linear variation of down force, frictional force, lateral force and acoustic emission (AE) sensor signal with time were monitored in situ. When critical load of the thin film delamination was reached, the AE sensor signal showed a significant increase in magnitude while there were prominent changes in the gradient of lateral force and frictional force. It was thus concluded, that the area of instability of these aforementioned signals represented the delamination process of the thin film from the underlying film from the stack (in this case, delamination of Cu from TaN). The load at which the AE signal, frictional force (F_f) and lateral force (F_x) again deviate from their trend of variation initially followed during the test, was assumed to the critical load P for the thin film interface. When F_f, F_x, and AE regain stability, the process of delamination is presumed to be complete.

المنارة للاستشارات
www.manaraa.com

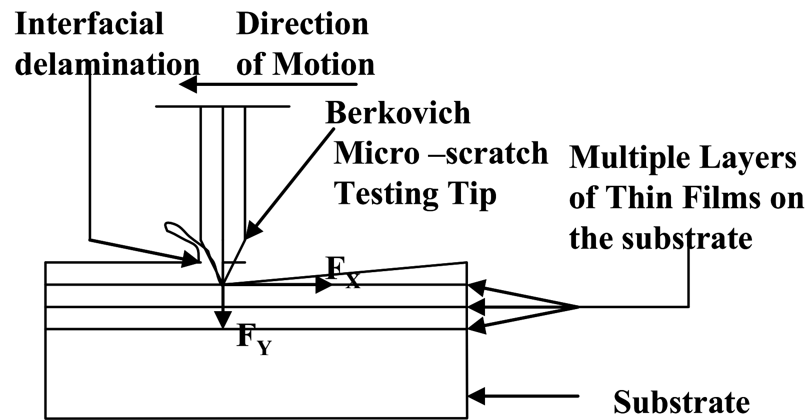

Fig. 4.4 Schematic of the Nanoscratch Testing Setup

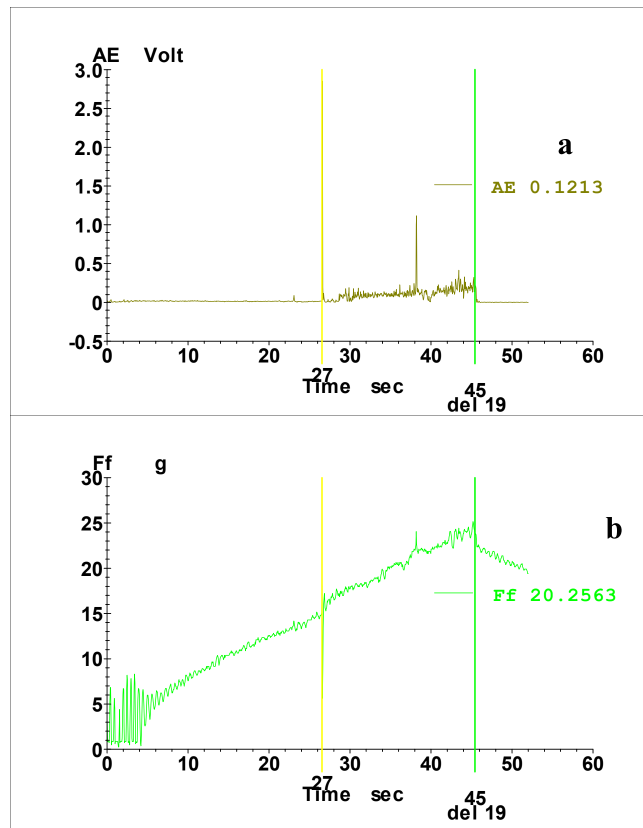

Fig. 4.5 Raw Data Showing the Variation of a) Acoustic Emission (AE), d) Frictional Force (F_f) with Time during a Scratch Test. (Sample 1 at Linearly Increasing Downward Force of 2 gm/sec Linear Velocity of 0.2 mm/sec)

www.manaraa.com

The raw data out put and variation of the different parameters such as: 1) variation of AE signal with time, and 2) variation of monitored during the scratch tests can be seen in Fig 4.5 (a, b). The critical load at which the delamination occurs is a measure of the practical work of adhesion (W) which can be evaluated using equation 3. In fig. 4.5 (a, b), it can be seen that delamination started after 27 seconds of loading at the downward 59 gm. The Cu thin film completely delaminated after 46 sec and the tip, then began its movement on Ta surface.

4.5.2.1 Failure Domain Analysis of Nanoscratch Tests

The increase in AE near the end of scratch tests reveals that there is some phenomenon occurring which brings about a significant dissipation of energy in form of an elastic wave in the ultrasound frequency range. Though, we had observed delamination of thin film interface that corresponded to the increase in AE signals during CMP, there was need conclusively prove that AE signal increase was due to delamination only and other phenomena such as crack initiation and propagation due to loading, or buckling of the buried layer, or purely cohesive failure of the material was not causing the increase in AE signals. For this purpose, failure domain analysis of the nanoscratch tests was performed using SEM/Auger Spectroscopy and FIB/SEM analysis.

4.5.2.1.1 SEM/Auger Spectroscopy Analysis

In order to conclusively prove that the increase in AE signal at the end of the scratch test is due to the delamination of the thin film from the buried layer, the surface SEM of the nanoscratch was performed (Fig. 4.6 a, b). Two points on the surface of the

المنارة للاستشارات
www.manaraa.com

nanoscratch were chosen as seen from Fig. 4.6. The first point (point 1 in Fig. 4.6 a) was chosen to evaluate the chemical composition of the surface before the significant penetration of the scratch tip beneath the film surface. The point 2 (Fig. 4.6 b) was chosen at a location where the delamination was complete (just after the elevation in the magnitude of the AE signal subsided). Auger electron spectroscopy (AES) analysis was carried on point 1 and 2 using the as received samples. An Ar back sputtering step was performed and the variation of elemental peak intensity with the respective binding energy was re-plotted. Similarly Auger analysis was performed on point 2 at the end of the scratch, before and after the Ar back sputtering. Table 4.3 shows the percentage elemental composition of points 1 and 2 before and after Ar back sputtering.

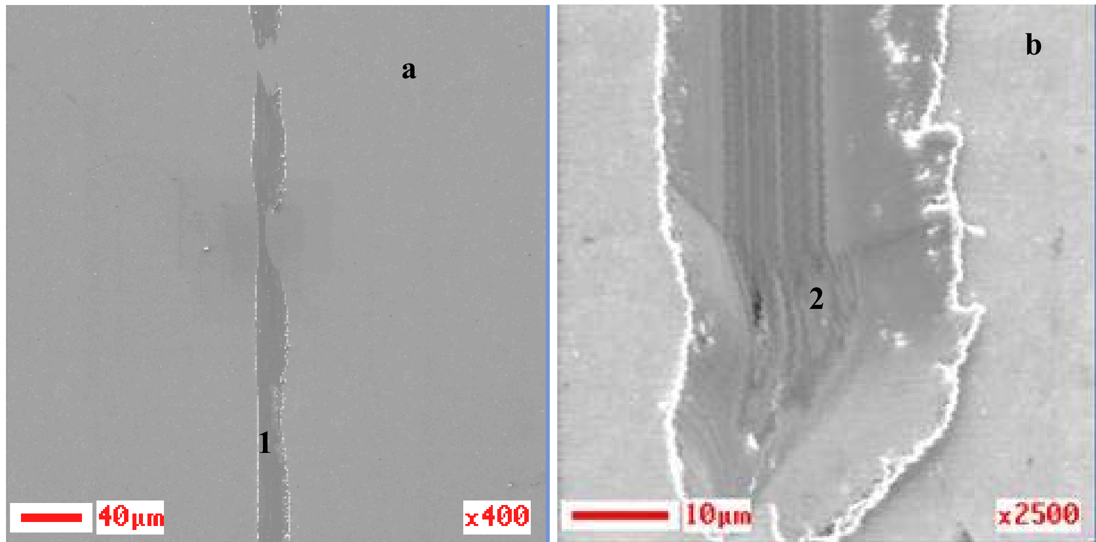

Fig. 4.6 Surface SEM of the Nanoscratch at Region a) at the Initial Stages of Microscratch, and b) Upon Completion of Delamination

المنارة للاستشارات
www.manaraa.com

Table 4.3 Relative Concentration of the Elements (at.%) on Scratch Surface

Element	C (0.128)	N (0.158)	O (0.371)	Cu (0.574)	Ta (0.194)
As-received					
Point 1	42	5	22	31	-
Point 2	30	8	37	3	22
After 12 s sputter					
Point 1	-	-	19	81	-
Point 2	15	22	9	14	40

It can be seen from Table 4.3 that when Auger analysis is done on the as received sample at point 1, there is an evidence of metallic Cu along with Carbon and oxygen on the surface. The presence of C could be traced on to surface organic contamination (in appropriate handling of the sample outside a clean room environment) which the presence oxygen is due to formation of passivating oxide of Cu. Upon back sputtering, the organic impurities are removed and presence of predominantly metallic copper with some oxide formation is seen. The Auger analysis performed at point 2 on the as received sample suggests that there is significant reduction in the metallic Cu on the surface. The surface is then comprised of predominantly Ta, which is consistent with the fact that TaN is the barrier layer used for Cu in the evaluated thin film stack. The presence of C again on the surface could be attributed to the impurities on the surface. Ar back sputtering of the region denoted at point shows that the extent on Ta and N on the surface increases showing that the tip moves on the barrier layer after the completion of

المنارة للاستشارات
www.manaraa.com

delamination. The increase in the presence of Cu on the surface could be attributed to the re-deposition of Cu from the surrounding debris on the scratched surface.

4.5.2.1.2 FIB Cross section and SEM Analysis

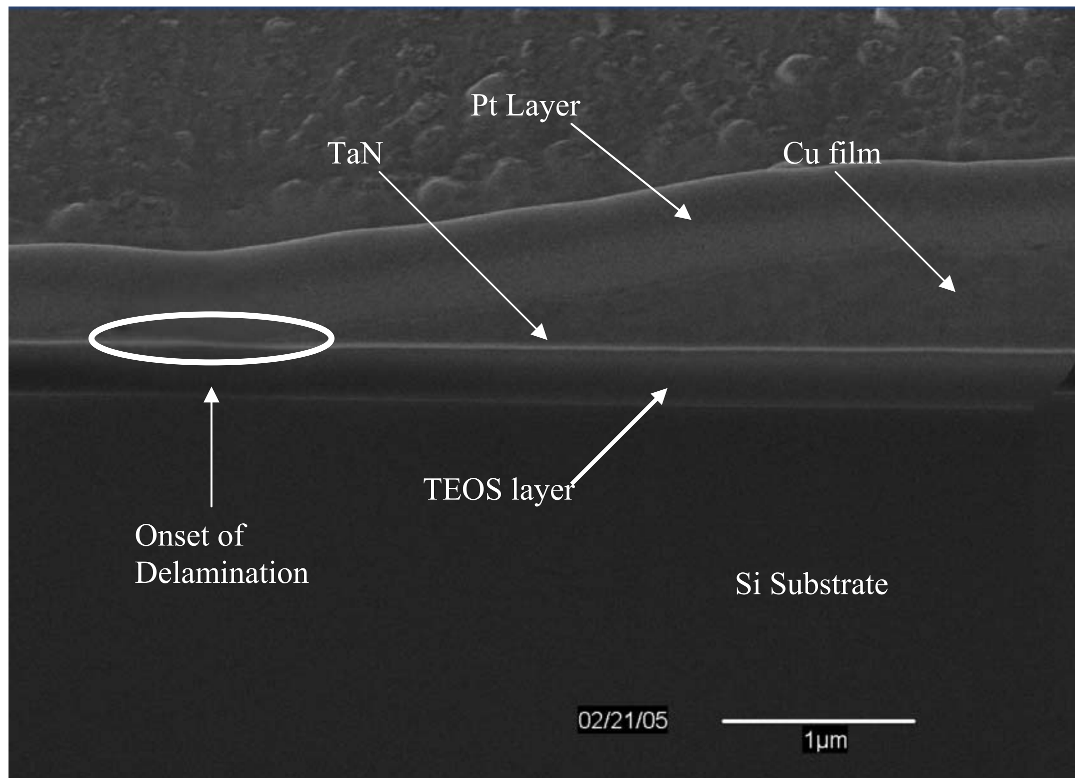

Fig. 4.7 FIB Cross-section and SEM Micrograph of the Thin Film Obtained a Region of Onset of Delamination

The Auger analysis proved that the scratch tip initially caused cohesive failure in Cu thin film by penetrating in it and then after delamination, the tip moved on the barrier thin film surface. However, in order to conclusive prove that the increase in AE signal did not result from phenomena such as buckling of the buried TaN or TEOS film,

المنارة للاستشارات
www.manaraa.com

cross section FIB and SEM analysis was performed at the Cu-TaN interface at a region where delamination began occurring. Fig. 4.7 shows the SEM of the FIB cross section of the thin film stack obtained at the position at which there is on set of delamination.

It can be seen from Fig. 4.7 that there are no obvious signs of buckling of the buried TEOS layer. Also there does not seem any crack initiation of propagation in any of the thin film layers below Cu. It can be thus concluded that the elevation in the magnitude of the AE signal is due to the peeling of the Cu thin film from TaN interface, as shown in Fig. 4.7. There also a reorganization of the Cu thin film grains due to external crack initiation and propagation under down loading and lateral velocity (nano-scratching), however, this subject is a separate investigation in itself and is beyond the scope of this research.

4.6 Quantitative Evaluation of Thin Film Adhesion energy

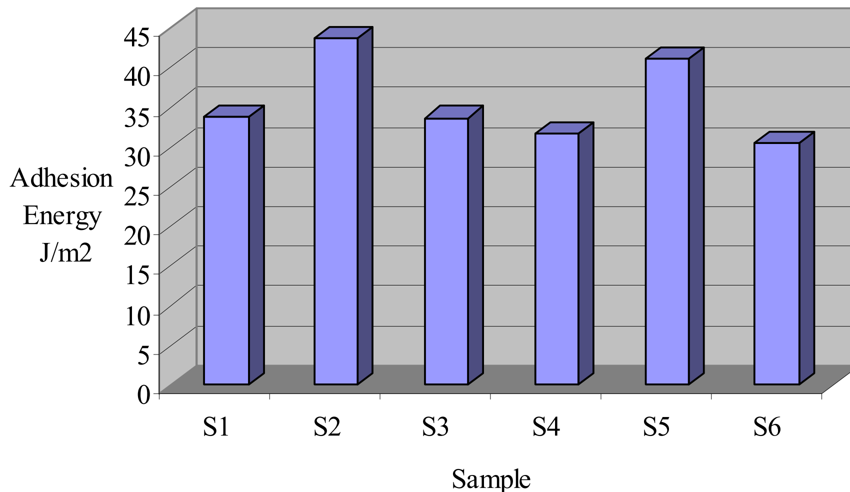

Fig. 4.8 Variation of Interfacial Adhesion Energy for the Different Samples Evaluated by Four Point Bend Technique

المنارة للاستشارات
www.manaraa.com

The results of the interfacial adhesion energy (G J/m^2) evaluated using the four point technique can be seen in Fig. 4.8. The sample dimensions were measured and substituted in equation 4.2 (ref. Fig. 4.2) for calculation of the adhesion energy for each of the sample. The average of 4 readings is shown as the adhesion energy for that particular sample in Fig 4.2. It can be seen from Fig. 4.2 that the interfacial adhesion energy does not show correlation with the Cu thin film thickness as the value of G in J/m^2 for sample 16 is seen smaller than sample 22 but the values of G for sample 21 is greater than sample 15. Figure 4.8 also shows that there is no significant difference in interfacial adhesion energy of samples that have been annealed at 150°C for 60min and later at 250° C for 60min, and samples which were annealed at 250° C for 60min and did not have a second annealing step. This held true for samples irrespective of their Cu thin film thickness. However, it can be seen that samples 2 and 5 showed markedly higher values of interfacial adhesion energy. These samples were annealed first at 200° C for 60min and the second stage annealing was done at 250° C for 60min. It can be thus concluded that duration of annealing along with temperature affected the interface. Annealing at a higher temperature as well as extended duration (200° C & 60min stage I and 250° C, 60min stage II), can bring about significant improvement in the interfacial adhesion. Even though optical evaluation of failed interface was sufficient to determine that the layer exposed was TaN failure domain analysis was done using EDS to reinforce this conclusion. The sample was subjected to EDS analysis and an elemental composition of the sample constituents was obtained. Although, due to the nature of the technique, constituent elements of all the thin films as well as substrate were obtained as results of EDS analysis, Fig. 4.9 shows the area which showed distinct presence of tantalum which

المنارة للاستشارات
www.manaraa.com

has been isolated for its distinct importance for the purpose of study. Apart from Ta, which existed in form of three different states (this goes on to show that Ta was combined with another element to form a compound in the thin film), elemental peaks of Si, O, C (impurities) and N were also observed (not seen in the Fig. 4.8). The element Cu was conspicuous by its absence. Taking all these factors in to consideration, it can be safely said that that thin film stack failed at the Cu-TaN interface.

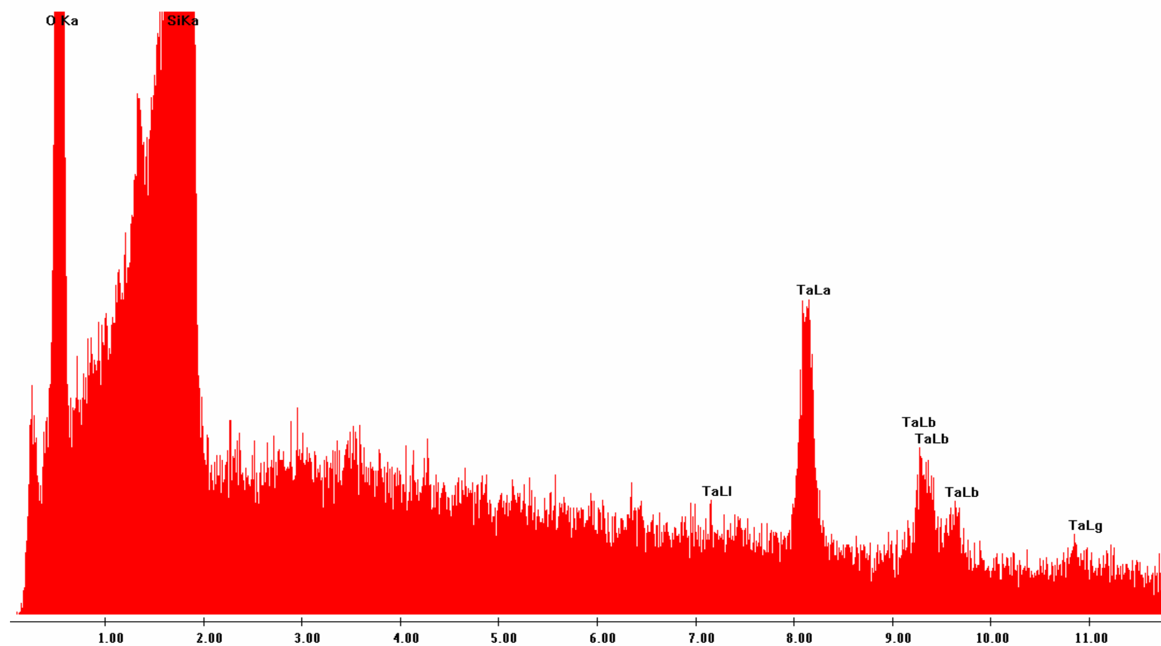

Fig 4.9 Elemental Dispersion Spectroscopy Analysis of the Failed Interface after Four Point Bend Analysis

www.manaraa.com

4.7 Qualitative Evaluation of Thin Film Adhesion energy

The interfacial adhesion was qualitatively evaluated using nanoscratch testing technique. In sharp contrast to the four point bending techniques discussed earlier, nanoscratch testing technique is fast, does not have excessive sample preparation time and has less chances of human error that might occur during bonding and notching the specimen before four point bend test. The variation of critical load for the candidate samples has been shown in Fig. 4.10. When the samples of a given Cu thin film thickness were compared, the critical load showed a higher value for sample that was annealed for 200° C & 60min in stage I and 250° C, 60min in stage II. There is a difference in the magnitude of the critical loading for sample with 650 nm Cu thickness and 1150 nm of Cu thickness could be attributed to the higher work done by the scratch tip to overcome the cohesive forces of a thicker film. The results of the scratch tests on the candidate samples also qualitatively showed the sample that were annealed for a relatively higher temperature and higher duration had an improved interfacial adhesion between Cu and TaN as compared to the other two samples. This is in agreement with quantitative evaluation of interfacial adhesion performed using four point bend test.

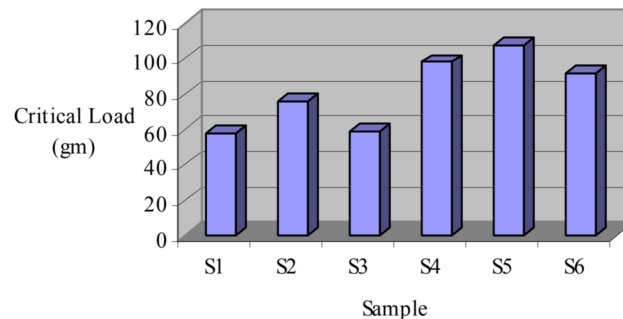

Fig. 4.10 Variation of Critical Load for Different Evaluated Samples obtained from the Nanoscratch Test

المنارة للاستشارات
www.manaraa.com

4.8 Low Dielectric Constant Materials (Low k Materials)

After evaluation of the Cu-TaN interface, the focus of study of material properties of potential materials undergoing CMP shifts to some candidate low k materials. CVD and spin-on methods are main deposition techniques of present generation low-*k* materials. Several spin-on low-*k* materials, like hydrogen silsesquioxane (HSQ), spin-on-glass (SOG), SiLK (trade mark of Dow Chemical Company), etc. have been studied [140]. Low-*k* dielectric materials can be categorized as follows: doped oxides (FSG, HSQ, MSQ and HOSP), organics (BCB, SiLK, FLARE and PAE-2), highly fluorinated materials (paryleneAF4, a-CF and PTFE), and porous materials (aerogel and xerogel) [140]. In some cases, combinations of these materials (for example, porous organics) are also being explored [140]. Silicon dioxide (SiO_2) has a dielectric constant of ∼4, while air is considered as the perfect insulator with a dielectric constant of ∼1. Porous materials can therefore achieve lower dielectric constants than the constituent materials [141]. Among many low-*k* candidates, however, only a few materials have shown all the required properties needed for integration into high-volume manufacturing processes.

Finding polymers with low-*k* value is a relatively easy task; but finding those with all the required chemical, mechanical, electrical and thermal properties for use in IC applications is more difficult. Proponents of CVD approaches, most notably carbon-doped siloxanes also known as organo-silicate glasses (OSGs) with *k* ranging below 2.5, claim the advantage of being able to reuse of existing tool sets and simpler integration due to the SiO_2-like structure of CVD siloxanes [142]. Alternatively, manufacturers of spin-on materials and spin-on equipments contend the better extendibility of future

المنارة للاستشارات
www.manaraa.com

generations' low-*k* dielectrics, especially in the sub-2.5 range when porous low-*k* materials will likely be used. Today, porous versions of many low-*k* spin-on materials are available for testing, whereas porous CVD low-*k* materials have yet to be demonstrated [142].

Most spin-on materials are organic polymers, some are inorganic and some are blends of the two. Their *k* values vary significantly from each other, depending on the material. However, in general the values are below 3.0. The semiconductor industry first broached the subject of new dielectrics in 1998 with the 0.18-µm circuitry that is now standard in high-end semiconductor chips like the Pentium 4. At this production node, manufacturers found a relatively easy answer for low-*k* material in fluorinated silicate glass (FSG), a CVD material created by doping traditional SiO_2 with fluorine from silicon tetra fluoride during the deposition [140].

4.8.1 CVD Based Low k Materials

Relative dielectric constant for conventional SiO_2 films is in the range of 3.9–4.6 at the frequency of 1 MHz. The values depend on the source materials and formation technique. Basically the dielectric constant is defined by the dielectric polarization, such as electronic polarization, ionic polarization and orientational polarization. Since the electronic polarization is basically defined by atomic radius, the molecular structure differences are essential. The dielectric constant is also increased by residual H–OH/or H–OH absorption, due to orientational polarization increment. One of the techniques to reduce the electronic polarization is to introduce an atom with a small atomic radius in the Si–O networks. Hydrogen (H), carbon (C) and fluorine (F) atoms are very effective

المنارة للاستشارات
www.manaraa.com

for this purpose. The binding energy of Si–F bond (129.3 kcal/mol) is higher than that of Si–O bond (88.2 kcal/mol), Si–F bond is thermally more stable. Therefore fluorination of SiO_2 films has been one of the main methods examined to reduce the dielectric constant of SiO_2 films [143]. Incorporation of fluorine in Si–O network causes a reduction of dielectric constant as a result of fluorine being the most electronegative and least polarizable element in the periodic table [144]. Additionally, precursors for depositing SiOF films are readily available and are inexpensive.

Several companies are developing low-*k* CVD films using a variety of carbon-containing precursors. The resulting organosilicate glass (OSG) films are also called carbon-doped silicon oxides (SiOC). The organic groups in OSGs invariably take the form of tetravalent silicon with a wide range of alkyl and alkoxy substitutions. In these films, the silicon–oxygen network seen in glass is occasionally interrupted, in a more or less homogeneous fashion, by the presence of organic functional groups, typically methyl ($–CH_3$) groups. Additionally, hydride (–H) substitution at silicon can also be present in the network. The film's lower *k* results due to these changes to the SiO_2 network and the reduced density of the OSG film relative to SiO_2. In typical CVD low-*k* films, 10–25% of the silicon atoms are substituted with organic groups. In amorphous OSG structure, the ratio of Si and carbon atom is typically 4:1 [145].

4.8.2 Spin On Low k Materials

The spin on deposition technique is particularly suited when good local planarization and gap fill is required for inter-metal dielectric. Both inorganic and organic films can be deposited by spin on methods and final structure of the film could be

المنارة للاستشارات
www.manaraa.com

amorphous or crystalline. The dielectric precursors are used in forma of “sol”. The thin film coating is performed by dispensing a liquid precursor on the center of the substrate which is spun on a spinner. The rotation of the spinner causes uniform dispersion of the solution. The resultant thin film is hard baked or soft baked and then sintered at an elevated temperature (300–400 °C). The sintering process ensures final cross-linking of polymer chains and results in mechanically stable thin film. Amorphous dielectric materials such as spin on glasses are coated using this method. A combination of hydrolysis in which there is a transition from Si–OR to Si–R functional groups takes place in presence of moisture and condensation process in which Si–O–Si structure is formed with elimination of H_2O to form the spin deposited film. The viscosity of the films increases sharply after spinning there by helping the film to settle on the substrate. Subsequently the gel is dried by baking or curing step [145].

In order to further reduce the dielectric constant of the ILD, porous films are made using spin on technique. The formation of more or less rigid skeleton before water extraction is important for formation of high porosity materials. The porosity can be induced in the material during the sol gel process or can be formed by using sacrificial nanoparticles or porogens. The details of various techniques to fabricate low-*k* dielectrics and methods to induce porosity have been extensively discussed in literature.

4.8.3 Potentially Feasible Low k Materials

Various oxide-based low-*k* materials were deposited using CVD as well as spin-on methods. Preparation technique and precursor gases for different types of doped and undoped oxides studied are briefly discussed in this section. Undoped silicon dioxide

المنارة للاستشارات
www.manaraa.com

(SiO_2 U) films were deposited on 8 in. Si wafer using PECVD method in a six-station sequential deposition system. The precursor gases were silane (SiH_4), nitrous oxide (N_2O) and nitrogen (N_2) and the substrate temperature was maintained at 400 °C.

SiOF is a fluorine-doped silicon dioxide film. It was deposited using inductively-coupled high-density plasma chemical vapor deposition (HDP CVD) method with SiF_4, SiH_4, O_2 and Ar at 400 °C. Details of the deposition method have been discussed earlier [146]. SiOF films grown by HDP CVD method has been shown to result in a film that has excellent film quality and gap fill characteristics [146, 147].

The dielectric film SiOC SP is a carbon-doped silicon dioxide, also known as carbon-doped siloxane, or organosilicate glass (OSG). This low-*k* film was grown on Si substrate using PECVD method at 400 °C in a six-station sequential deposition system. The precursor used in this process is a cyclic 1,3,5,7-tetramethylcyclotetrasiloxane (TMCTS). TMCTS is prepared through hydrolysis of methyldichlorosilane to firstly form a linear siloxane polymer that is end capped with trimethylsilyl groups.

Another carbon-doped low-*k* film (SiOC NSP) was deposited using a different and non-standard precursor tetramethylsilane gas, with N_2O and N_2 using PECVD method at 400 °C in a six-station sequential deposition system. It is similar to the film SiOC SP.

In order to investigate the difference in CVD deposited low-*k* with the spin-on low-*k* we have also used a carbon-doped oxide-based low-*k* (SiOC SO), deposited by spin-on method. SiOC SO is siloxane polymer-based material and is an organic and inorganic hybrid. As this dielectric film was deposited by a spin-on method, it has flowable and planarizing characteristics.

المنارة للاستشارات
www.manaraa.com

Silica aerogel/xerogel which is known as nanoporous silica, has numerous properties which suggest applications such as low dielectric constant ($1.1 < K < 2.5$) materials for inter-level dielectrics for the next generation. The advantages of these materials, in addition to the low dielectric constant, include high temperature stability, pores much smaller than microelectronic feature sizes, deposition using conventional spin-on and vapor deposition methods, and precursors similar to those currently used in the microelectronic industry. SiLK is a new polymer from the Dow Chemical Company which does not contain silicon. A valuable feature of SiLK is its high thermal stability. SiLK films are prepared by spin-coating of dissolved initial products in organic solvents and curing [148].

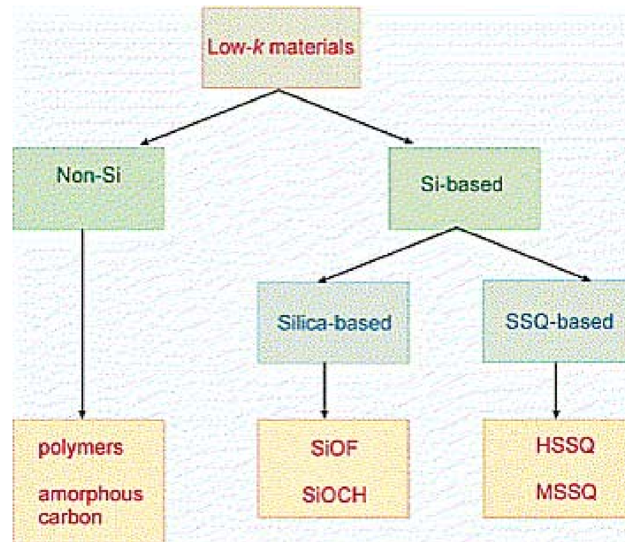

Fig. 4.11 Simplified Classification of Low k Dielectrics [205]

As the dielectric constant decreases the mechanical properties of the materials deteriorate. This is undesirable for interconnect materials. A material with optimized

المنارة للاستشارات
www.manaraa.com

mechanical strength is very much required for successful chemical mechanical polishing of these interlayer dielectric materials. Thus to ensure a low-cost packaging solution for low-*k* devices, issues regarding mechanical properties must be understood and considered as carefully as electrical properties [149, 150]. In the case of porous materials of dielectric constant ~2, porosity near 65% are utilized. These materials are so weak mechanically that they may not be robust enough for the CMP process. Simplified classification of the low-*k* materials can be seen in Fig. 4.11.

4.9 Mechanical Characterization of Low k Materials

To evaluate the mechanical properties, nano-indentation over a small scale has been used extensively in recent years [151-155]. This is a depth sensing indentation at low loads and is a well-established technique for the investigation of localized mechanical behavior of materials. The displacement and load resolution can be as low as 0.02 nm and 50 nN, respectively. A typical load versus displacement curve showing contact depth (h_c), and maximum depth (h_t) after unloading is shown in Fig. 4.12. Hardness and Young's modulus of elasticity are derived from the experimental indentation data by an analytical method using a number of simplifications [156]. Contact depth h_c can be calculated by:

$$h_c = h_t - \frac{\varepsilon F}{S} \quad (4.2)$$

where h_t is maximum depth of penetration including elastic deformation of the surface under load, F is the maximum force, and $\varepsilon = 0.75$ is a geometrical constant associated with the shape of the Berkovich indenter [156]. Once h_c is determined, the projected area

المنارة للاستشارات
www.manaraa.com

A of actual contact can be calculated from the cross-sectional shape of the indenter along its length. S is the stiffness, which can be derived experimentally from the following equation:

$$S = \frac{dF}{dh} = \frac{2}{\sqrt{\pi}} E_r \sqrt{A} \quad (4.3)$$

where E_r is the reduced modulus. Hardness is then calculated from the simple relation:

$$H = \frac{F}{A} \quad (4.4)$$

The reduced modulus E_r is normally defined as:

$$\frac{1}{E_r} = \frac{1 - \nu^2}{E} + \frac{1 - \nu_i}{E_i} \quad (4.5)$$

Details of the samples along with their refractive index, *k*-values, and density information are shown in Table 4.4. Mechanical properties of the films were measured using nanoindentation technique using Nano Indenter® XP (MTS System Corporation, Oak Ridge, TN). A three-sided Berkovich-shaped diamond indenter is used to indent on the material surface. The load and displacement data obtained in the nanoindentation tests were analyzed according to the method of Oliver and Pharr [151, 152]. The continuous stiffness measurement (CSM) technique was used for measuring absolute and depth dependent hardness and modulus values. Values were calculated by averaging a number of separate indentations at particular depth specifications. Initially the instrument was calibrated with the standard sample (fused silica) provided by MTS and other single crystal metal samples.

المنارة للاستشارات
www.manaraa.com

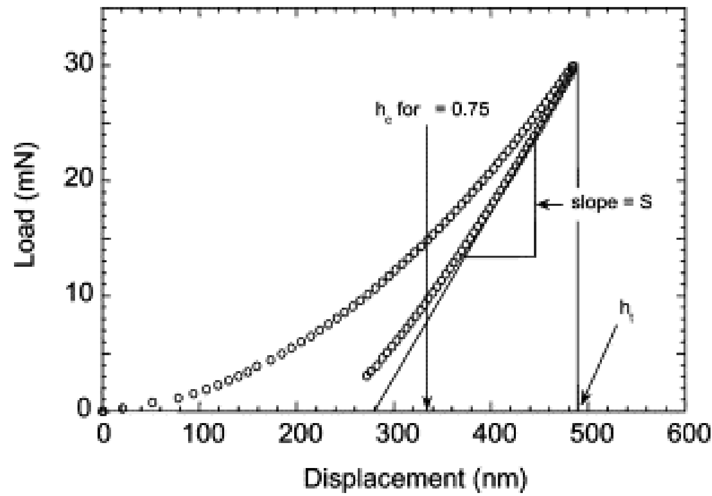

Fig. 4.12 Typical Curve Showing the Loading and Unloading as a Function of Indenter Penetration Depth

Table 4.4 Details of the Different Low k Materials Evaluated

#	Sample	Thickness (Å)	Grown by	Refractive Index	κ
1	SiO_2 (U)	3850	PECVD	1.474	~ 4.0
2	SiOF	1700	HDPCVD	1.430	~3.7
3	Polyimide	16000	Spin-On	1.920	~2.9
4	BCB	17000	Spin-On	1.542	~2.6

The mechanical properties of the candidate samples were evaluated by nanoindentation. The depth of penetration for the indenter was fixed at ~50 % of the sample film thickness. The calculation of mechanical properties was performed at 50 % of the indentation depth (i.e. ~25 % of the film thickness). This depth of calculation of the mechanical properties chosen to avoid the substrate effects as well as the effect of the surface oxide or other complex that might be present due to the reaction of the film with

المنارة للاستشارات
www.manaraa.com

ambient air. The values of the mechanical properties i.e. hardness and Young's modulus have been tabulated in Table 4.5. The normalized hardness of the dielectric materials in comparison with the hardness of SiO_2 is shown in Fig.4.13. It can be seen from Table 4.4 and Fig. 4.13 that there is almost an exponential decrease in the hardness and Young's Modulus of the material with a decrease in the dielectric constant. These reduced mechanical properties adversely impact the ability of the material to withstand down pressure and shear during CMP. The material removal during three body contact abrasion mechanism (most likely) during CMP takes place when the particles abrade the surface layer complex formed by the chemically active slurry [157].

Table 4.5 Results of Nanoindentation of the ILD materials

#	Sample	Thickness (nm)	Indentation Depth (nm)	Hardness (Gpa)	Young's Modulus (Gpa)
1	SiO_2 (U)	385	200	6.3±1.2	68.1±1.2
2	SiOF	170	100	4.3±0.7	42.4±3.4
3	Polyimide	1563	750	0.335±.0.03	3.2±.0.25
4	BCB	1665	800	0.29±0.08	3.5±0.4

The particles suspended in the slurry are significantly harder than all the ILD materials except SiO_2. In the event of agglomeration of the slurry particles or due to any other reasons, if the depth of particle indentation is greater than the thickness of the surface layer formed in the slurry, then a materials with lower hardness is more susceptible to deep surface scratches. Usually, a buffing step accompanies every CMP

المنارة للاستشارات
www.manaraa.com

polishing run. However, in the event of a deep surface microscratch, it is difficult for the buffing step to produce a mirror flat surface after CMP.

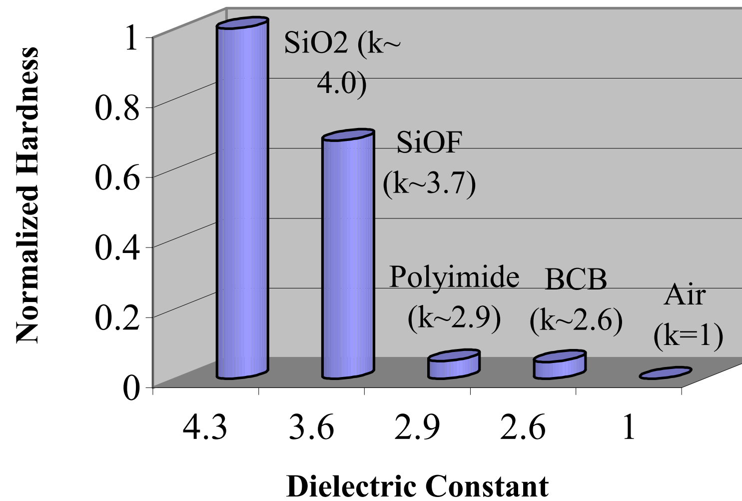

Fig. 4.13 Variation of the Normalized Hardness with Dielectric Constant of the Candidate ILD Materials

4.10 CMP of Low k Materials

Before we discuss the result of the CMP of low k materials, it is necessary examine the theory behind the material removal of the candidate dielectric materials. Material removal mechanisms for: 1) ceramics (doped and undoped SiO_2) and 2) polymeric (Polyimide and BCB) have been discussed in this section. The material removal mechanism of the ILD is strictly dependant on the chemistry of the slurry used. However, for the scope of this study, the generic mechanism of removal in alkaline ILD polishing slurry with colloidal silica particles as abrasives has been discussed.

المنارة للاستشارات
www.manaraa.com

4.10.1 Doped and Undoped Ceramic Material Removal

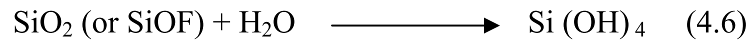

$$SiO_2 \text{ (or SiOF)} + H_2O \longrightarrow Si(OH)_4 \quad (4.6)$$

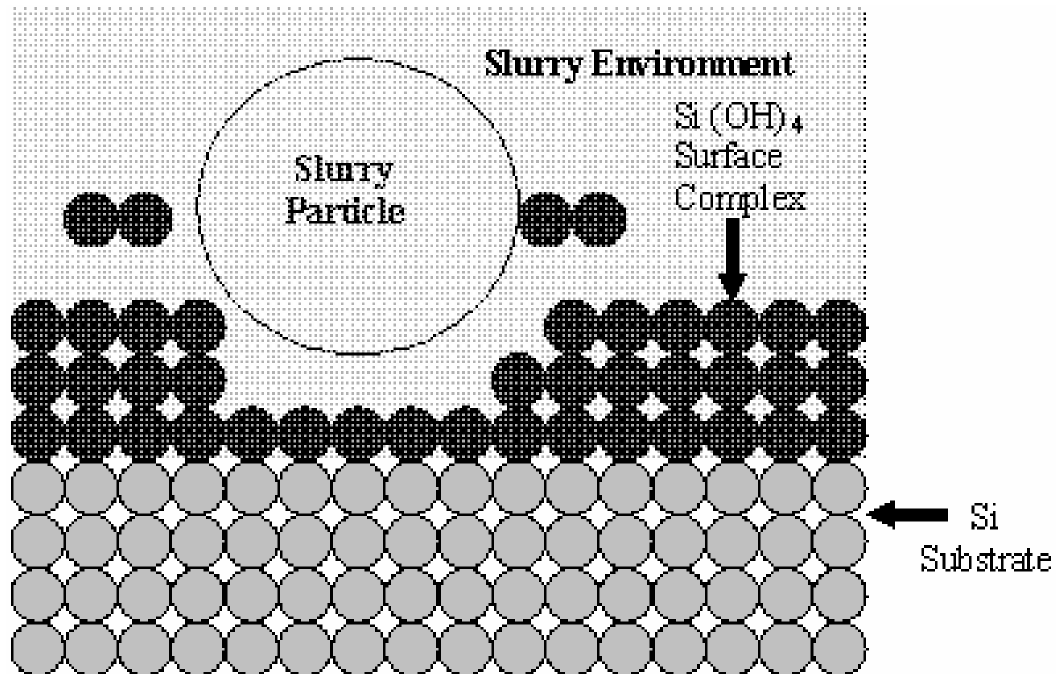

Fig 4.14. Material Removal Schematic during Ceramic ILD CMP

The fumed or colloidal silica abrasives in the slurry and the ceramic dielectric surface are of comparable hardness. During polishing of dielectrics such as SiO_2 or SiOF, the alkaline slurry hydrolyzes the few surface atomic layers into relatively softer $Si(OH)_4$. This material can then be easily removed with the help of slurry abrasive particles in pressure of the polishing pad for given operating CMP conditions [114]. The chemical reaction (unbalanced) indicative of the material surface transformation is shown in equation 2, and schematic of the material removal is shown in Fig. 4.14.

المنارة للاستشارات
www.manaraa.com

4.10.2 Doped and Undoped Ceramic Material Removal

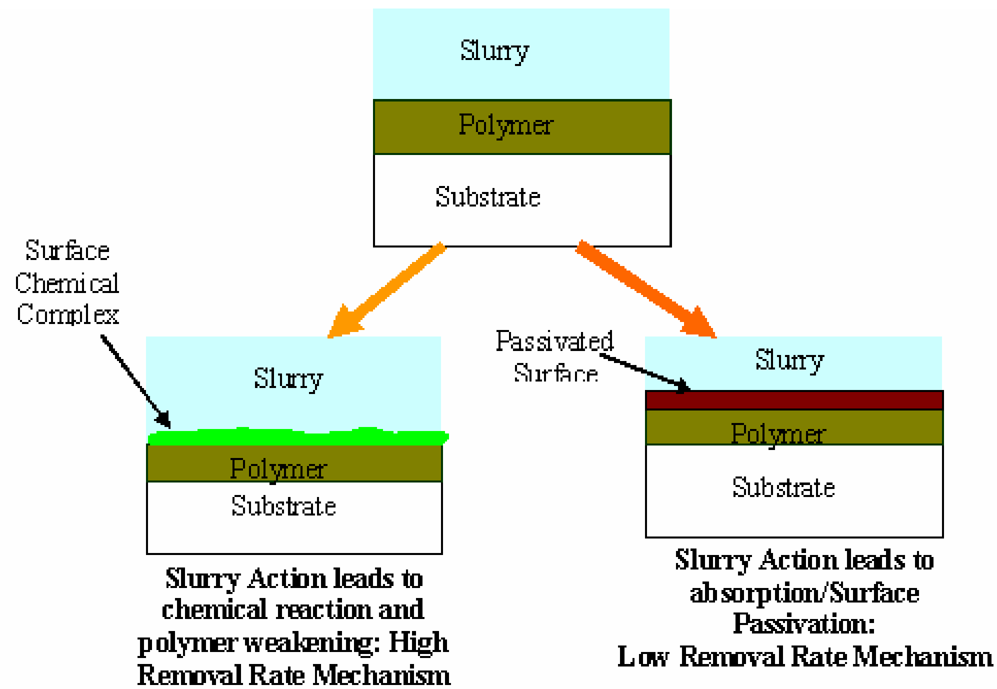

Fig. 4.15 Schematic showing the Action of ILD Slurry on the Polymer Surface during CMP

When the polymeric ILD materials are polished using alkaline slurry with silica abrasive particles, the slurry can either 1) effectively react with the surface producing a thicker and weaker polymeric layer there by yielding high removal rates or 2) passivate the surface and produce low removal rates primarily due to mechanical abrasion. The reaction at the surface and properties of the surface layer are dependent upon the physical characteristics of the polymer. For the high removal rate polymer CMP process, the material removal mechanism can be divided in to the following parts: 1)

المنارة للاستشارات
www.manaraa.com

adsorption of the slurry on the surface of the polymer if the material is hydrophilic, 2) diffusion of the slurry in the polymer surface, 3) reaction of the alkaline slurry with the polymer surface to create a significantly softer and weaker surface or breaking of the polymer bonds by the slurry diffused in the polymer thereby creating a thick surface polymer complex, 4) removal of the surface layer with abrasives in the slurry in presence of the polishing pad and 5) dissolution of the removed material [2]. The schematic of the slurry attack on the polymer surface is shown in Fig. 4.15.

4.10.3 CMP Process Conditions

The experiments for this study were performed using: 1) commercial IC 1000 Suba IV polyurethane pad manufactured by Rodel, Inc, 2) Rodel, Inc. Klebesol 1501 commercial polishing slurry. The pad was subjected to break in for 20 minutes before each set of material polishing runs with flowing DI water using TBW grid-abrade diamond pad conditioners. A conditioning run lasting 20 sec was performed using DI water between every two CMP runs. The experiments were performed at 1, 3, and 6 PSI down pressure. At each value of down pressure, CMP runs were performed at three different values of platen rotation: 1) 42.4 RPM, 2) 148.5 RPM and 3) 254.6 RPM. The values of platen rotation corresponded to an average linear velocity of: 1) 0.2 m/s. 2) 0.8 m/s, and 3) 1.2 m/s. This study being comparative, the upper carrier rotation action of CMP tester was not used. The movement of the polished sample was restricted to slider oscillation. The details of the experiments have been tabulated in Table 4.6.

المنارة للاستشارات
www.manaraa.com

Table 4.6: ILD Material CMP Experimental Details

#	Parameter	Conditions
1	Down Pressure	Variable (1-6 PSI)
2	Platen Rotation	Variable (42.4-254.6 RPM) or (0.2 m/s-1.2 m/s)
3	Slider Position and Movement	45mm ± 5mm @ velocity of 5 mm/ sec
4	Slurry	Oxide Slurry Rodel, Inc. Klebesol 1501 (pH~10.5) with colloidal silica abrasive particles.
5	Pad	Rodel, Inc. IC1000 Suba IV A4 perforated with specific gravity ~745
6	Time of polishing	120 sec (Values of AE and COF noted in the first 30 seconds have been plotted)
7	Polishing Specimen	1" X 1" coupon

The process parameters specifically studied were: 1) variation of COF with time and 2) variation of material removal rate (MRR) for different sets of polishing conditions, for each material. The removal of the material was calculated as shown in equation 4.6. The thickness of the thin film was measured using He-Ne Laser Ellipsometry.

$$MRR = \frac{Thickness_{Initial} - Thickness_{Final}}{Time} \quad (4.6)$$

المنارة للاستشارات
www.manaraa.com

4.10.4 Tribological Properties of Low k Materials

A total of 9 CMP experiments were performed on each of the candidate ILD samples at the pressure and linear velocity conditions mentioned in the experimental section of the paper. The variation of COF for the entire duration of the CMP run (120 sec) was noted. For the purpose of comparative ILD study, the variation of COF for the first 30 seconds was considered. The variation of AE signal was also noted in situ. However, off hand there was no distinct trend in AE signals. To explore the subtle phenomena occurring during each polishing run, the AE signals need to be filtered using the wavelet based approach [156]. This study does not fall within the scope of this current research.

The variation of COF with time for the different conditions of down pressure and velocity for all the samples are shown in Fig. 4.16 a-d. It can be seen from Fig. 4.16 that the magnitude of COF (COF= $\frac{F_s}{F_N}$; where F_s is the shear force and F_N is the normal force during the CMP run) [40] is strongly dependent on 1) the down pressure, 2) platen velocity and 3) material that is being polished. Every material for given conditions of pressure and velocity shows a unique value of COF. This principle is used for effective end point detection (EPD) of the CMP process. The change in the value of COF upon complete material removal depends upon the tribological properties of the buried layers. This transition can be attributed to the complete material removal. Details of the EPD using COF and AE have already been reported [64]. The end point obtained using in-situ data is not sharp. Further signal filtering is currently being carried out for accurate estimation.

www.manaraa.com

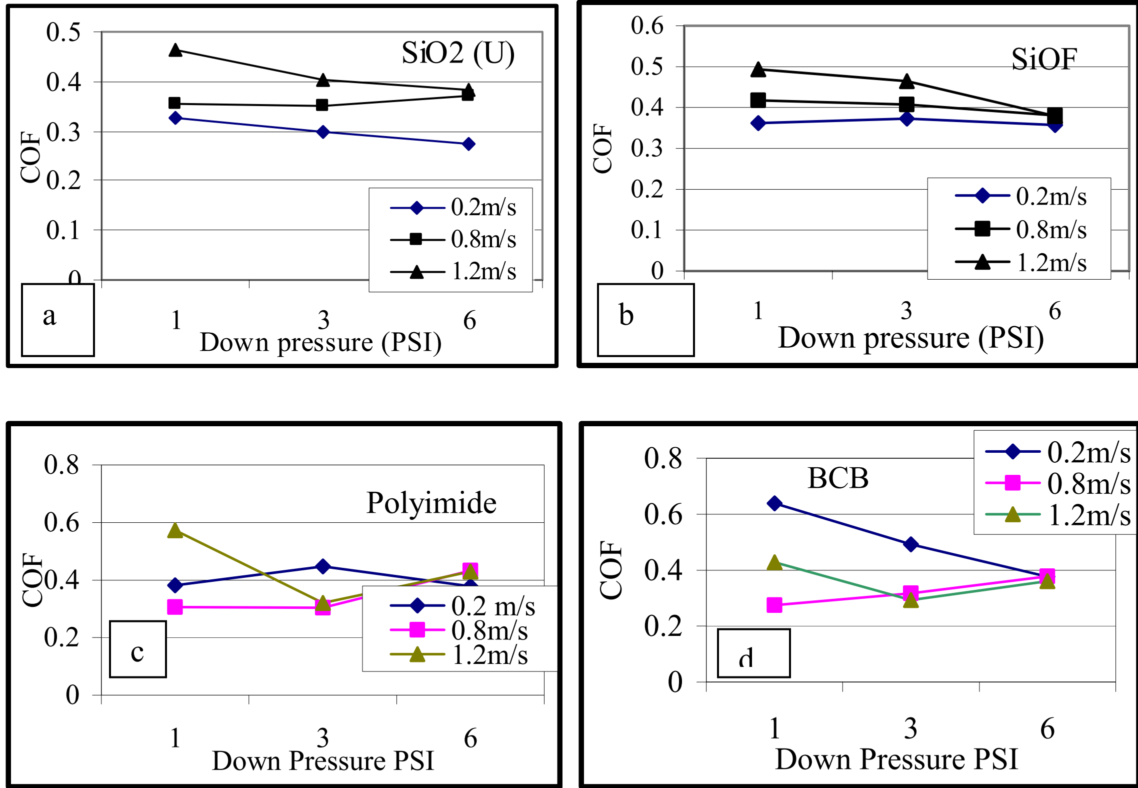

Fig. 4.16 Variation of COF with Down Pressure (PSI) and Linear Velocity (m/s) for a) SiO_2U, b) SiOF, c)Polyimide, and d) BCB

Normally, the values of COF should decrease with the increase in platen velocity. This is due to the fact that friction is generated at the interface of the pad and wafer is not only due to the interaction of the high points on the wafer and the slurry but also due to the interaction of ceramic slurry abrasive particles with the pad and wafer. With the increase in their speed due to high platen velocity, the depth of indentation of the particles on the surface of the pad decreases. Due to the partial elastic behavior, at shallow depth of indentation, the response of the pad is brisk and there is lesser drag to the particle motion on the surface of the polishing pad. Hence, there is lesser dynamic friction at the pad-wafer interface [158]. Previous experiments carried out with carrier

المنارة للاستشارات
www.manaraa.com

rotation have shown the verification of this phenomenon [159]. However, anomalies can be seen in some cases (ref Fig. 4.16 a-d) due to lack of upper rotation of the sample coupon. The lack of sample rotation causes non uniform material removal. More material is removed from the leading edge as compared to the lagging edge. The variable thickness on the surface of the sample contributes to the variation of the COF value during the polishing run.

Fig 4.16 (a-d) shows an overall trend of decrease in the value of COF with an increase in down force. These results are in agreement with those obtained previously on this set up [160]. It must be noted here that, the increase in down force brings about a corresponding increase in the shear force (F_s) as shown in equation 4.7 [161].

$$F_s \propto W \frac{\sigma}{H} \tan \delta \quad (4.7)$$

where W is the downward loading, σ is the maximum shear stress on the given area, H is the hardness of the polishing pad and tan δ is the ratio of the loss modulus to the storage modulus (which is also a measure of the toughness) of the pad. The applied down force F_z on a viscoelastic polishing pad can be written as shown in equation 4.8:

$$F_z = F_v + F_N \quad (4.8)$$

where F_v is the force dissipated for pad deformation due to the viscous nature and F_N is the normal force due to the elasticity of the polishing pad. Due to non linearity of the strain displacement reactions in the viscoelastic materials like polyurethane, second order geometric non linearity is observed in the polishing pads upon application of down force. This geometric non linear expansion of the pad produces an axial normal tensile force in the polishing pad. The second order normal force (F_{SN}) for a rotating pad with radius r,

المنارة للاستشارات
www.manaraa.com

modulus of rigidity G and uniform angle of twist ψ is expressed as shown in the equation 4.9 [162].

$$F_{SN} = \frac{1}{4} G\pi\psi^2 r^4 \quad (4.9)$$

The term $G\psi^2 r^4$ is nothing but the shear force (F_s) acting on the surface of the pad under the given loading. Thus, the second order normal force can be expressed in terms of the shear force as shown in equation 4.10.

$$F_{SN} = \frac{1}{4}\pi F_s \quad (4.10)$$

Hence, the COF during a polishing run can be expressed as a function of elastic recovery and shear force as shown in equation 4.11

$$COF = \frac{F_s}{F_{ER} + \frac{1}{4}\pi F_s} \quad (4.11)$$

where F_{ER} is the first order elastic normal reaction (recovery) component of the normal force. It can be concluded from equation 4.11 that the increase in shear force with the increase in the down force, brings about a corresponding increase in the normal force due to the increase in the shear component and normal elastic reaction of the pad. This can explain an overall decrease in the values of COF with the increase in the down pressure.

4.10.5 Variation of Material Removal Rate for Low k Materials

The variation of MRR of all the ILD samples under variable pressure and linear velocity conditions is shown in Fig. 4.17 a-d. An average of thin film thickness readings at the leading edge was used for MRR calculation due to more material removal

المنارة للاستشارات
www.manaraa.com

near it. It can be seen from the Fig. 4.17 that the candidate ILD samples follow the Preston's equation. Material removal is strongly dependent on solution chemistry of the slurry as well as the CMP process conditions. To achieve highest defect free MRR, the material passivation or surface reaction at the pad wafer interface should more or less match the abrasion of material due to the process conditions. If the material removal is lesser than the surface chemical complex formation, there is a decrease in the removal rate. In case of the lesser material passivation, partial material removal takes place due to mechanical abrasion. This increases the chances of the defects on the surface of the wafer and also reduces the removal rate.

It can be seen from Fig. 4.17 that the MRR for the same process conditions is higher for SiOF as compared to SiO_2. The higher Preston's coefficient, which is indicative of the dependence of the MRR on the pressure and velocity conditions during CMP for a given material, is higher for SiOF (1.903) as compared to SiO_2 (U) (1.468). Fig. 4.17 c, d shows that the variation of MRR of the polymers (Polyimide and BCB) does not follow the Preston's equation accurately. Materials in the past, especially ILD, have exhibited two Preston's coefficients [163, 164]. Further polishing investigations are needed at low values of down pressure and linear velocity to ascertain whether evaluated polymers display this phenomenon of having two different values of Preston's coefficients governing their MRR with process conditions.

www.manaraa.com

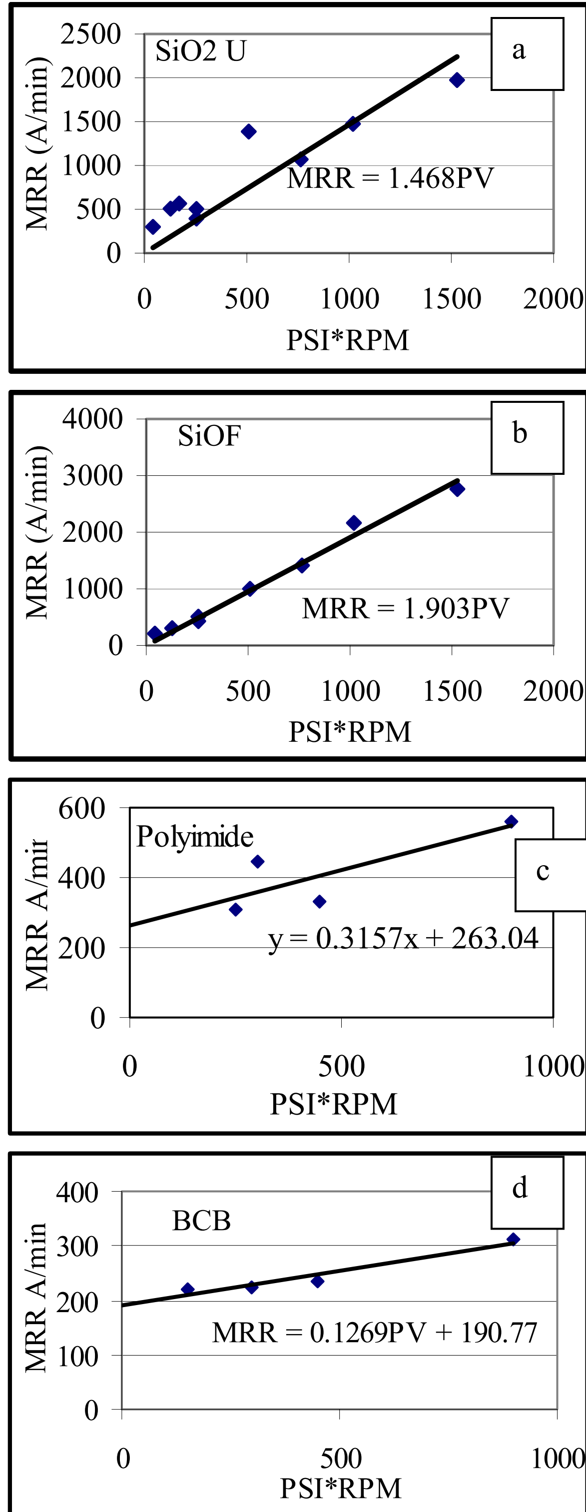

Fig.4.17 Variation of MRR with Pressure (P) and Platen RPM (Linear Velocity V) for a) SiO_2 (U), b) SiOF, c) Polyimide, d) BCB

www.manaraa.com

The MRR for SiO_2 (U) and SiOF (ceramics) is significantly greater than that of the polymers. The rate at which the surface is softened and directly attacked is more for the ceramics as the slurry is tailor made and commercialized for SiO_2. The chemical attack of the slurry on the polymers is relatively subdued due to their chemical composition. Hence, even though the extent of mechanical forces contributing to the material removal is almost the same, MRR is more for SiO_2 and SiOF. Both BCB and Polyimide have the tendency to uptake moisture. BCB moisture uptake (after being fully cured), however, is much less than Polyimide after cure. BCB moisture weight uptake or absorption is $< 0.2\%$, while Polyimide moisture uptake is about 1-2%. Though this data was obtained in air at around 80% relative humidity, similar behavior is expected to persist when the polymers are in contact with the slurry. Thus, when Polyimide and BCB wafers are subjected to CMP, there may be slightly more "bond breaking" due to higher moisture uptake in Polyimide than BCB in addition to the slurry chemical attack.

4.10.6 Surface Characterization of Low k Materials

As a part or the comparative study, pre and post CMP AFM was performed on ILD samples that underwent CMP at 3 PSI down force and 148.5 RPM (0.8 m/s linear) platen rotation. The surface morphology and roughness before and after CMP were evaluated. The change in R_{rms} due to CMP for each of the sample at the aforementioned polishing conditions is shown in Table 4.7. The AFM images for the sample before and after CMP can be seen in Fig. 4.18 a-d.

It can be seen from Table 4.6 and Fig. 4.18a that the surface roughness of SiO_2 (U) decreases significantly upon polishing. As the slurry has been commercialized

المنارة للاستشارات
www.manaraa.com

for SiO_2, this factor must have been taken in to account in the slurry design. The sample SiOF shows a very smooth surface before CMP. However, there is an increase in surface roughness after CMP. This may be due to the fact that the surface complex formed during CMP of SiO_2 (U) and SiOF may be similar or even the same. Hence after planarization, the ILD surface may display similar properties including surface roughness. Further XPS analysis is however needed to confirm the occurrence of this phenomenon. Also, due to the lesser hardness of the SiOF as compared to SiO_2, there might be slightly greater indentation of the ILD surface leading to a slightly rougher surface. However, the threshold of surface scratch does not appear to be reached in case of SiOF, despite its lower hardness.

Both the polymeric ILD materials show a very smooth surface before CMP. However, the surface roughness of both Polyimide and BCB increases very significantly after CMP (Polyimide has a rougher surface as compared to BCB). Due to the low hardness of the polymers films, numerous scratches caused by slurry abrasives or agglomerates can be seen on the surface of the both the polymers after CMP. There may formation of a passivated surface complex and lack of polymer weakening in presence of the slurry. Thus, the material removal may be primarily due to mechanical abrasion. This explains the significantly lower material removal of the polymers as compared to the ceramics. The scratches left on the surface of Polyimide are far numerous when compared with those occurring on BCB, in spite of the fact that hardness of the Polyimide is slightly greater than BCB. As the water in the slurry attacks Polyimide more than BCB, the surface layer formed due to the reaction of the Polyimide with the slurry may be softer due to relatively higher water content or absorption in comparison with

المنارة للاستشارات
www.manaraa.com

BCB. This explains almost two and half times higher post CMP roughness, more surface scratches and slightly higher removal rate shown by Polyimide. Details investigation of the wear and removal mechanism of these polymers needs to be carried out in the future.

Table 4.7 Surface Roughness (R_{rms}) of the ILD samples before and after CMP

#	Sample	R_{rms} Before CMP (nm)	R_{rms} After CMP (nm)
1	SiO_2 (U)	3.42	0.37
2	SiOF	0.18	0.40
3	Polyimide	0.529	8.326
4	BCB	0.657	3.658

4.10.7 Findings of Low k Materials Evaluation

There is a decrease in the mechanical properties of the materials with the decrease in their dielectric constant. The COF of the material is an individual characteristic which changes with a change in the CMP input parameters. This can be used for accurate EPD, MRR estimation, qualitative estimation of the selectivity of the slurry towards the material etc. There is an overall decrease in the COF with increase in down pressure. However, there is an increase in the removal rate with the increase in pressure. This is due to the fact the normal force exerted by the pad is also partly comprised of the shear force experienced by the material due to the viscoelastic nature of the pad.

المنارة للاستشارات
www.manaraa.com

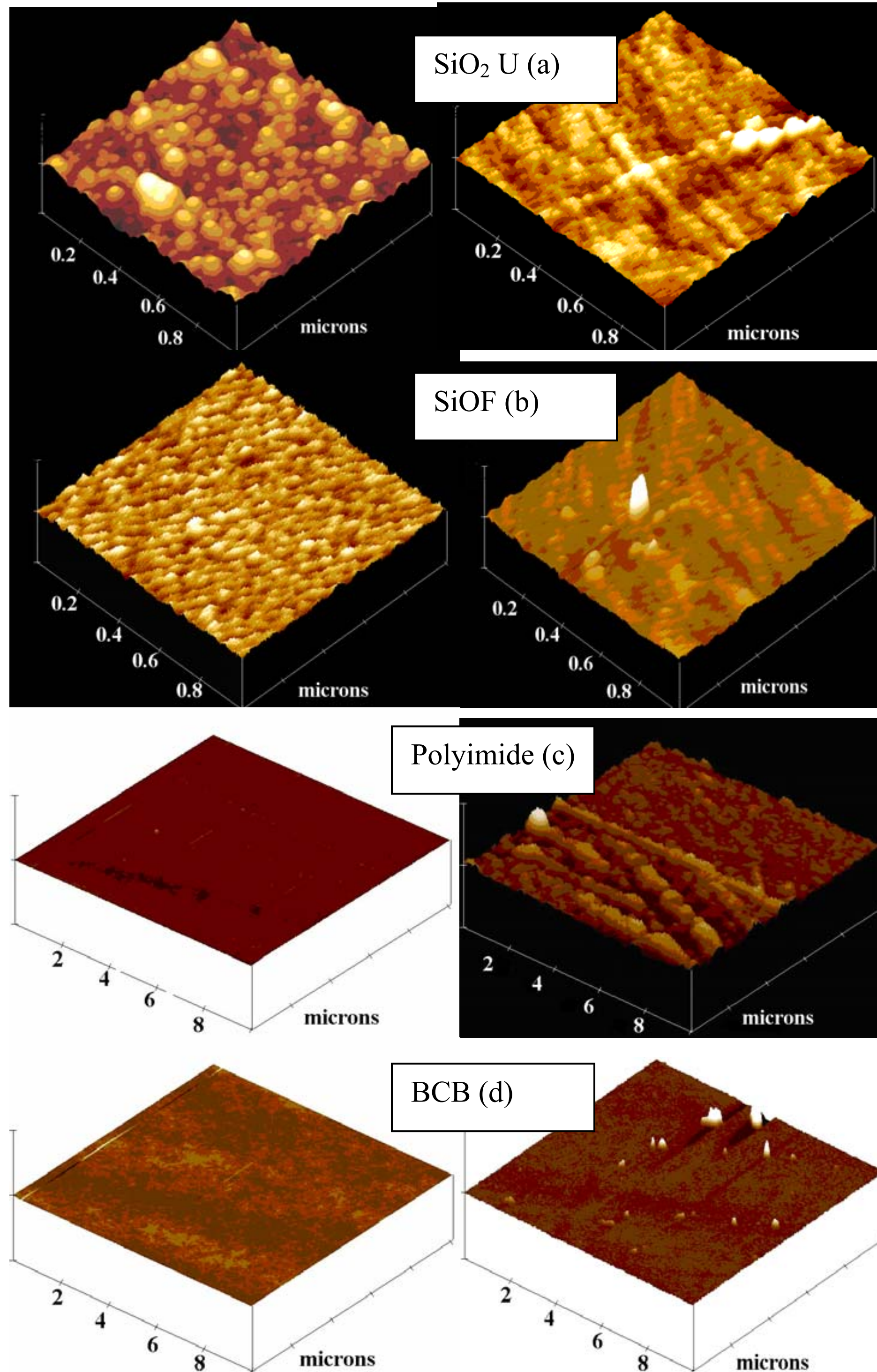

Fig. 4.18 Surface Morphology of the Candidate ILD Samples Before and After CMP for:

a) SiO_2 (U), b) SiOF, c) Polyimide and d) BCB

المنارة للاستشارات
www.manaraa.com

As there is an increase in the magnitude of the shear force with the increase in down pressure, MRR increases with pressure, even though the value of COF decreases. There should be a decrease in COF with increase in linear velocity. The anomalies observed in the study are due to the non-uniform material removal due to the absence of upper rotation. The sample SiO_2 (U) and SiOF follow the Preston's equation accurately while the polymeric samples do not. The possibility of the polymeric samples showing two Preston's coefficient needs to be investigated by carrying out experiments at lower values of pressure and velocity. There is a sizable increase in the surface roughness of the polymeric materials after CMP. Surface of the polymeric materials shows the existence of scratches after CMP which are absent in case of the ceramic samples materials. There is weakening and softening of the polymer in presence of the slurry but the passivating layer formation and removal is not as effective as demonstrated by the ceramic samples. This explains the relatively higher material removal rate shown by the ceramics. The lower removal rates, high surface roughness, existence of microscratches coupled with lower hardness are definitely some of the integration challenges that need to be overcome before successful integration of polymeric materials.

المنارة للاستشارات
www.manaraa.com

CHAPTER FIVE

INVESTIGATION OF NON UNIFORMITIES IN POLISHING PAD

5.1 Significance of Polishing Pad

The polyurethane CMP polishing pad forms a very integral part of any CMP process. The choice of the pad depends upon the CMP polishing equipment, nature of material polished and polishing output requirements. For all practical purposes, commercial polishing pads are of viscoelastic nature and, are mostly used are made up of a matrix of cast polyurethane foam with filler material to control hardness or polyurethane impregnated felts [165, 166]. The pad carries the slurry on top of it, executes the polishing action, and transmits the normal and shear forces for polishing. At the pad wafer interface, the slurry acts on the wafer and forms a compound with the material that is being polished. This compound is then removed when by the abrasive particles that act between the asperities of the pad and high points on wafer. The material removed, is then washed away due to the constant slurry flow on the pad.

There is ongoing research to investigate the dependence of various pad material properties on the CMP process. Some of the findings thus far show that: 1) there is a drop in material removal rate, as a function of time due to the varying mechanical response under conditions of critical shear; [77] 2) wafer planarity is a function of pad stiffness, which is determined by the elastic properties of the pad material [77, 103]. The

المنارة للاستشارات
www.manaraa.com

pad might be directly responsible for several process defects like wafer to wafer non uniformity (WTWNU) where there is non homogeneity of polishing when one wafer is compared to another or within wafer non uniformity (WIWNU) where there is non homogeneity of polishing at different areas of the same wafer. Several techniques have been used before for characterization of the CMP polishing pad with Dynamic Mechanical Analysis (DMA) being the most prominent one [167-169]. However, almost all these techniques are destructive. A novel non destructive Ultrasound Transmission (UST) developed at USF can be effectively used for evaluation of the CMP pads [170, 171]. This technique works on the principle of ultrasound permeability through absorbing viscoelastic medium. The difference in the ultrasound transmission is used to determine the non uniformity or variation of specific gravity within a single pad (Fig. 5.1).

5.2 Method for Mapping and Isolation of Non Uniformities in Pad

The UST technique has been used to study 32" and 20" diameter commercial polyurethane pads with and without sub-pads. The regions of the pad which showed very high and low amplitude of UST ("regions of interest") were subjected to further evaluation. One inch coupons from the regions of interest were punched and its impact on the pad uniformity was studied. Material from the regions of interest was then evaluated using DMA to estimate their mechanical properties. Finally 6 inch coupons from the regions of interest were subjected to CMP process evaluation to understand the impact of pad non uniformity on its CMP performance. Commercial CMP polyurethane pads were used for this study. The first evaluated pad was a closed cell polyurethane polishing pad with pores created usually with a blowing agent. This pad was attached with a soft sub

المنارة للاستشارات
www.manaraa.com

pad which comprised of non woven polyester fibers impregnated with polyurethane to leave open porosity. This pad sub pad combination henceforth will be referred to as Pad 1. The second type of polishing pad used for the study comprised of the same aforementioned polishing pad without the sub-pad. This pad will henceforth be referred to as Pad 2. Both the pads were 32” in diameter had concentric grooves on them (K grooves).

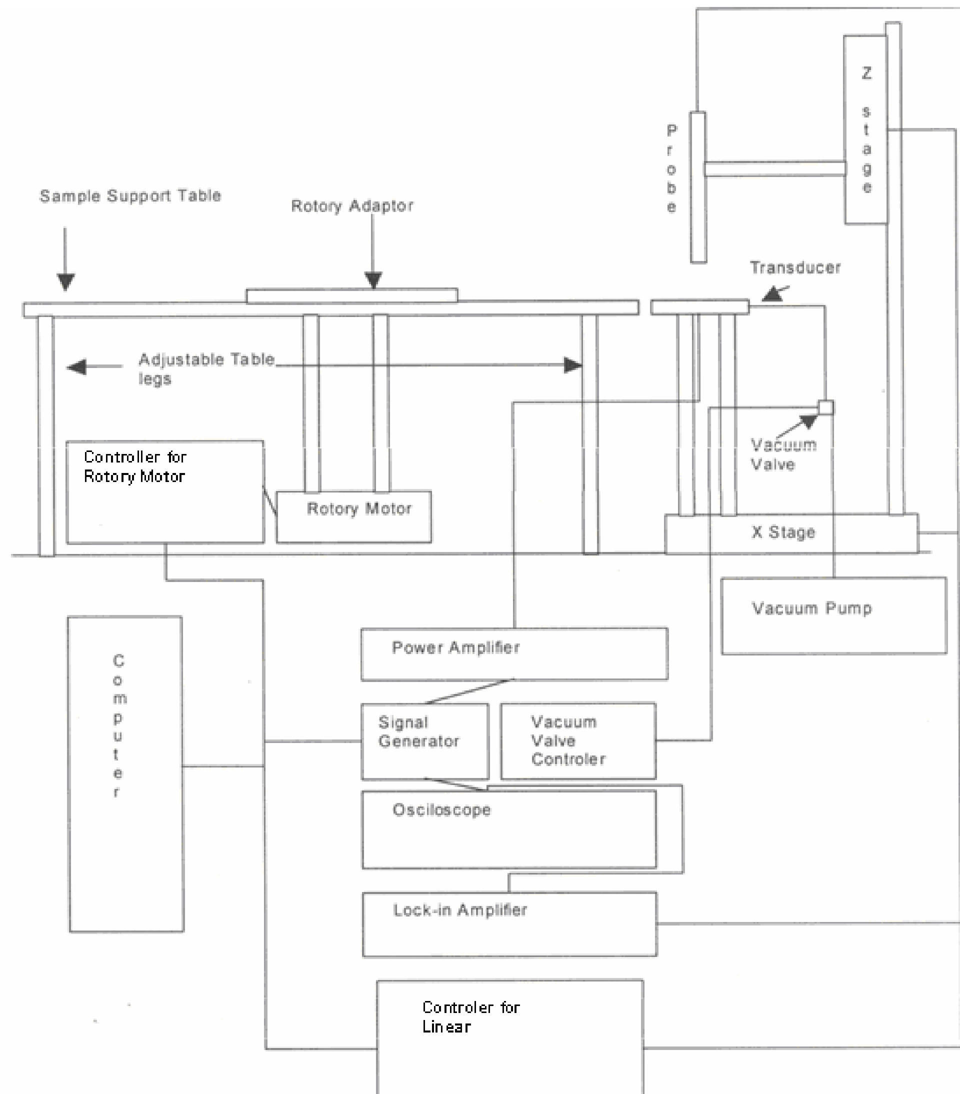

Fig. 5.1 Schematic of the Construction of the Ultrasound Testing Equipment

المنارة للاستشارات
www.manaraa.com

The combined thickness of pad 1 (polishing pad + sub pad + 2 pressure sensitive adhesive layers) was measured to be around 110 ± 7 mils. The thickness of Pad 2 (polishing pad + pressure sensitive adhesive layer) was 50 ± 4 mils.

5.3 Ultra Sound Testing (UST) System

The UST system consists of a flat square table that can accommodate polishing pads as big as 32" in diameter. The center of the table has a circular hole that allows the two screws that holds the pad to pass through. One side of the table has a slot which enables the transverse movement of a 3" Valpey Fisher piezoceramic transducer along the radial direction of the polishing pad. The transducer has a hole in the center and has trenches in the sides which help in generation of the vacuum which is used to hold the pad on the surface during UST measurement. The piezoceramic transducer emits resonance ultrasound vibrations at 26 KHz (first resonant frequency of the piezoceramic transducer), while a 7 mm diameter quartz rod or a pinducer housed in aluminum casing aligned directly above the transducer acts as the receiver. The received ultrasound frequency is then converted in to electrical energy and the raw output is seen on the oscilloscope. The signal from the probe and reference input are both sent to a lock in amplifier which records the amplitude of the received signal at the same frequency as the emitted signal. Different sections of the polishing pad are scanned be rotating the pad using the mounting screws by a step motor with 2 degrees angular steps, and moving the emitting piezoceramic transducer and the aligned receiver using another step motor at 7mm radial steps with help of a threaded spindle and screw. There is a provision for vertical movement of the receiving pinducer with the help of vertically positioned spindle

المنارة للاستشارات
www.manaraa.com

and screw. The regions of polishing pad having variations in specific gravity transmit different amplitudes of UST at a same frequency. The amplitude of the ultrasound permeability with in a pad obtained as a result of UST is normalized to against the average UST amplitude to estimate the comparative variations in specific gravity in the different regions of the same polishing pad. The output of the measurement is a Doppler diagram in which different colors correspond to different amplitudes of UST with in the pad. The measurements are taken at a distance of 100 μm below the pad surface to eliminate the presence of possible "air pockets". It must be understood here that due to the viscoelastic nature of the cross linked polymer material of the polishing pad, all measurements taken are "curve fitted" taking the effect of measurement stress and temperature on the material into consideration. The details of the UST set up, measurement techniques, characterization procedures and operation have already been published in literature [170, 171]. The UST experiments were performed on the "as received" polishing pad with the plastic release liner below it. It is assumed that the bottom PSA and the plastic liner are uniform and will have a similar effect on the ultrasound transmission. These effects could then be filtered out when the entire data is normalized against the mean UST. The area showing the highest ultrasound transmission over the entire pad was designated as "high transmission" or 'HT', while the areas showing the lowest ultrasound transmission were designated as "low transmission" or 'LT'. After the UST mapping, 1", 3" and 6" diameter coupons were punched out of the HT and LT regions for subsequent experiments. The pad was remapped using the same procedure discussed above without the 1" and 3" coupons being replaced. In case of 6" coupons, the coupons were replaced and partial remapping of the pad was done.

للاستشارات
www.manaraa.com

5.4 Evaluation of Mechanical and Tribological Properties of Polishing Pad

Mechanical properties of small sections of the pads from the HT and LT regions were evaluated using DMA to examine the possible change in structure-property relationship of these regions. It has been shown before, that orientation of the polishing pad grooves or the directional orientation of the pad surface perforations directly affect the values of loss and storage modulus of the pad materials that are evaluated using DMA [167, 169]. The pad displays higher mechanical properties when the perforations or grooves are oriented parallel to the length of the coupon used in the DMA. Two coupons (20mm X 10mm) were cut from Pad 1. The grooves on the pad were kept parallel to the length of the coupon used in DMA. The plastic release liner is removed as it's relatively adhesion with PSA was an impediment during flexural loading of the sample during DMA. To facilitate the clamping of the coupon, even the PSA is scrubbed off to before DMA. The bottom glue layer was scrubbed off of the coupon, allowing more efficient clamping in the holder. Data was obtained on a TA Instruments DMA 2980 (New Castle, DE) at temperature increments of 4°C with an isothermal time of 1 min. per increment starting from room temperature (20°C) and going up to 80°C. The flexural mode was used with single cantilever clamp and 3.0 μm amplitude. Frequencies ranged from 0.6 – 30 Hz for all measurements. The set up and working of the DMA has been elaborately discussed in literature [172-174].

المنارة للاستشارات
www.manaraa.com

Table 5.1 Details of the CMP Experiments Performed on the Polishing Pad evaluated by UST

Sr. No	Item	Description
1	Polishing Sample Materials	1. Patterned HDP 5000° A ILD (2 cm X 2 cm) (HDP 5K) 2. Blanket SiO_2 ILD (2 cm X 2 cm)
2	Polishing Pad	Pad 1 and Pad 2 (described before)
3	Slurry	Cabot SSK 12 (ILD slurry)
4	Slurry Flow rate	52 ml/min
5	Conditioning	1. Break-in 20 min. with 3M diamond conditioner with DI water **2.** Conditioning for 2min with D.I. water after ever set of three polishing runs of 90 seconds each
5	Down force	1. 1, 3, 6 PSI for Patterned HDP 5000° A ILD 2. 3 PSI for Blanket SiO_2 ILD
6	Platen Rotation/Carrier Rotation (RPM)	1. 100/95, 200/195, 300/295 for Patterned HDP 5000° A ILD 2. 200/195 Blanket SiO_2 ILD

The polishing experiments were done using the CETR CP- 4 bench top CMP tester which is a stand-alone bench-top simulator with instrumented process control. The

المنارة للاستشارات
www.manaraa.com

CMP tester provides real-time measurements of tribological parameters such as coefficient of friction (COF). The CMP performance of the pads was evaluated at different conditions of down force (PSI) and rotation (RPM). Experiments were performed on 1” X 1” coupons having 5000Å high density plasma (HDP) dielectric material using Cabot Microelectronics SSK 12 commercial ILD slurry. The values of down force and bottom platen rotation used were: 3 and 6 PSI, and 100, 200 and 300 RPM respectively. The carrier rotation was maintained at 5 RPM lower than the platen rotation. The slurry flow was maintained at 40 ml/min. The process conditions during all the experiments have been tabulated as shown in Table 5.1. The details of the CMP tester have been discussed before.

5.5 SEM Evaluation of Polishing Pad

Usually, commercial polyurethane pads, either perforated or grooved consist of pores of approximately 30 μm in diameter and account for around 30 % of the volume of the pad. Fig 5.2 shows the cross-section of Pad 1. It can be seen from the figure that there are two layers of pad held together with the help of a pressure sensitive adhesive. The entire stack is attached to the platen with the help of another layer of PSA. In case of Pad 2, there is only one layer of PSA that is needed to attach the pad on the platen, due to the absence of a sub-pad.

المنارة للاستشارات
www.manaraa.com

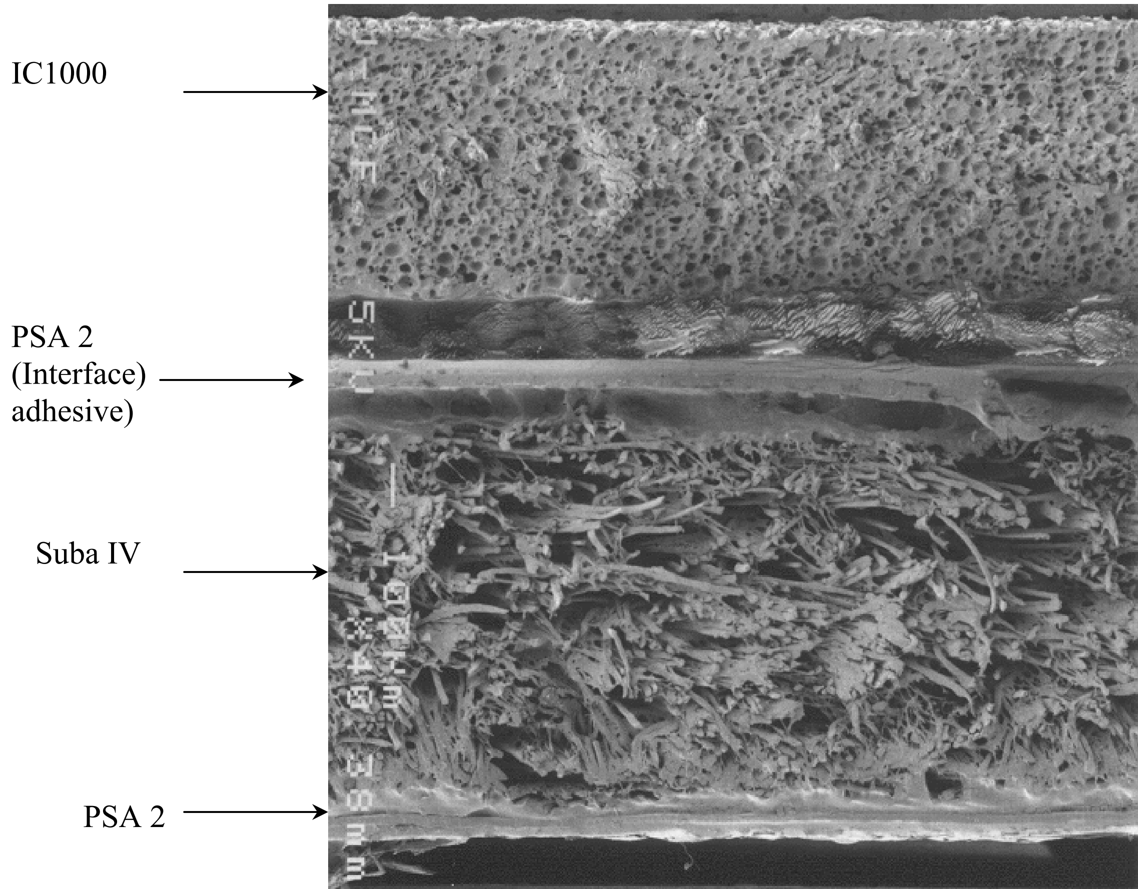

Fig. 5.2 Cross-section Scanning Electron Micrograph of the Evaluated Commercial Polyurethane Polishing pad with a Sub-pad

5.6 Isolation of Polishing Pad Coupons

The results of UST scan over one quarter (90° scan) of the donut shaped Pad 1 are shown in Fig. 5.3 a-d. There are distinct HT and LT regions on the surface of the pad with UST amplitude variation changing by a factor of two. The variation of the ultrasound transmission is normalized. Fig 5.3 b shows the histogram of the distribution of the intensity of the ultrasound transmission over the section of the pad. There is a large variation in ultrasound transmission within a quarter of the donut shaped pad. A set of 1

www.manaraa.com

inch coupons were punched out from HT and LT regions. The pad was then remapped and results of the ultrasound scan are shown in Fig. 5.3 c. Dark areas can be seen on the pad due to the presence of an air gap in region from where the coupons were punched out. There is a significant change in the intensity in ultrasound transmission of the pad without the coupons.

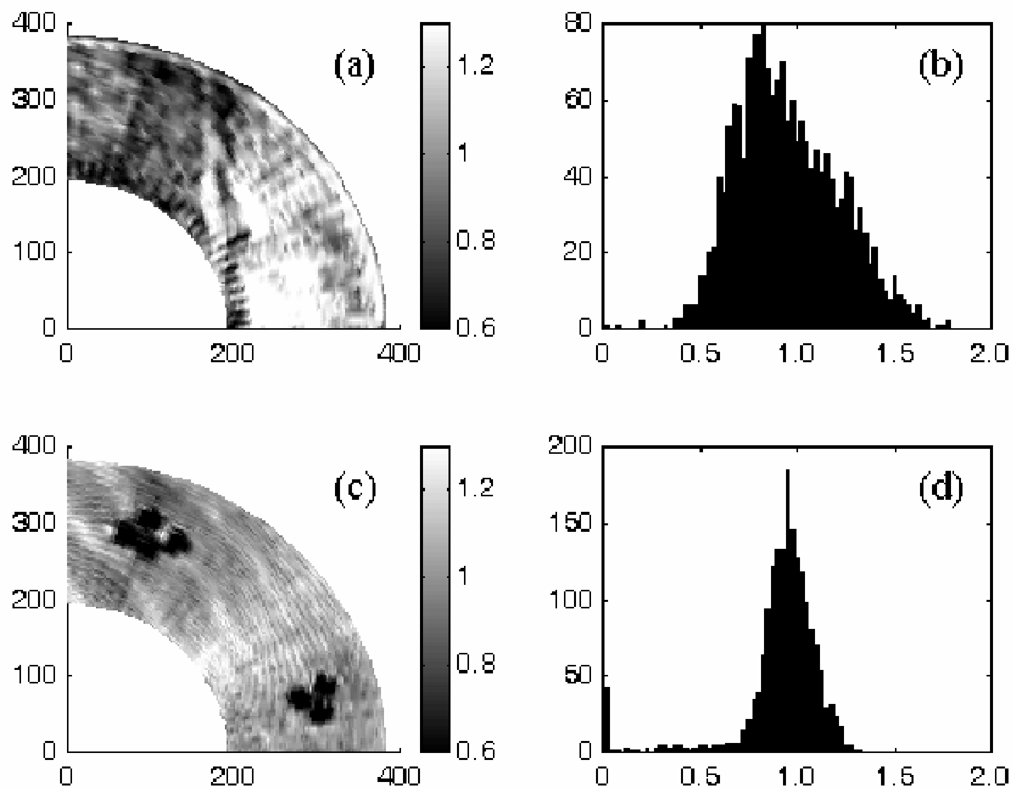

Fig. 5.3 Ultrasonic Transmission Maps of the Quarter IC1000/SubaIV pad a) Before and b) After punching of the 1” coupons. Three coupons were punched at the High-Intensity (white) Area and Four Coupons at Low-Intensity (Black) Area. The Effect of Pad Acoustic Homogenization after Punching is Illustrated in Respective Histograms (b, d)

المنارة للاستشارات
www.manaraa.com

The “dark areas” of LT are virtually absent, except from the region from where coupons were punched out. Fig. 5.3 c shows a more homogenous distribution profile of the ultrasound transmission over the entire pad. The region of the pad which showed high ultrasound transmission and from where the pad coupons were previously punched showed significantly lower ultra sound transmission, while the regions of the pad which previously showed low ultrasound transmission exhibited an increase in ultrasound transmission. A reduced inhomogeneity in the histogram shown in Fig. 5.3 d can be attributed to the strain relaxation accompanied with elastic stress release due to punching of coupons. It can be thus said that the built in stresses in the polishing pad bring about a variation in the specific gravity.

5.7 Isolation of 6 Inch Polishing Pad Coupons

Fig. 5.4 a shows the ultrasound map of the 360° scan of Pad 1. The variation of the ultra sound permeability through the region was normalized over a scale from 0.8 to 1.2. Upon identification of the HT and the LT regions of the pad, coupons of 6” diameter were punched out with the intention of entrapping the entire non-homogeneous region. (It was also chosen to make sure no superfluous effects from cutting the wafer were seen in the interior of the coupon as was seen with the 3 inch and 1 inch coupons.) Fig. 5.4 (b, c) shows the partial scans of the polishing pad when the HT and LT pad coupons were put back in the region from where they were isolated. It can be seen from Fig. 5.4 b that there was a reduction in the ultrasound transmission in the HT coupon after punching and remapping. Also, the coupon showed reduced ultrasound signal transmission in comparison to the surrounding pad. This indicates that HT region in the

www.manaraa.com

full map corresponds to the pad region under compressive stress which is relaxed when coupon was punched. When the 6" coupon from the LT area of the pad was punched and remapped after placing it in its original position (ref. Fig 5.4c) the ultra sound transmission over the entire coupon remains approximately same as seen in the previous scan (ref Fig. 5.4a). However, there is an increase in the UST amplitude in the center of this coupon suggesting that certain regions corresponding to the LT area of the pad were under tensile stress. After the coupon was punched out, there was a stress release from these areas there by making them denser. This increases the ultrasound permeability due to the localized increase in the pad specific gravity. The distinct lower ultrasound transmission seen at the edge of both the coupons in the scans obtained during remapping (ref Fig. 5.4(b, c)) shows the presence of an air gap at the boundary of the pad and the coupons. Certain distinct areas of significantly reduced UST amplitude in the coupon shown in Fig. 6b also indicates that there is an air gap underneath the coupon when it is put back in place. This may be due to the loss of flatness on the bottom of the coupon after stress release. We estimated that 20% variation of the UST permeability between high and low intensity areas corresponds to 10% relative change of the pad density (specific gravity). It must be mentioned here that previously experiments were performed by isolating 3" inch coupons from the pad. The results of this experiment were found to be similar to those reported in Fig.5.4. The coupons punched out of the pad to entrap the regions of non-uniformity bring about a generate change in the stress distribution regime in the pad. Hence, the local density variation needs to be examined on the Pad 1n its entirety.

المنارة للاستشارات
www.manaraa.com

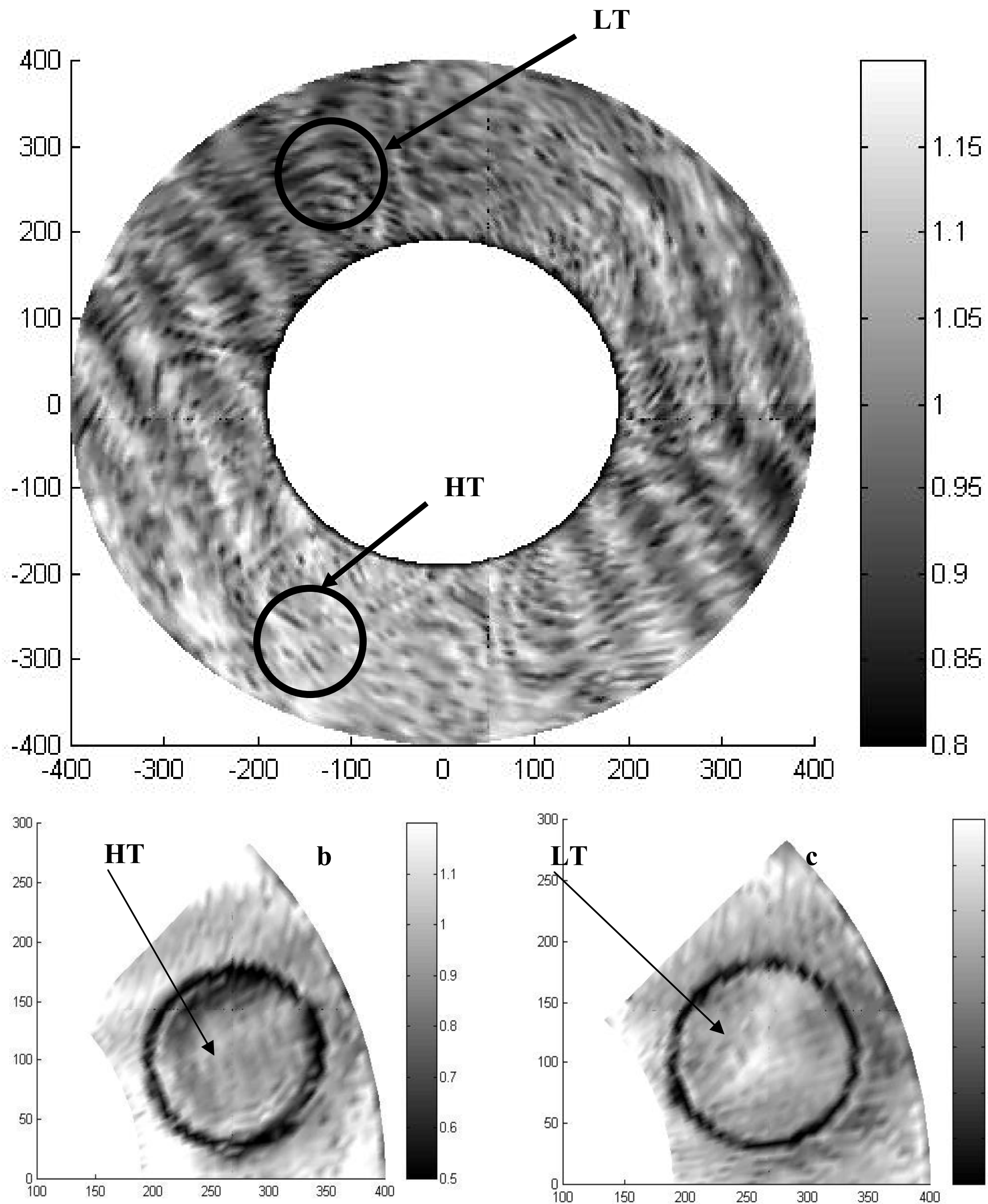

Fig. 5.4 a) Pad Mapped Before Punching 6-inch Coupons, b) Area of Pad Remapped after Replacing the Punched HT Coupon, c) Area of Pad Remapped after Replacing the Punched LT Coupon (All the Values have been Normalized over the Entire Area)

المنارة للاستشارات
www.manaraa.com

5.8 Pad Dynamic Mechanical Analysis

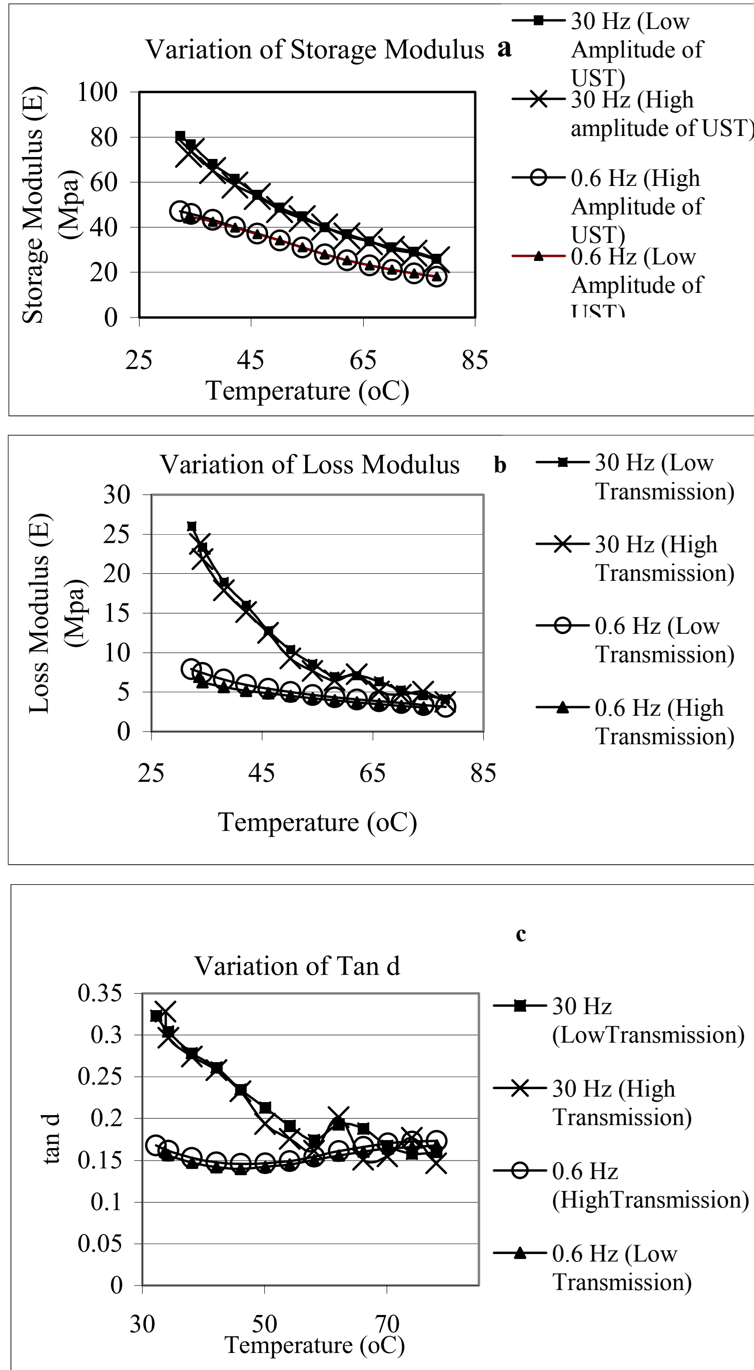

Fig 5.5 a) Variation of storage modulus Vs temperature, b) Variation of loss modulus Vs temperature c) Variation of tan δ Vs temperature of samples tested from low and high intensity region of the pad

www.manaraa.com

In order to evaluate a possible variation in the viscoelastic properties of the HT and LT, DMA was performed on pieces of pads from the HT and LT coupons that were punched out. Fig 5.5 (a, b, c) shows the variation of storage modulus, loss modulus and tan δ with temperature respectively as evaluated by DMA experiments carried out at 30 Hz and 0.6 Hz frequency (two extreme frequency values in the data set reported). There is no significant difference between the magnitude and variation of storage modulus, loss modulus and tan δ for HT and LT samples. It can be thus said that though DMA gives an estimate of the bulk viscoelastic properties of the polishing pad materials (polyurethane), and is not the best technique to characterize the entire polishing pad.

5.9 Frictional Characteristics Polishing Pad Regions

For evaluation of tribological properties (which would directly correlate with the CMP performance) of the regions of non-homogeneity of the polishing pad, new samples of Pad 1 and Pad 2 were mapped using the same UST system. The 360° scans of both these samples are shown in Figs. 5.6 and 5.7. It appeared that there was a lesser area with extreme amplitude (very high or very low) amplitude of ultrasound transmission and hence less variation of specific gravity in Pad 2 as compared to Pad 1. We propose that the relatively lesser variation of specific gravity in Pad 2 could be attributed to the absence of an additional layer of the PSA which joins the pad and sub-pad. The variation of the thickness of the PSA at the interface, in addition to the possible contact stresses can generate variable pressure in the body of the polishing pad. Due to the viscoelastic nature of the polishing pad, these variable stresses may cause variable deformation in the pad matrix which in turn causes the variation in the specific gravity in pad material.

المنارة للاستشارات
www.manaraa.com

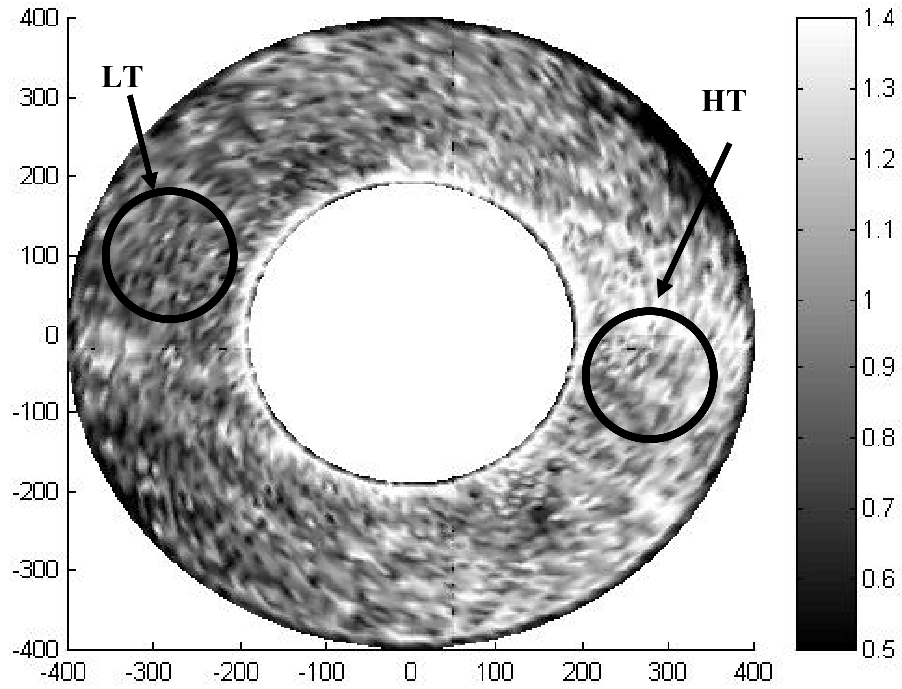

Fig.5.6 Ultrasound Transmission Scan of Pad with Sub-pad

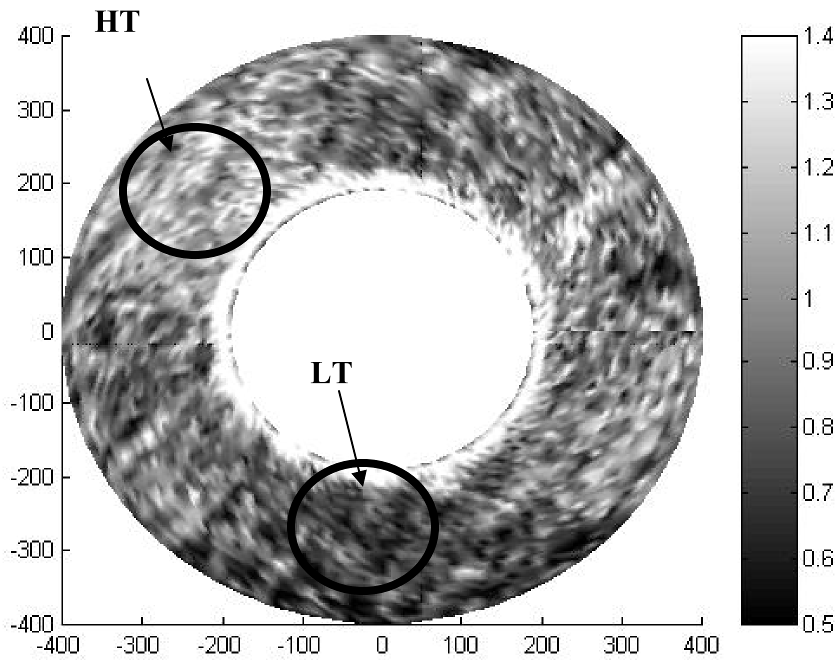

Fig. 5.7 Ultra-sound Transmission Scan for Pad without Sub-pad

المنارة للاستشارات
www.manaraa.com

It must be mentioned here that there was no transient variation of in the density of different polishing pad regions when the same pad was remapped in its entirety after an interval of 24 hours. When HT and LT coupons were punched out, there was a general stress release in the pad matrix. The histograms of the pad ultra sound permeability obtained before and after punching coupons out of the pad also support this hypothesis (ref. Fig. 5.3 (b, d)). When 6" coupons are pressed out of the pad, there might not be complete relaxation of the built in stresses due to the partially viscous nature of polyurethane. However, as can be see from Fig. 5.4 (a, b, c), there is a definite reorganization of the stress topography. Due to the nature of pad fabrication and viscoelastic properties of polyurethane material a complete uniform and stress free Pad 1s difficult to fabricate and there will be minor variations of specific gravity in the polishing pad. However, it is necessary to ensure that specific gravity variations in the pad stay to the absolute unavoidable minimum in order to obtain uniform CMP output.

The 6 inch diameter HT and LT both Pad 1 and Pad 2 (ref Figs. 5.6, 5.7) were used to polish 5000 Å HDP ILD material at the conditions elaborated in the experimental section of this paper to evaluate their CMP performance. Each polishing run was performed for 90 seconds. The COF, which is the ratio of the shear force (F_s) to the normal force (F_N) ($COF = \frac{F_s}{F_N}$), was measured in situ. The average of the values of COF obtained for the first 30 seconds of polishing has been reported as the characteristic COF value of the pad coupon. Fig. 5.8 (a, b) shows the variation of COF with down force and platen rotation for 3, 6 PSI and 100, 200 and 300 RPM respectively for Pad 1 and 2. It can be safely said that the HT and LT regions show different values of COF during CMP

المنارة للاستشارات
www.manaraa.com

under the various CMP conditions of PSI and RPM.

There is a general trend of a decrease in the values of COF values with the increase in platen velocity. It must be noted here that, the values of COF reported are an average of 5 CMP runs with a ± error of 5-7%. The COF for a given process condition is due to the combination of shear at the pad asperity heights and shear due to the slurry film. The shear or friction produced by the “two body abrasion” at the pad wafer interface is higher than the “three body abrasion”. With increase in the platen velocity, there is an increase in the slurry film thickness on the surface of the pad. This in turn increases the part of the down pressure supported by slurry film and decreases the pad asperity contact with the wafer. Due to increase in the extent of three body contact abrasion at the pad wafer interface, there is a decrease in COF with increase in platen velocity and slurry film thickness [175, 176]. Figs. 5.8 (a, b) also shows a decrease in COF for both Pad 1 and 2 with an increase in down force. These results are in agreement with those obtained previously on this set up.

Fig. 5.8 a shows the comparative COF values for HT and LT regions of Pad 1. At 3 PSI, the LT region shows consistently higher values of COF for all the different values of platen rotation. However, at 6 PSI the COF values for HT region are mostly higher. Similar trend can be seen from Fig. 5.8b, where the values of COF for HT region of Pad 2 are consistently higher as compared to the corresponding LT region for the given set of machine input parameters. It has been shown previously, that there is no change in the mechanical properties (storage modulus, loss modulus and toughness) the HT and LT regions (ref Fig. 5.6 a-c). Hence, when the values of COF are compared at the given set of machine conditions, for the different regions of ultrasound permeability, it

www.manaraa.com

can be expected that the mechanical response of pad under those conditions should remain consistent for both types of the pad samples. The change in COF can be thus attributed to the change in the shear force experienced on the pad under the same machine conditions. The values of applied down pressure W, tan δ and H remaining the same, the shear force changes due to the change in shear stress per unit area experienced by the pad. This may be a function of the variable specific gravity of the pad. A comparison of this pad behavior could be made with a spring coil mattress wherein, certain different small regions are kept under constant compressive and tensile loading for sustained period of time. After the pressure on all the regions is released, there is, in general, a relaxation of stress in the spring coils of the mattress. However, the equilibrium state of the coils that were formerly under tensile loading is different from the spring coils form the regions that were previously under compressive stress. In the same way, upon stress relaxation due to isolation from the parent pad, the different HT and LT regions of the pad show slight variation in their respective specific gravity at equilibrium. This difference in the specific gravity may thus be responsible for the slight variation of COF seen during the CMP experiments (ref Figs. 5.8 a, b). The dependence of the maximum shear stress of the pad surface on its specific gravity needs to be further investigated. The material removal during CMP directly depends upon the shear force exerted on the material surface. In the event of the variation in shear force for given polishing conditions, there is a chance of non uniform material removal. This phenomenon thus has the potential to cause the WIWNU and WTWNU defects during the CMP process.

www.manaraa.com

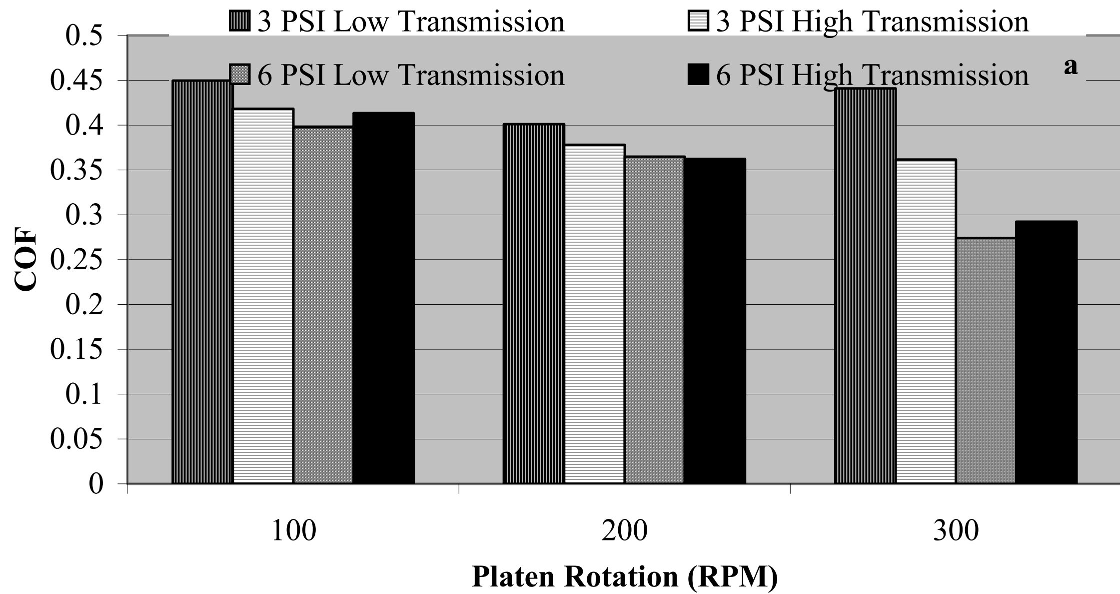

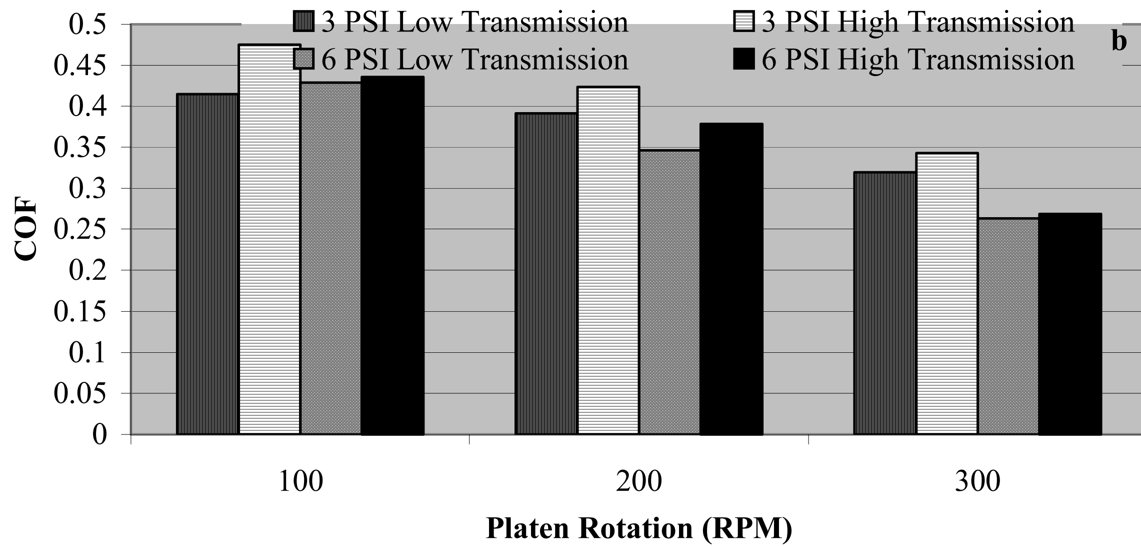

Fig. 5.8 Variation of COF for a) Pad 1 and b) Pad 2 during the CMP process for the Various Values of PSI and RPM

www.manaraa.com

5.10 Summary of Investigations of Polishing Pad Non-uniformities

The spatial variation of the ultrasound permeability in the polishing pad measured by the scanning UST metrology is an excellent indicator of the specific gravity variation in the CMP polishing pad. The most prominent reason for the variation in the specific gravity is the variation of PSA layer which bonds the pad with the sub-pad. The built in stresses are entrapped in the pad and hence, isolation of the “high” and “low” ultrasonic transmission regions brings about an overall redistribution (relaxation) of the stresses in the pad and improves pad uniformity. The polishing pad must be evaluated as whole in a non-destructive manner, as the mechanical properties of the small pad’s portion represent the bulk mechanical properties of the pad polyurethane materials and are not adequate indicators of the pad CMP performance. The pad when subjected to CMP evaluation shows a decrease in COF with increase in platen rotation and down pressure due to the mechanical response characteristics of polymers. There is a variation in the polishing performance of the different isolated regions of non uniformity. This may be translated in to variation in material removal during the CMP and cause the WTWNU and WIWNU defects. Such a variation in the shear force occurs in spite of HT and LT region isolation. Hence, CMP performed with the polishing pads with built in stress and having areas of varying specific gravity will have a direct impact on the process repeatability.

المنارة للاستشارات
www.manaraa.com

CHAPTER SIX

INVESTIGATION AND OPTIMIZATION OF APPLICATION SPECIFIC CMP PADS

6.1 Application Specific Pad (ASP) for CMP

Due to its crucial role in CMP, the mechanical, chemical, and physical properties of the polishing pad play a significant role in the material removal and final global planarization of the wafer surface. The properties of the pad are both intrinsic and extrinsic functions of the polymer or the foam from which the pad is made [177-179]. Historically, polyurethane-based pads (e.g., IC1000 / Suba IV stacked pad (Rodel, Newark, DE)) have been used to obtain both good uniformity and efficient topography reduction, due to their unique property of combining high strength with high hardness and modulus, plus high elongation at break [77, 103]. With increased polishing cycles, slurry particles and polishing debris can be trapped on the surface pores. Also, the pad surface becomes *glazed* due to: 1) deposition of worn/abraded material and 2) smoothing effect of the slurry residue, causing a decrease in pad surface micro-roughness [180]. This causes a drop in the material removal rate (MRR) during the CMP process. The conditioning process done typically using diamond grit restores pad surface asperities, removes worn out debris and the reaction products of the pad and the slurry. However, the process of conditioning accelerates pad wear, reduces the pad life and modifies pad

المنارة للاستشارات
www.manaraa.com

surface after every run. The modified surface may even affect the CMP resulting wafer uniformity after polishing [181-183]. If the conditioning step is bypassed, there will be far reaching benefits in terms of: 1) operator convenience, 2) process optimization, 3) process down time and 4) uniformity of process output.

It has been shown that the material properties of the polishing pad directly impact its CMP output [184, 185]. There is a drop in MRR, as a function of time due to the varying mechanical response under conditions of critical shear [184]. There is also a variation in wafer planarity as a function of pad stiffness, which is determined by the elastic properties of the pad material [186, 187]. Also, there can be numerous other process defects such as dishing [188], erosion [189], non planarity etc. due to the mismatch of the pad wafer hardness.

The use of a surface coating on the pad is becoming increasingly widespread as an effective means of enhancing and modifying the surface mechanical properties by "surface engineering" [190]. The mechanical and viscoelastic properties of the pad material are altered if the polishing pad is coated appropriately. Variation in the thickness of coating can yield a thin film of varying hardness which can be then matched with the hardness of the wafer [190]. The matching of mechanical properties inherently affords polishing rate selectivity and reduces process induced defects.

Taking the aforementioned factors into account a novel polishing pad using polyolefin [191] instead of polyurethane has been developed. This pad is coated with a ceramic on top to tune the mechanical properties of pad surface during the CMP process [192]. The coatings lend application specificity to the pad by matching its surface hardness to that of the material being polished. The salient features of this pad are: 1) no

المنارة للاستشارات
www.manaraa.com

need for the traditional pad 'break-in' before polish, no conditioning / dressing ever, 2) no need to keep pads wet in idle mode, 3) long pad life, 4) high selectivity, 5) ergonomically friendly / easy pad changes due to a redesigned pressure sensitive adhesive and 6) demonstrated pad-to-pad reproducibility.

6.2 Scheme for Optimization of ASP Properties

In this research, we have performed metrology, characterization and prototype CMP performance evaluation of different variants of ASP for Tungsten polishing. The cross section analysis, surface characterization, estimation of surface and bulk mechanical properties, evaluation of static and dynamic tribological properties for different candidate polishing pads coated with ceramic material for different time durations has been performed. The pads with varying total thickness and fixed optimum ceramic surface coating time were then subjected to the prototype CMP process. The results of the experiments were directly used to finalize: 1) surface ceramic coating time and 2) pad thickness, prior to commercialization.

The polishing pad used in this research was made up of talc and calcium carbonate ($CaCO_3$) filled EVA-polyethylene blend thermoplastic. Cross linking is done via a free-radical mechanism, catalyzed by cumyl-peroxide, during the thermal extrusion process [193]. The use of metal-oxides or ceramics such as Tetraethylorthosilicate (TEOS) (used in this case) to coat the pad surface makes the pad permanently hydrophilic. The surface modification of the psiloQuest's application specific pads (ASP) was accomplished through plasma enhanced vapor deposition (PECVD) from organometallic precursors. The details of the surface coating technique have already been

المنارة للاستشارات
www.manaraa.com

elaborated elsewhere [192]. The surfaces of five different pads (for convenience referred to Pad 1, Pad 2, Pad 3, Pad 4 and Pad 5) were coated with TEOS for five different time durations of 10, 20, 30, 40 and 60 minutes respectively.

6.3 Experimental Techniques for ASP Property Evaluation

Scanning Electron Microscopy (SEM) was used to examine the pad surface and cross section, while nanoindentation was used to evaluate the surface micro-mechanical properties as a function of coating time. Nanoindentation technique is widely used for estimation of the mechanical properties of thin films on a substrate [194, 195]. The mechanical response to the indentations, usually by diamond indenters, is used to evaluate the mechanical properties such as Hardness and Young's modulus. In this case, indentation experiments were carried out on the surface modified/grafted pads using a NANOTEST 600®. Indentations were performed under ultra low load range. Initial load was 0.1mN, which is a machine parameter. The control parameter was set to 'depth controlled' and each pad was indented for varying depth with a maximum depth of 10000 nm. The results reported are an average of 10 indentations performed for the constant depth of 1600 nm.

The surface modification of the polymer pad for different deposition time was characterized using PHI 5400 X -Ray photoelectron spectrometer. The base pressure used was 10^{-10} Torr. The spectrometer was calibrated using a metallic gold standard (Au ($4f_{7/2}$): 84.0 ± 0.1 eV). Non- monochromatic Mg K$\propto$ X-ray source with energy 1253 eV at a power of 250 W was used for the analysis. Charging shifts produced by the sample were removed by using binding energy scale referenced with respect to the binding

www.manaraa.com

energy of the hydrogen part of adventitious carbon line at 285.0 eV. Peak deconvolution was carried out using PEAK FIT Software.

The static coefficient of friction (COF) of the candidate pads was evaluated using the wear test was run with a Kiedon U45 static COF tool [196]. The variation of static coefficient of friction and static wear rate was plotted against the surface coating time of the candidate pad. The prototype CMP testing was performed on the CETR CP-4 bench top CMP tester. The Si wafers having 6000 Å tungsten over buried SiO_2 layer were used during the CMP run. The polishing was performed at an optimized set of machine parameters known as "best known method" (BKM). The details of the CMP experimental conditions can be seen in Table 6.1. The coefficient of friction (COF), acoustic emission (AE) and MRR for a given process run were determined in-situ. To examine the interdependence of the parameters evaluated during all the aforementioned metrology experiments, a cross tabulation of the different variables was done using the commercial JMP software. Finally, after optimization of pad surface coating time, candidate pads with different total thickness (thin film + polishing pad), starting from 70 mils and going up to 135 mils (intermediate pad thickness in mils were: 75, 85, 95, 110, 115), and having an optimized coating time were subjected to prototype CMP performance evaluation. It must be noted here, that CMP polishing runs were repeated for 8-10 times for a given condition. The values of data for samples with very high surface microscratching defects were discarded. The surface microscratching may sometimes result from slurry particle agglomeration or impregnation of abraded chip on the pad. The average values (with an error of ± 5 %) MRR and COF were reported.

المنارة للاستشارات
www.manaraa.com

Table 6.1 Experimental details of CMP process used for ASP evaluation

#	Parameter	Conditions
1	Down Pressure	2 PSI
2	Platen Rotation	150 RPM
3	Carrier Rotation	145 RPM
3	Slider Position and Movement	Stationary at 40 mm from platen center
4	Slurry	Commercial Cabot W-2000 (pH 2.5)
5	Pad	Different psiloQuest ASP with spiral grooves
6	Time of polishing	90 sec (Values of AE and COF noted in the first 30 seconds have been plotted)
7	Polishing Specimen	1" X 1" coupon of 6000 Å $W/SiO_2/Si$ (wafer)

6.4 Evaluation of ASP Surface Micro-mechanical Properties

The surface of the ASP can be permanently modified when the pad asperities and troughs are covered with TEOS. The cross section the ASP in comparison with a commercial IC1000 Suba IV polishing pad can be seen in Fig. 6.1 a, b. The commercial polyurethane pads need two layers of pressure sensitive adhesive (PSA) when a sub pad is attached to the polishing pad to impart better conformability. The variation in the thickness and expansion of the PSA with time and temperature in conjunction with the interfacial contact stresses is known to cause several specific gravity variations in the body of the polishing pad [197].

المنارة للاستشارات
www.manaraa.com

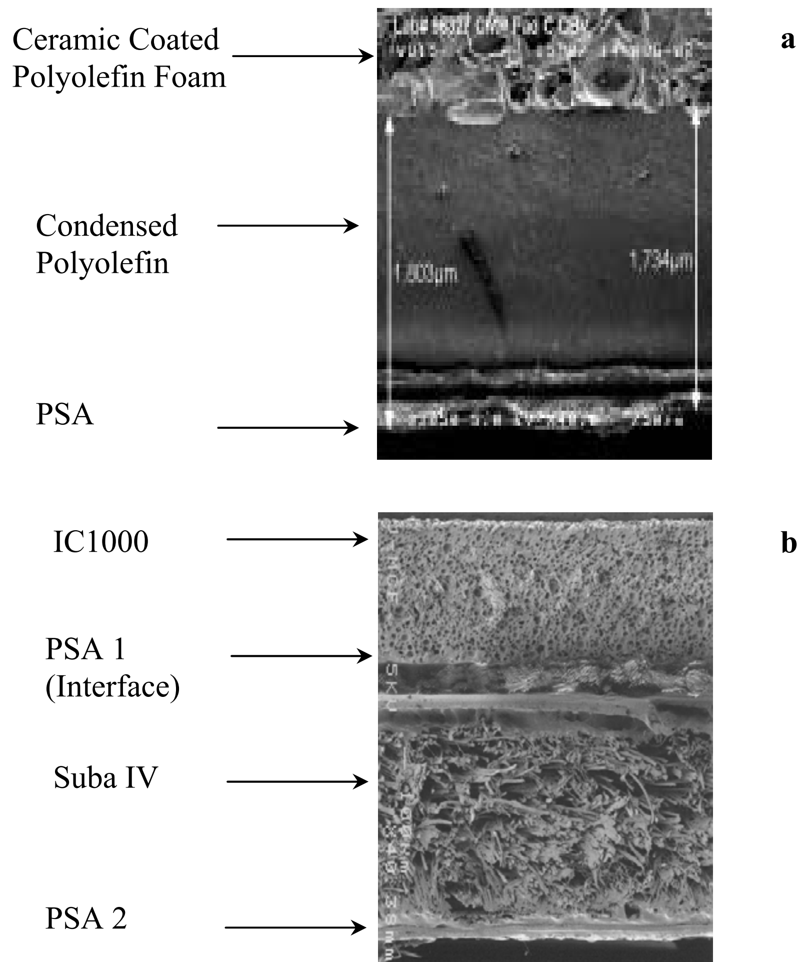

Fig. 6.1 Cross-sectional SEM micrograph of a) PsiloQuest's ASP and b) Commercial Polyurethane Polishing pad with a sub pad

The load vs. displacement data curves obtained from nanoindentation were analyzed using the Oliver and Pharr Method to estimate the micromechanical properties of the surface TEOS film [155, 156]. The viscoelastic nature of the substrate may directly affect the surface penetration of the nanoindentation [198, 199]. Fig. 6.2 shows the

المنارة للاستشارات
www.manaraa.com

loading-unloading curve when nanoindentation was performed on Pad 1. During loading, several nodes of non-uniform tip penetration were observed with increasing load (X_b: pop in). Conversely during unloading, the tip showed exactly the opposite phenomenon of non uniform withdrawal (X_c: pop out). The depth at which the non-linearity in the loading curve occurs for the first time is marked as X_a. Such non-uniform penetration of the indenter tip into the coatings probably results from the initiation and/or propagation of the crack in the ceramic coating [200]. It is well known that plastic deformation under indentation, which is analogous to the impregnation of abrasives on the surface, is a critical attribute of CMP pads. Thus, these 'events' in the load-depth curves may be good predictors of pad performance when put in to service. The studies revealed that X_a is a function of PECVD coating time.

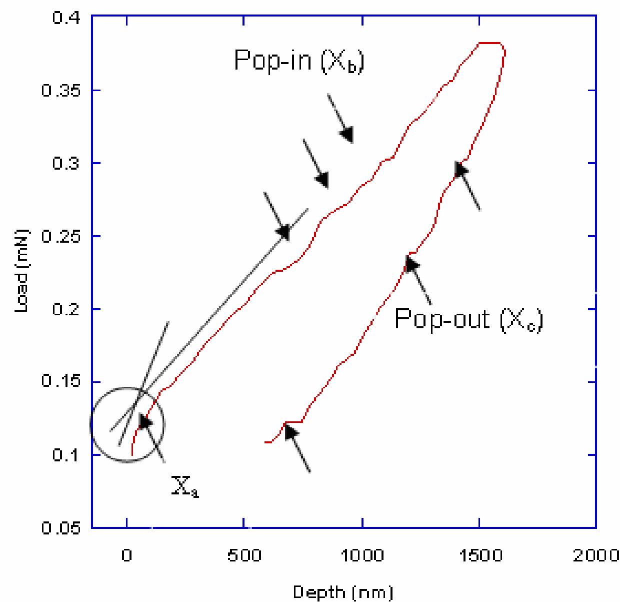

Fig. 6.2 Loading and Unloading Behavior Exhibited by the PsiloQuest's ASP coated for 10 minutes (Pad 1). Note the non-linearity at the Specific Sites of the Loading and Unloading Curve Represent Plastic Deformation under Indentation

المنارة للاستشارات
www.manaraa.com

Fig. 6.3 shows the correlation of X_a on PECVD-TEOS coating time for all the candidate pad samples with 1600 nm deep indentations. The data suggest that X_a is related to the thickness of the ceramic coated on the surface of the pad foam. The depth of penetration before plastic deformation increases with increase in TEOS thickness, till it reaches a plateau for a coating time of 40 minutes. The mechanical properties (Hardness and Young's Modulus) derived from the loading unloading curve are shown in Fig. 6.4.

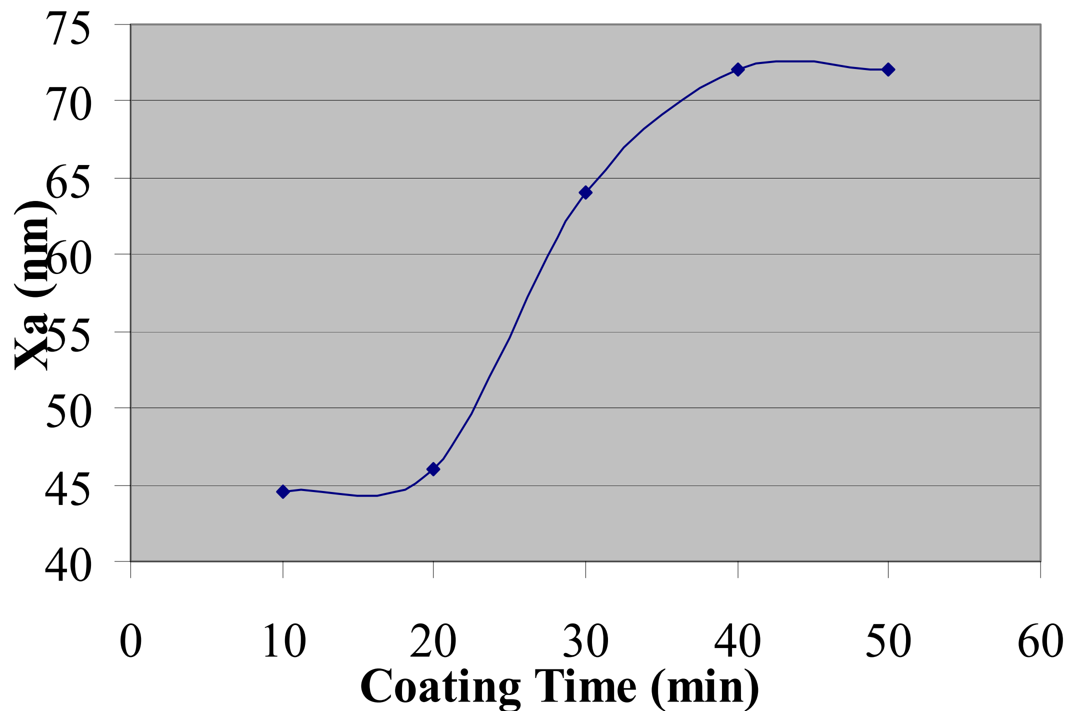

Fig. 6.3 The Variation of Depth of First Non-linearity of in the Loading Curve (Xa) as a Function of PECVD-TEOS Coating Time for Different Pads Evaluated

The increase in pad coating time: 1) will increase the thickness of the surface coating and 2) can possibly improve the density and conformability of the surface

المنارة للاستشارات
www.manaraa.com

coating. There is an increase in the hardness and Young's Modulus of the surface with the increase in PECVD-TEOS deposition time. This may be primarily due to the fact that as the thickness of the rigid film on the compliant substrate increases, for a given depth of penetration, nanoindentation predominantly tends to yield the actual thin film mechanical properties with decreasing substrate compliance effect.

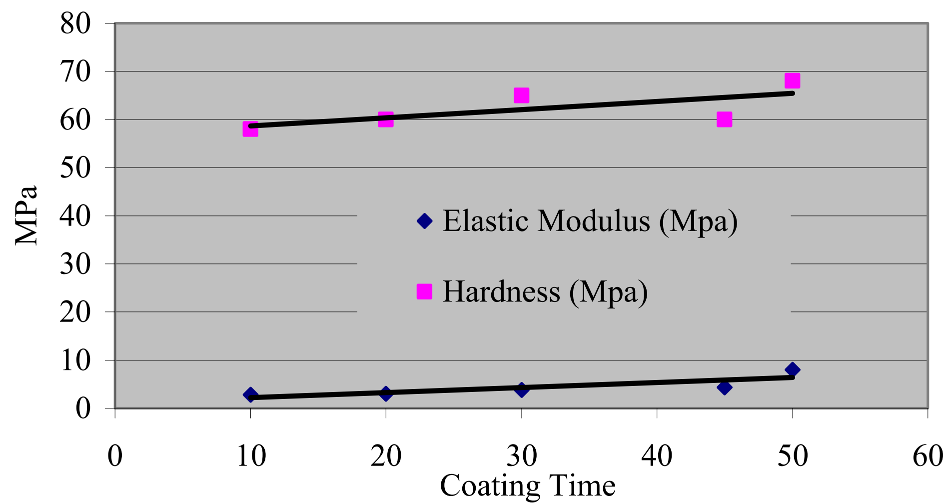

Fig. 6.4 Variation of Elastic Modulus and Hardness with TEOS Coating Time Evaluated by Nanoindentation for Different Evaluated Polishing Pads

6.5 Evaluation of ASP Surface Micro-mechanical Properties

The information on the variation in the pad surface chemistry with the change in coating time was obtained using XPS analysis. The C (1s) signal resolved into three major peaks: a peak at 285.0 eV represents the C-C and C-H bonds and a peak observed at 286.5 eV represents the C-O bond. These results agree with the previously published literature [201]. A peak component centered at 289-289.3 eV can be attributed to carbamide [-O-C (NH_2) =O] functional group from the residues of the blowing agent

www.manaraa.com

used in the pad substrate manufacturing process. For the specimens coated for 40 and 45 minutes respectively, an additional peak was observed near 283.6 eV. This peak can be assigned to a C-Si bond. The XPS Si (2p) spectrum was deconvoluted into two major peaks at 102.3 and 103.4 eV, which represent the silicate and Si-O species, respectively. The data indicate that PECVD processes produced surface films rich in silanol, consistent with TEOS films deposited at low process temperatures [202-207].

Fig. 6.5 shows the XPS results for pad samples coated with PECVD-TEOS for the given different time durations. Fig. 6.6 shows the oxygen to silicon (O/Si) intensity ratio values calculated from the XPS data. This ratio is proportional to the concentration of the silanol in the deposited coatings. There was a decrease in the silanol concentration with the increase in the coating time up to coating time of 30 minutes; beyond which the silanol concentration again showed an increase. Furthermore, a small peak is observed at 102.1 eV, which represents Si-N bond for Pads 3, 4 and 5. There is also an abrupt reduction in Si to N ratio, which indicates an increase in nitrogen species on the surface. The XPS observations suggest that as the deposition time increases, substrate (polymer pad) temperature also increases, which causes outgassing of the nitrogen used in foaming the substrate. The nitrogen reacts with the Si species on the pad surface, which causes formation of Si_3N_4 species in stoichiometric conversion from SiO_4 to Si_3N_4 [208-210]. At higher coating times, the ion bombardment of the foam surface may generate appreciable amounts of C radicals on the surface of the pad. These radicals react with the silicon species to form silicon carbide (SiC), which is subsequently incorporated in surface coating of the pad.

المنارة للاستشارات
www.manaraa.com

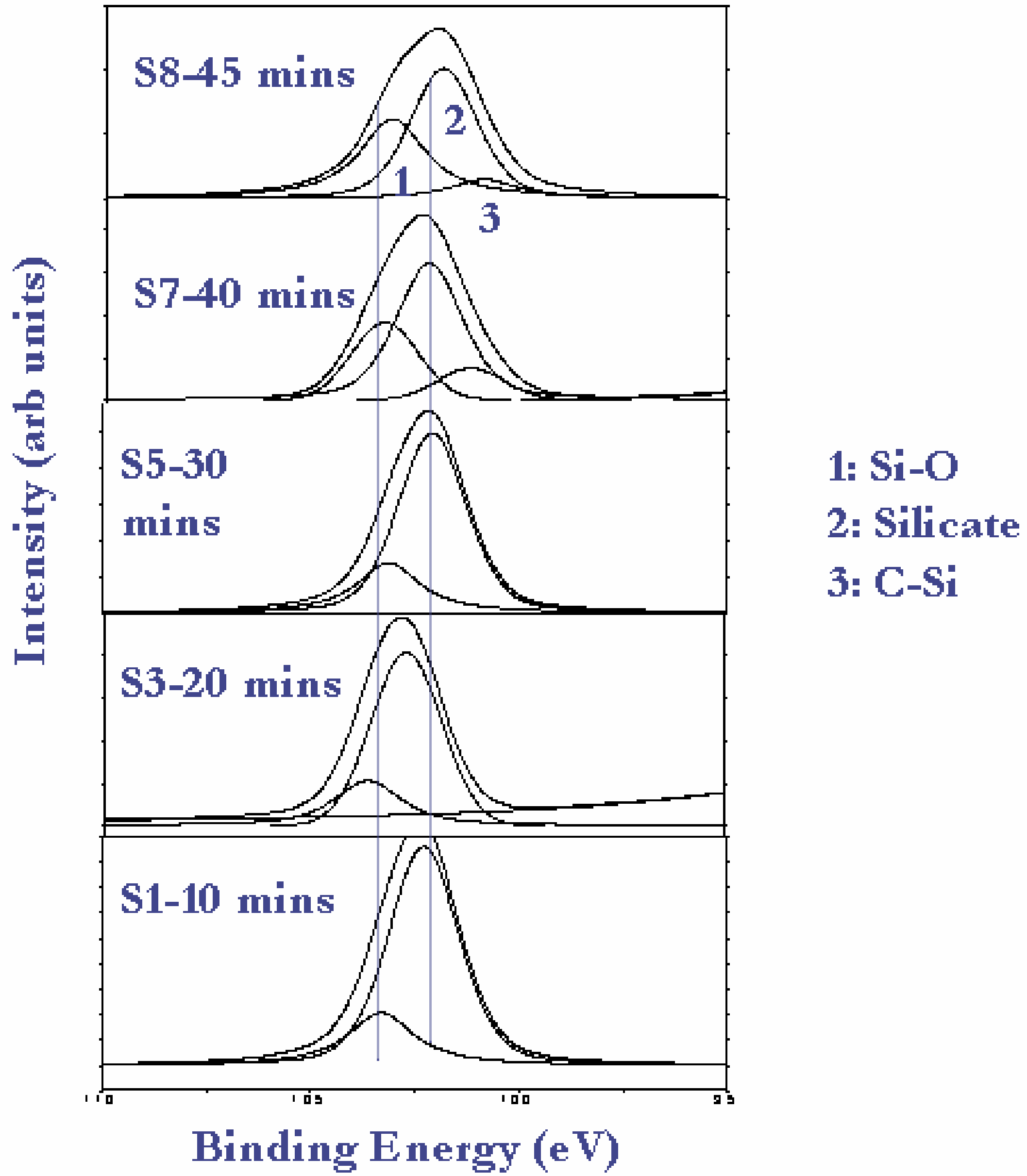

Fig. 6.5 X-Ray Photoelectron Spectroscopy (XPS) Data for Polishing Pads with Different TEOS Surface Coating Time

المنارة للاستشارات
www.manaraa.com

The incorporation of Si_3N_4 and SiC species would certainly be expected to make the pad surface stiffer and may contribute towards the improvement in its mechanical properties. The XPS results also show that the PECVD TEOS forms a very complex compound on the surface of the polyolefin foam due to the combination of several elementary reactions. The PECVD-TEOS coating process produces both silica and silicates (SiOX and SiO_2) on the foam surface. The change in the surface chemistry of the substrate as a function of deposition time at a fixed TEOS/O_2 mixture can be progressively observed from the XPS results.

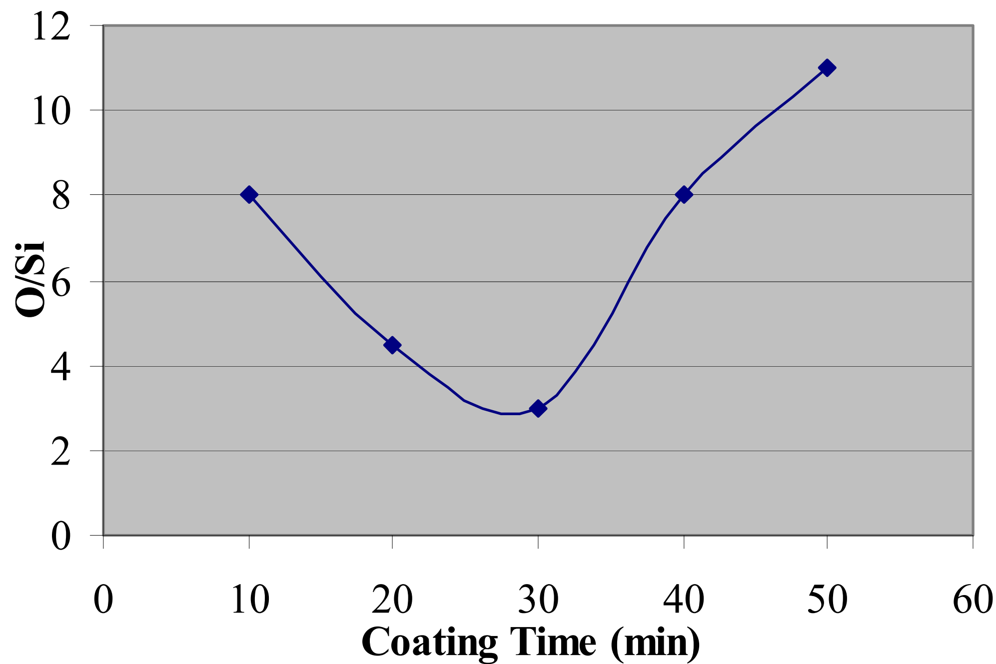

Fig. 6.6 Variation in Surface Silanol / Silicates in PECVD-TEOS Coating as a Function of TEOS Deposition Time

المنارة للاستشارات
www.manaraa.com

6.6 Evaluation Static Tribological Properties of ASP

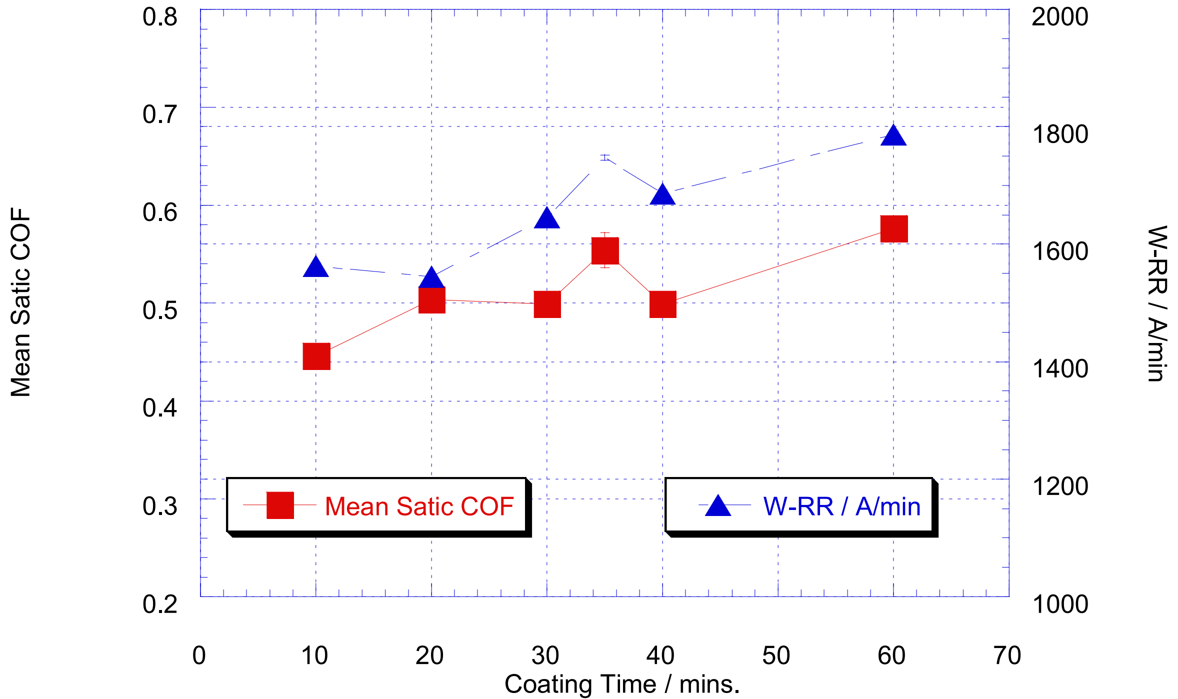

Fig 6.7 Variation of Static Wear Rate and Static Coefficient of Friction for Pads with Different PECVD TEOS Surface Coating Time

A static wear test was performed to gauge the impact of the variation of the surface chemistry on the tribological properties of the pad. The variation of pad surface wear rate and the static COF for different pads evaluated using the blanket W wafers is shown in Fig. 6.7. There was a general trend showing an increase in the static COF and wear rate with the increase in pad surface coating time. Initially there was a plateau observed when COF and Wear rate for Pads 3 and 4 were evaluated. A special case of pad coated with 35 minutes of PECVD TEOS coating was evaluated specifically for this experiment. The 35 minutes PECVD TEOS coated pad showed a higher wear rate and static COF as compared to Pad 3 and 4. The increase in the static COF and wear rate for

المنارة للاستشارات
www.manaraa.com

the 35 minutes coated pad correlates very well with the previous XPS observation of decrease in O/Si ratio or increase in Si content on the surface with coating time. Also, the further increase in static COF and W wear rate is due to combination on Si with Carbon and Nitrogen on the surface to SiC and Si_3N_4 (as verified by XPS).

6.7 CMP (Dynamic Tribological Properties)Evaluation of ASP

The sample-to-sample variation of dynamic COF during prototype CMP experiments for different candidate pads is shown in Fig. 6.8. There does not appear to be a definitive trend in the variation of COF (COF of 5 CMP runs is reported here without averaging) with increasing coating time.

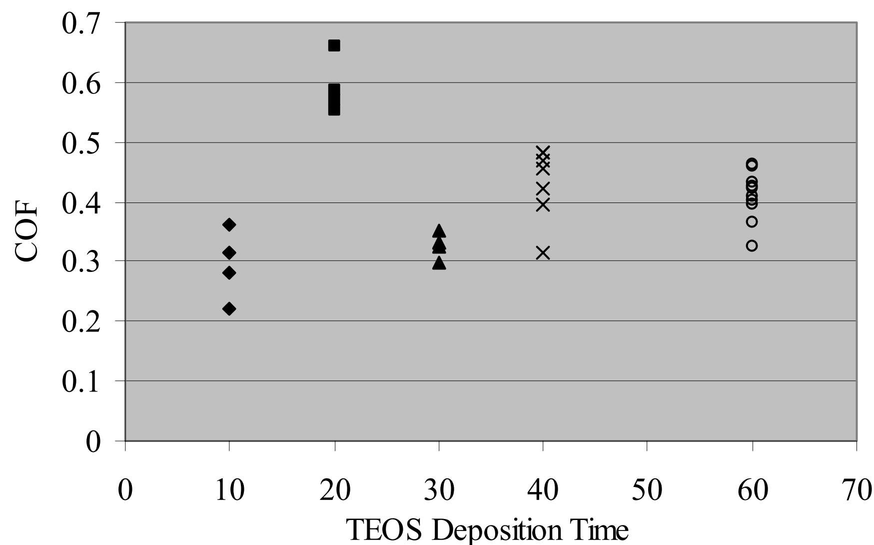

Fig. 6.8 Variation of the Average Value of COF (taken for First 60 Seconds) for the Different Candidate Pads during the Polishing Runs at 2 PSI Down Force and 150 RPM Platen Rotation

www.manaraa.com

The variation of average MRR with coating time for different evaluated polishing pads is shown in Fig. 6.9. It can be seen from the figure, that there was a general decrease in MRR with increase in coating time from Pad 1 to 3. The subsequent increase in coating time brings about an increase in MRR for Pad 4 but saturation is reached at this level. It must be noted here that the pad MRR is significantly lower than accepted standards for W polishing because of: 1) use of prototype CMP experimental set up, 2) no slider oscillation, 3) relatively lower values of down force and platen rotation chosen for CMP evaluation.

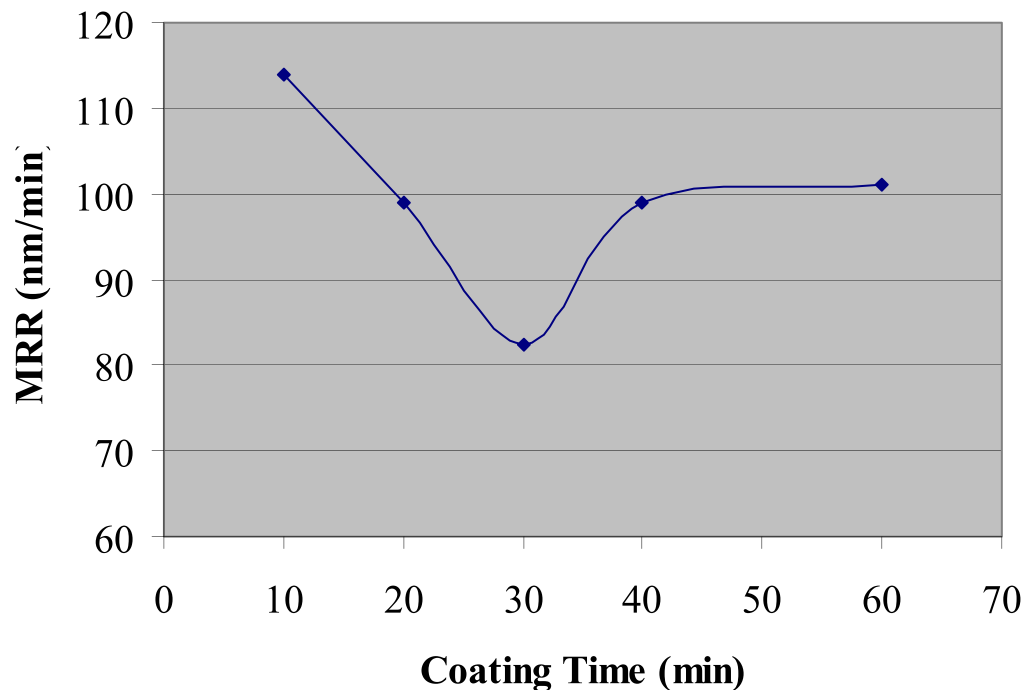

Fig. 6.9 Variation of the Average Value of MRR for the Different Candidate Pads during the Polishing Runs at 2 PSI Down Force and 150 RPM Platen Rotation

المنارة للاستشارات
www.manaraa.com

In order to find the interdependence of the different evaluated pad metrology parameters namely: 1) coating time, 2) mean static COF, 3) mean static wear rate, 4) mean dynamic COF and 5) mean MRR, multivariate cross correlation was done using the JMP ™ software. The correlation coefficients of the different evaluated materials have been shown in Table 6.2. It can be seen from the table that there is a direct dependence of static surface properties such as wear rate and static COF with the pad coating time. However, there was little or no direct correlation of pad surface coating time duration with the CMP output parameters of dynamic COF and MRR. Thus, any trend in the variation of dynamic COF and MRR with the pad coating time can only be considered as the secondary effects of polishing. There is a very good correlation between the static COF and static wear rate of the pad surface, but there is very little correlation between the dynamic COF and MRR. The static tribological property evaluation, which is non destructive, was done in order to correlate it with the CMP performance of the polishing pad. However due to their inadequate correlation with the dynamic tribological properties, the static tribological properties cannot be considered as good indicators of pad CMP performance.

The static COF is the ratio of the lateral frictional force to the normal reaction when two surfaces come in contact, while the dynamic COF during CMP the ratio of the shear force (F_s) to the normal force (F_N) ($COF = \frac{F_s}{F_N}$)[56]. The increase in down force brings about a corresponding increase in the shear force (F_s) as shown in Eqn. 6.1[57]

$$F_s \propto W \frac{\sigma}{H} \tan \delta \quad (6.1)$$

المنارة للاستشارات
www.manaraa.com

where W is the downward loading, σ is the maximum shear stress on the given pad area, H is the hardness of the polishing pad and $\tan \delta$ is the ratio of the loss modulus to the storage modulus (which is also a measure of the toughness) of the pad. The dynamic shear is a function of the loading, pad hardness, stiffness and the pad asperity contact with the wafer. The normal reaction upon loading depends upon the storage modulus (elastic component) of the polishing pad. The MRR during CMP on the other hand partially depends upon the surface shear and is also governed by factors such as slurry film thickness, abrasive size, pad compliance, surface reaction kinetics and heat dissipation from the interface. Hence, dynamic COF and MRR show very weak correlation between themselves. The increase in pad surface micromechanical properties with the increasing in coating time however causes an increase in the wear of the W samples. The static wear of W is only due to the lateral frictional force between W and pad surface. Thus a very good correlation between pad coating time with static friction and wear is seen. The static friction and static wear also have a good correlation due to the very same reason.

As the surface film coating time increases, the thickness and conformability of the film on the surface increases. This may bring about an increase in the stiffness of the pad at and near the surface. This may decrease the MRR due to decrease in pad compliance and asperity contact under the applied load as seen from the MRR data for Pad 1, 2 and 3 (ref. Fig. 6.9). Though the substrate is maintained at room temperature, the electrode used to strike the plasma in the PECVD chamber operates at an elevated temperature. Due to heat dissipation by radiation, there is an increase in the substrate temperature which becomes pronounced when coating time exceeds 30 minutes. This

www.manaraa.com

increase in substrate temperature may strain or even break the bonds between the atoms in the cross-linked polyolefin foam. The return of the polishing pad to the room temperature after surface coating may not re-establish all the bonds and the foam may not regain its original properties. This hypothesis is supported by the evaluation of the bulk mechanical properties using Dynamic Mechanical Analysis of similar ASP surface coated for different times reported elsewhere [168]. The reported data show that there is a general trend showing a decrease in storage modulus and an increase in the loss modulus of the pad with increase in coating time. Hence, even as the surface mechanical properties of the pad increase with the coating time in excess of 30 minutes, the overall compliance of the polyolefin substrate increases the pad asperity contact with the wafer, thereby improving the MRR for Pad 4 and 5. The O/Si ratio on the surface appears to vary in synchronization with the MRR. However, there does not seem to be any direct correlation between the chemical properties of the surface and MRR during CMP.

Table 6.2 Multivariate Correlations between Various Independent Results and PECVD Coating Time

	Coating Time / min	Mean Static COF	W-RR / A/min	Mean (Dynamic COF)	W CMP-RR / A/min
Coating Time / min	1.0000	0.9168	0.9668	0.0495	-0.9735
Mean (Dynamic COF)	0.0495	0.2897	-0.2022	1.0000	-0.1584
Mean Static COF	0.9168	1.0000	0.8140	0.2897	-0.9558
W-RR / A/min	0.9668	0.8140	1.0000	-0.2022	-0.9155
W CMP-RR / A/min	-0.9735	-0.9558	-0.9155	-0.1584	1.0000

للاستشارات المنارة
www.manaraa.com

Though the MRR was found to be highest for Pad 1, nanoindentation studies suggested that the initial surface penetration for the onset of plastic deformation for Pad 2 was the lowest (ref. Fig. 6.3). Therefore, this pad was found to be most susceptible to wear and damage caused by the impregnation of slurry abrasive particles. The value of X_a seemed to reach a plateau for Pad 4 and 5. Thus a TEOS surface coating time of 40 minutes was decided to be optimum from a MRR perspective.

6.8 Optimization of ASP Total Thickness

It is difficult to theoretically quantify the appropriate thickness of the pad foam for which a surface TEOS coating of 40 min. would prove optimum in terms of CMP performance, especially MRR. Hence, polishing pads of different total thickness (film + foam) ranging from 75 to 135 mils were subjected to CMP performance evaluation on the CETR bench top CMP tester. The variation of COF for different pad coating thickness can be seen in Fig. 6.10. The COF shows an increase with the increase in pad thickness. The combined mechanical properties of the polyolefin pad comprise of a combination of mechanical properties of the hard ceramic surface and compliant polyolefin substrate. The effective contribution to the mechanical properties of the polyolefin substrate in comparison with the surface increases with increase in the pad thickness for the same coating time. The thicker foam adds pad compliance and increases the extent of viscous deformation for a given down force. This results in the decrease in the normal reaction of the polishing for the given set of process parameters. As discussed earlier, the COF being the ratio of the shear force to normal reaction, the decrease in the normal reaction with the increase in the viscous nature of the polishing pad brings about

المنارة للاستشارات
www.manaraa.com

progressive increase in the pad COF with increase in total thickness. The variation of MRR for different pad thickness is shown in Fig. 6.11. There is an increase in MRR up to pad thickness of 95 mils; however there is a sharp decrease in MRR for pad thickness of 110 mils. The further increase in pad thickness does not seem to impact the MRR significantly as further increase in the viscous nature of the pad in not translated in to the compliance of the surface due to the inherent stiffness of the ceramic coating. Thus the thickness of pad (95 mils) showing the maximum removal rate was chosen as the optimum pad thickness from the MRR perspective. Finally, it must be noted that considerations besides MRR were taken in to account before the polishing pad was actually commercialized and these findings were interpreted in context of other investigations dedicated towards studying other CMP output variables such as non-uniformity, dishing, erosion etc.

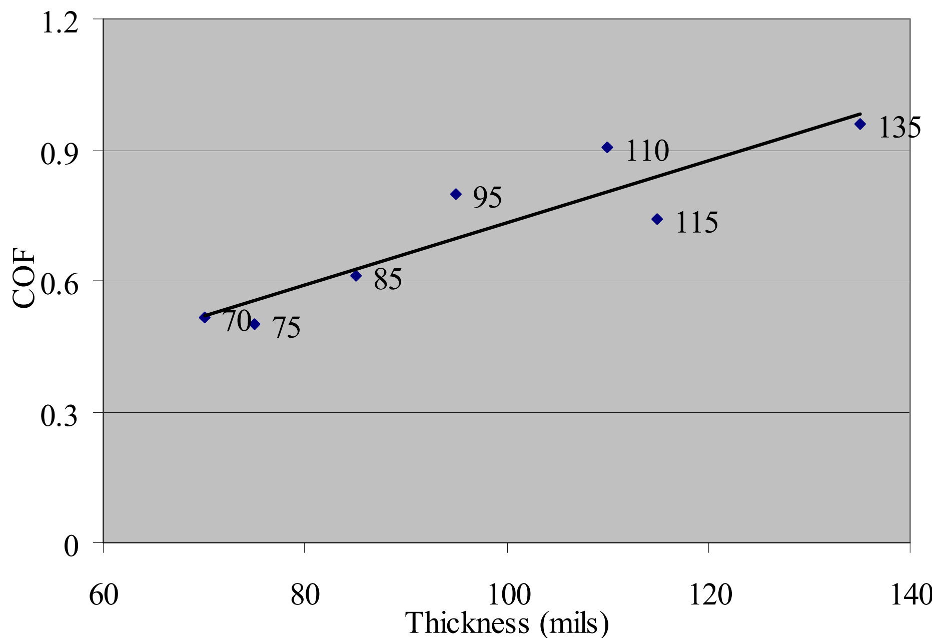

Fig. 6.10 Variation of COF for Different Total ASP Thickness for an Optimized Surface Coating Time of 40 Minutes

المنارة للاستشارات
www.manaraa.com

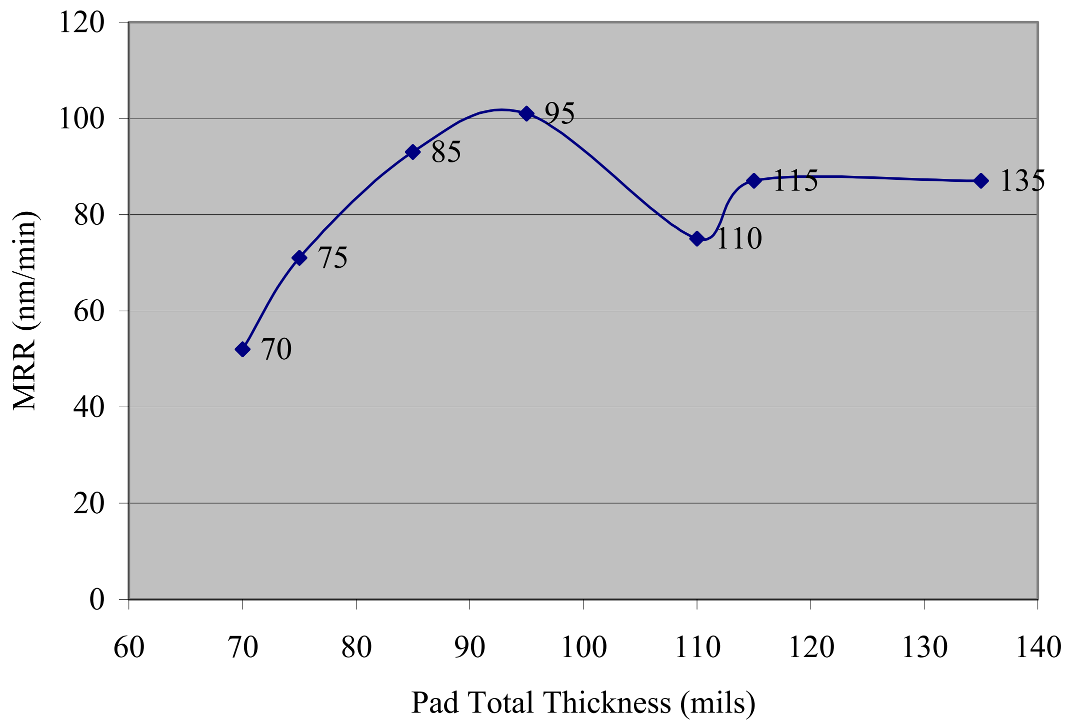

Fig. 6.11 Variation of MRR for Different Total ASP Thickness for an Optimized Surface Coating Time of 40 Minutes

6.9 Summary of ASP Optimization and Characterization

Polyolefin could be effectively used to replace the traditional polyurethane in CMP polishing pads. Polyolefin shows excellent adhesion when coated with a ceramic surface layer using PECVD to fine tune pad wafer hardness without the sub pad. Due to inherent resistance of polyolefin to slurry chemical and with the added chemical protection and hydrophilicity of TEOS, no conditioning is required during entire pad lifetime. An elaborate pad metrology matrix has been developed to evaluate the polishing pad before being put in service. There does not seem to be any correlation with pad static

المنارة للاستشارات
www.manaraa.com

tribological properties and dynamic tribological properties. The quality and durability of the surface can be judged by the surface penetration of the nanoindentation tip. The materials removal rate being one of the vital CMP output variables, the pad surface TEOS coating time can be finalized to 40 minutes taking in to account the occurrence of plastic deformation of the surface under incident loading. The pad thickness for enhanced MRR was experimentally finalized to 95 mils. When interpreted with the findings of the experiments performed to optimize other CMP output variables such as dishing, erosion, non-uniformity, this methodology of pad metrology would be useful for characterization and evaluation of different pads with novel architecture before their commercialization.

المنارة للاستشارات
www.manaraa.com

CHAPTER SEVEN

INVESTIGATION AND MODIFICATION OF CMP SLURRY

7.1 Background of CMP Slurry

CMP is a process that is influenced to a great extent by numerous slurry parameters such as pH, solution chemistry, charge type, concentration and size of abrasives, complexing agents, oxidizers, buffering agents, surfactants, corrosion inhibitors, etc. [56, 106, 211, 212]. The specific and proprietary nature of the slurry manufacture makes it difficult to elucidate the exact effects of slurry on the particular thin films that are polished in it. The slurry interactions at the pad wafer interface are probably therefore, the least understood mechanisms in entire semiconductor fabrication process technology [101]. An ideal CMP slurry should be able to achieve high removal rate, excellent global planarization, should prevent corrosion (in case of metal, especially Cu), good surface finish, low defectivity and high selectivity. The typical design criteria for slurry are given in Fig. 7.1. These criteria have been broadly identified after survey of literature [111-117].

7.2 Effect of CMP Slurry in Global Planarization

As discussed in the previous section, the global planarization as a result of CMP process is one of the key outputs of the process. As suggested in Fig. 7.1 the slurry,

المنارة للاستشارات
www.manaraa.com

plays a key role in achieving global planarization. To achieve the requisite level of global planarization without compromising on the removal rate and producing a defect free wafer surface needs optimization of the slurry parameters.

Global Planarization
- Formation of a thin passivated surface layer
- Minimization of chemical etching
- Minimization of mechanical polishing

Removal (Polishing) Rate
- Rapid formation of a thin surface layer
- Control of the mechanical/interfacial properties of the surface layer
- Stress induction by abrasion to remove the surface layer
- Indentation-based wear
- Fracture/delamination-based removal

Surface Defectivity
- Rapid formation of a thin surface layer
- Minimization of mechanical polishing
- Control of particle size and hardness
- Control of particle size distribution

Selectivity
- Top-layer chemomechanical polishing
- Bottom-layer mechanical polishing
- Reduction of mechanical component in slurry

Slurry Handling
- Formation of stable slurries
- Control of interparticle and particle–surface interactions
- Steric-force-based repulsion in ionic systems

Fig. 7.1 Prime Criteria for Slurry Design [101]

المنارة للاستشارات
www.manaraa.com

The slurry parameters must be so optimized that the mechanical removal of the material is minimized as slurry depending upon excessive mechanical removal produces high frictional forces and can thus damage the surface topography. Following are the some of the salient issues that must be considered before specific slurry design: 1) To minimize the frictional forces, the removal rate needs to be compromised and thus the process runs for a longer period of time, 2) also variation in local polishing pressure leads to variable removal rates within the wafer, which seriously compromises global planarization [101], 3)Excessive chemical etching adversely affects surface planarity and induces defects on the surface such as corrosion [220]. Thus, the key to a good polishing step is achievement of synergy between chemical etching and mechanical planarization with minimization of both the phenomena. For this purpose there is a need for the formation of a passivation layer at the interface of the wafer and pad as seen in Fig. 7.2., 4) The passivation layer has to be thinner that the difference in the height between high and low regions in order to avoid within wafer non-uniformity [101]. In case of Cu polishing, the formation of the passivation layer is accelerated by oxidizers such as H_2O_2, potassium ferricynate, ferric chloride, and ferric iodate and corrosion damage to the surface is prevented by corrosion inhibitors such as benzotriazole (BTA) [221]. For tungsten, there is rapid formation of surface passivation layers due to the use of peroxygen compounds and stabilizing agents [222]. The purpose of passivation layer in case of silica polishing is to soften the surface which is inherently hard. Maintenance of alkaline pH in most cases is sufficient [223] for appropriate passivation. During Ta polishing, formation of stable Ta_2O_5 helps in uniform removal of material from the surface [224].

المنارة للاستشارات

www.manaraa.com

To avoid numerous surface defects, the time to achieve the formation of thin passivation layer should be minimized. All these aspects were taken in to account before the evaluation and design of novel slurries.

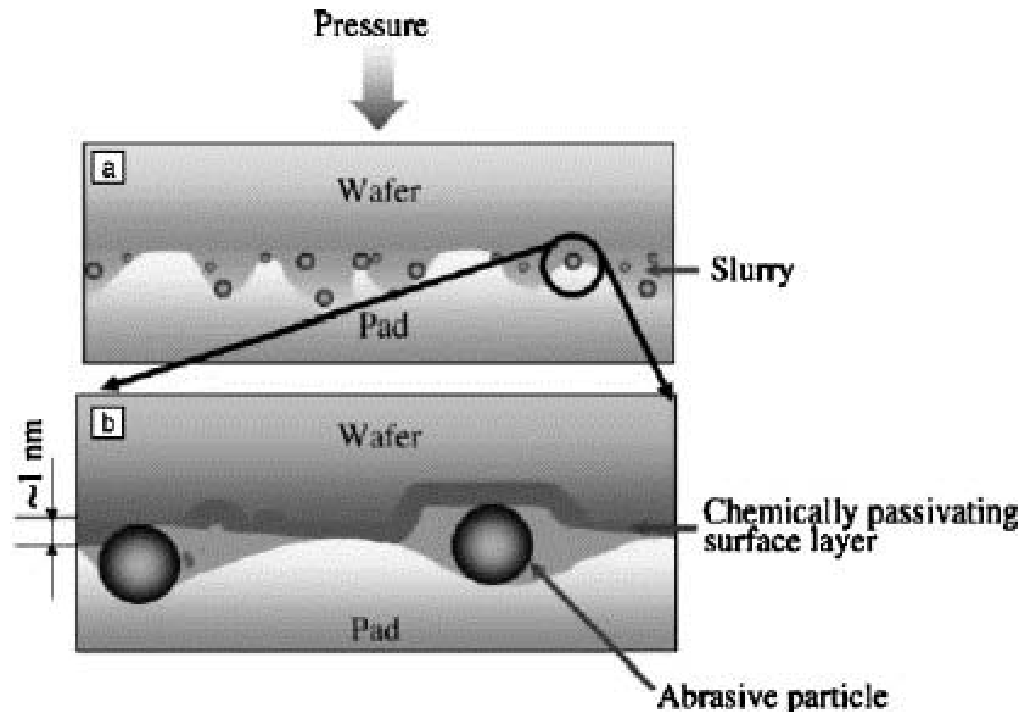

Fig. 7.2 Schematic of Microscale and Nanoscale Phenomena during CMP [218]

7.3 Effect of Slurry on Removal Rate

The chemical action of the slurry chemicals on the material, the mechanical abrasion of the particles on the polished materials, interplay of the different complexing agents, oxidizers and corrosion inhibitors. Chemicals such are oxidizers and corrosion inhibitors vastly affect the reaction rate of the slurry with similar particle nature, size and distributions. Fig. 7.3 shows the variation of the reaction rate of the different slurry components on Cu when the reaction kinetics were studied using electrochemical

المنارة للاستشارات
www.manaraa.com

chronoamperometry [224, 225]. From the electrochemical data, it can be seen from the figure that the surface rate kinetics reaches about 60 Å/s when Cu is immersed in DI H_2O. The reaction rate increases to around 120 Å/s when 5% H_2O_2 is added. However upon addition of 10 mM BTA, the reaction rate came down considerably.

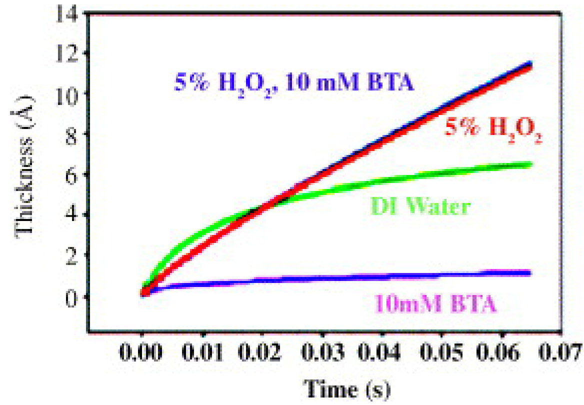

Fig. 7.3 Variation of Rate of Surface Layer Formation in Cu with Different Slurry Chemistry [101]

7.3.1 Effect of Slurry Chemistry on Removal Rate

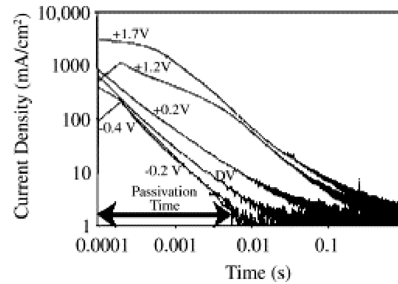

Fig. 7.4 Transient Electrochemical Chronoamperometry Measurements of W [101]

The surface reaction is not the only contributing factor for achievement of high removal rate during CMP. The time scale at which the passivation layer is formed

المنارة للاستشارات
www.manaraa.com

before the average time of successive particle interaction with the wafer for abrasion is also important to produce a defect free, fast CMP process. Fig. 7.4 shows the electrochemical chronoamperometry (potentiostatic) analysis of Tungsten by first keeping the samples at cathodic potential to avoid surface oxidation and then “anodizing” them. The generation of current, which corresponds to surface reaction rate, is monitored on a millisecond scale as shown in Fig. 7.4. It can be seen form the figure, that Tungsten surface quickly passivates which is conducive for mechanical removal of the material.

7.3.2 Effect of Slurry Particle Size, Hardness and Concentration

The generalized materials removal rate (MRR) for oxide has been modeling in the literature and be expressed as shown in Eq.7.1 [225]:

$$MRR = n\mathrm{Vol}_{removed} \quad (7.1)$$

The variable n is number of active abrasives taking part in the process and $\mathrm{Vol}_{removed}$ is the volume of material removed by each abrasive. To estimate the total volume of material removed, it is necessary to estimate the total area of the pad–wafer and wafer-abrasive contact. The area of active abrasive contact is given by:

$$A = \pi x \delta \quad (7.2)$$

where A is the area of contact x is diameter of abrasive and δ is the depth of indentation on the passivating film made by the abrasive particle [226].

المنارة للاستشارات
www.manaraa.com

If one assumes elastic contact between the particles and the surface, the indentation depth as a function of particle size is given by:

$$\delta = \frac{3}{4}\phi\left(\frac{\text{Papp}}{2KE}\right)^{2/3} \quad (7.3)$$

where Φis the particle size, *K* is the particle fill factor at the surface and *E* is the Young's modulus of the surface layer [101, 226, 227]. This equation assumes that the particles are much harder than the surface layer. (7.1), (7.2) and (7.3) show that the area of contact and indentation depth increase with increase in particle size and hardness. It is thus implied that as particle size and hardness increases the removal rate increases. The increase in particle concentration will increase the number of active particles, there by causing more number of indentations to the passivating film and increasing the removal rate. Fig. 7.5 indicates the increase in removal rate of tungsten with increase in particle size and concentration. The details of the experiments can be obtained in the relevant literature [101].

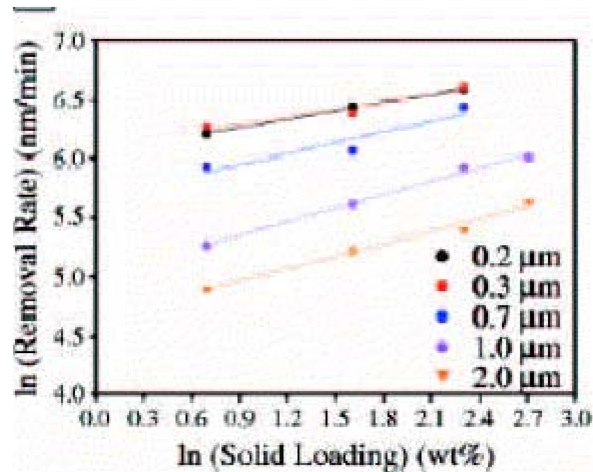

Fig. 7.5 Variation of Removal Rate with Particle Size and Concentration [101]

المنارة للاستشارات
www.manaraa.com

Increase in particle size or hardness also gives rise to surface defects such as micro-scratches that cause fatal long-term device failure. Bigger and harder particles would cause deeper micro-scratches, which will be very difficult to eliminate even by the final buffing CMP step. The increase in particle concentration translates in to increase in removal rate only up to a certain extent. As seen in Fig. 7.6 shown by Singh and Bajaj [101] and Mahajan et al. [215], the removal rate of the silica increases with increase in particle size and concentration at low particle concentration, however after a particular threshold for every given particle size the mechanism of removal changes and there is considerable decrease in removal rate with increase in particle concentration. For the purpose of this experiment, spherical monosized particles were used in slurry of pH 10. Change in material removal mechanism is expected to be the reason of this phenomenon [215].

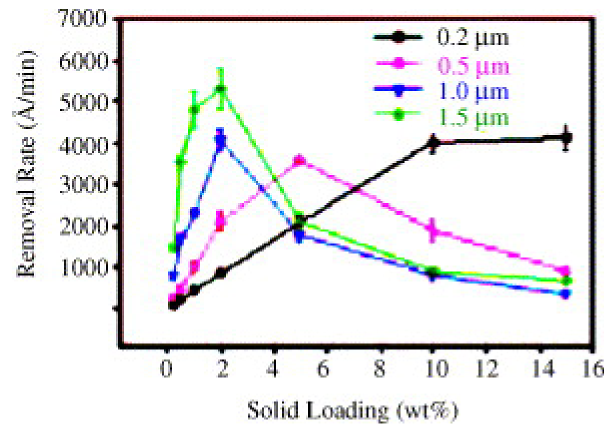

Fig. 7.6 Removal Rate of Silica with Different Particle Size and Concentration [215]

7.4 Effect of Temperature on CMP Slurry Performance

We have studied the impact of slurry temperature on the CMP performance of the slurry. For this study, we maintained the slurry in a range of temperature from 18.5^{o}C

المنارة للاستشارات
www.manaraa.com

to 30°C. Electroplated Copper blanket films of 15000 Å thick were polished using the CETR^{TM} bench top CMP tester using a 6" diameter polishing pad coupon attached to the bottom platen and a 1" X 1" sample coupon faced down onto the pad. Cabot iCue 5001 slurry and IC1000/Suba IV polyurethane perforated pads were used to polish the copper samples. Polishing conditions were maintained at 3 PSI, 100 RPM bottom platen rotation, 95 RPM carrier rotation, slurry flow rate 50 ml/min. The slurry was maintained at the predetermined temperature (both above and below room temperature) for the duration of the polishing experiment. Removal rates were calculated from the in-situ endpoint detection ability of the machine, which shows a change of the COF at the complete removal of the thin film. The time for removal was noted, which gives the removal rate information. The variation of the removal rate along with COF with change in slurry temperature is plotted in Fig.7.7. An overall increase in the removal rate with temperature can be observed from the figure. This increase of the removal rate can be attributed to changes in both mechanical and chemical nature of the polishing process. The change of the mechanical component of the process has two reasons: Firstly, as a result of polishing pad softening (change in mechanical properties of the pad due to the increase in temperature) the area of contact increases [228], thus increasing the number of abrasive particles coming in contact with the wafer surface. This is supported by the COF increase with increase in slurry temperature as shown in Fig. 7.7. These results are in agreement with the results from previous investigations by other authors [228-230]. Secondly, a decrease of the viscosity of the slurry occurs with increasing temperature, which increases the friction at the interface and hence increases shear resulting in higher removal rates [231]. Thus, increase in the removal rate and friction with temperature can

المنارة للاستشارات
www.manaraa.com

be attributed to: 1) increase in reaction kinetics at the pad-wafer interface, 2) softening of polishing pad there by increasing the contact area and hence shear, 3) decrease in the viscosity of the slurry due increase in temperature [232].

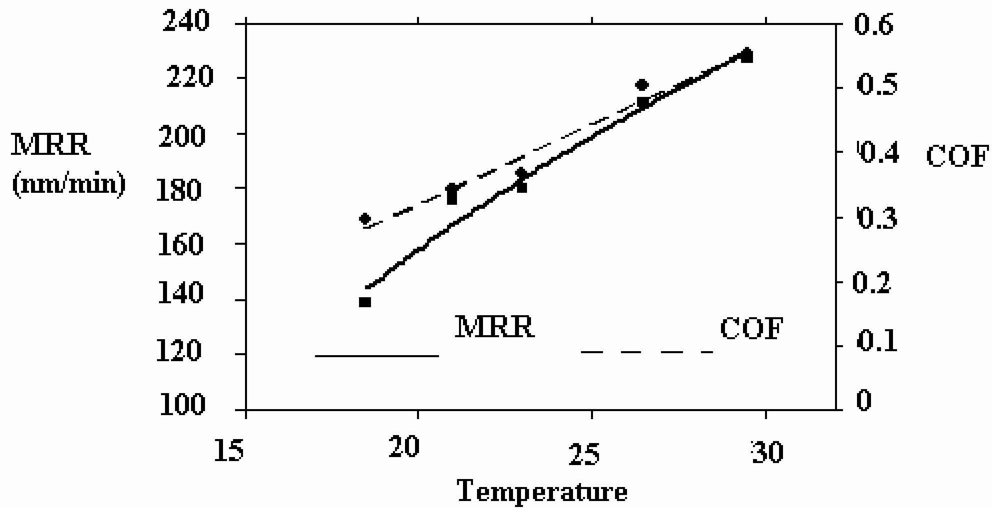

Fig. 7.7 Variation of COF and MRR with Increase in Slurry Temperature

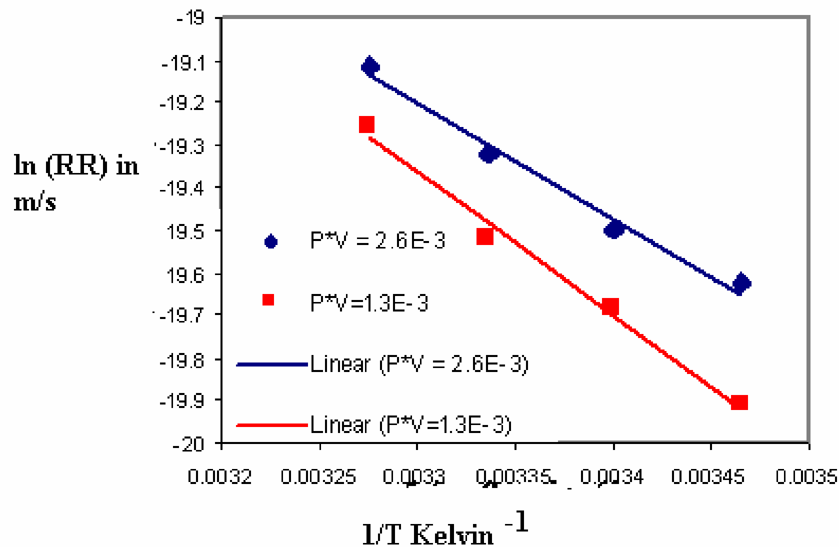

Fig. 7.8 Variation of ln of MRR in m/s with Inverse of Temperature (1/T) Showing an Arrhenius Relationship

المنارة للاستشارات
www.manaraa.com

It must also be mentioned that the increase in MRR during CMP with increase in the slurry temperature is governed by an Arrhenius type relationship. The variation of ln of removal rate with temperature (1/T) is a straight line with a negative slope (Fig. 7.8). The slope of this curve can be used to determine the activation energy of the Cu-slurry system. If the increase in reaction kinetics can be achieved at room temperature with the help of the chemical action of slurry additives, then there can be an enhancement in slurry performance without the corresponding increase in thermal overheads. For this purpose, we have a proposed a novel slurry design (chemistry) which used a surface catalyst to enhance the slurry performance of Cu slurry. The details of this novel nanoparticle based slurry are discussed in the subsequent section.

7.5 Novel Nanoparticle based Cu slurry

Compared to the other materials involved in the IC fabrication, (eg Silicon, Tungsten, Silica, etc.), Cu is much softer as compared to the abrasive particles used in the chemical active solution used (CMP Slurry) during the its polishing process. Controlling Cu polishing to meet the stringent demands of the semiconductor industry and producing Cu wiring without: 1) corrosion, 2) micro/nano scratching, 3) over polish, pattern damage, trough formation, etc, 4) material delamination, etc. is of paramount importance to make more sophisticated and cost effective chips of tomorrow. Due to the inherent soft nature of Cu, there are severe restrictions in obtaining the desired removal rate by purely mechanical means (increase in down pressure and platen rotation). There is a need to chemical enhance the performance of a CMP process step without significant increase in the applied surface shear to the wafer. The proposed slurry promises to be helpful in

المنارة للاستشارات
www.manaraa.com

achieving the aforementioned demands of the semiconductor industry within the strict tolerances prescribed. Thus, this new technology will facilitate in the achievement of the widely published objectives of the semiconductor industry. Additionally this proposed slurry does not require any special conditions for operation. These and other advantages will significantly bring down the cost of ownership (CoO) of the CMP operations. The universal benefits of this technology include: 1) decrease in the IC cost, 2) wide implementation of the IC, 3) more versatility and faster operation the next current electronic products.

7.5.1 Composition of Novel Nanoparticle Based Cu Slurry

The proposed slurry consists of colloidal suspension of nanoparticle abrasives derived from Tetraethylorthosilicate (TEOS), its derivatives and any materials modified from TEOS, in a chemically active medium. The base solution of the slurry consists of deionized (DI) water, buffering agents like organic and inorganic buffers, cleansing agents, surface modified catalysts, and surface reagents. The chemically active medium is additionally comprised of acids such as HCl, H_2SO_4, HNO_3, and other inorganic acids in different concentrations, anti corrosive compounds like Benzotriazole (BTA) ranging from 0.0001 to 4 % by volume, oxidizing agents such as H_2O_2, $KMnO_4$ or other oxidizing agents ranging from 1 % to 8 % by volume.

The details of the chemical composition of the slurry are as follows[233: 1)Base Solution: DI water, 2) Buffer: Inorganic Buffer (HCl, HNO_3, H_2SO_4) pH: 5-7, 3) Nanoparticles Particles: TEOS based, 4) Size distribution: 80-120 nm, 5) Shape: Spherical, 6) Dispersion: Colloidal Suspension, 7) Oxidizing Agent: H_2O_2, $KMnO_4$, (1-5

المنارة للاستشارات
www.manaraa.com

vol%), 8) Surfactants: TWEEN X 100 (0.01 to 1 vol %), 9) Concentration: 2-10 wt %, 11) Chelating Agents: Organic Acids and others, 12) Corrosion Inhibitor: BTA (0.01 to 1 vol %)

7.5.2 Mechanism of Polishing of Novel Nanoparticle Cu Slurry

The proposed slurry consists of similar and variable sized TEOS nanoparticle abrasives ranging from 10 nm to 200 nm. The particle concentration of the nanoparticles in the slurry solution ranges from 2 to 12 % by weight. The primary objective to the nanoparticle slurry is to precisely control the desired CMP output variables and prevent defects such as: 1) high surface roughness, 2) micro/ nano scratching, 3) dishing, erosion or pattern damage, 4) delamination, 5) surface corrosion, pits and craters. The slurry solution is made of DI water, glycene and organic acids like acetic acid. The slurry buffer contains acids solutions, specifically 25 to 75 vol. % HNO_3 to optimize the reaction over the Cu surface. Other inorganic acids such as HCl and H_2SO_4 have also been explored to optimize the surface reactions. The pH of the slurry can be maintained within the range of 2.0 to 10.0. The surface reactions are carried out in presence of catalysts such a TiO_2, ZnO, SnO_2, other metal oxides, ceramics, and elements and compounds derived and modified from them. Ionic and Anionic surfactants specifically TWEEN X100 have been used in the range of 0.001 to 4 vol. % to eliminate surface corrosion and impart hydrophobicity to the surface. To trigger and enhance the accelerated surface oxidation for effective material abrasion, oxidizing agents, specifically H_2O_2 and others such as KMnO4, NH_4MnO_4, Cr $(NO_3)_2$ etc. have been used in the range of 1 to 8 vol. %. The slurry employs compounds such as KOH, KCl, and other organic and inorganic salts in

المنارة للاستشارات
www.manaraa.com

isolation and/or in combination for generation of active ions for maintaining and balancing the slurry pH. The aforementioned organic and inorganic salts also serve the purpose of generating counter ions to prevent the diffusion of K^+ ions in Cu due to their competitive reactions. The competitive reactions are also employed on a stand-alone basis or in series to minimize the heat generated as a result of the chemical action of the slurry on the Cu surface. This prevents the adverse process effects that may be caused due to pad surface heating and viscoelastic material reflow which inevitably leads to pad compliance and loss in planarity. The mechanism for polishing action of the CMP slurry has been illustrated in Fig. 7.9.

المنارة للاستشارات
www.manaraa.com

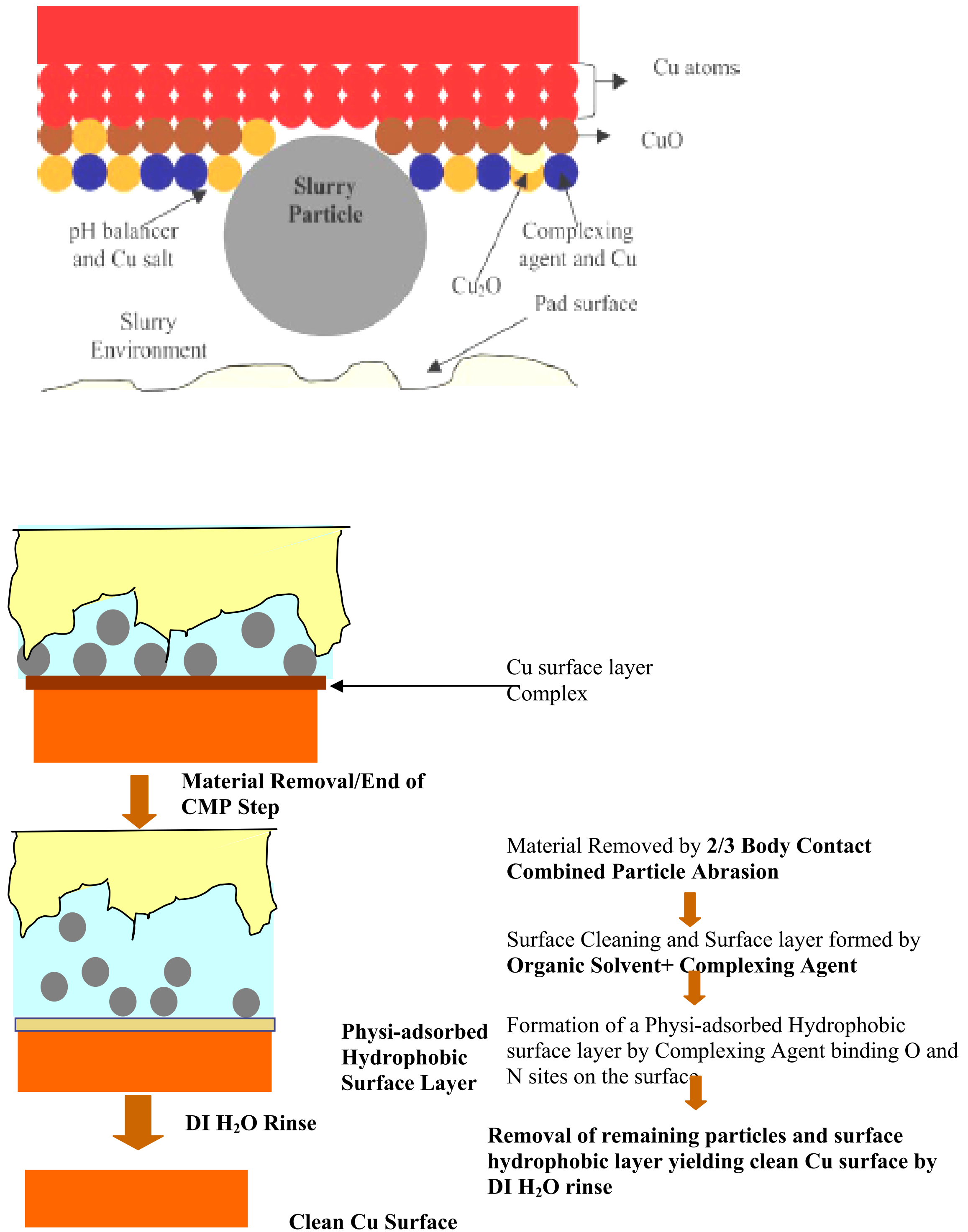

Fig. 7.9 Schematic Showing Mechanism of Polishing Action of Novel Nanoparticle CMP slurry

المنارة للاستشارات
www.manaraa.com

7.5.3 Polishing Performance of Novel Nanoparticle Cu Slurry

The CMP experiments using the novel slurry were performed using Electroplated Copper blanket films of 15000 Å thick were polished using the CETR™ bench top CMP tester using a 6" diameter polishing pad coupon attached to the bottom platen and a 1" X 1" sample coupon faced down onto the pad. IC1000/Suba IV polyurethane perforated pads were used to polish the copper samples. Polishing conditions were maintained at 3 PSI, 100 RPM bottom platen rotation, 95 RPM carrier rotation, slurry flow rate 50 ml/min (polishing conditions were maintained similar to previous slurry temperature analysis). Fig. 7.10 shows the variation of MRR for EP Cu for different trials performed without the addition of metal oxide surface catalysts. It can be seen from the figure that the MRR performance is well below the industrial standards with the highest MRR obtained being 55 nm/min.

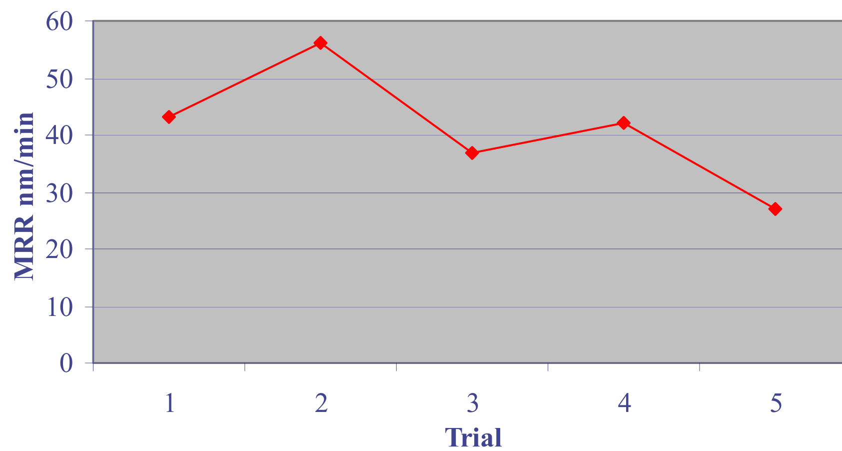

Fig. 7.10 Variation of MRR for Different Trials Using Nanoparticle Slurry without the Surface Catalyst

المنارة للاستشارات
www.manaraa.com

Upon addition of the surface catalyst, there was a dramatic improvement in the slurry performance. Fig. 7.11 shows the MRR during CMP for different trials performed with newly developed slurry with the metal oxide ceramic surface catalyst. There is at least a 100 % improvement in the MRR upon addition of the surface catalyst.

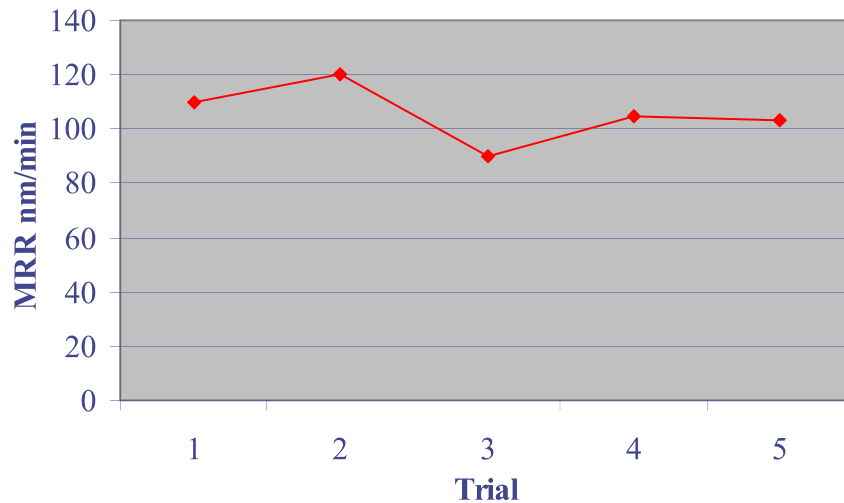

Fig. 7.11 Variation of MRR for Different CMP Trials for Nanoparticle Slurry with Surface Catalyst

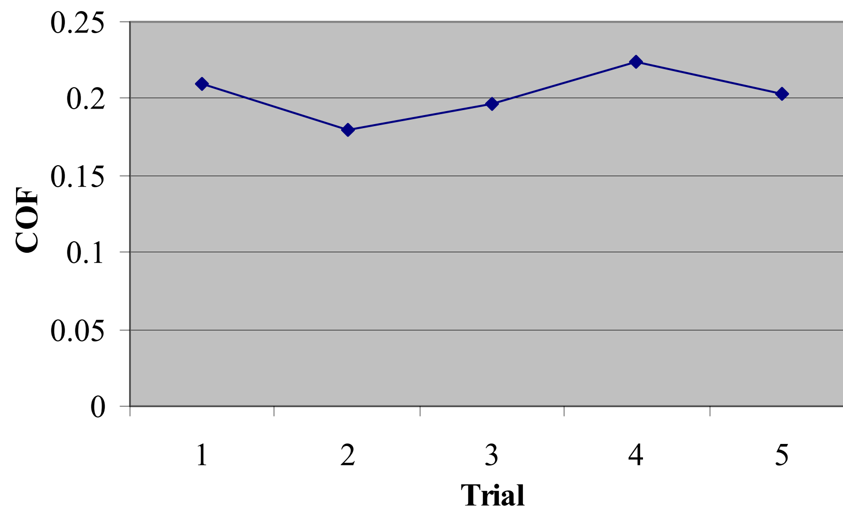

Fig. 7.12 Variation of COF for Different CMP Trials Using Novel Nanoparticle Based CMP slurry

المنارة للاستشارات
www.manaraa.com

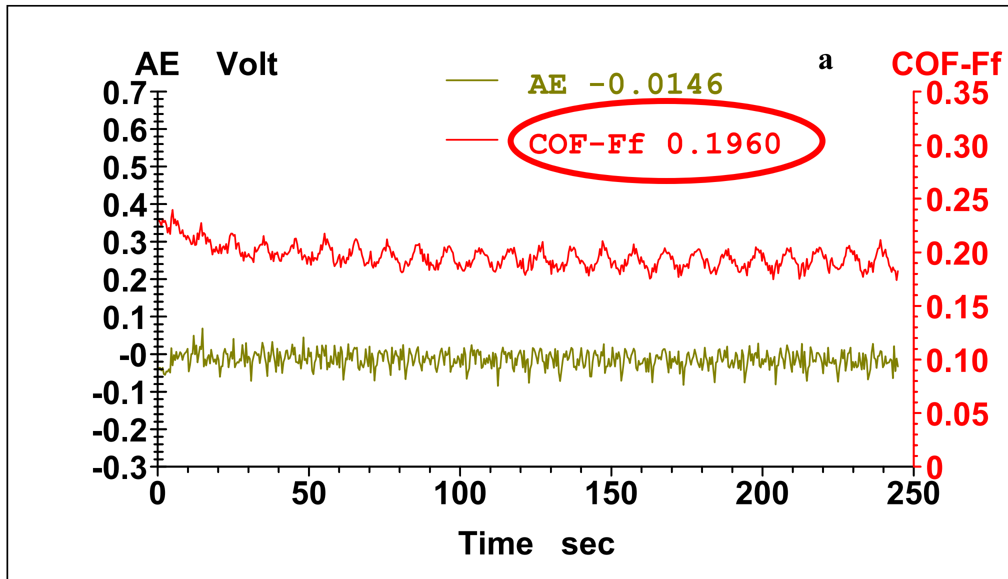

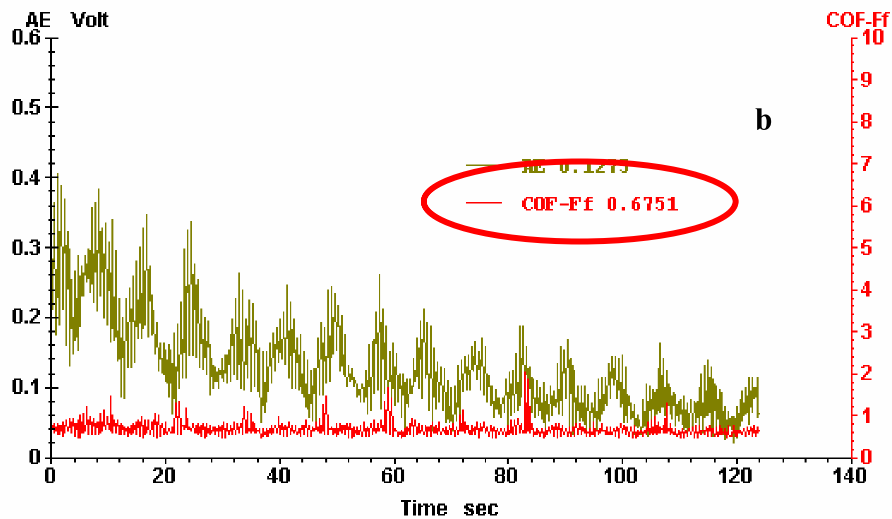

Fig. 7.13 Variation of COF with Time Measured In-situ for Polishing of EP Cu Samples Under 3 PSI Down Pressure and 100 RPM Platen Rotation Using a) Novel Nanoparticle Cu Slurry, and b) Commercial Cu Slurry

Another salient feature of this slurry is that there relatively low amount of shear generated during polishing. The MRR mechanism being predominantly chemical

www.manaraa.com

ensures that the contribution of shear remains at its bare minimum. Also, due to the competing reactions of Cu^{2+} ions and K^{+} ions, there is effective exchange of heat at the pad wafer interface. This does not cause the polishing pad to soften and then excessively comply with the wafer topography. The enhancement of MRR without excessive pad compliance will have benefits in terms of enhanced global planarization, extended pad life. Fig. 7.12 shows the variation of COF for different trials of the slurry for which removal rate have been reported in Fig. 7.11. There is a significant different between the COF values obtained when the developed slurry when compared to an industrial slurry when used in polishing under the same conditions as seen from Fig. 7.13 a, b.

7.6 Summary of Investigation and Modification of CMP Slurry

The CMP slurry has a delicate balance of different chemicals which significantly affect the CMP process output. In case of metal polishing the reaction occurring at the pad wafer interface are highly dominated by the chemical composition of the CMP slurry. The most significant attributes of the CMP slurry that affect CMP output are: 1) pH, 2) particle shape, 3) particle hardness, 4) particular concentration and distribution. The increase in temperature of slurry significantly increases the reaction kinetics, there by increasing the removal rate. However the adverse effects of slurry heating are: 1) decreased pad wear life, and2 inhibition of global planarization. For this purpose we have leveraged the phenomenon of surface catalysis in the CMP slurry which enables the slurry to predominantly employ chemical means for material removal. There is a lower COF observed during the operation of this slurry which means lower surface shear during CMP. This property of the slurry is beneficial as lower surface shear

المنارة للاستشارات
www.manaraa.com

automatically translates in: 1) lower pad wear, 2) reduced defects. It is predicted that predominantly chemically acting slurries will be used in the future as Cu and low k ILD materials are incorporated.

المنارة للاستشارات
www.manaraa.com

CHAPTER EIGHT

SUMMARY

8.1 Summary of the Research

Chemical Mechanical Polishing being the process of choice for achieving local and global planarization on the surface of the wafer, needs to be extensively studied in order to deal with certain teething challenges presented by it. In situ CMP process monitoring is one of the methods by CMP process can be analyzed and controlled. Monitoring the COF during the CMP process can give indications of the process end point and slurry selectivity in situ. The acoustic emission signal can detect delamination during the process. These two signals if employed in conjunction together with a feed back loop can ensure significant reduction in CMP process defectivity along with a reduction in cost of ownership. The process CMP needs to be studied by taking in to account the properties of the materials that undergo CMP, the polishing pads used for it, at the same time by evaluating the slurry that enables preferential removal of materials.

The mechanical and tribological properties of materials significantly impact their CMP performance. Certain CMP attributes such as wear mechanism, defectivity are based upon the mechanical properties of the materials undergoing CMP. There is evidence that pre CMP treatment of thin films undergoing CMP can allow higher freedom for developing CMP process for some materials such as Cu.

المنارة للاستشارات
www.manaraa.com

Previous reports of evaluation of CMP polishing pads were based upon evaluation of materials that constitute the polishing pad. The ultra sound testing, which is a non destructive polishing pad evaluation technique is explored to evaluate the non uniformity in the pad specific gravity. However, the polishing pad a whole may contain certain non uniformities in their specific gravity which may not be observed if small coupons of the polishing pads are evaluated. When attempts were made to isolate the regions of non uniformity of the polishing pad, the coupons showed bulk properties of constituent materials. Thus, it can be said that the polishing pad as a consumable needs to be evaluated as whole without breaking its integrity

Surface modification of the polishing pad is a feasible and encouraging direction for development of novel polishing pads. When coated with a ceramic, the polishing pad surface remains insulated from the slurry chemical attack. Therefore, there in no need for conditioning of the polishing pad during operation. The static tribological properties and the mechanical properties do no correlate very well with the pad polishing performance. Hence, the CMP evaluation of the polishing pad cannot be predicted using these statically evaluated pad properties. The increase in polishing pad surface mechanical properties with increase in polishing pad coating time brings about a decrease in material removal rate. The reason being this counter intuitive phenomenon is: 1) decrease in pad surface compliance, 2) increase in slurry film thickness on the surface of the pad due to decrease in the pad surface roughness. The impact of pad foam thickness and slurry film thickness can be gauged by experimentally evaluating polishing pads with different total thickness.

المنارة للاستشارات
www.manaraa.com

The advent of Cu and ultra low k dielectrics, it is crucial to perform CMP in a low force and low linear velocity regime (low stress). The slurry which is a combination of chemically active agents as well as mechanically acting abrasives is crucial in maintaining the optimum and delicate balance of chemical and mechanical component of CMP. The slurry chemical attack and temperature determines the reaction kinetics at the pad wafer interface. The increase in metal oxidation and dissolution enhances the material removal rate during CMP. This enhancement in the oxidation and dissolution at the pad wafer interface can also be done using a surface catalyst such as metal oxides in the slurry. The use of surface catalysts to enhance slurry performance increases the chemical component during the CMP process. Hence enhanced material removal rate can be obtained at lower surface shear.

Finally, understanding the process aspects, material properties, polishing pad behavior and slurry performance gives a holistic perspective of the process of CMP. This could be treated a contribution towards transforming CMP in to more of a science from the present stage, where in it is more of an art.

8.2 Major Findings and Contributions

The process of CMP has been extensively investigated during this research. As mentioned before, the process of CMP being a complex interplay of different variables, it is very important to isolate the each of them and understand their impact on the process output. This research has been an effort to isolate some of the variables and study their specific characteristics and gauge their impact on CMP.

The process of understanding CMP began my monitoring the polishing runs

المنارة للاستشارات
www.manaraa.com

in-situ. Though there are some techniques available to monitor the process end point, in-situ monitoring of polishing behavior of different materials and consumables has not been extensively done before. Thus findings in this area identify a range in which CMP outputs such as MRR, End Point, slurry selectivity for a combination of polishing pad, slurry, material, as well defects such as delamination, at a given polishing condition. This in-situ monitored data also served as a starting point for further investigations in area of heuristic training of the CMP apparatus to engineer a feed back mechanism for accurate process control. This research also helped elucidate wear mechanisms of novel materials such as cross linked polymers and doped oxides used as ILD.

The findings of the research were then extended in three different directions namely: 1) Pre-CMP material evaluation and improvement: The significance of annealing over the interface of the thin films in the damascene structure was investigated and correlation of the interfacial adhesion energy with standard process data available was made. 2) Investigation of Polishing Pads: Novel application specific polishing pads that do not require conditioning was evaluated for the first time ever during this research. The contributions were made to the architecture of these polishing pads which end up being a commercial product.Though evaluation of application specific pads was done on 6 inch coupons, some of the findings on commercial polishing pads suggested that polishing pad needs to be evaluated as a consumable on the whole. If the integrity of the polishing pad was broken, the properties evaluated are those of the material that constitutes the polishing pad and do not give an idea of the pad CMP performance in its entirety. The findings of the experiments on novel pads were always implemented with this in mind. 3) Novel Slurry Formulation: The CMP consumable market is booming and expected to

المنارة للاستشارات
www.manaraa.com

soar. With newer and softer materials being implemented in the IC, CMP slurry with a predominant chemical component was formulated during this research. The approach of using a surface catalyst to enhance CMP slurry performance was used for the first time in this research.

The research thus makes a scientific and technical contribution to the field of CMP, and adds its two cents in transforming the process of CMP from being more of an art to being more of a science.

8.3 Future Trends in CMP and Potential Areas for Investigation

There are several innovations and modifications such as slurry free approach, low down force polishing, abrasive less and nanoparticle slurry approach, etc. that are being carried out in the CMP process. Process such as reverse electroplating and combination of different planarization process, are also trying to compete with CMP for achievement of effective global and local planarization of the wafer.

The process of chemical mechanical polishing is also finding increasing application in the field of giant magneto resistive (GMR) and colossal magneto resistive (CMR) disc drives for polishing successive layers of thin films (Co and Ni). Special emphasis is laid on successful endpoint detection and selectivity of the slurry. CMP is used to polish multi-level thin film structure of the drives.

The field of Microelectromechanical systems (MEMS) is also increasing adapting the process of CMP. As MEMS structures implement smaller and smaller features as constituents, the planarity of the thin films becomes an important issue. For optical MEMS applications the mirror like smooth surface of the thin films is of utmost

المنارة للاستشارات
www.manaraa.com

importance for reliable and repeatable functioning of the device, for example, optical features.

Metal and high-*k* insulators have replaced the dummy gates, which were used to preserve self-alignment of gate electrode. These metal and insulator layers need to be planarized with utmost control, where CMP has to play a significant role. Deposition techniques for such metal and high-*k* insulator films are yet to be defined and CMP of films deposited by such atomic layer depositions need to be investigated to get optimum polishing performance. Also, CMP of noble metals, which are used to make gate electrodes in p-channel devices need to be investigated to achieve optimum removal performance.

المنارة للاستشارات
www.manaraa.com

REFERENCES

1. J.G. Ryan, R.M. Geffken, N.R. Poulin and J.R. Paraszczak, IBM J. Res. Dev. 39, 371 (1995).

2. C.L. Borst, W.N. Gill and R.J. Gutmann, Chemical–Mechanical Polishing of Low Dielectric Constant Polymers and Organosilicate Glasses: Fundamental Mechanisms and Application to IC Interconnect Technology, Kluwer Academic Publishers, Boston (2002).

3. Y. Taur, Y.-J. Mii, D.J. Frank, H.-S. Wong, D.A. Buchanan, S.J. Wind, S.A. Rishton, G.A. Sai-Halasz and E.J. Nowak, IBM J. Res. Dev. 39 , 245 (1995).

4. Internet web site: http://www.intel.com/labs/features/si11032.htm, Intel, 2002.

5. J. Givens, S. Geissler, O. Cain, W. Clark, C. Koburger and J. Lee, Proceedings of the 11th International VLSI Multilevel Interconnection Conference, 43, (1994).

6. P. B. Zantye, A. Kumar and A. K. Sikder, Mat. Sci. Eng. R 45, 3-6, 89, (2004).

7. A.K. Bates, M. Rothschild, T.M. Bloomstein, T.H. Fedynyshyn, R.R. Kunz, V. Liberman and M. Switkes, IBM J. Res. Dev. 45, 605 (2001).

8. F. Bernard, Micro. Eng. 61–62, 11 (2002).

9. B. Michel, A. Bernard, A. Bietsch, E. Delamarche, M. Geissler, D. Juncker, H. Kind, J.-P. Renault, H. Rothuizen, H. Schmid, P. Schmidt-Winkel, R. Stutz and H. Wolf, IBM J. Res. Dev. 45, 5, 697 (2001).

المنارة للاستشارات
www.manaraa.com

10. S. Wolf and R. Tauber, Silicon Processing for VLSI Era, McGraw-Hill, New York (1991).

11. R.W. Keyes, Proc. IEEE 69, 267 (1981).

12. S.P. Murarka, Metallization: Theory and Practice for VLSI and ULSI, Butterworth-Heinemann, Boston (1993).

13. J.A. Lee, M. Moinpour, H.-C. Liou and T. Abell, Proceedings of Materials Research Society San Francisco, CA (2003), p. F7.4.

14. International Technology Roadmap for Semiconductors, 2001.

15. K. Shenai, VLSI Metallization: Physics and Technologies, Artech House Inc. (1991).

16. V.K. Tripathi and R.J. Bucolo, IEEE Trans. Electron Dev. 34, 3, 650 (1987).

17. G. Leibmann, Br. J. Al. Phys. 1, 4, 92 (1950).

18. R.F. Harrington and C. Wei, IEEE Trans. Microwave Theory Tech., 32, 705 (1984)

19. P. Wolters, Internet web site: http://www.peterwolters.com/cmp/cmpmultilevel.htm, © (2003).

20. W.-S. Lee, S.-Y. Kim, Y.-J. Seo and J.-K. Lee, J. Mater. Sci.: Mater. Electron. 12, 1, 63 (2001).

21. W.J. Patrick, W.L. Guthrie, C.L. Standley and P.M. Schiable, J. Electrochem. Soc. 138, 555 (1991).

22. S. Wolf, Silicon Processing for VLSI Era II, Process Integration 45, McGraw-Hill, New York (1991).

23. P. Sallagoity, F. Gaillard, M. Rivoire, M. Paoli and M. Haond, Microelectron. Reliab. 38, 271 (1998).

المنارة للاستشارات
www.manaraa.com

24. S.-Y. Jeong, S.-Y. Kim and Y.-J. Seo, Microelectron. Eng. 66, 480 (2003).

25. S.-Y. Kim, C.-I. Kim, E.-G. Chang, Y.-J. Seo, T.-H. Kim and W.-S. Lee, Proceedings of 4th IUMRS-ICEM-98 Cheju Korea, 24–27 August 1998, 468 (1998)

26. S.-Y. Kim and Y.-J. Seo, Microelectron. Eng. 60, 2-4, 357 (2002).

27. Y.-J. Seco, S.-Y. Kim and W.S. Lee, Mech. Eng. 65, 4, 371 (2003).

28. Y.-J. Seo, G.-U. Kim and W.S. Lee, Microelectron. Eng. 71, 209 (2004).

29. C. Chen, J.-Y. Wu, W. Lur, US Patent 6,169,012 (2001).

30. C. Chen, J.-Y. Wu, W. Lur, US Patent 6,486,040 (2002).

31. C. Chen, J.-Y. Wu, W. Lur, US Patent 6,448,159 (2002).

32. D.G. Thakurta, D.W. Schwendeman, R.J. Gutmann, S. Shankar, L. Jiang and W.N. Gill, Thin Solid Films 414, 78 (2002).

33. C. Zhou, L. Shan, J. Robert Hight, S.H. Ng and S. Danyluk, Wear 253, 3-4, 430 (2002).

34. X. Li, T.K.S. Wong, Rusli and D. Yang, Diamond Relat. Mater. 12, 3-7, 963 (2003).

35. G. Schindler, G. Steinlesberger, M. Engelhardt and W. Steinhögl, Solid State Electron. 47, 7, 1233 (2003).

36. R.F. Schnabel, D. Dobuzinsky, J. Gambino, K.P. Muller, F. Wang, D.C. Perng and H. Palm, Microelectron. Eng. 37–38, 59 (1997).

37. L. Shon-Roy, Integrated Circuit Engineering Corporation Handbook, 1999.

38. K. Kobayashi, Mater. Sci. Eng. 98, 2-15, 181 (2003).

39. K. Kobayashi, J. Phys. Chem. Solids 59, 9, 1671 (1998).

40. K. Kobayashi and I. Mizushima, Mater. Sci. Eng. B 39, 224 (1996).

المنارة للاستشارات
www.manaraa.com

41. K. Kobayashi and H. Sasaki, Mater. Res. Bull. 33, 5, 811 (1998).

42. K. Kobayashi, J. Non-Cryst. Solids 217, 2-3, 323 (1997).

43. J. Levert, S. Mukherjee and D. Debear, Semicon, Japan (1999).

44. J.-H. Zhao, I. Malik, T. Ryan, E.T. Ogawa, P.S. Ho, W.-Y. Shih, A.J. McKerrow and K.J. Taylor, Appl. Phys. Lett. 74, 7, 944 (1999).

45. M.P. Petkov, M.H. Weber, K.G. Lynn, K.P. Rodbell and S.A. Cohen, J. Appl. Phys. 86, 6, 3104 (1999).

46. A. Kuntman, R. Yenidünya, A. Kaşgöz and H. Kuntman, Microelectron. J. 30, 127 (1999).

47. A. Maddalon, K. Barla, E. Denis, E. Lous, E. Perrin, S. Lis, C. Lair and E. Dehan, Microelectron. Eng. 50, 1-4, 33 (2000).

48. L. Trabzon and O.O. Awadelkarim, Microelectron. Eng. 65, 4, 463 (2003).

49. C.T. Chua, Y.-P. Lee, M.S. Zhou, L. Chan, US Patent 6,121,130 (2000).

50. A.E. Braun, Semicond. Int. 11 May 2003.

51. M. Köhler, Etching in Microsystem Technology, Wiley, Weinheim (1999).

52. M. Esashi, Microsyst. Technol. 1, 2 (1994).

53. K. Suzuki, S. Hiraoka and S. Nishimatsu, J. Appl. Phys. 64, 3697 (1988).

54. D.M. Knotter, J. Am. Chem. Soc. 122, 18, 4345 (2000).

55. AT&T Bell Laboratory, Solid State Technol. 37, 12, 26 (1994).

56. J.M. Steigerwald, S.P. Murarka, and R. J. Gutmann, Chemical Mechanical Planarization of Microelectronic Materials, Wiley, New York (1997).

57. D.J. Stein, J.L. Cecchi and D.L. Hetherington, J. Mater. Res. 14, 3695 (1999).

المنارة للاستشارات

www.manaraa.com

58. H. Landis, P. Burke, W. Cote, W. Hill, C. Hoffman, C. Kaanta, C. Koburger, W. Lange, M. Leach and S. Luce, Thin Solid Films 220, 1 (1992).

59. Internet web site: http://www.memc.com/MEMC.nsf/0/6D86FAED316FE14686256AE80058166D/$File/Ultraflat_wafers.pdf?OpenElement, © MEMC, 2003.

60. Internet web site: http://www.komsil.co.jp/en/office/hist.htm, © Komatsu, (2003).

61. Internet web site: http://www.research.ibm.com, © IBM, (2004).

62. Internet web site: http://www.sematech.org/corporate/index.htm, © Sematech Inc., (2004).

63. Internet web site: http://www.mitsubishi.or.jp/e/monitor/monitor_old/97version/monitor9802/wafer.html, © Mitsubishi, (2004).

64. A.K. Sikder, P. Zantye, S. Thagella, A. Kumar, B. Michael Vinogradov, N.V. Gitis, Proceedings of 8th CMPMIC Conference, 120, 2003.

65. S.H. Li, R. Miller, Chemical Mechanical Polishing in Silicon Processing, vol. 63, Academic Press, New York, 2000,

66. J. Hernandez, P. Wrschka, Y. Hsu, T.-S. Kuan, G.S. Oehrlein, H.J. Sun, D.A. Hansen, J. King and M.A. Fury, J. Electrochem. Soc. 146, 4647 (1999).

67. G.B. Basim, J. Colloid Interface Sci. 256, 1, 137 (2002).

68. Internet web site: http://www.pall.com/catalogs/microelec/cmp, © Pall, 2003.

69. Internet web site: http://www.amat.come, © Applied Materials Inc., 2003.

70. W.J. Patrick, W.L. Guthrie, C.L. Standley and P.M. Schiable, J. Electrochem. Soc. 138, 555 (1991).

المنارة للاستشارات

www.manaraa.com

71. W.L. Guthrie, W.J. Patrick, E. Levine, H.C. Jones, E.A. Mehter, T.F. Houghton, G.T. Chiu and M.A. Fury, IBM J. Res. Dev. 36, 845 (1992).

72. Internet web site: http://www.sea.rl.ac.uk/oldsea/oldpubs/Ale/desc.htm, Semiconductor Equipment Assessment, 2002.

73. D.G. Thakurta, C.L. Borst, D.W. Schwendeman, R.J. Gutmann and W.N. Gill, Thin Solid Films 366, 1-3, 181 (2000).

74. W. Li, D.W. Shin, M. Tomozawa and S.P. Muraka, Thin Solid Films 270, 601 (1995).

75. T.F.A. Bibby, J.A. Adams, K. Holland, G.A. Krulik and P. Parikh, Thin Solid Films 308–309, 1-4, 538 (1977).

76. B.J. Hooper, G. Byrne and S. Galligan, J. Mater. Process. Technol. 123, 1, 107 (2002).

77. H. Lu, B. Fookes, Y. Obeng, S. Machinski and K.A. Richardson, Mater. Charact. 49, 1, 35 (2002).

78. B. Mullany, J. Mater. Process. Technol. 132, 1–3, 10, 28 (2003).

79. Internet web site: http://www.sfamipec.com/product/polish_sing.html, Speed Fam, 2004.

80. T.-H. Tsai and S.-C Yen, Appl. Surf. Sci. 210, 3-4, 190 (2003).

81. S.-Y. Kim, C.-J. Park and Y.-J. Seo, Microelectron. Eng. 66, 1-4, 472 (2003).

82. J.M. Boyd, H.E. Litvak, US Patent 6,612,902 (2003).

83. C.-H. Lu, M.-Y. Li, US Patent 6,307,628 (2002).

84. N. Saka, J. Nam, H.L. Oh, US Patent 6,476,921 (2001).

85. A.K. Sikder, private communication, 2003.

المنارة للاستشارات
www.manaraa.com

86. A.K. Sikder, private communication, 2002.

87. F.-S. Lee, C.-C. Chen, J.-C. Lee, H.-C. Huang, US Patent 6,503,124 (2003).

88. T. Shih, C.-H. Yu, US Patent 6,682,396 (2004).

89. S.R. Roy, US Patent 6,547,652 (2003).

90. E.C. Wilson, H.A. Anderson, G. Appel, US Patent 6,149,512 (2000).

91. Internet web site: http://www.lamrc.com, © Lam Research Inc., 2001.

92. N. Shendon, US Patent 5,899,800 (1999).

93. N. Shendon, D.R. Smith, Patent 5,582,534 (1996).

94. T. Laursen and M. Grief, J. Electron. Mater., 31, 10, 1509, (2002).

95. L.P. Lai, J.L. Tucker, R.J. Lujan, US Patent 6,224,472 (2001).

96. Internet web site: http://www.nikon.co.jp/main/eng/products/cmp_e.htm, Nikon Corporation, 2003.

97. Infenion Corporation, http://www.infenion.com/, © Infenion Corporation, 2003.

98. O. Kuhn, H. Drummer, I. Dresden and F. Stanke, Proceedings of the 2nd European AEC/APC Conference, 308, (2001).

99. F. Preston, J. Soc. Glass Tech. 11, 214 (1927).

100. C. Rogers, L. Racz, J. Coppeta, A. Philipossian and F. Kaufman, J. Electrochem. Soc. 147, 5, 1903 (2000).

101. R.K. Singh and R. Bajaj, MRS Bull. 27, 10, 743 (2002).

102. A.K. Sikder, F. Giglio, J. Wood, A. Kumar and J.M. Anthony, J. Electron. Mater. 30, 1522 (2001).

103. H. Lu, H. Lu, Y. Obeng and K.A. Richardson, Mater. Charact. 49, 2, 177 (2002).

104. B.-S. Chen, J.S. Steckenrider, B.L. Mueller, US Patent 6,464,562 (2002).

المنارة للاستشارات
www.manaraa.com

105. J.-C. Twu, Y.-H. Chen, T. Shih, S.-M. Jang, US Patent 6,589,872 (2003).

106. S. Kondo, N. Sakuma, Y. Homma, Y. Goto, N. Ohashi, H. Yamaguchi and N. Owada, J. Electrochem. Soc. 147, 3907 (2000).

107. M. Hanazono, J. Amanokura and Y. Kamigata, MRS Bull. 27, 10, 722 (2002).

108. W.R. Morrison, K.P. Hunt, US Patent 5,938,505 (1999).

109. S.-Y. Kim, K.-J. Lee and Y.-J. Seo, Microelectron. Eng. 66, 1-4, 463 (2003).

110. S.-Y. Kim, J.-H. Lim, C.-H. Yu, N.-H. Kim and E.-G. Chang, KIEEME Trans. Electr. Electron. Mater. 4, 2, 1 (2003).

111. J. Reynolds, A. L. Swecker, A. J. Strojwas, A. Levy and B. Bell, Solid state technology 39, (1998)

112. T. Park, T. Tugbawa and D. Boning, Proc. CMP-MIC, Santa Clara, CA, March, 196, (2000).

113. M. Oliver, Ed., Chemical Mechanical Planarization of Semiconductor Materials, Springer, NY, © 2004.

114. L.M. Cook, J. Non-Cryst. Solids 120, 152 (1990).

115. David Evans, Sharp Labs of America, Camas, WA, Private Communication, (2005).

116. T. K. Das, R. Ganesan, A. K. Sikder, A. Kumar, IEEE Transactions on Semiconductor Manufacturing, Accepted for publication (U.S. Patent pending).

117. A. K. Sikder and A. Kumar, M. Vinogradov and N. V. Gitis, Delamination studies on Cu-low-K stack, to be submitted

المنارة للاستشارات

www.manaraa.com

118. R. Ganesan, T. K. Das, A.K., Sikder, A. Kumar, IEEE Transactions on Semiconductor Manufacturing 16, 4, 677 (2003);(U.S. Patent # 60/521,357 filed on April 8th 2004, Approval pending).

119. S. Lagrange, S.H. Brongersma, M. Judelewicz,, A. Saerens, I. Vervoort, E. Richard, R. Palmans and K. Maex, Microelectron. Eng. 50, 449-457 (2000).

120. J. M. Harper, C. Cabral, Jr., P.C. Andricacos, L. Gignac, I.C. Noyan, K. P. Rodbell and C.K. Hu, J. Appl. Phys. 86, 2516-2525 (1999).

121. A. Furuya, Y. Oshita and A. Ogura, J. Vac. Sci. Technol. A, 18, 2854-2857 (2000).

122. C. Lingk, M.E. Gross, and W.L. Brown, J. Appl. Phys. 87, 2232-2236 (2000).

123. S.H. Brongersma, E. Richard, I. Vervoort, H. Bender, W. Vandervorst, S. Lagrange, G. Beyer and K. Maex, J. Appl. Phys. 86, 3642-3645 (1999).

124. L. Vanasupa, Y-C. Joo, P.R. Besser and S. Pramanick, J. Appl. Phys., 85, 2583-2590 (1999).

125. C-Y. Yang, J.S. Jeng and J.S. Chen, Thin Solid Films 420-421, 398-402 (2002).

126. M.T. Perez-Prado and J.J. Vlassak, Scripta Mater. 47, 817-823 (2002).

127. H. Lee, S.S. Wong and S.D. Lopatin, J. Appl. Phys. 93, 3796-3804 (2003).

128. K. Ueno, T. Ritzdorf and S. Grace, J. Appl. Phys., 86 4930-4935 (1999).

129. C. Lingk, and M.E. Gross, J. Appl. Phys., 84, 5547-5553 (1998).

130. W.H. The, L.T. Koh, S.M. Chen, J. Xie, C.Y. Li and P.D. Foo, Microelectron. J., 32, 579-585 (2001).

131. J. Proost, T. Hirato, T. Furuhara, K. Maex and J.-P. Celis, J. Appl. Phys. 87, 2792-2802 (2000).

132. T.-H. Fang and W.-J. Chang, Microelectron. Eng. 65, 231-238 (2003).

المنارة للاستشارات
www.manaraa.com

133. S.H. Kang, Y.S. Obeng, M.A. Decker, M. Oh, S.M. Merchant, S.K. Karthikeyan, C.S. Seet and A.S. Oates, J. Electron. Mater., 30, 1506-1512 (2001).

134. J. Ye, N. Kojima, K. Ueoka, J. Shimanuki, T. Nasuno, and S. Ogawa, J. Appl. Phys. 95, 3704, (2004).

135. P.G. Charalambides, J. Lund, A. G. Evans and R. M. McMeeking, J. Appl. Mech. 56, 77, (1989).

136. P.G. Charalambides and A.G. Evans, J. Am. Ceram. Soc. 72, 746, (1989).

137. R. H. Dauskardt, M. Lane, Q. Ma and N. Krishna, Engg Fract Mech 61, 1411, (1998).

138. A. A. Volinksy, N. R. Moody and W. W. Gerberich, Acta mater. 50, 441, (2002).

139. N. X. Randall and R. Consiglio, Rev. Sci. Instrum. 71, 2796 (2000).

140. T . Homma, Mater. Sci. Eng. R23, 243 (1998).

141. D.W. Gidley, W.E. Frieze, T.L. Dull, J. Sun, A.F. Yee, C.V. Nguyen and D.Y. Yoon, Appl. Phys. Lett. 76, 10, 1282 (2000).

142. L. Peters, Semicond. Int., 108, (2000).

143. L. Pauling, The Nature of the Chemical Bond (third ed.), Cornell University Press, Ithaca, NY (1960).

144. J.W. Yi, Y.H. Lee and B. Farouk, Thin Solid Films 374, 103 (2000).

145. R.K. Laxman, N.H. Hendricks, B. Arkles and T.A. Tabler, Semicond. Int. (2000).

146. A.K. Sikder, A. Kumar, S. Thagella and J. Yota, J. Mater. Res., 19, 4, 996 (2004).

147. E. Korczynski, Solid State Technol. 39, 4, 63 (1996).

148. M.R. Baklanov, M. Muroyama, M. Judelewicz, E. Kondoh, H. Li, J. Waeterloos, S. Vanhaelemeersch and K. Maex, J. Vac. Sci. Technol. B17, 5, 2136 (1999).

المنارة للاستشارات
www.manaraa.com

149. X. Xiao, N. Hata, K. Yamada and T. Kikkawa, Rev. Sci. Instrum. 74, 10, 4539 (2003).

150. D. Shamiryan, T. Abell, F. Lacopi and K. Maex, Mater. Today 7, 1, 34 (2004).

151. M.R. McGurk and T.F. Page, J. Mater. Res. 14, 2283, (1999)

152. C. Taylor, R. Prince, A.P. Malshe, L. Riester, G.J. Salamo and S.O. Cho, , Proc. SPIE Int. Soc. Opt. Eng. 4936, 424, (2002).

153. J.-H. Ahn and D. Kwon, Mater. Sci. Eng. A285, 172**,** (2000).

154. N.X. Randall and A. Harris, Wear 245, 1-2, 196, (2000).

155. G.M. Pharr, Mater. Sci. Eng. A253, 151, (1998)

156. W.C. Oliver and G.M. Pharr, J. Mater. Res. **7,** 1564, (1992).

157. S. Thagella, A. K. Sikder, and A. Kumar, J. Electrochem. Soc. 151, 3, 205 (2004)

158. K. Ludema, Friction, Wear, Lubrication: A Text Book in Tribology, p. 90, CRC Press, Boca Raton, © (1996).

159. P. B. Zantye, A. Kumar, S. Ostapenko, A. Sikder, M. Dallas, Submitted to the J. Vac. Sci Tech. A, (2005).

160. A.K. Sikder, I.M. Irfan, A. Kumar and J.M. Anthony, J. Electron. Mater. 30, 12, 1527, (2001).

161. Maria Ronay and Charles L. Rohn, Tribol. Lett. 14, 3, 205 (2003).

162. Maria Ronay, J. Electrochem. Soc.151, 12, G 847 (2004).

163. D.O. Ouma, Modeling of Chemical Mechanical Polishing for Dielectric Planarization, Ph.D. Thesis, Massachusetts Institute of Technology, USA, (1999).

164. K. Qin, B. Moudgil and C.W. Park, Thin Solid Films 446, 2, 277 (2004).

165. C. Hepburn, Polyurethane Elastomers, Applied Science Publishers, London, (1982).

المنارة للاستشارات
www.manaraa.com

166. K.L. Johnson, Contact Mechanics, Cambridge University Press, Cambridge (1985).

167. M. Moinpour, A. Tregub, A. Oehler and K. Cadien, MRS Bull. 27, 10, 766, (2002).

168. P. B. Zantye, S. Mudhivarthi, A.K. Sikder, A. Kumar and Y. Obeng, Mater. Res. Soc. Symp. Proc. 816, K 5.6 (2004).

169. A. K. Sikder, I. M. Irfan, Ashok Kumar, A. Belyaev, S. Ostapenko, M. Calves, J. P. Harmon and J. M. Anthony, Mat. Res. Soc. Sym. Proc., 670, M 1.8, (2001)

170. D. G. Totzke, Ultrasound diagnostic of chemical mechanical planarization pads, MS Thesis, University of South Florida, Tampa, FL, May 2000.

171. D. G. Totzke, A. Belyaev, W. Moreno, S. Ostapenko, I. Tarasov, W. Easter, A. Maury, and A. Crevasse, AIP Conf. Proc. 550, 1, 259 (2001).

172. I. Lacík, I. Krupa, M. Stach, A. Ku č ma, J. Jur č iová and I. Chodák, Polym. Test. 19, 7, 755 (2000).

173. L. Woo, M. T. K. Ling and S. P. Westphal, Thermochim. Acta 272, 171 (1996).

174. F. Podczeck and S. M. Almeida, Eur. J. Pharm. Sci. 16, 3, 209 (2002).

175. A. Philipossian and S. Olsen, J. Electrochem. Soc 151, 6, G 436 (2004).

176. F. Podczeck and S. M. Almeida, Eur. J. Pharm. Sci. 16, 3, 209, (2002).

177. D. Castillo-Mejia, J. Kelchner and S. Beaudoin, J. Electrochem. Soc. 151, G 271, (2004).

178. C.-Y. Chen, C.-C. Yu, S.-H. Shen and M. Ho, J. Electrochem. Soc. 147, 3922, (2000).

179. Y.-R. Jeng, P.-Y. Huang and W.-C. Pan, J. Electrochem. Soc. 150. G630, (2003).

180. S. Machinski, Wear characterization of polyurethane chemical mechanical polishing pads, MS Thesis, University of Central Florida, FL, Summer, (2001).

المنارة للاستشارات

www.manaraa.com

181. A. S. Lawing, Proceedings of the Mat. Res. Soc. Symp. Proc., Vol. 732E, I 5.3.1. (2002),

182. A.S. Lawing, Proceedings of the Seventh International Chemical Mechanical, Planarization for VLSI/ULSI Interconnection Conference (CMP-MIC), San Jose CA, Feb. 27-March 1, 310,(2002).

183. A.S. Lawing, Proceedings of the Fifth International Symposium on Chemical Mechanical Planarization, Philadelphia, PA, May 12-17, (2002).

184. R. K. Singh, S.-M. Lee, Low Stress Polishing of Copper / Low-K Dielectric Structures, Proceedings of the 8th CMP-IMC Conference, Marina Beach Marriott Hotel, Marina Del Rey, CA, February 19-21, 129, (2003).

185. R. Bajaj, M. Desai, R. Jairath, M. Stell and R. Tolles, Mater. Res. Soc. Symp. Proc. 337, p. 637**,** (1994).

186. K. Nakamura, S. Kishii and Y. Arimoto , Jpn. J. Appl. Phys. 36, 1525, (1997).

187. T. Gan, Modeling of chemical mechanical polishing for shallow trench isolation. MS thesis, Massachusetts Institute of Technology, Cambridge (MA), May 2000

188. S.-H. Chang, Microelectronic Engineering, 77, 1, 76, (2005).

189. R. Saxena, D. G. Thakurta, R. J. Gutmann and W. N. Gill Thin Solid Films, 449, 1-2, 192, (2004).

190. D.S. Rickerby, S.J. Bull, Engineering with surface coatings: The role of coating microstructure, Surf. Coat. & Technology, Volume 39/40, (1989), pp. 315.

191. A. G. Sirota, Polyolefins: modification of structure and properties, Israel Program for Scientific Translations, Jerusalem, © (1971).

المنارة للاستشارات

www.manaraa.com

192. Y.S. Obeng, E. M. Yokley, Method of Altering the Surface Properties of a Polishing Pad and Specific Application Thereof, US Patent # 6579604, Issued on June 17, (2003).

193. I. Chodák, A. Romanov, M. Rätzsch, G. Haudel, Acta Poly. 38, 12, 672, (2003).

194. J.-H. Ahn and D. Kwon, Mat. Sci. Eng., A 285, 172, (2000).

195. A.C. Fischer-Cripps. Nanoindentation, Springer-Verlag, New York, © (2002).

196. Internet website: http://www.kett.com/files/br94ai.pdf, Kett USA, © (2002).

197. P. B. Zantye, A. Kumar, W. Dallas, S. Osteapenko, A. K. Sikder, J. Vac. Sci Technol. A, In Review (2005).

198. W.D. Nix, Metallurgical Transactions A, 20A, 2217, (1989).

199. A.K. Bhattacharya and W.D. Nix, Intl. Journal of Solids and Structures, 24, 1287, (1988).

200. T.F. Page, W.C. Oliver and C.J. McHargue, J. Mater. Res., 7, 450, (1992).

201. G. Beamson, D. Briggs, High Resolution XPS of Organic Polymers, The Scienta ESCA300 Database, John Wiley & Sons NY, © 1992.

202. Y. Obeng, Proceedings of the 204th Electrochemical Society Meeting, Orlando, FL, Editors: S. Seal, R. L. Opila, K. Sundaram, and R. K. Singh, pp. 156.

203. S. Deshpande, S. Kuiry, M. Klimov, Y. Obeng, S. Seal, J. Electrochem. Soc. 151, G788, (2004); S. Deshpande, S. Dakshinamurthy, S.C. Kuiry, R. Vaidyanathan, Y.S. Obeng and S. Seal, Thin Solid Films 483,1-2 261, (2005).

204. S. C. Kuiry, S. Seal, E. Megan and B. Heinman, Thin Solid Films, 423, 243, (2003).

205. S. C. Kuiry, S. Seal, W. Fei, B. Heinman, J. Ramsdell, S. V. Babu, Y. Li and B. Wood, J of Electrochemical Society, 150, 1, C 36, (2003).

المنارة للاستشارات
www.manaraa.com

206. D. Tamboli, S. Seal, V. Desai and A. Maury, Journal of Vacuum Science and Technology A 17, 4, 1079, (1999).

207. S. C. Kuiry, Y. Obeng, S. Deshpande, S. Seal, Symposium M1, Sixth International Symposium on Chemical Mechanical Polishing, as a part of the 204th Meeting of The Electrochemical Society in Orlando, FL from October 12- 16, pp. 52, (2003).

208. F. Fracassi, R. d'Agostino, P.Favio, J. Electrochem Soc. , 139, 9, 2636, (1992).

209. Alexandra Fidalgo and Laura M. Ilharco, Journal of Non-Crystalline Solids, 283, 1-3, 144, (2001).

210. M. S. Hegde, R. Carracciolo, K. S. Hatton, and J. B. Wachtman, Jr., Appl. Surf. Sci., 37, 16, (1989).

211. J. S. Steckenrider, B.L. Mueller, US Patent 6,533,832 (2003).

212. T.-H. Tsai and S.-C. Appl. Surf. Sci. 210, 3-4. 190, (2003).

213. G. Bahar Basim and B. Moudgil, KONA Power Technol. Jpn. 21, 178, (2003).

214. M. Bielmann, U. Mahajan and R.K. Singh, Electrochem. Solid-State Lett. 2, 401, (1999).

215. U. Mahajan, S.-M. Lee and R.K. Singh, Mater. Res. Soc. Symp. Proc. 613, E 1.7 (2000).

216. H. Li, M. VanHaneham, J. Quanci, Mater. Res. Soc. Symp. Proc. 767, F 5.3, (2003).

217. F.B. Kaufman, D.B. Thompson, R.E. Broadie, M.A. Jaso, W.L. Guthrie, D.J. Pearson and M.B. Small, *J. Electrochem. Soc.* 138, 11, 3460 (1991).

218. R.K. Singh, S.-M. Lee, K.-S. Choi, G.B. Basim, W. Choi, Z. Chen and B.M. Moudgil, MRS Bull. 27, 10, 752 (2002).

المنارة للاستشارات

www.manaraa.com

219. T.-H. Tsai and S.-C. Yen, Appl. Surf. Sci. 210, 3-4, 190 (2003.

220. T.-H. Tsai, Y.F. Wu and S.C. Yen, Appl. Surf. Sci. 214, 1-4, 120 (2003).

221. A. Misra, US Patent 6,530,967 (2003).

222. A. Vijayakumar, T. Du, K.B. Sundaram and V. Desai, Polishing, Microelectron. Eng. 70, 1, 93 (2003).

223. C. Kourouklis, T. Kohlmeier and H.H. Gatzen, Sens. Actuators A: Phys. 106, 263 (2003)

224. J. Luo and D.A. Dornfeld, Material removal mechanism in chemical mechanical polishing: theory and modeling, IEEE Trans. Semicond. Manuf. 14, 2, 112 (2001).

225. S.R. Runnel and L.M. Eyman, J. Electrochem. Soc. 141, 1698 (1994).

226. Y.-R. Jeng and P.-Y. Huang, Electrochem. Solid-State Lett. 7, 2, G40 (2004).

227. N.J. Brown, P.C. Baker and R.T. Maney, Proc. SPIE 306, 42 (1981).

228. J. Sorooshian, D. Hetherington and A. Philipossian, Electrochem. Solid State Lett., 7 (10), G222, (2004).

229. I. Kojima and M.Kurahashi, J. Electron. Spectr. Rel. Phen. 42, 177 (1987).

230. W. Li, D. W. Shin, M. Tomozawa, S. P. Murarka, Thin Solid Films 270, 601, (1995).

231. B. Mullany, G. Byrne, J. Mater. Process. Technol. 132, 28, (2003).

232. S. Mudhivarthi, P. B. Zantye, A. Kumar, A. Kumar, M. Beerbom and R. Schlaf, Electrochemical and Solid State Letters, Accepted for Publication, (2005).

233. P.B. Zantye, A. Kumar and A. Kumar, Novel Nanoparticle based CMP slurry for Cu planarization, US Patent Procedures Pending (Ref No.: 05A023PR).

المنارة للاستشارات

www.manaraa.com

ABOUT THE AUTHOR

The author received his Master's degree in field of Mechanical Engineering in May 2002 at University of South Florida, Tampa, FL, USA. He will be receiving his Doctoral degree in Mechanical Engineering in August 2005 from the same university, for his work in the area of Chemical Mechanical Planarization. Apart from CMP, the author's research interests include: MEMS, microelectronic thin film synthesis and metrology, and chemical and biological sensors. He has also pursued his research interests overseas at the Institute of Microelectronics, Singapore during his internship. The author currently has filed 2 Patents, has 8 journal articles either published or under the process of being published, besides 21 conference papers. He received the Sigma Xi Outstanding Graduate Researcher Award (Tampa Bay Chapter) for the year 2004. The author has been elected a full member of the American Society of Mechanical Engineers and is also affiliated to the Materials Research Society and the Electrochemical Society.

المنارة للاستشارات
www.manaraa.com